Pediatr Radiol (2017) 47 (Suppl 2):S297–S421
DOI 10.1007/s00247-017-3820-2

ABSTRACTS

Pediatric Radiology Supplement

Founded in 1963
The European Society of Paediatric Radiology

53rd Annual Meeting and 39th Post Graduate Course of the European Society of Paediatric Radiology

May 30 – June 03, 2017

Davos, Switzerland

TABLE OF CONTENTS

Welcome Words

Dear colleagues,

Paediatric imaging and dedicated radiological care of children has become an integral part of modern paediatric healthcare.

It is with great pride, that we welcome you to the 53rd Annual Meeting and the 39th Post Graduate Course of the European Society of Paediatric Radiology, which will be held in Davos/Switzerland, from May 30 – June 03, 2017!
It has been more than 20 years since our meeting was held in Lugano/Switzerland, and so much has changed in the world of paediatric radiology, but the only thing that has remained constant is the commitment and the talent of the ESPR community!

We sincerely hope that this meeting will provide a platform for networking, will advance education and provide the frame for both, making new and renew old friendships in our alpine city.
The ESPR 2017 course builds on the spirit of previous years and is structured around six pathology-based sessions with functional correlation, one session dedicated to neonatal imaging and one session focused upon radiation protection. The highlight of this course is an international discussion panel with renowned experts who will demonstrate the clinical and radiological features in a case-based session dedicated to child abuse and genetic-metabolic mimickers.

We are living in a rapidly evolving world, in which new diseases and an intensive population exchange across countries are deemed to have a long lasting and global financial and epidemiological impact. We will have two special focus sessions dedicated to emerging infectious diseases like ZIKA virus and to the problem of age assessment in juvenile migrants, highlighting the clinical and radiological aspects of these two new and poorly investigated topics.

To underscore the importance of international communication, two “ESPR meets CHOP” Mini-Symposia will be held, in which eminent European and American experts will exchange their radiological experience and knowledge about various specific diseases including neuroblastoma, sarcoma and many more.
This exciting, thoughtful and stimulating programme would not be possible without the commitment of dozens of members, non-members and vendors willing to support the ESPR by sharing their expertise, time and resources.

We are confident that you will find the venue and networking, research and educational opportunities inspirational and fun.

We are looking forward to seeing you in Davos!

Yours,
Jacques Schneider & Georg Eich
ESPR Congress President & Congress Secretary

ESPR 2017 Congress organisation

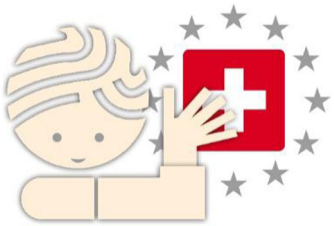

Congress President
Jacques Schneider, Basle/CH

Congress Secretary
Georg Eich, Aarau/CH

Scientific Committee
Jacques Schneider, Basle/CH
Georg Eich, Aarau/CH
Sylviane Hanquinet, Geneva/CH

ESPR 2017 Congress Office
Education Congress Research GmbH
Neutorgasse 9/2
1010 Vienna/Austria
Tel.: +43 1 533 40 64
Fax.: +43 1 533 40 64 445
Email: office@espr2017.org
www.espr2017.org

General Information
European Society of Paediatric Radiology

Officers

President	Catherine M. Owens (London, United Kingdom)
General Secretary	Maria I. Argyropoulou (Ioannina, Greece)
Treasurer	Philippe Petit (Marseille, France)
Congress President	Jacques Schneider (Basel, Switzerland)
Congress Past President	Karen Rosendahl (Bergen, Norway)
	James Donaldson (Chicago, USA)
Council of Trustees	Veronica Donoghue (Dublin, Ireland)
	Fred Avni (Brussels, Belgium)
	Paolo Toma (Genoa, Italy)

Honorary members

1964 J. Caffey USA
1964 L. Schall Germany
1965 S.R. Kjelberg Sweden
1965 E.B.D. Neuhauser USA
1966 J. Lefèbvre France
1973 H.M. Gefferth Hungary
1973 K. Rowinski Poland
1974 F.N. Silverman USA
1975 U.G. Rudhe Sweden
1979 J.A. Kirkpatrick, Jr USA
1979 A. Lassrich Germany
1979 J. Sauvegrain France
1982 C. Fauré France
1982 A. Giedion Switzerland
1983 E. Willich Germany
1984 R. Astley United Kingdom
1987 J. Bennet France
1987 O.A. Eklöf Sweden
1987 C.A. Gooding USA
1987 D.C. Harwood-Nash USA
1987 J.F. Holt USA
1987 A.K. Poznanski USA
1987 H. Taybi USA
1988 H.J. Kaufmann Germany
1989 B.J. Cremin South Africa
1989 K-D. Ebel Germany
1989 H. Fendel Germany
1989 E.M. Sweet United Kingdom
1990 D.R. Kirks USA
1991 A. Chrispin United Kingdom
1991 E.A. Franken USA
1991 D. Nussle Switzerland
1991 B.P. Wood USA
1992 W.E. Berdon USA
1993 W. Holthusen Germany
1993 J. Lucaya Spain
1994 N.C. Perlmutter Belgium
1994 H.G. Ringertz Sweden
1994 D.G. Shaw United Kingdom
1996 R. Lebowitz USA
1996 B. Lombay Hungary
1997 Y. Briand France
1997 N. T. Griscom USA
1997 P. Small United Kingdom
1998 A. Daneman Canada
1998 G. Kalifa France
1999 M. Grunebaum Israel
1999 P. Thomas Ireland
2000 N. Blake Ireland
2000 P. Kramer The Netherlands
2000 G. Stake Norway
2001 J. Bar-Ziv Israel
2001 R.C. Brasch USA
2001 M. Hassan France
2001 J.L. Strife USA
2002 S. Laurin Sweden
2003 G. Beluffi Italy
2003 H. Carty United Kingdom
2003 B. Parker USA
2003 A. Pelizza Italy
2004 C. Hall United Kingdom
2004 A. Marcinski Poland
2005 U. Willi Switzerland
2005 J.P. Montagne France
2005 G. Farielo Italy
2006 A.E. Oestreich USA
2006 L. Garel Canada
2006 M. Mearadji The Netherlands
2006 F. Brunelle France
2007 R. Fotter Austria
2007 P.A.N. Daltro Brasil
2007 G. Benz-Bohm Germany
2007 M. Spehl-Robberecht Belgium
2008 R. Teele USA (New Zealand)
2008 T. Slovis USA
2008 I. Gassner Austria
2008 J. Fonseca Santos Portugal
2009 R. Schumacher Germany
2009 N. Gourtsoyiannis Greece
2009 I. Boechat USA
2009 S. Chapman United Kingdom
2009 J. Troeger Germany
2009 E. Richter Germany
2010 F. Avni Belgium
2010 V. Donoghue Ireland
2010 P. Toma Italy
2010 F. Diard France
2011 R. De Bruyn United Kingdom
2011 G. Enriquez Spain
2011 C. Garcia Chile

2011 P. Kleinman USA
2011 G. Taylor USA
2012 C. Veyrac France
2013 D. Pariente France
2014 R. Arthur Scotland
2014 M. Haliloglu Turkey
2016 C. Owens United Kingdom
2016 D. Bulas United States
2016 E. Kis Hungary
2017 M. Riccabona Austria
2017 G. Pena Spain

Gold medallists

2007 J. Lucaya Spain
2008 G. Kalifa France
2010 U. Willi Switzerland
2011 R. Fotter Austria
2012 F. Brunelle France
2013 F. Avni Belgium
2014 V. Donoghue Ireland
2015 G. Sebag France
2016 P. Toma Italy

Jacques Lefèbvre awards

1977 H. Ringertz (Norway)	The Width of the Cranial Sutures in the Neonate: An Objectif
1978 L. Garel (France)	Xanthogranulomatous Pyelonephritis in Children: 19 cases
1979 M. Brauner (France)	Metrizamide Myelography in Infants with Brain Injury to the Brachial Plexus
1980 M. Spehl-Robberecht (Belgium)	Ultrasonic Study of Pancreas in Cystic Fibrosis
1981 L. Garel (France)	The Renal Sinus: An Important Anatomical Landmark in Children
1982 A. Couture (France)	Ultrasonographic Exploration of Cerebral Malformations
1983 F. Brunelle (France)	Percutaneous Cholecystography in Children
1984 C. Veyrac (France)	Ultrasound of Normal and Pathologic Choroid Plexus
1985 F. Avni (Belgium)	Ultrasonic Demonstration of Abnormal and Atypical Gallbladder Content in Newborns
1986 D. Pariente (France)	Biliary Tract invovement in Children with Histiocytosis X
1987 N. Sellier (France)	Focal Cortical Dysplasia: A rare Cause of Epilepsy
1988 K-H. Deeg (Germany)	Pulsed Doppler Sonographic Measurement of Normal Values for the Flow Velocities in the Cerebral Arteries of Healthy Infants
1989 P. Winkler (Germany)	Major Pitfalls in the Doppler Examination of the Cerebral Vascular System
1990 C. Garel (France)	Laryngeal Ultranographic Study in Infants and Children: Pathological Findings
1991 J-P. Pracos (France)	Systematic Study of Superior Mesenteric Vessels in Abdominal US
1992 A. Hollman (United Kingdom)	Colour Doppler Imaging of the Acute Pediatric Scrotum
1993 M. Chami (France)	Ultrasound Contribution in the Analysis of the Newborn and Infant Normal Foot and Club Foot: Preliminary Study
1994 C. Adamsbaum (France)	Vermian Agenesis without Posterior Fossa Cyst
1995 G. Sebag (France)	Magnetic Resonance Angiography of Pediatric Rena Transplants with Quantification of Allograft Blood Flow
1996 W.K. Rohrschneider (Germany)	US, CT and MR imaging Characteristics in Nephroblastomatosis: Evaluation of 23 patients
1997 L. Hertz-Pannier (France)	Non-Invasive Preoperative Motor Mapping in Children with Brain Functional MRI
1998 N. Nicaise (Belgium)	Dynamic Gd DTPA Enhanced T1W Turbo Field Echo Imaging: Interest in Pediatric Renal Evaluation
1999 F. Rypens (Belgium)	Fetal Lung Volume Estimation by MRI: Normal Values and Potential Use
2000 F. Ziereisen (Belgium)	Doppler assessment of pulsatility index (PI) of the uterine artery in girls around puberty
2001 M.K. Lidegran (Sweden)	MRI and echocardiography in assessment of ventricular function in atrially corrected transposition of the great arteries
2002 M. Cassart (Belgium)	The Assessment of Fetal Uronephropathies by MR Imaging
2003 N. Boddaert (France)	18F-fluoro-L-DOPA PET SCAN in focal forms of hyperinsulinism of infancy
2004 C. Jourdan (Germany)	US Evaluation of Intima-media Thickness (IMT) and Elastic Properties – Distensibility, Stiffness, and Incremental Modulus of Elasticity – of the Common Carotid Artery as Marker of Early Vascular Damage in Children with Chronic Renal Failure and Reference Values
2005 C.J. Kellenberger (Switzerland)	Cardiovascular MRI for Investigating Newborns and Infants with Congenital Heart Disease
2006 P. Ou (France)	Magnetic resonance assessment of aortic flow dynamics and aortic arch geometry in patients with successful repair of coarctation of the aorta
2007 C. Sporcq (Belgium)	Reappraisal of the sonographic characteristics of the fetal and newborn kidney: introducing the cortico-medullary ratio
2008 M.B. Damasio (Italy)	Which is the best imaging modality to capture bone erosions in juvenile idiopathic arthritis?
2009 K. McDonald (United Kingdom)	DWI to assess chemotherapy response in solid tumours
2010 L.S. Ording-Müller (Norway)	Development of the wrist. Normal standards based on MRI for 6-15 year-olds
2011 C. Duran (Spain)	Voiding urosonography: normal and abnormal appearance of the urethra
2012 J. Vazquez (Spain)	External manual reduction with US assistance: a new procedure for pediatric idiopathic ileocolic intussuseption
2013 A. Viehweger (Germany)	The Gini-coefficient: A new method to assess fetal brain development
2014 S. Kinner (Germany)	MR colonographywith diffusion weighted imaging (DWI) in childrenand adolescents with inflammatory bowel disease (IBD)
2015 J. Shur (United Kingdom)	Size matters – Dose reference levels (DRL's) based on patient thickness, instead of age
2016 L. Laborie (Norway)	Fetal, infant, and childhood growth and acetabular hip dysplasia at skeletal maturity: findings from a prospective study with follow-up from newborn to adult life
2017 C. Zollikofer (Switzerland)	Hominid Evo-Devo: Reconstructing the evolution of human development

Poster awards

1994 H. Gomes (France)	Neonatal Hip Sonography from Anatomy to Sonography
1995 P. Schmit (France)	Imaging of Cystic Mesenchymal Hamatomas of the Liver. Review of 13 Patients
1997 P. Schmit (France)	Congenital Hepatic Vascular Malformations in Children
1998 H. Brisse (France)	In Utero MRI Normal Gyral Development of the Human Brain
2000 M. Valle (Italy)	High-frequency US detection of the brachial plexus in newborns and infants
2001 W.K. Rohrschneider (Germany)	Static Dynamic MR-Urography – Simultaneous Morphological and Fonctional Evaluation of the Urinary Tract
2002 C.M. Owens (United Kingdom)	The Utility of MRI in the Assessment of Symptomatic Adenoidal Hypertrophy and Rhynosinusitis in Children – Pre-And-Post – Medical Therapy
2003 R. Schumacher (Germany)	Sonographical anatomy of the Anal Sphincter Complex (ASC) and levator ani muscle in neonates and infants
2004 H.J. Mentzel (Germany)	Comparison of Whole-Body STIR-MRI and 99mTc-Methylene Diphosphonate Scintigraphy in the Examination of Children With Suspected Multifocal Bone Lesions
2005 G. Enriquez (Spain)	Prenatal assessment of lung hypoplasia in congenital diaphragmatic hernia: correlation between volumetric MRI and biometric ultrasound measurements
2006 I. Sorge (France)	Reduction of radiotherapy in children with early stages of Hodgkin's lymphoma, Influenced by a new imaging and FDG-PET based strategy
2007 S. Punwani (United Kingdom)	Effects of reducing radiation dose on lung nodule detection.
2008 J-F. Chateil (France)	Imaging of acquired spinal cord lesions and spinal canal pathology in children
2009 G.M. Barez (Spain)	Spectrum of Imaging findings in the brachial apparatus anomalies
2010 M. Brun (France)	Diffusion tensor imaging in attention deficits in children treated for posterior fossa tumours: preliminary results
2011 C. Fonda (Italy)	3T arterial spin labelling (ASL) in pediatric patients
2012 O. Arthurs (United Kingdom)	Diffusion weighted MRI of the fetal brain in intrauterine growth restriction.
2013 C. Duran (Spain)	Voiding urosonography: a pictorial essay of the lower urinary tract pathology
2014 A. Tanase (France)	Ultra low dose imaging for the follow up of idiopathic scoliosis: feasibility of spinal 3D reconstructions and reproducibility of 3D parameters reproducibility- a pilot study
2015 M. Napolitano (Italy)	MR assessment of Crohn's disease activity in a paediatric population:correlation with clinical index of disease (SP)
2015 D. Kljucevsek (Slovenia)	Contrast- enhanced Ultrasound (CEUS) of bowel wall with quantitative assessment of Crohn's disease activity in child: a case report (EP)
2016 J. Adu (United Kingdom)	Early Onset Infantile Inflammatory Bowel Disease (EP)
2016 J.E. Park (Korea)	Three-dimensional, T1-weighted Gradient-Echo Imaging of the Brain with a Radial Sampling of K-Space: An Alternative Technique to Reduce Motion Artifacts in Breathless Children (SP)

Young researcher awards

2003 M. Brun (France)	Phonological decoding in dyslexic children: activation pattern in FMRI
2004 A.B. Barnacle (United Kingdom)	Image-guided Percutaneous Biopsy of Soft Tissue Masses in Children
2005 M. Raissiki (Greece)	Eye-Lens Bismuth Shielding in Pediatric Head CT Examinations
2006 I. Sorge (Germany)	Reduction of radiotherapy in children with early stages of Hodgkin's lymphoma, influenced by a new imaging and FDG-PET based strategy
2007 M. Alison (France)	In vivo targeting of macrophagic activity with MRI contrast agent (USPIO) in an experimental model of neonatal brain lesions
2008 J. Herrmann (Germany)	Capsular arterial collateralisation after paediatric liver transplantation
2010 O. Arthurs (United Kingdom)	MR Voiding cystourethrography for vesico-ureteric reflux in unsedated infants
2011 N. Gupta (United Kingdom)	Predictors of vesicoureteric reflux in infants with UTI using NICE criteria
2012 L.B. Laborie (Norway)	Associations between femoroacetabular impingement and hip dysplasia as demonstrated radiographically. Preliminary results
2013 N. Lochbühler (Switzerland)	MRI assessment of inflammatory activity and mandibular growth following intra-articular TMJ steroid injection in children with JIA
2014 A. Slaar (The Netherlands)	A clinical decision rule for acute wrist trauma in children
2015 S. Shelmerdine (United Kingdom)	Achondroplasia: Really Rhizomelic
2016 M. Paddock (United Kingdom)	What is the value of spine, hand and foot radiographs as part of the skeletal survey for diagnosing suspected physical child abuse?

President's awards

2004 A.K. Kilian (Germany)	Prenatal Magnetic Resonance (MR) Lung Volumetry of Congenital Diaphragmatic Hernia (CDH): Comparison with the Clinical Outcome and the Necessity of Extracorporeal Membrane Oxygenation (ECMO)
2005 A. Larke (Ireland)	MRI findings as an indication of underlying genetic lesions in congenital malformations of the brain
2007 C. Duran (Spain)	Voiding cystosonography for the study of the urethra
2008 A. Calder (United Kingdom)	Computed tomography compared with ultrasound and chest radiography in children with pleural empyema
2009 E. Senocak (Turkey)	MRI and DWI findings in children with hemophagocytic lymphohistiocytosis: tendancy for symmetricity
2010 S. Franchi-Abella (France)	Congenital portosystemic shunt: complications and outcome after closure: about 19 pediatric cases
2011 S. Punwani (Greece)	MRI vs. PET/CT for detection of focal splenic lesions in paediatric and adolescent lymphoma at initial staging

2012 P. Xenophontos (Greece)	Detection of primary sclerosing cholangitis (PSC)-type lesions in children with inflammatory bowel disease via MRCP: a relative risk measures analysis
2013 G. Pasztor (Hungary)	The importance of pyelectasis – report of a clinical study in progress
2014 A.S. Littooij (The Netherlands)	Whole-body MRI for staging of paediatric lymphoma: prospective comparison to an FDG-PET/CT-based reference standard
2015 C. Wieser (Austria)	Vessel flexibility index as a new marker for cardio-vascular disease – a pilot study
2016 L.K Suther (Norway)	Image Quality Assessment of 3T MR Coronary Angiography (3D SSFP) In Patients Operated For Transposition of the Great Arteries with Three Qualitative Methods

Past presidents and meeting sites

1964 J. Lefèbvre, Paris/France
1965 U.G. Ruhde, Stockholm/Sweden
1966 J. Sutcliff, London/United Kingdom
1967 H.J. Kaufmann, Basel/Switzerland
1968 A. Lassrich, Hamburg/Germany
1969 K. Rowinsky, Warsaw/Poland
1970 G. Iannacone, Rome/Italy
1971 G. Thomsen, Copenhagen/Denmark
1972 J. Sauvegrain, Paris/France
1973 R. Astley, Birmingham/United Kingdom
1974 P.E. Heikel, Helsinki/Finland
1975 K. Knapp, Madrid/Spain
1976 O. Eklöf, Stockholm/Sweden
1977 A. Giedion, Lucern/Switzerland
1978 N. Perlmutter-Cremer, Brussels/Belgium
1979 K.D. Ebel, Cologne/Germany
1980 The Dutch Group of Paediatric Radiologists, The Hague/The Netherlands
1981 G. Stake, Oslo/Norway
1982 A. Rubin, Prague/Czechoslovakia
1983 C. Fauré, Paris/France
1984 G.F. Vicchi, Florence/Italy
1985 E. Sweet, Glasgow/Scotland
1986 J. Lucaya, Barcelona/Spain
1987 D. Lallemand (ESPR) & D. Harwood-Nash (SPR), Toronto/Canada
1988 D. Nusslé, Montreux/Switzerland
1989 N. Blake, Dublin/Ireland
1990 H. Fendel, Munich/Germany
1991 H.G. Ringertz (ESPR) & D. Kirks (SPR), Stockholm/Sweden
1992 B. Lombay, Budapest/Hungary
1993 D.G. Shaw, London/United Kingdom
1994 F. Avni, Brussels/Belgium
1995 P. Kramer, Utrecht/The Netherlands
1996 P. Thomas, (ESPR) & K. Fellows (SPR) Boston/USA
1997 U. Willi, Lugano/Switzerland
1998 B. Theodoropoulos, Rhodes/Greece
1999 J. Bar-Ziv & G. Kalifa, Jerusalem/Israel
2000 J. Fonseca Santos, Lisbon/Portugal
2001 F. Brunelle (ESPR) & J. Strife (SPR), Paris/France
2002 T. Nordshus, Bergen/Norway
2003 P. Toma, Genoa/Italy
2004 J. Troëger, Heidelberg/Germany
2005 V. Donoghue, Dublin/Ireland
2006 R. Fotter (ESPR) & G. Taylor (SPR), Montreal/Canada
2007 G. Enrìquez, Barcelona/Spain
2008 S. Chapman, Edinburgh/United Kingdom
2009 M. Haliloglu, Istanbul/Turkey
2010 J.F. Chateil, Bordeaux/France
2011 C.M. Owens (ESPR) & Dorothy Bulas (SPR) London/United Kingdom
2012 M.I. Argyropoulou, Athens/Greece
2013 E. Kis, Budapest/Hungary
2014 R.A.J. Nievelstein, Amsterdam/Netherlands
2015 M. Riccabona & E. Sorantin, Graz/Austria
2016 K. Rosendahl (ESPR) and J. Donaldson (SPR), Chicago/United States

Future ESPR meeting
2018 Berlin, Germany, June 18-22

Future SPR meeting
2017 Vancouver, Canada, May 16-20

Future IPR meeting
2021 Rome, Italy

European courses of paediatric radiology (ECPR)
1992 F. Brunelle, Biarritz/France (Abdomen)
1993 P. Toma, Genoa/Italy (Musculoskeletal)
1994 G. Enrìquez, Barcelona, Spain (Thorax)
1995 C. Raybaud, Marseille/France (Neuroradiology)
1996 G. Benz-Bohm, Cologne/Germany (Abdomen)
1997 H. Carty, Liverpool/United Kingdom (Thorax)
1998 C. Adamsbaum & G. Sebag, Montpellier/France (Musculoskeletal)
1999 P. Tortori-Donati, Genoa/Italy (Neuroradiology)
2000 R.Fotter, Graz/Austria (Abdomen)
2001 S. Laurin, Lund/Sweden (Thorax)
2002 B. Lombay, Budapest/Hungary (Musculoskeletal)
2003 E. Martin-Fiori & T. Huisman, Zurich/Switzerland (Neuroradiology)
2004 T. Berrocal, Madrid/Spain (Abdomen)
2005 M. Spehl & C. Christophe, Brussels/Belgium (Thorax)
2006 J-N. Dacher, Rouen/France (Emergencies)
2007 R. Schumacher, Mainz/Germany (Musculoskeletal)
2008 K. Chong, London/United Kingdom (Neuroradiology)
2009 R. van Rijn, A. Smets & E. Deurloo, Amsterdam/The Netherlands (Abdomen)
2010 C. Fonda, Firenze/Italy (Thorax)
2011 I. Barber, Barcelona/Spain (Musculoskeletal)
2012 H.J. Mentzel, Jena/Germany (Abdomen)
2013 M.H. Lequin, Rotterdam/the Netherlands (Thorax)
2014 D.C. Hughes, Sheffield/United Kingdom (Musculoskeletal)
2015 A. Rossi, N. Girard & M. Argyropoulou, Ioannina/Greece (CNS)
2016 C. de Lange & L. S. Ording Müller, Oslo/Norway (Pediatric Abdominal Imaging)

Future ECPR course
2017 Utrecht/Netherlands, October 11-13 (Paediatric Musculoskeletal Imaging)

European courses of paediatric neuroradiology (ECPNR)

Courses run jointly by ESPR, the ESNR and the ESMNR

2011 M. I. Argyropoulou (ESPR), A. Rossi (ESNR) & N. Girard (ESMNR), Marseille/France
2013 M. I. Argyropoulou (ESPR), A. Rossi (ESNR) & N. Girard (ESMNR), Genoa/Italy
2015 M. I. Argyropoulou (ESPR), A. Rossi (ESNR) & N. Girard (ESMNR), Ioannina/Greece
2016 M. I. Argyropoulou (ESPR), A. Rossi (ESNR) & N. Girard (ESNR), P. M. Sundgren (ESNR), Marseille/France
2017 M. I. Argyropoulou (ESPR), A. Rossi (ESNR) & N. Girard (ESNR), P. M. Sundgren (ESNR), Genoa/Italy

ESPR Honorary members 2017

Dr. Pilar García-Peña and Prof. Michael Riccabona

We have the pleasure and honour to introduce Dr. Pilar García-Peña and Prof. Michael Riccabona as our ESPR Honorary Members for ESPR Davos in June 2017.

ESPR honorary membership is awarded to acknowledge, commend and thank recipients for all of their hard work and dedication in contributing to the care of children within Europe and for their exceptional dedication and commitment over many years to the ESPR.

Dr. Pilar García-Peña

Dr. Pilar García-Peña is a graduate of Medicine and Surgery in the Medical Faculty of the Central University of Barcelona, Spain.

Pilar was born in San Sebastian, in the Basque Country, Spain. She is the mother of one son and a proud grandmother to three grandchildren, and she currently resides in the city where she started her career, Barcelona, Spain.

Dr. García-Peña is a talented polymath and greatly values precious time with family and friends, classical music and opera, art exhibitions, worldwide travelling and is a keen and talented photographer.

Pilar trained first as a clinical Paediatrician, at Hospital Clinico of the Central University, subsequently working as a Paediatrician at this centre for three happy years.

She then subspecialised in Paediatric Radiology at the University Hospital Materno-Infantil Vall d'Hebron, Universidad Autónoma, Barcelona, Spain, and in addition, she completed post-graduate training at the Hospital Clinico of the Central University in Madrid, Spain; at the Royal Hospital for Sick Children in Edinburgh, United Kingdom; and at the Curie Foundation and Trousseau Hospital in Paris, France.

Dr. García-Peña practiced Paediatric Radiology at the University Hospital Materno-Infantil Vall d'Hebron of the Universidad Autonoma in Barcelona where she was Chief of the CT Unit of Paediatric Radiology for 15 years.

Pilar has had a long and distinguished academic career and has been a reviewer and collaborator for many different national and international medical journals including the American Journal of Radiology (AJR), Radiology, Radiographics, European Radiology, Paediatric Radiology, Acta Radiológica Escandinava, Radiología, and many more with extensive publications and book chapters in national and international reputable journals.

She is an international celebrity lecturer, with multiple lectures and presentations in numerous high profile national and international congresses.

She has been made an honorary member of several international societies and – is Editor of 'Paediatric Chest Imaging in Infants and Children', 3rd edition, 2014, with many renowned American, European and Asian Paediatric Radiology co-authors, who respect and admire her greatly.

She is now Emeritus in Paediatric Radiology, University of Barcelona and National Health Institutions and Vice-President of the International Society of Thoracic Paediatric Imaging.

Dr. García-Peña has devoted a lifetime to her profession, helping, training and inspiring young doctors, collaborating with colleagues, and being actively involved in developing Paediatric Radiology in Spain and other countries.

She is much beloved of her colleagues, and her charm, beauty and charisma have shone through her considerable intellectual prowess to inspire many aspiring radiologists throughout the world. It is a pleasure to award her honorary membership of a Society to which she has contributed so much over a very distinguished career.

Dr. C.M. Owens, February 2017

Prof. Michael Riccabona

Prof. Michael Riccabona undertook his Medical school & University training at the University of Innsbruck, Tirol, Austria, completing his MD at Karl Franzens University in Graz, Austria.

Following an internship in neurology, surgery and internal medicine he then specialized in Paediatrics at the Dept. of Paediatrics, University Hospital in Graz. There he took charge of the paediatric radiology and sonography sections at University Hospital in Graz, as associate professor of paediatrics. In 1993 he additionally started to specialise in radiology, becoming associate professor of radiology in 1998 - then taking charge of the subsection of paediatric sonography at the Dept. of Radiology, University Hospital in Graz, where in March 2006 he was appointed full Univ. Prof at the Medical University Graz, Austria.

He has a distinguished academic career and written over 200 papers, more than 50 chapters and several textbooks, and is a very popular international speaker, delivering numerous lectures at many high profile scientific meetings.

He is an active member of several reputable international societies, has been chair of the paediatric ultrasound section of the Austrian ultrasound society since 2003, and president of the society of German speaking paediatric radiologists (2010-2016). He is a constant source of inspiration within his subspecialist areas of interest in ultrasound and abdominal radiology in children.

He has been course director at several important meetings and served as President of ESPR in Graz in 2015 and as lead of the Paediatric Subcommittee at ECR in 2012.

He has provided inspirational leadership as Chair of the ESPR task force on uroradiology since 2002 – writing state of the art guidelines and procedural recommendations to facilitate standardised best practice for imaging within paediatric uroradiology.

He has been a reviewer for many international journals.

He has on-going active roles in postgraduate education for medical colleagues from Eastern Europe, including basic ultrasound education and refresher courses, and workshops.

Michael Riccabona is very deserving of honorary membership of ESPR, which reflects his seminal role within Paediatric Radiology in Europe and his tireless dedication working for the good of children.

Dr. C.M. Owens, February 2017

ESPR 2017 Programme at a glance

ESPR 2017 Post Graduate Course Programme

TUESDAY, MAY 30, 2017
POST GRADUATE COURSE

	ROOM 1 – ASPEN
08:00-09:00	**Radiation protection**
09:00-09:30	Break
09:30-12:30	**Thoraco-abdominal imaging**
12:30-13:30	Break
13:30-15:30	**Trauma**
15:30-16:00	Break
16:00-18:00	**In depth: Spine and spinal cord**

WEDNESDAY, MAY 31, 2017
POST GRADUATE COURSE

	ROOM 1 – ASPEN
08:00-10:00	**Anything new about functional imaging?**
10:00-10:30	Break
10:30-13:00	**Systemic disorders**
13:00-14:00	Break
14:00-15:30	**Tumors of the head and neck**
15:30-16:00	Break
16:00-17:30	**Syndromes and genetics**
17:30-18:15	**Panel Discussion: Radiologic challenge: Child abuse or genetic/metabolic disease: A case-based session**

ESPR 2017 Annual Meeting Programme

THURSDAY, JUNE 01, 2017

	ROOM 1 – ASPEN	ROOM 2 – SANADA I	ROOM 3 – SANADA II
07:45	Opening Ceremony		
08:00	Special Focus Session: Emerging infectious diseases: ZIKA Virus infection		
08:15			
08:30			
08:45			
09:00	ESPR meets CHOP		
09:15			
09:30			
09:45			
10:00	Break		
10:15			
10:30		Task Force Session: Neuro	Task Force Session: MSK – Imaging in juvenile idiopathic arthritis (JIA) – An update
10:45			
11:00			
11:15			
11:30		Scientific Session: Neuro	Scientific Session: MSK
11:45			
12:00			
12:15			
12:30	Industry sponsored symposium		
12:45			
13:00			
13:15			
13:30		Scientific Session: Abdominal (GI & GU) Imaging	Task Force Session: CT and radiation dose
13:45			
14:00			
14:15			
14:30		Task Force Session: Abdominal (GI & GU) Imaging	Scientific Session: CT and radiation dose
14:45			
15:00			
15:15			
15:30	Case Report Presentation Session	Scientific Session: Abdominal (GI & GU) Imaging	Scientific Session: MSK
15:45			
16:00			
16:15			
16:30	Break		
16:45			
17:00	Jacques Lefèbvre Lecture		
17:15			
17:30			
17:45			
18:00			

ESPR 2017 Key messages/Objectives

- To learn about and update your knowledge on state of the art paediatric imaging approaches, and to get inspired by new scientific results and endeavours.
- To revisit basic imaging rules and methods, and to hear about new technologies for paediatric imaging.
- To discuss how to optimally adapt the various imaging techniques minimising radiation exposure and risks during diagnostic imaging in children.
- To consider common restrictions, challenges, and possible solutions in Paediatric Radiology within the different settings in different countries, regions, continents and clinical scenarios - discussing all these aspects with colleagues, and to mingle with experts from all over the world learning from each other and fostering networking in Paediatric Radiology to try to grant optimal imaging for all children.

CME - Continuing Medical Education

An application for the 53rd Annual Meeting as well as for the 39th Post Graduate Course has been submitted to the EACCME® for CME accreditation of this event. The EACCME is an institution of the UEMS (www.uems.net). The number of CME points will be announced at the ESPR 2017 Congress Website.

Each medical specialist should only claim those hours of credit that he/she actually spent in the educational activity. Certificates of attendance will be available in the ESPR MyUserArea after the meeting.

Programme - 39th Post Graduate Course

Programme - 39th Post Graduate Course

Tuesday, May 30, 2017

Time	Room 1 - Aspen
08:00-09:00	**Radiation protection**
	Moderator: R.W. Wolf, Bern/CH
	Xray: Can we still improve the technique/protection?
	R.W. Wolf, Bern/CH
	Computed tomography: Are we doing enough?
	E. Sorantin, Graz/AT
09:00-09:30	Break
09:30-12:30	**Thoraco-abdominal imaging**
	Moderators: L. Alamo, Lausanne/CH; P. Petit, Marseille/FR
	Prenatal thoracic MRI
	L. Alamo, Lausanne/CH
	Genital malformation: Müller and Wolff
	K. Darge, Philadelphia/US
	Neonatal liver tumors and hepatic vascular malformations
	D. Pariente, Le Kremlin Bicetre/FR
	Imaging in Crohn disease: State of the art in diagnosis, prognosis and followup
	P. Petit, Marseille/FR
	Heterotaxy and isomerism
	Ch. Lapierre, Montreal/CA
	Congenital lung disease: The role of ultrasound
	G. Enriquez, Barcelona/ES
12:30-13:30	Break
13:30-15:30	**Trauma**
	Moderator: A. Offiah, Sheffield/UK
	Traumatic injuries of the skull base
	S. Blaser, Toronto/CA
	Abdominal injuries
	S. Toso, Geneva/CH
	Sport injuries
	D. Jaramillo, Philadelphia/US
	Inflicted injuries in children
	A. Offiah, Sheffield/UK
15:30-16:00	Break
16:00-18:00	**In depth: Spine and spinal cord**
	Moderator: A. Rossi, Genoa/IT
	Imaging and clinical challenges in scoliosis
	J-F. Chateil, Bordeaux/FR
	Tumors of the osseous spine
	S. Blaser, Toronto/CA
	Spinal malformations
	A. Rossi, Genoa/IT
	Spinal infection and inflammation in childhood
	N.M. Canto-Moreira, Stockholm/SE

Wednesday, May 31, 2017

Time	Room 1 - Aspen
08:00-10:00	**Anything new about functional imaging?**
	Moderator: M. Argyropoulou, Ioannina/GR
	CNS (fMRI, MRS, more?)
	M. Argyropoulou, Ioannina/GR
	Advances in Blood Flow imaging
	J-P. Vallee, Geneva/CH
	Kidney (Obstruction/perfusion/excretion)
	K. Darge, Philadelphia/US
	Imaging of regional lung function by MRI: Methods and clinical value for paediatric lung disorders
	J. Schaefer, Tuebingen/DE
10:00-10:30	Break
10:30-13:00	**Systemic disorders**
	Moderator: R. Nievelstein, Utrecht/NL
	Intestinal bowel disease and related arthropathies
	D. Jaramillo, Philadelphia/US
	Juvenile onset spondyloarthropathies (SpAs)
	E. Von Brandis, Tromso/NO
	Juvenile idiopathic arthritis (JIA)
	O. Olsen, London/UK
	Pulmonary manifestation of connective tissue disorders and the vasculitides
	C.M. Owens, London/UK
	Whole body imaging: Sonography, CT, MRI, PET - What and when? Diagnosis versus pathology
	R. Nievelstein, Utrecht/NL
13:00-14:00	Break
14:00-15:30	**Tumors of the head and neck**
	Moderator: T. Huisman, Baltimore/US
	Soft tissue tumors and pseudotumors
	T. von Kalle, Stuttgart/DE
	Bone tumors
	M. Elmaleh-Bergès, Paris/FR
	Vascular tumors and malformations
	T. Huisman, Baltimore/US
15:30-16:00	Break
16:00-17:30	**Syndromes and genetics**
	Moderator: G. Eich, Aarau/CH
	X-ray of the hand: Don't miss the syndrome
	G. Eich, Aarau/CH
	Brain and bone
	T. Huisman, Baltimore/US
	The funny looking child: Gen-ethics
	A. Superti-Furga, Lausanne/CH
17:30-18:15	**Panel Discussion: Radiologic challenge: Child abuse or genetic/metabolic disease: A case-based session**
	Moderator: G. Eich, Aarau/CH
	S. Blaser, Toronto/CA; T. Huisman, Baltimore/US; A. Superti-Furga, Lausanne/CH

Invited Abstracts - 39th Post Graduate Course

Abstracts appear as submitted to the online submission system and have not been checked for correctness and completeness.

TUESDAY, MAY 30, 2017

SESSION: RADIATION PROTECTION

Xray: Can we still improve the technique/protection?

R.W. Wolf; Bern/CH

Summary:
The answers right away is: yes we can and we constantly have to. It is part of human nature to recognize problems and to find solutions. We define ideals but we also face reality. Being aware of the gap in between we are constantly driven to improve. This overview will highlight some milestones and disputes throughout the 100 years of development in the use of plain X-ray imaging. It will hint on scientific literature and sources of information. And it will hint on some Swiss contributions as the ESPR meeting 2017 will be held in Davos, Switzerland.
Fighting the glow not the fire - 122 years of X-ray imaging development and improvement:

In the beginning of the clinical use of X-ray imaging, there was great enthusiasm in its potential without knowing the unfavorable dangers of uncontrolled use of X-ray. The dangers were recognized and the 'beast' was tamed and domesticated. In respect to radiation protection, the most significant achievements took place in the first half of that development. Throughout the recent decades, some further considerable steps in dose reduction took place mainly by the improvement of film-screen systems and the recent introduction of computed (CR) and digitized radiography (DR). Even if the early computerized X-ray imaging brought a slight increase in patient doses (which was overcompensated later on by direct digital radiography) a whole new world of further advantages launched the digital era in which we live today. As we all know new dangers arose with these techniques as the uncontrolled distribution of images and thereby confidential patient data over hospital departments and across borders throughout. Also, the risk of an evitable overexposure in digital radiography is a significant issue.
Throughout the process of taming the radiation and controlling it, today's doses are attained within the lowest range of the danger scale. This range still is perceived as a black box within which we do not exactly know which concept reflects the potential harm best. The linear no-threshold model [LNT] is acknowledged as the concept which most reliably supports the idea of radiation protection. Other concepts partly oppose the linear idea and question the relevance of that dose range because there lie so much greater health benefits in the appropriate use of diagnostic X-

rays. Several scientists even propagate the idea that very low levels are producing health benefits instead of physical harm [hormesis model]. Nevertheless, the LNT model is widely accepted as the most helpful in the context of diagnostic radiology.
Some recent studies were able to support the idea of potential harm at very low dose levels as they were able to prove the induction of attributable cancers in the pediatric age group. So today we are fighting the glow, not the fire. As trained medical professionals we are fully aware of the fact that there is only little potential harm to the patient by using X-rays in the current state of the art. But on the other hand, we also have to be aware of the fact that our patients and their parents still fear the fire. One of our main tasks, therefore, is to explain the risks and benefits to the patients and their advocates and to educate the public.

State of the equipment and perspectives
Developed straight from the first radiographic technique's digital radiography today is state-of-the-art in plain 2D-imaging. Throughout the last decade, it has replaced CR and conventional radiography In many institutions. In the United States of America, one of the most developed healthcare systems, healthcare authorities propagate incentives to abolish CR and older imaging systems by making them financially unattractive. The market is fully concentrated on the spread of DR systems. Momentarily there are no real milestones but many refinements of existing systems such as tomosynthesis, dual energy subtraction and advanced auto-stitching, fluoroscopy capability, basic angiography applications and 3-D cone-beam CT images are made available. Combinations of these features can be found in some recently designed X-ray machines. Grid-less imaging software can reduce patient dose significantly. Concerning detectors, there are CR retrofit systems which will support the easy upgrade of existing systems to DR capability. Wireless detectors with large internal storage, different sizes and high resolutions of 100 microns are available.

DR is becoming a part of the system
In the current era of full digitalization of our lives and big data, digital radiology is a cornerstone of our healthcare systems. RIS and PACS as part of integrated healthcare (IHS) systems are widely disseminated. At the next step, all accessible data will be used for analyses. The major vendors of imaging systems, as well as PACS suppliers and independent companies, offer readymade software tools for reports and evaluations of all kind. The doses from different X-ray sources can be screened internally and be used for optimization purposes. They also can be sent to remote servers for dose monitoring, comparison and optimization in multi-hospital health care provider settings or to comprehensive databases like The American College of Radiology dose index registry, cancer registries, or for central billing.

Has everything been invented?
Many technologies have been declared dead before a new transformation appeared. This was the case for example with single slice CT before the invention of spiral CT by Willi Kalender, Germany and Peter Vock, Switzerland in 1988. Often the plain X-ray image was meant to be needless or redundant as newer technologies like CT or MRI approached. But it still is of value because of different reasons as the low dose, high availability, well known and easy interpretation to name a few. There are some new and sophisticated techniques on the way like the "Smart X-ray Source" which uses coherent beams of X-rays from an array of micron-sized point sources, developed by scientists at the Massachusetts Institute of Technology (MIT). The developers promise less radiation, less weight of the equipment and a far better soft tissue resolution. Another promising approach is phase contrast X-ray imaging which has the potential to reduce the dose up to 1/100 of the actual value. It also has its strengths in additional soft tissue information as recent experimental publications show (Paul Scherrer Institute Switzerland) e. g. in functional evaluation of lung fluid (Munich, Germany). Functional imaging of the lungs can also be achieved without any radiation as the development of the known concept of electrical impedance tomography highlights. This functional imaging method usually is not within the modality spectrum of radiologists.

Dose control and reduction - local - regional - international
The most effective measures to achieve significant dose reductions in your own department are still the same strategies which are based on the "eternal rules" as we know them from our teachers: Avoiding unnecessary exposures by strictly controlling the appropriateness of a referral. Justification is a shared responsibility between radiologists and clinicians. There are many tools available for justification like the appropriateness criteria, guidelines or rules (like wrist or ankle rules) of several national societies and different study groups.
The process of optimization is mainly in the hands of the technicians. As many studies show, the proper collimation still has the greatest effect on dose reduction. Other important factors are the positioning of the patient and the shielding of radiosensitive organs which are not relevant for image interpretation so that they may be covered by lead shields. The proper use of the grid in bigger children can now partially be replaced by software solutions. In digital radiography, a profound knowledge of postprocessing possibilities is mandatory as well as the active control of the exposure indices. Dose limitation procedures should be regularly checked in a team-based approach to avoid overexposure by less experienced staff or "exposure creep". Existing standards should be actively used to guarantee a constant satisfactory image quality.
In 2011, the image gently campaign released a safety checklist for performing digital radiography examinations on pediatric patients which is easily applicable to every radiology service.
Organizational improvements: At regional and national level, efforts should be made to check for best practice use in the departments and to compare and discuss imaging strategies. The establishment of national and international dose reference levels helps to keep the overall doses low and to protect the population from unnecessary overexposure.
The PiDRL Project prepared the "European diagnostic reference levels for pediatric imaging" as part of the EuroSafe project. Momentarily the results of PiDRL-workgroup are harmonized with international organizations. The European Guidelines on DRLs for Paediatric Imaging can be accessed as a preliminary final for workshop drafts on the internet.
On a worldwide basis, the World Health Organization has published a fundamental information brochure concerning radiation risks and the communication of health professionals and patients. Health care professionals have a shared responsibility for communicating risks and benefits of imaging procedures to patients, especially in the case of pediatric patients.
The document "Communicating radiation risks in paediatric imaging-Information to support health care discussions about benefit and risk" is intended to serve as a tool for health care providers, to communicate known or potential radiation risks associated with pediatric imaging procedures and to support risk-benefit dialogue in health care settings.

Responsibilities
As said before we are fighting the glow, not the fire. The paper of the Swiss pediatric oncology group stirred a broad discussion. Among other issues, there was a question if it shouldn't be a logical consequence to transfer kids from areas with higher background radiation to safer areas. The author's answers were clear: that Swiss health authorities better concentrate their efforts more effectively and with greater benefit for more people by supporting prevention "toward modifiable environmental factors leading to larger numbers of deaths from several causes, such as exposure to radon, air pollution, and second-hand tobacco smoke".
This leads to the conclusion that we as medical radiological professionals do have the obligation to make every effort to prevent our patients and personnel from harm of the usage or non-usage of radiation. As health specialists, we also should support the fields of prevention with broad mass effects as far as we have the opportunity. And as human beings, we are summoned to do so in respect to other beings, to our environment and to the resources we all share. Radiation protection and quality improvement is just a small part of it all, but it is our field - and 'yes we can'.

References:

1. 2014-stellungnahme-lnt-modell.pdf [Internet]. [zitiert 2. February 2017]. under: https://www.bag.admin.ch/dam/bag/de/dokumente/str/kommission-strahlenschutz/stellungnahmen-strahlenschutz/2014-stellungnahme-lnt-modell.pdf.download.pdf/2014-stellungnahme-lnt-modell.pdf

2. Matthews K, Brennan PC, McEntee MF. An evaluation of paediatric projection radiography in Ireland. Radiography. August 2014;20(3):189–94.

3. Applications -> Phase-Contrast Imaging –> Application - DECTRIS [Internet]. [zitiert 3. February 2017]. under: https://www.dectris.com/pci_application.html

4. Spycher BD, Lupatsch JE, Zwahlen M, Röösli M, Niggli F, Grotzer MA, u. a. Background Ionizing Radiation and the Risk of Childhood Cancer: A Census-Based Nationwide Cohort Study. Environmental Health Perspectives. Juni 2015;123(6):622.

5. Herrmann TL, Fauber TL, Gill J, Hoffman C, Orth DK, Peterson PA, u. a. Best practices in digital radiography. Radiologic technology. 2012;84(1):83–89.

6. Communicating radiation risks in paediatric imaging [Internet]. [zitiert 27. April 2016]. under: http://apps.who.int/iris/bitstream/10665/205033/1/9789241510349_eng.pdf?ua=1

7. Deutsches Ärzteblatt: Kinderradiologie–Besonderheiten des Strahlenschutzes (17.06.2011) [Internet]. [zitiert 3. Juni 2014]. under: http://www.aerzteblatt.de/archiv/93819/Kinderradiologie-Besonderheiten-des-Strahlenschutzes

8. Diagnostic Imaging and Ionizing Radiation - Canadian Nuclear Safety Commission [Internet]. [zitiert 4. February 2017]. under: http://nuclearsafety.gc.ca/eng/resources/infographics/di-ir/index.cfm

9. DRWhitepaper-Optimizing-image-quality.pdf [Internet]. [zitiert 27. November 2013]. under: http://www.healthcare.philips.com/main/about/events/ecr/assets/documents/DRWhitepaper-Optimizing-image-quality.pdf

10. Sacks B, Meyerson G, Siegel JA. Epidemiology Without Biology: False Paradigms, Unfounded Assumptions, and Specious Statistics in Radiation Science (with Commentaries by Inge Schmitz-Feuerhake and Christopher Busby and a Reply by the Authors). Biol Theory. 2016;11:69–101.

11. Tschauner S, Marterer R, Gübitz M, Kalmar PI, Talakic E, Weissensteiner S, u. a. European Guidelines for AP/PA chest X-rays: routinely satisfiable in a paediatric radiology division? Eur Radiol. Februar 2016;26(2):495–505.

12. EuroSafe Imaging Together - for patient safety [Internet]. [zitiert 6. February 2017]. under: http://www.eurosafeimaging.org/

13. Don S, Macdougall R, Strauss K, Moore QT, Goske MJ, Cohen M, u. a. Image gently campaign back to basics initiative: ten steps to help manage radiation dose in pediatric digital radiography. AJR Am J Roentgenol. Mai 2013;200(5):W431-436.

14. Bech M, Tapfer A, Velroyen A, Yaroshenko A, Pauwels B, Hostens J, u. a. In-vivo dark-field and phase-contrast x-ray imaging. Scientific Reports [Internet]. 13. November 2013 [zitiert 3. February 2017];3. under: http://www.nature.com/articles/srep03209

15. Safety Commission CN. Linear-Non-Threshold Model [Internet]. 2014 [zitiert 2. February 2017]. under: http://nuclearsafety.gc.ca/eng/resources/health/linear-non-threshold-model/index.cfm

16. MEDICAL X-RAY IMAGING, CURRENT STATUS AND SOME FUTURE CHALLENGES - v49_01.pdf [Internet]. [zitiert 3. February 2017]. under: http://www.icdd.com/resources/axa/vol49/v49_01.pdf

17. Kostova-Lefterova D, Taseva D, Hristova-Popova J, Vassileva J. Optimisation of paediatric chest radiography. Radiat Prot Dosimetry. 1. Juli 2015;165(1–4):231–4.

18. Willis CE. Optimizing digital radiography of children. European Journal of Radiology. November 2009;72(2):266–73.

19. Tomà P, Cannatà V, Genovese E, Magistrelli A, Granata C. Radiation exposure in diagnostic imaging: wisdom and prudence, but still a lot to understand. Radiol Med. 25. November 2016;

20. Martin CJ. Radiation shielding for diagnostic radiology. Radiat Prot Dosimetry. Juli 2015;165(1–4):376–81.

21. Seidenbusch MC, Schneider K. Strahlenhygienische Aspekte bei der Röntgenuntersuchung des Thorax. Radiologe. 1. Juli 2015;55(7):580–7.

22. John SD, Moore QT, Herrmann T, Don S, Powers K, Smith SN, u. a. The Image Gently Pediatric Digital Radiography Safety Checklist: Tools for Improving Pediatric Radiography. Journal of the American College of Radiology. Oktober 2013;10(10):781–8.

23. Seibert JA, Morin RL. The standardized exposure index for digital radiography: an opportunity for optimization of radiation dose to the pediatric population. Pediatr Radiol. 1. Mai 2011;41(5):573–81.

24. The Think A-Head campaign: an introduction to ImageGently 2.0 | SpringerLink [Internet]. [zitiert 6. February 2017]. under: http://link.springer.com/article/10.1007/s00247-016-3739-z

25. Yaroshenko A, Pritzke T, Koschlig M, Kamgari N, Willer K, Gromann L, u. a. Visualization of neonatal lung injury associated with mechanical ventilation using x-ray dark-field radiography. Sci Rep [Internet]. 13. April 2016 [zitiert 3. February 2017];6. under: http://www.ncbi.nlm.nih.gov/pmc/articles/PMC4829826/

Images:

http://nuclearsafety.gc.ca/images/readingroom/healthstudies/linear-non-threshold-fig1-eng.jpg

"The linear non-threshold model." Spycher BD, Lupatsch JE, Zwahlen M, Röösli M, Niggli F, Grotzer MA, u. a. Background Ionizing Radiation and the Risk of Childhood Cancer: A Census-Based Nationwide Cohort Study. Environmental Health Perspectives. Juni 2015;123(6):622.

"Background radiation in Switzerland. From: Background Ionizing Radiation and the Risk of Childhood Cancer: A Census-Based Nationwide Cohort Study. " http://apps.who.int/iris/bitstream/10665/205033/1/9789241510349_eng.pdf

"Communicating radiation risks in paediatric imaging. Freely available at the WHO homepage."

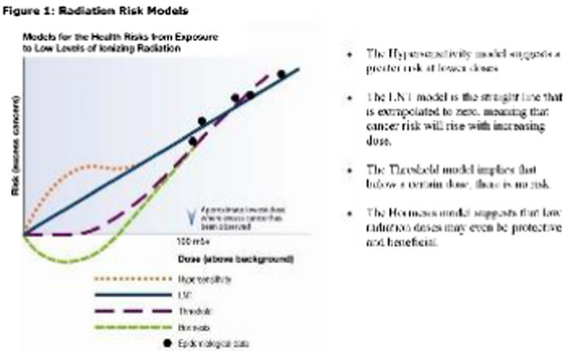

"The linear non-threshold model."

"Background radiation in Switzerland. From: Background Ionizing Radiation and the Risk of Childhood Cancer: A Census-Based Nationwide Cohort Study."

"Communicating radiation risks in paediatric imaging. Freely available at the WHO homepage."

Computed tomography: Are we doing enough?
E. Sorantin; Graz/AT

Summary:
Already in 1912 the ALARA principle was published – but the implementation is still far from complete. According to the surveys of the EC Tender Project "PiDRL – European Diagnostic Reference Levels for Paediatric Imaging" the most frequent Computed Tomography (CT) examinations in children are, in descending order, head/neck, chest and abdomen thus counting for about 75% of all pediatric CT's. Therefore it makes sense to optimize these examinations first.
Surveys of the "International Atomic Energy Agency (IAEA)" in 40 countries have shown, there is considerable lack of organization – eg in about 50% of facilities protocols for children were missing, indication based protocols available only in 57%, CTDI values for head and chest two to five times of those for adults.
All of these simple facts indicate we are not doing enough for radiation protection in pediatric CT. Actions to lower dose in CT can be categorized in organisational, optimization and alternatives.
The interdisciplinary implementation of international guidelines for CT in minor head trauma with trauma surgeons could serve as an example of organisational actions.
For dose optimization knowledge about dose relevant factors according the „Imaging Chain" is mandatory as well as adjusting kV to pediatric needs. Dose influence on image quality must be known,
By exploiting the fact, that, if all CT parameters are kept constant but hte slice thickness is just halve there must be an increase in noise – in particular about two times more. Therefore if a standard examination is reconstructed at half slice thickness and image quality is still appropriate the amount of waste radiation is in the range of 100%. Therefore if the next examination will be reduced with eg 20% mAs setting less will be for sure in appropriate quality and the process can be started again. After a couple of examinations the optimal dose will be reached. Thus the „half slice thickness" approach is easy to do, does not need special equipment or human resources and will help to find the appropriate dose.
The third point is alternatives – Ultrasound and MRI being the candidates in the first row. New, radiation free, techniques like electrical impedance tomography and others are already developed and can be expected to be release soon.

Take home points:
- We are not doing enough for CT dose saving – even more than 100 years after release of ALARA principle
- Dose saving actions can be categorized inthe subtasks organisation, optimization and alternatives
- "The half slice thickness approach" is an easy to do technique to elaborate the optimal dose on an particular CT machine.

SESSION: THORACO-ABDOMINAL IMAGING

Prenatal thoracic MR
L. Alamo; Lausanne/CH

Summary:
The generalization of screening US has considerably increased the detection of congenital anomalies *in utero*. In the last years, important technological advances and especially, the development of fast heavily T2-weighted sequences has led to an increasing use of prenatal MRI as additional diagnostic imaging method. MRI is increasingly used for evaluation of thoracic pathology, including tumours and vascular malformations as well as anomalies of the diaphragm, the lungs and more recently, even of the foetal heart:
– Thoracic tumours and vascular malformations: The diagnosis of a congenital tumor during pregnancy involves a tremendous emotional impact for a family. The most frequently observed thoracic tumours are teratoma, myocardial rhabdomyoma and exceptionally, pleuropulmonary blastomas. MRI may provide relevant additional information concerning the origin of the lesion and its real anatomical extent.
– Diaphragmatic pathology: Congenital hernia is by far the most commonly reported foetal diaphragmatic anomaly. The large field of view and the multiplanar possibilities of MRI may help to clarify the position of the herniated organs and to evaluate the severity of lung hypoplasia, considered the most important parameter for predicting outcome. Other rare pathologies include eventration, paralysis and diaphragmatic lung sequestrations.
– Lung anomalies: Congenital lung abnormalities are a heterogeneous group of pathologies consisting of isolated bronchopulmonary or vascular anomalies or a combination of both of them. Congenital pulmonary airway malformation, bronchopulmonary sequestration and bronchial atresia are the most often observed pathologies but they present significant overlap imaging findings. MRI allows accurate information concerning the location and extension of the lesion and the volume of the normal and abnormal lung.
– Heart pathology: The evaluation of the foetal heart remains extremely difficult because of its small size and high rate of battements. The unpredictable foetal motions during data acquisition and the absence of a foetal ECG signal to synchronize data acquisition are additional problems. In the last years, different approaches have been made to overcome these challenges.

Take home points:
Radiologists should know the typical imaging findings of the thoracic pathology most often observed in foetuses. Prenatal MRI may provide additional relevant information in a wide spectrum of congenital thoracic anomalies, but in general, it should only be performed if it is considered that additional results might influence the management of the pregnancy and/or the therapeutic approach. Therefore, it is important to know the right indications for MRI and to recognize the limits of the method.

Genital malformation: Müller and Wolff

K. Darge; Philadelphia/US

Summary:

Interruptions during embryogenesis of the Muellerian or Wolffian ducts result in various, potentially complex genitourinary abnormalities of a wide spectrum or combinations. Multiple imaging modalities are employed to evaluate patients with these abnormalities. Ultrasound is the frontline imaging modality. MR imaging is mostly reserved for complex cases and may incorporate an MR urography, too. Other imaging modalities are less frequently used or provide only ancillary information. This presentation will demonstrate the utility of ultrasound and MR imaging, in particular, in the routine diagnostic imaging of patients with the wide spectrum of Muellerian and Wolffian duct abnormalities.

Take home points:

- Muellerian and Wollfian duct abnormalities can have a wide range of genitourinary manifestation.
- Ultrasound is the primary imaging modality for Muellerian and Wolffian duct abnormalities.
- MR imaging is reserved for more complex cases.

Neonatal hepatic tumors and vascular malformations

D. Pariente, S. Franchi-Abella; Le Kremlin Bicêtre/FR

Summary:

Neonatal hepatic tumours and vascular malformations are rare but imaging plays a key role in diagnosis and treatment. The most frequent hepatic tumour is haemangioma (fig1) which often is asymptomatic but may be complicated by cardiac failure, coagulopathy or compartment syndrome. The differential diagnosis mainly includes hepatoblastoma, hematoma (Fig2), abscess, mesenchymal hamartoma, choriocarcinoma in the solitary form and metastatic neuroblastoma, cirrhosis, neonatal leukemia in the multifocal form. Pertinent biological data are alpha-fetoprotein (but level may be normally high in neonate), betaHCG, and urinary catechol amines. Hepatic vascular malformations are rarer and include intra or extra porto-systemic shunts (PSS), arterio-portal fistula or complex mixed forms. Intrahepatic PSS may be associated with haemangioma and regress in most cases rapidly (Fig3). On the contrary the extrahepatic PSS which are located below the portal vein, should be urgently closed to avoid occurrence of agenesis of the portal vein. The best imaging modality is US which must be performed with high frequency probes and colour Doppler to identify hepatic vessels and assess patency, direction of flow, abnormal communication. MRI and CT with contrast injection may also be useful.

Hepatic mass in a 12 do neonate with increased CRP and AFP. US showing a hyperechoic mass with thrombosis of the left portal vein (black arrow) and a track (white) extending to the mass: hematoma due to malposition of an umbilical vein catheter.

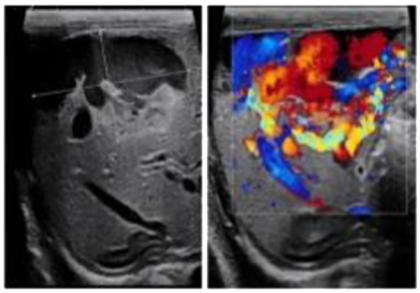

Hemangioma of antenatal diagnosis on D1. The mass is composed of a large anterior vascular lake corresponding to a porto-systemic shunt and a tissular hyperechoic part. The infant has remained asymptomatic.

Intrahepatic porto-systemic shunt between the left portal branch of segment 2 (white arrow) and the left hepatic vein (black arrow) in a neonate. At 3 months of age this shunt has completely resolved.

Take home points:

Haemangioma is the most frequent hepatic tumour in the neonate and is often asymptomatic with spontaneous resolution. Levels of alpha-fetoprotein are physiologically high in the neonate, and can be misleading. Hepatic hematoma can be secondary to traumatic delivery, to coagulation disorders or to umbilical vein catheterization. Intrahepatic porto-hepatic shunts are the most frequent vascular malformations and regress in most of the cases in the first year of life. US with colour Doppler remains the best imaging modality in the neonatal period.

Imaging in Crohn disease: State of the art in diagnosis, prognosis and followup

N. Colavolpe, A. Aschero, B. Bourliere-Najean, C. Roman, F. Khachab, H. Pico, M. Kheiri, G. Gorincour, C. Desvignes, P. Petit; Marseille/FR

Summary:

During the past years the inflammatory bowed diseases (IBD) have increase in frequency (1). Less than twenty-five percent of them occur in children of less than 18 years (2) and Crohn's disease (CD) is twice as frequent than ulcerative colitis (UC) in the pediatric age group. Specific phenotypic and genotypic subtype of IBD occur in younger children. Early onset (EO) pediatric IBD (before 5 years of age) represent 11% of childhood IBD (3). UC and undetermined colitis are more frequent in this age group. EO CD showed a more frequent isolated colonic and upper gastrointestinal involvement than later-onset disease where locations are predominantly colic and terminal ileum later on childhood.

Some pediatric IBD specificities exist than can interfere with the imaging findings:

- CD can be limited to the terminal ileum or to the colon in up to 20% of children (4). Isolated jejunal involvement is reported to occur in 5-6% of children. This location is more frequent in the youngest and is more at risk of complicated course of disease (2). For Auvin et al. (3) the small bowel is involved in 80% of cases with less involvement of the terminal ileum than in the adult population.
- UC: the classical contiguous alteration of the bowel wall from the rectum to the caecum is inconstant. A macroscopic rectal sparing is reported from 5 et 30% and the absence of continuous disease from rectum to caecum (caecal patch) described in 2% of children. Transmural inflammation may be present in severe form as well as terminal ileitis without granulomata (backwash ileitis) (2).

In order to assess these pathologies, and more specifically CD small bowel locations which are difficulty explored by others modalities, small bowel follow-through, barium enema, ultrasound, computed tomography and MR imaging have been widely used.
Among them, MR-Enterography has gained worldwide acceptance due to multiple factors including: a high contrast resolution, a multiplanar ability, an absence of radiation, the possibility to explore in the same exploration the whole bowel and the extra-bowel diseases (perianal fistulae, sacroiliac joint, biliary tract), the ability to compare of side by side consecutive studies in a reproducible manner, a more easily understood exploration by the clinicians than ultrasound, and first of all for its performances.
In order to technically harmonize this exploration a recent consensus statements on MRE protocol has been published by the ESGAR and the ESPR Societies (5).

Preparation:

- Depending on their age children must not have solid oral intake from 2 to 6 hours prior to the examination to reduce bowel wall motility. Morning MR appointment is more favorable for this purpose. No gasless fluid restriction is recommended but is reabsorbed too quickly to distend enough the small bowel. None hyperosmolar non absorbable solution is superior to another. Its ingestion must start 45 to 60 minutes prior to MRE. The recommended volume is 20 ml/kg with a maximum up to 25 ml/kg. Explanations long before the MRE concerning the importance of such absorption and the use of a refreshed product mixed with aromatized flavors will facilitate the child's participation.
- The use of spasmolytic agents is optional. However, there are recommended in adults by multiple societies including ESGAR (5), the Society of Abdominal Radiology (6) and the ACR (www.acr.org/Quality-Safety/Standards-Guidelines). But, MRE without antiperistaltic agents result has reached a high diagnostic confidence and excellent agreement with CT enterography for the presence of CD (7). If used, they need to be administered immediately prior to motion sensitive sequence (T1W dynamic enhanced sequences). If the pictures obtain with these medications are of better quality, there is no evidence that they change the final diagnosis and the children's therapeutic management (8). The use of these products increase the length of the exploration and their side effects are frequent (nausea > vomiting) which balance their visual benefice (8). If a spasmolytic agent is used, the recommended first line spasmolytic agent is i.v. hyoscine butylbromide (0.5mg/kg i.v). The recommended second line agent is i.v. glucagon, 0.5mg (<24.9kg) and 1mg (>24.9kg), given as a slow infusion with i.v. saline at an infusion rate at 1ml/s.
- No rectal enema is needed.
- Exploration can be performed either at 1.5Tesla or 3Testla. More chemical shift and susceptibility artifacts are present with the latter. Prone position has been demonstrated to allow better small bowel distension than the supine one with reduction of the peristaltism but without better lesion detections (9,10). Large multi-elements coils are needed to cover with high resolution from the perineum up to the left colonic flexure.

Sequences: Both morphologic steady state free precession gradient echo and 2D -T2-weighted images are needed in the axial and coronal planes. Fat saturation in one of this plane is recommended and maximal slice thickness of 5 mm is required. Nowadays, non-enhanced then enhanced 3D T1-Fat saturation weighted sequences are mandatory. Slice thickness does not exceed 3 mm. Enhance sequence need to be acquired at the portal phase of injection. However, in recent studies the need for gadolinium has been questioned when DWI is added to the morphologic sequences. DWI sequences have been considered optional (5,6) but we consider their place essential in pediatric practice. They must be done with high b values, from 600 up to 800 in the coronal and axial planes with 5 to 8 mm contiguous cut in free breathing. Axial plane is less prone to artefact than the coronal plane. Interestingly enough Shenoy et al (11) report in 27 pediatric patients that DWI does not perform as well as standard MRE for detection of active Crohn disease but the combination of DWI and MRE increases imaging accuracy for determining disease activity compared with either technique alone. Seo et al (12) in 44 young adults said that DWI MRE was noninferior to contrast-enhanced MRE for the evaluation of inflammation in CD. Based on the exploration of 130 CD adult and pediatric population, DWI proved to be efficient and would avoid gadolinium injection (14). Sirin et al. (14) report in 37 children that DWI revealed lesions that were not detectable with MRE done with gadolinium injection. Finally, respectively Dubron et al. (15) in 48 children and Neubauer et al (16) in 33 children and young adults demonstrate better performance of DWI than gadolinium enhanced imaging. Like the existing MR protocols for suspected appendicitis (17) it will not be surprising to see fast MR IBD explorations becoming an alternative to emergency US as already proposed (16). This fast MR limited to a morphologic T2 sequence in two planes associated with DWI sequences will allow a positive diagnosis and the IBD work up. Apart from bowel obstruction and its spontaneous bowel distension one of the limiting factors will be the need for an oral water agent uptake in a potential surgical patient. However, it has been published in the adult literature than an oral or rectal preparation was not necessary to rule out UC (18) nor a CD (19). The other limiting factor is the length of exploration. MRE can be shorten especially if the patient's positioning is easy to do (dorsal decubitus) (20) and if there is no need for injection, either for spasmolytic agent and for gadolinium chelates. The suppression of the IV line, the absence of potential side effects (nausea, vomiting) of paralytic agents and the decreased of repeated long apneas with no loss of significant information will be strong progresses toward the Holy Grail.

- *Positive diagnosis, disease activity, prognosis and follow-up*: MRE has a better accuracy to detect inflammation for the small bowel than for the colon (21). One of its goal is to try to accurately identify features of active inflammation vs fibrotic disease. This is of paramount importance since the former may respond to medical treatment and the latter may need surgical resection. However, inflammation and fibrosis are associated within the same bowel segment and progress in a parallel way making the goal difficult to reach (22-24). In their study based on the analyze of 20 children operated for CD strictures, Barkmeier et al. (24) report than strictures demonstrating >3 cm upstream dilatation with associated feces sign were highly associated with transmural fibrosis. The most severely fibrotic strictures were associated to the greatest amount of inflammation and there was no significant correlation between stricture length, mural thickness, degree of post-contrast enhancement (arterial and delayed venous phases), diffusion-weighted imaging apparent diffusion coefficient, pattern of post-contrast enhancement, or normalized T2-weighted signal intensity and histological fibrosis or inflammation scores. However, correlation with histological specimens of CD done on a other series

demonstrated that the enhancement ratio of the wall is positively correlated with disease chronicity due to a possible increasing microvessels permeability and inversely correlated to acute disease (25). On the other hand, several authors have tried to correlate the ADC values to CD activity. Fibrotic tissue does not restrict diffusion and presents a decrease of signal at high b values and high ADC values whether acute inflammation shows decrease ADC values. Variable thresholds from 1.6 x10^{-3} mm^2/s to 2.4 x10^{-3} mm^2/s have been proposed to separate active vs non active disease (21). However, others authors have reported low ADC value of fibrosis compare to histology (26). Even if promising results have been published with high correlation with the Crohn Disease Endoscopic Index of Severity (13), ADC measurements are associated with sever limitation factors including sample size overlap between the bowel wall and its atmosphere, lack of reproducibility between MRI-Units and MRI- vendors, non-standardized sequence b-values parameters (21). Two MRE scores are available to quantify the activity of CD. One is using gadolinium injection (27) and the other DWI (13). Due to the complexity of the formula, both are difficult to use in daily practice and have not been evaluated in paediatric practice.

Interestingly enough if a simplify MRE paediatric protocol appears to become a reality, US stays a good imaging challenger and (28). In a recent meta-analysis, based on adult and pediatric series, Calabrese et al (29) reported that bowel US showed 79.7% sensitivity and 96.7% specificity for the diagnosis of suspected CD, and 89% sensitivity and 94.3% specificity for initial assessment in established patients with CD. Bowel US identified ileal CD with 92.7% sensitivity, 88.2% specificity, and colon CD with 81.8% sensitivity, 95.3% specificity, with lower accuracy for detecting proximal lesions. The absence of abnormal thickness wall would have a negative predictive value, high enough to exclude the need for further exploration, especially when CD is concerned (30,31). Concordance between US and MRE have been variably reported from excellent (32) to just correct (33).

Rosembaum and al (22) report that the US findings present in children operated for CD include: bowel wall thickness above 4.3 mm (mean, 6.1 mm) and an increased frequency of loss of mural stratification and fibrofatty proliferation.

Others US technologies are used in children to better approach the disease activity. It includes, hydrosonograpy using specific oral agents (Mannitol, Sorbitol, PolyEthylene Glycol, etc…), contrast-enhanced ultrasound and dynamic contrast-enhanced ultrasound (nowadays, contrast agent is off-label in children) (34) and elastography (35). Their enthusiastic results and their efficiency to assess disease activity need to be confirmed (36).

In conclusion, as we suspected 7 years ago (37), MRE has dramatically modified our approach of pediatric IBD especially when considering its orientation toward a less invasive exploration and the increasing importance of DWI imaging. A cost benefice between MRE and US remains to be done on this increasing disease.

References:

1) Kim SC, Ferry GD. Inflammatory bowel diseases in pediatric and adolescent patients: clinical, therapeutic, and psychosocial considerations. Gastroenterology 2004; 126:1550–60.

2) Levine A, Koletzko S, Turner D, et al; ESPGHAN revised Porto criteria for the diagnosis of inflammatory bowel disease in children and adolescents. J Pediatr Gastroenterol Nutr. 2014;58(6):795-806.

3) Aloi M, Lionetti P, Barabino A, et al; SIGENP IBD Group. Phenotype and disease course of early-onset pediatric inflammatory bowel disease. Inflamm Bowel Dis. 2014;20(4):597-605

4) Paolantonio P, Ferrari R, Vecchietti F, et al. Current status of MR imaging in the evaluation of IBD in a pediatric population of patients. Eur J Radiol 2009;69:418–24.

5) Taylor SA, Avni F, Cronin CG, et al The first joint ESGAR/ ESPR consensus statement on the technical performance of cross-sectional small bowel and colonic imaging. Eur Radiol. 2016 Oct 18. Epub Ahead of print

6) Grand DJ, Guglielmo FF, Al-Hawary MM. MR enterography in Crohn's disease: current consensus on optimal imaging technique and future advances from the SAR Crohn's disease-focused panel. Abdom Imaging 2015; 40:953–96

7) Grand DJ, Beland MD, Machan JT, et al. Detection of Crohn's disease: Comparison of CT and MR enterography without anti-peristaltic agents performed on the same day. Eur J Radiol 2012; 81:1735–1741

8) Dillman JR, Smith EA, Khalatbari S, Strouse PJ. I.v. glucagon use in pediatric MR enterography: effect on image quality, length of examination, and patient tolerance. AJR Am J Roentgenol. 2013 Jul;201(1):185-9.

9) Alexopoulou E, Roma E, Loggitsi D, et al. Magnetic resonance imaging of the small bowel in children with idiopathic inflammatory bowel disease: evaluation of disease activity. Pediatr Radiol 2009;39: 791–7.

10) Cronin CG, Lohan DG, Mhuircheartaigh JN. MRI smallbowel follow-through: prone versus supine patient positioning for best small-bowel distension and lesion detection. Am J Roengenol 2008; 191:502–506

11) Shenoy-Bhangle AS, Nimkin K, Aranson T, et al. Value of diffusion-weighted imaging when added to magnetic resonance enterographic evaluation of Crohn disease in children. Pediatr Radiol. 2016;46(1):34-42

12) Seo N, Park SH, Kim KJ, et al. MR Enterography for the Evaluation of Small-Bowel Inflammation in Crohn Disease by Using Diffusion-weighted Imaging without Intravenous Contrast Material: A Prospective Noninferiority Study. Radiology 2016;278(3):762-72

13) Hordonneau C, Buisson A, Scanzi J, et al. Diffusion-weighted magnetic resonance imaging in ileocolonic Crohn's disease: validation of quantitative index of activity. Am J Gastroenterol. 2014;109(1):89-98

14) Sirin S, Kathemann S, Schweiger B, Hahnemann ML et al. Magnetic resonance colonography including diffusion-weighted imaging in children and adolescents with inflammatory bowel disease: do we really need intravenous contrast? Invest Radiol. 2015;50(1):32-9.

15) Dubron C, Avni F, Boutry N, et al. Prospective evaluation of free-breathing diffusion-weighted imaging for the detection of inflammatory bowel disease with MR enterography in childhood population. Br J Radiol. 2016;89(1060):20150840.

16) Neubauer H, Pabst T, Dick A, et al. Small-bowel MRI in children and young adults with Crohn disease: retrospective head-to-head comparison of contrast-enhanced and diffusion-weighted MRI. Pediatr Radiol 2013;43:103–14

17) Dillman JR, Gadepalli S, Sroufe NS, et al. Equivocal Pediatric Appendicitis: Unenhanced MR Imaging protocol for nonsedated children-A clinical effectiveness Study. Radiology 2016;279(1):216-25.

18) Oussalah A, Laurent V, Bruot O, et al. Diffusion-weighted magnetic resonance without bowel preparation for detecting colonic inflammation in inflammatory bowel disease. Gut 2010;59:1056–65.

19) Kiryu S, Dodanuki K, Takao H, et al. Free-breathing diffusion-weighted imaging for the assessment of inflammatory activity in Crohn's disease. J Magn Reson Imaging 2009;29:880–886.

20) Cronin CG, Lohan DG, Mhuircheartaigh JN. MRI smallbowel follow-through: prone versus supine patient positioning for best small-bowel distension and lesion detection. Am J Roengenol 2008;191:502–506

21) Dohan A, Taylor S, Hoeffel C, et al. Diffusion-weighted MRI in Crohn's disease: Current status and recommendations. J Magn Reson Imaging. 2016;44(6):1381-1396.

22) Rosenbaum DG, Conrad MA, Biko DM, et al. Ultrasound and MRI predictors of surgical bowel resection in pediatric Crohn disease. Pediatr Radiol. 2016 29 Epub ahead of print

23) Punwani S, Rodriguez-Justo M, Bainbridge A, et al. Mural inflammation in Crohn disease: location-matched histologic validation of MR imaging features. Radiology 2009; 252:712–20.

24) Barkmeier DT, Dillman JR, Al-Hawary M, et al. MR enterography-histology comparison in resected pediatric small bowel Crohn disease strictures: can imaging predict fibrosis? Pediatr Radiol. 2016 46(4):498-507

25) Taylor SA, Punwani S, Rodriguez-Justo M, et al. Mural Crohn disease: correlation of dynamic contrast-enhanced MR imaging findings with angiogenesis and inflammation at histologic examination–pilot study. Radiology. 2009;251(2):369-79

26) Tielbeek JA, Ziech ML, Li Z, et al. Evaluation of conventional, dynamic contrast enhanced and diffusion weighted MRI for quantitative Crohn's disease assessment with histopathology of surgical specimens. Eur Radiol 2014;24:619–629
27) Rimola J, Ordás I, Rodriguez S, et al. Magnetic resonance imaging for evaluation of Crohn's disease: validation of parameters of severity and quantitative index of activity. Inflamm Bowel Dis. 2011;17(8):1759-68.
28) Dillman JR, Smith EA, Sanchez RJ, et al. Pediatric Small Bowel Crohn Disease: Correlation of US and MR Enterography. Radiographics. 2015;35(3):835-48
29) Calabrese E, Maaser C, Zorzi F, et al. Bowel Ultrasonography in the Management of Crohn's Disease. A Review with Recommendations of an International Panel of Experts. Inflamm Bowel Dis. 2016;22(5):1168-83.
30) Alison M, Kheniche A, Azoulay R, et al. Ultrasonography of Crohn disease in children. Pediatr Radiol 2007;37:1071–82.
31) Bremner AR, Griffiths M, Argent J, et al. Sonographic evaluation of inflammatory bowel disease: a prospective, blinded, comparative study. Pediatr Radiol 2006;36:947–53
32) Magnano G, Granata C, Barabino A, et al. Polyethylene glycol and contrast-enhanced MRI of Crohn's disease in children: preliminary experience. Pediatr Radiol 2003;33:385–91
33) Dillman JR, Smith EA, Sanchez R, et al. Prospective cohort study of ultrasound-ultrasound and ultrasound-MR enterography agreement in the evaluation of pediatric small bowel Crohn disease. Pediatr Radiol. 2016;46(4):490-7.
34) Kljucevsek D, Vidmar D, Urlep D, et al. Dynamic contrast-enhanced ultrasound of the bowel wall with quantitative assessment of Crohn's disease activity in childhood. Radiol Oncol. 2016 9;50(4):347-354
35) Fufezan O, Asavoaie C, Tamas A, et al. Bowel elastography – a pilot study for developing an elastographic scoring system to evaluate disease activity in pediatric Crohn's disease. Med Ultrason. 2015;17(4):422-30.
36) Serafin Z, Białecki M, Białecka A, et al. Contrast-enhanced Ultrasound for Detection of Crohn's Disease Activity: Systematic Review and Meta-analysis. J Crohns Colitis. 2016;10(3):354-62)
37) Gorincour G, Aschero A, Desvignes C, et al. Chronic inflammatory diseases of the bowel: diagnosis and follow-up. Pediatr Radiol. 2010;40(6):920-6.

Take home points:
Whatever is the CD presentation, US remains the first imaging modality for its exploration. US and MR-enterography (MRE) are both widely used to reach the following goals:
- To confirm the diagnosis,
- To characterize, describe the extension and define the activity of the disease,
- To depict complications,
- To evaluate response to therapy
- To look for the presence of extraintestinal manifestations

CT is limited to interventional procedure or in case of emergency when US and MRI are not available.

Heterotaxy and isomerism

C. Lapierre; Montreal/CA

Summary:
Objectives: To review the classification of visceroatrial situs To describe the associated cardiac and non-cardiac anomalies To illustrate typical findings in fetuses, neonates and children To discuss the surgical consideration and the long-term follow-up in these patients
Abstract:
By definition, the type of situs is determined by the relationship between the atria and the adjacent organs. Anatomically, the atrial chamber differentiation is based on the morphologic aspect of the atrial appendages, earlike extensions of the atria. Three types of situs exist: solitus (normal), inversus (mirror image) and ambiguus.

A single type of situs is present in a patient. When the situs is neither solitus nor inversus, it is referred to as situs ambiguus or heterotaxy. Heterotaxy may manifest with various abnormal visceroatrial configurations that are associated with cardiac (in 90-100% of cases) and extracardiac anomalies such as splenic abnormalities, biliary atresia and intestinal malrotation.
Two subsets of situs ambiguus are well-recognized: right isomerism (asplenia) and left isomerism (polysplenia). In heterotaxy, the venoatrial connections are frequently abnormal.
Left isomerism is usually indicated by bilateral bilobed lungs, interruption of the IVC and multiple spleens. The more likely found cardiac anomalies are: pulmonary or aortic stenosis, isolated atrial and ventricular septal defects, cardiac arrhythmia due to sinus node dysfunction as well as pulmonary veins that drain into both the right and the left atria. In the presence of right isomerism, bilateral trilobed lungs, a large symmetric liver, and absence of the spleen are frequently observed. At the cardiac level, patients are more likely to have a common atrioventricular defect, a double outlet right ventricle and pulmonary stenosis. Total anomaly of the pulmonary venous return and absence of coronary sinus will always be present in right isomerism.
Heterotaxy can be diagnosed with high accuracy by prenatal echography. A diagnosis should be suggested in the presence of congenital heart disease, visceroatrial heterotaxy and interruption of inferior vena cava with azygos continuation for left isomerism or abnormally closed juxtaposition of inferior vena cava and descending aorta in right isomerism. The mortality in fetuses is high in the presence of heart block and hydrops whereas the cardiac anomalies influence the long-term outcome.
As discussed in the literature, the clinical outcomes and long-term prognosis in these patients are relatively poor when compared with non-heterotaxy patients. The risk factors are cardiac (underlying anatomy and arrhythmia risk) and non-cardiac. Based on the cardiac anatomy, one of the main determinants is left versus right isomerism. With right isomerism, the cardiac malformation is more severe and an univentricular correction is more frequent. Another predictor of mortality is pulmonary vein stenosis/obstruction. Whatever the severity of cardiac lesions, the postoperative or discharge mortality is higher in patients with heterotaxy. Prenatal diagnosis seems not improve the survival.
Extracardiac anomalies also contribute to the increased morbidity and mortality. Three of the more challenging entities are respiratory, immunologic and gastrointestinal.
Recurrent respiratory infections, failed extubation or chronic respiratory failure are frequently observed in patients with heterotaxy. Recent studies revealed an association between heterotaxy and primary ciliary dyskinesia which can explain the increased postoperative respiratory complications. The spleen is important for the bacterial clearance. Patients with asplenia or polysplenia are thought to have “functional asplenia”. So, they are at risk for sepsis and severe bacterial infection. The incidence of intestinal malrotation is high, approximately 40% to 90%. Observation versus prophylactic Ladd procedure and screening for asymptomatic intestinal malrotation are a growing area of debate. The trend seems to go along conservative management and surveillance of malrotation.

Take home points:
- Three types of visceroatrial situs exist: solitus, inversus and ambiguus.
- Cardiac (90-100% of cases) and extracardiac anomalies/ splenic abnormalities and intestinal malrotation are found with heterotaxy.
- Venoatrial connections are frequently abnormal in heterotaxy.
- The clinical outcomes are poor in patients with heterotaxy when compared to non-heterotaxy patients.

Congenital lung disease: The role of ultrasound
G. Enriquez; Barcelona/ES

Summary:
Bronchopulmonary malformations, such as congenital pulmonary airway malformation (CPAM), bronchopulmonary sequestration (BPS), and congenital lobar emphysema (currently known as congenital lobar overinflation [CLO]), are common congenital lung diseases. These conditions are detected prenatally, usually in the second trimester, in countries where obstetric sonography is routinely performed. The malformations are seen as hyperechoic images with respect to normal fetal lung parenchyma, with a mass effect and homogenous appearance or with coexisting cysts. The lesions usually decrease in size along gestation. A residual mass is seen on postnatal chest radiography, the first imaging technique performed, in only 40% of cases.
CPAM and BPS are predominantly located in the posterior lower chest and can be identified postnatally on ultrasound using a small vector probe and a subcostal and subxiphoid approach. Potential feeding arteries can be visualized using color or power Doppler. Based on clinical and sonographic findings, the differential diagnosis between congenital lung malformations and tumors such as neuroblastoma, type I pleuropulmonary blastoma, and myofibroblastic tumor will be discussed.
Postnatal management and imaging of newborns with congenital lung malformations is controversial, particularly in asymptomatic patients (approximately 80% of cases). Chest radiography is mandatory at birth and chest ultrasound is also recommended to confirm the prenatal diagnosis. Computed tomography (CT) or magnetic resonance imaging (MRI) using angiographic techniques should be performed some months (8 months) after birth in asymptomatic patients. These techniques are also recommended in symptomatic newborns and before surgery to characterize the arterial supply and venous drainage in CPAM and BPS, as ultrasound is limited in this regard.
In premature infants, sonography complements radiography in the study of prematurity-related lung diseases such as respiratory distress syndrome and its pulmonary complications (eg, pneumothorax), in predicting bronchopulmonary dysplasia, and in diagnosing transient tachypnea of the newborn when clinical and radiographic features are inconclusive. The main ultrasound finding in these conditions is visualization of numerous "B-lines", vertical narrow-based hyperechoic bands extending from the pleural surface to the end of the field of view, representing what is currently known as "sonographic interstitial syndrome". B-lines are artifacts originating from variations in the air-fluid relationship of the lung and are better seen using high-frequency linear probes (7.5-12 MHz). Use of sonography for follow-up of these patients will reduce the number of the chest plain films performed, and therefore, the amount of radiation exposure in this vulnerable population.
For proper interpretation of the sonographic findings in these conditions, the radiologist should be familiar with current related terms, such as *lines A, lines B*, *comet tail artifact*, *interstitial-alveolar syndrome*, *septal syndrome*, and *white lung*.

Take home points:
- To revisit prenatal and postnatal sonographic findings of congenital lung malformations and provide a differential diagnosis with congenital lung tumors
- To illustrate the sonographic findings of interstitial lung syndrome that enable the diagnosis of several prematurity-related lung lesions and complications
- To provide a summary of the terms essential for proper interpretation of ultrasound images in these conditions

SESSION: TRAUMA

Abdominal: Pediatric Abdominal Trauma: What we know, what we think we know and what we should remember
S. Toso; Geneva/CH

Summary:

1. To underline the specific biomechanical and pathophysiologic implications of abdominal trauma on children.
2. To discuss the gamut of available algorithms and the institutional limitations in the diagnostic work-up.
3. To present established and new techniques in imaging of the acute pediatric abdomen.
4. To illustrate typical findings and imaging pitfalls.

Trauma is the leading cause of mortality and morbidity in children after the first year of life. Motor vehicle accidents are the leading cause of death from unintentional injury in children up to the age of 15. Of these cases, the abdomen is the fourth most commonly injured area. In pediatric patients non-operative management of these injuries predominate, hence the importance of early radiologic assessment for appropriate clinical follow-up.
Anatomically, compared to adults, childrens' abdomens are more square, less muscular and with less intraperitoneal and subcutaneous fat to absorb impact. The diaphragm is more horizontal causing downward displacement of the liver and the spleen outside the protective casement of the ribs. The pelvis is smaller and hence the bladder is displaced upward, also resulting in more vulnerability to this organ. The organ surface area is larger in children and they have a smaller body mass—hence more force applied per-unit of body surface area. The ribs are flexible, and although we see fewer rib fractures, this results in more internal damage.
Physiologically, children maintain hemodynamic stability longer, often presenting with only mild tachycardia, even when in severe hemodynamic shock. Decrease in blood pressure may not be evident before the loss of 30% blood volume. Nevertheless, bleeding is less severe and operative intervention is rarely performed.
Mechanics of blunt abdominal trauma include organ compression from seat belt injury with the presence of erythema, ecchymossis or abrasion on the abdominal wall increasing the likelihood of internal organ injury (55% likelihood of injury). Other common mechanisms include pedestrian-car collisions(4% with intra-abdominal injuries), falls (4% with intra-abdominal injuries), or handle bar injuries (54% with intra-abdominal injuries).
After the child arrives in the hospital, a trauma algorithm is initiated. Generally, for the unstable patient, algorithms are similar and require a rapid ATLS protocol, followed by a FAST ultrasound to confirm free fluid prior to operation. In stable patients, institutional algorithms vary greatly between countries and in different centers. Some rely solely on mechanism to determine the need for FAST vs CT (not complete ultrasound), others will rely on clinical exam (in a conscious patient with reliable exam) and blood work to determine the need for imaging (CT or US) and others may chose to perform an initial US and complete the exam with a constrast-enhanced US during work hours. In the literature many management prediction rules exist based on the history, physical examination, mechanism of injury and are supplemented by blood work and/or intial imaging. Most are based on retrospective reviews, with only a few controlled clinical trials. However, the validity of these studies is limited because of different populations, institutional policies and variable radiological practices in terms of when imaging is performed, which modalities are most beneficial and which are less valuable, all the while, considering the utilization of the least irradiating techniques. A representative sample of such algorithms will be discussed.
Routine and extensive initial trauma panels are not required according to a number of studies. Abdominal ultrasound and urinalysis together have been found to confirm 98% of all intra-abdominal injures, in some studies. Serial haemoglobins/hematocrit is valuable for determining ongoing

blood loss and assists clinical surveillance. Electrolyte abnormalities are uncommon in children unless severe shock is present (metabolic acidosis). Liver function tests are elevated in most cases of blunt abdominal trauma, hence, are often performed for its high sensitivity, to avoid CT if the liver panel is negative. Imaging, however, is needed for grading of the potential liver injury if the liver panel is positive.

Abdominal xray is not useful in blunt abdominal trauma, and is usually normal. Ultrasound has an important role in the pediatric community, as a sensitive and non-irradiating modality. However, this sensitivity is dependent on the type of ultrasound performed (FAST vs. complete abdominal ultrasound vs. contrast-enhanced ultrasound) but also on the qualifications and experience of the performing physician.

A meta-analysis of FAST in pediatrics demonstrates that it has a sensitivity of 66% (grade I-II evidence) for identifying hemoperitoneum. A negative FAST is not sufficient to rule out intra-abdominal trauma. One prospective observational trial demonstrasted that 34 % of patients without free fluid on FAST (performed by formally trained pediatric truama surgeons demonstrated at least grade III liver or splenic injuries on CT). We know that pediatric ultrasound is operator-dependent, and generally an ultrasound performed by the skillful hand of a pediatric radiologist is more sensitive than that performed by surgeons or by adult radiologists. Furthermore, we know that the benefits of contrast-enhanced ultrasound in pediatric trauma exist—highly accurate in visualising lesions, hence avoiding non-contributive CT imaging, however, the feasibility of providing 24-hr contrast-enhanced ultrasound by a qualified radiologist is resource intesive: both structurally and with respect to personnel.

Published indications for abdominal CT in stable pediatric patients included suspected mechanism of blunt abdominal trauma, significant fluid resusitation without apparant blood loss, hemoglobin <100mg/L without obvious blood loss, multisystem trauma and unreliable abdominal exam. One series with 1500 children undergoing CT for blunt abdominal trauma demonstrate postive findings in 388 (26%), of which all solid organ injuries and 96% of hollow viscus injuries were identified on CT. However, CT has its limitations: it was found to identify gastrointestinal perforation in only 47% of patients with known perforation, but with findings of free fluid, wall thickening and/or bowel dilatation. It is also less accurate in identifying pancreatic trauma, with normal scans in 33-53% of children with pancreatic trauma. Again, findings of pancreatic trauma can be non-specific: free fluid or, less commonly, thickening of the gerota's fascia, presence of mesenteric fluid or of fluid between the pancreas and the superior mesenteric vein. When and where to perform CT depends on the imaging algorithms established by individual centers. Generally, unstable patients with very high grade visceral injuries are taken to surgery. The stable patients are treated with non-operative management. The literature on angiographic embolization in pediatric blunt trauma is limited to case series that demonstrate a limited utility in hemodynamically stable patients with ongoing blood loss or for the definitive treatment of traumatic pseudoanevryms. A dialogue with the interventional radiologist is imperative in such cases.

Common imaging findings and pitfalls will be illustrated with case examples.

In conclusion, a child's anatomy and physiology must be taken into account when determing the level of urgency and appropriate imaging work-up in blunt abdominal trauma. Imaging of these patients cannot follow a standard algorithm as institutions vary with respect to types of personel, training, frequency of trauma, emergency department trauma protocols and availability of an in-house pediatric radiologist. Ultrasound and CT have their advantages and disadvantages with associated pitfalls that the pediatric radiologist must recognize to provide an optimal diagnostic workup with minium irradiation.

Take home points:

A child's anatomy and physiology must be taken into account when determing the level of urgency and appropriate imaging work-up in blunt abdominal trauma. Imaging of pediatric abdominal trauma cannot follow a standard algorithm as institutions vary with respect to types of personel, training, frequency of trauma, emergency department trauma protocols and availability of a pediatric radiologist. Ultrasound and CT have their advantages and disadvantages with associated pitfalls that the pediatric radiologist must recognize to provide an optimal diagnostic workup with minium irradiation.

Sport injuries

D. Jaramillo; Miami, FL/US

Summary:

The growing skeleton has unique vulnerabilities to acute and chronic injuries due to sports. The practice of intensive sports during puberty and adolescence has led to a great increase in the incidence of sports-related injuries. During the growth spurt of early adolescence, the physis becomes weak, and is the site of fractures and avulsions (particularly in the apophyses) and of physeal widening due to repeated stresses, such as the wrist in gymnasts or the proximal humerus of baseball pitchers. Both lesions can result in growth arrest. The chondro-osseous junctions of the ossifying epiphyses and apophyses are also vulnerable to avulsions, and the avulsed fragment may be entirely cartilaginous and not visible radiographically (such as in the patellar sleeve fracture). Repeated trauma to epiphyses or round bones can lead to osteonecrosis (Panner's disease) but more often to osteochondritis dissecans (OCD). In adolescents, OCD occurs most frequently in the medial femoral condyle, the capitellum of the elbow and the talar dome. Juvenile OCD has a better prognosis than the adult form. When the skeleton begins to mature, there are fractures unique to partially closing physes such as the triplane and Tillaux fracture. Some sturctures have propensity to unique injuries during adolescence. A stress on the anterior cruciate ligament (ACL) can lead to a tibial eminence avulsion in puberty (Figure), an incomplete ACL tear in early adolescence or a complete ACL tear later. Meniscal tears are almost always vertical and often involve large meniscal fragments that can flip. Patellar dislocations often result in osteochondral injuries.

This review will cover the main types of sports-related injuries and the imaging modalities used to diagnose them.

11 year-old with pain and popping sensation during a fall on a football game. AP radiograph is normal

Sagittal PD shows avulsion of the tibial eminence by the ACL

Coronal T2 shows that the avulsion involves the cartilaginous insertion almost exclusively

Take home points:

- The immature skeleton is vulnerable in unique ways to stresses related to the increased practice of intensive sports during puberty and adolescence.
- The physis and the unossified portions of the epiphyses are particularly susceptible to injury. The chondro-osseous junctions are the weakest.
- Many of the cartilaginous injuries are not detected radiographically and require advanced imaging by ultrasound or MRI.
- It is important to take into account the specific sport in order to anticipate subtle injuries that may be difficult to detect.

Inflicted injuries in children

A. C. Offiah; Sheffield/UK

Summary:

The radiographs obtained when inflicted injury is suspected are collectively termed the "skeletal survey". A full skeletal survey should be performed in all children below 2 years of age in whom abuse is suspected. The investigation is not complete until follow-up skeletal imaging has been performed in the 11 to 14 days following the initial survey. Children below one year of age should also receive a CT brain. Neurological imaging in older children will depend on the clinical scenario. CT chest/abdomen is indicated when visceral injury is suspected.

In terms of imaging in suspected abuse, ESPR has adopted the RCR guidelines.

In the absence of a history of significant trauma, fractures highly specific for abuse in pre-ambulatory children include rib, metaphyseal and diaphyseal fractures. Simple linear skull fractures have a relatively low specificity for abuse.

The combination of subdural haemorrhage, retinal haemorrhage and diffuse cerebral oedema/encephalopathy (the so-called, "triad") suggests shaking. Whereas the presence of a skull fracture implies impact.

Visceral injury often results from direct blunt trauma and may therefore be accompanied by anterior and/or costochondral rib fractures. The posterior rib arcs are protected by soft tissue and posterior rib fractures result from compressive/squeezing forces rather than direct trauma.

The dating of fractures has a subjective element and it is more important to recognise that fractures are in different stages of healing, rather than to assign a definite age/age range to the injuries.

The major differential diagnoses are accidental trauma and osteogenesis imperfecta. If rickets is the cause of the fractures, then radiology and/or biochemistry will show evidence of rickets. A low vitamin D level, in the absence of rachitic features, is not the cause of fractures.

Close liaison between radiologists and paediatricians is vital and any siblings/children in the same household who are below 2 years of age should also receive a skeletal survey.

Remember that the presence of injury does not always mean abuse and that the absence of injury does not always exclude abuse.

Take home points:

- Image according to the RCR Guidelines (revised guidelines soon to be published)
- Rib, metaphyseal and long bone fractures have a high specificity for abuse in pre-ambulatory children
- Presence of the triad suggests shaking; a skull fracture requires impact
- Do not attempt to precisely date fractures - if you must, then apply broad ranges
- Low vitamin D in the absence of radiological/biochemical features of rickets is not a cause of fractures in infants and young children

SESSION: IN DEPTH: SPINE AND SPINAL CORD

Imaging and clinical challenges in scoliosis

J.-F. Chateil, P. Bessou, M. Havez-Enjolras; Bordeaux/FR

Summary:

Disorders of the spinal posture are common in children and adolescents. Scoliosis may be primitive, structural, particularly during adolescence; during this period, careful follow-up is mandatory, because worsening is frequent. Clinical examination with evaluation of a hump (gibbosity) with a scoliometer is mandatory, with also neurological assessment. Beside radiography, additional tools have been developed to avoid X-ray exposure: “spinal mouse”, back surface topography systems, ultrasound and other computer-assisted systems. But scoliosis can also be secondary, and imaging is important to find a cause and adapt management. Among the etiologies, radiologist must recognize spine malformations, dysplastic and neuromuscular scoliosis. In addition, scoliosis may also be in relation with a primitive lesion, tumor-related or not, whether the initial disease could be within the spinal canal, spinal or paravertebral.

Imaging studies lies first on PA and lateral full spine x-rays, if possible with a low dose device (flat panel, slot-scanning system), keeping in mind that follow-up with repetitive exposures may be necessary. Reproducible measures of different curvatures help to assess the overall static spine and the importance of scoliosis with Cobb angle. The assessment of axial rotation can be obtained through 3D simulations, with frontal and axial views (see figure). Morphologic evaluation of the

spine is mandatory: if a secondary scoliosis is suspected, the research to etiology needs to perform CT or MRI, depending on the clinical signs and the results of plain X rays evaluation. Similarly, these explorations are useful in the preoperative assessment when surgical treatment is necessary.

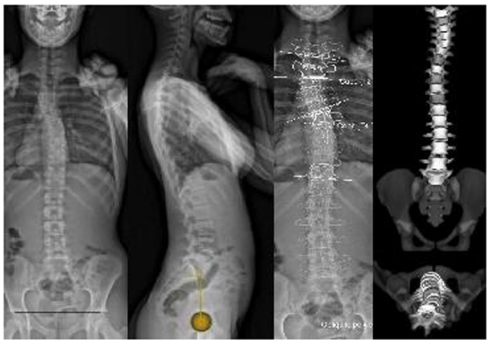

Girl scoliosis, PA and lateral views with EOS®, 3D simulation, coronal and axial views

Take home points:
Clinical evaluation is always the first step in subject with suspected scoliosis
Radiation burning is quite low with new devices, but repetitive exposures for follow-up need to carefully respect justification for X-rays exposures
New tools are available to appreciate 3D spinal deformation and evaluate prognosis and surgical procedures
CT and/or MRI are useful in presurgical assessment and to look for etiologies in suspected secondary scoliosis

Malformations of the spine and spinal cord
A. Rossi; Genoa/IT

Summary:
Embryology and classification:
Spinal cord development occurs through three consecutive periods: (i) *gastrulation* (2nd gestational week): the embryonic disk is converted from a bilaminar into a trilaminar arrangement, with formation of the intervening mesoderm; the notochord is laid down along the midline, identifying the craniocaudal embryonic axis; (ii) *primary neurulation* (18th-27th day): under the induction of the notochord, the midline ectoderm specializes into neural ectoderm. The initially flat neural plate progressively bends and folds until it fuses in the midline to form the neural tube. The primary neural tube produces the uppermost 9/10 of spinal cord; (iii) *secondary neurulation* (28th-48th day): a secondary neural tube is laid down caudad to the termination of the primary neural tube. Retrogressive differentiation of the secondary neural tube results in the tip of the conus medullaris and filum terminale.
Defects in one of these three embryological steps produce *spinal dysraphisms*, characterized by anomalous differentiation and fusion of dorsal midline structures. Spinal dysraphisms may be categorized clinically in two subsets: open and closed spinal dysraphisms.

Open spinal dysraphisms:
In open spinal dysraphisms (OSD) the placode (non-neurulated neural tissue) is exposed to the environment through a cutaneous defect along the child's back. OSD include myelomeningocele, myelocele, hemimyelomeningocele and hemimyelocele, and are associated with a Chiari II malformation. Myelomeningocele is by far the most common of these forms; the placode protrudes through a posterior defect and is elevated above the skin surface due to concurrent dilatation of the subarachnoid spaces.

Closed spinal dysraphisms:
Closed spinal dysraphisms (CSD) are covered by intact skin, although cutaneous stigmata usually indicate their presence. Two subsets may be identified based on whether a subcutaneous mass is present. *CSD with tumefaction* comprise lipomas with dural defect (lipomyelocele and lipomyelomeningocele), meningocele, and myelocystocele. Lipomas with dural defect are more common; they are differentiated from one another based on the position of the cord-lipoma interface, that lies within the spinal canal in lipomyelocele, and outside the spinal canal (ie, into a meningocele) in lipomyelomeningocele. *CSD without tumefaction* comprise complex dysraphic states (ranging from complete dorsal enteric fistula to neurenteric cysts, diastematomyelia, dermal sinuses, caudal agenesis, and spinal segmental dysgenesis), bony spina bifida, tight filum terminale, filar and intradural lipomas, and persisting terminal ventricle. The most complicated forms (*complex dysraphic states*), including diastematomyelia, caudal regression, and segmental spinal dysgenesis) are related to faulty gastrulation. Diastematomyelia (literally, split cord) is caused by failure of midline notochordal integration, resulting into two separate hemineural plates. Caudal agenesis and segmental spinal dysgenesis are related to defective notochordal formation, characterized by absence or hypoplasia of a segment of the notochord, in turn resulting into absence or hypoplasia of a corresponding segment of the spinal cord.

Take home points:
Correlation of neuroradiological features of spinal dysraphisms with corresponding embryologic derangements is the basis of the clinical-neuroradiological classification, which can be successfully used in the everyday clinical practice

WEDNESDAY, MAY 31, 2017

SESSION: ANYTHING NEW ABOUT FUNCTIONAL IMAGING?

CNS (fMRI, MRS, more?)
M. Argyropoulou, L. Astrakas; Ioannina/GR

Summary:
Functional neuroimaging of CNS is a fast advancing field with frequent new developments in scanner's hardware, protocols, clinical indications, and post-processing techniques. For radiation safety reasons in the case of children, functional neuroimaging is mostly based on MR techniques especially designed to focus on the assessment of functional tissue characteristics, such as neuronal activity (fMRI),, metabolism (MRS) and perfusion (DSC perfusion, ASL). Pediatric coils with multiple elements, multiple slice excitation, 3D spectroscopy, 3D ASL, reduced FOV (zoom) and improved motion compensation techniques are important tools available to meet the permanent challenges of pediatric MR functional imaging: fast motionless acquisitions and increased resolution.
Functional MRI (fMRI) reveals brain activation during performance of behavioral tasks, based on the blood oxygen level dependent (BOLD) MRI signal, which is modulated by neural activity via a process of neurovascular coupling. For children, especially of younger age unable to follow a task, resting-state fMRI (rfMRI) can be performed and correlates brain areas with similar spontaneous fluctuations in the BOLD signal — thereby enabling estimates of 'functional connectivity.' Main clinical applications of fMRI are the delineation of eloquent cortex near a space-occupying lesion and the determination of the "dominant hemisphere" for language. Intense research is conducted in the areas of language organization and development, brain plasticity, and neurobehavioral disorders (e.g. ADHD).
Magnetic resonance spectroscopy (MRS) is a noninvasive MR technique, that detects intracellular metabolites, and may provide neuroimaging biomarkers of normal biological and pathological processes or response to a therapeutic intervention. Although the main field of application of MRS is the brain tumors, it has also been of particular

usefulness in assessing ischemic or traumatic brain injury and neurometabolic disorders.
Perfusion MR imaging methods detect signal changes that accompany the passage of a tracer through the cerebrovascular system. A less invasive approach is arterial spin labeling (ASL) that uses arterial water as an endogenous tracer to measure CBF and thus it is more suitable for pediatric studies. MR perfusion is applied in the evaluation of brain tumors, neurological diseases and developmental disorders.
Functional neuroimaging clinical applications are expected to expand greatly in the future due to the increasing availability of their techniques, as well as the continuous advancements in the field of pediatric research. Good knowledge of these techniques will become more necessary for an effective clinical practice and will enhance the role of radiology in the healthcare system.

Take home points:
Functional neuroimaging advanced techniques based on MRI allow us to study complex CNS processes such as cerebral perfusion (DSC, ASL), metabolic activity (MRS) and brain activation (fMRI).
Functional neuroimaging techniques already have significant clinical pediatric applications and assisted by recent advances in MR technology are expected to become even more powerful in the near future.

Kidney: Perfusion, Excretion, Obstruction
K. Darge; Philadelphia/US

Summary:
The functional imaging of the urinary tract entails the evaluation of the renal perfusion and excretion. In this complex process the sites of the main abnormalities could be pre-renal, renal parenchymal, renal pelvicalyceal or post-renal or even a combination at different sites. Functional MR urography (fMRU) is an advanced tool that not only allows the exquisite morphological depiction of the urinary tract, but also makes it possible to generate comprehensive functional data. These provide information about the function of the kidney as well as the excretion of urine from the renal parenchyma into the pelvicalyces and ureter. The functional results are mainly divided into two groups: 1. Transit times – these are recorded in minutes and a side comparison gives idea how much time it takes for the contrast to go through the renal parenchyma – the longer the more abnormal in general. 2. Differential renal functions – these can be based on the enhanced renal parenchymal volume or the Patalk number generated from this area and provides in percentage the split renal function. This presentation will discuss in detail the functional aspect of MR urography and demonstrate its utility in routine pediatric uroradiologic imaging.

Take home points:
- Functional MR urography provides comprehensive functional information
- Transit time results in functional MR urography inform about passage of the contrast through the kidney
- Differential renal functions can be based on parenchymal volume or Patlak and serve for calculating the split function

Imaging of regional lung function by MRI: Methods and clinical value for paediatric lung disorders
J. F. Schäfer; Tübingen/DE

Summary:
In chronic childhood lung disease (e.g. cystic fibrosis) global pulmonary function tests (PFT) can be normal although lung damage is already present. Moreover, in comparison to imaging, PFT is challenging in young children. Thus, cross-sectional imaging became more important in the past two decades. Regarding morphological evaluation, multidetector computed tomography (MDCT) serves as the most sensitive and reproducible modality. For functional evaluation perfusion/ventilation scintigraphy remains the reference standard. Although the individual radiation burden by a single chest CT has decreased significantly in the past, radiation doses can cumulate considerably when repeated examinations are performed in a long-term follow-up. Pulmonary MRI exists as an alternative method, especially for paediatric patients. However, standard H+MR sequences do not demonstrate small airway disease due to inherent limitations of low signal and rapid T2* signal decay of lung tissue. For comprehensive diagnosis, functional MRI offers the unique possibility to measure regional ventilation and perfusion, and mapping relaxation times and diffusion. Focussing on research applications, a variety of methods are available for these purposes. In this context, ventilation imaging using inert fluorinated gas indicates to overcome the limitations of the expensive setting necessary for imaging with hyperpolarized noble gasses. Regarding lung perfusion, dynamic contrast-enhanced MRI (DCE-MRI) is the most established method in clinical practice. However, especially in children, techniques that are completely non-invasive and do not require i.v.-contrast agents administration or gas inhalation could be promising to achieve broad acceptance. Concerning non-invasive methods, ventilation can be assessed by sequences with ultra-short echo times (UTE), perfusion by arterial-spin-labeling (ASL) and both by Fourier decomposition MRI (FD-MRI).

Take home points:
In conclusion, pulmonary MRI offers both, the assessment of morphology and the unique possibility to measure regional ventilation and perfusion, and mapping relaxation times and diffusion. New MR techniques that are completely non-invasive are now available. However, further scientific evaluation is needed.

SESSION: SYSTEMIC DISORDERS

IBD and related arthropaties
D. Jaramillo; Miami, FL/US

Summary:
Musculoskeletal diseases affect about 5% of patients with Crohn's disease and are the most frequent extra-intestinal manifestation of inflammatory disease. The articular manifestations of inflammatory bowel disease (IBD) are one of the seronegative arthritides, although they have a lower incidence of HLA –B27 than other seronegative arthritis such as ankylosing spondylitis.
There are manifestations in the joints of the extremities, and findings in the pelvis, especially in the sacro-iliac joints, and spine. Involvement of the extremities occurs in about 10% of patients with IBD related arthropathies, are more common with Crohn's disease, and can have either manifestations related olygoarticular JIA, or can have symmetrical involvement of smaller joints. The axial manifestations include ankylosing spondylitis and sacro-iliitis. Sacroilliitis is typically bilateral (Figure) and often has radiographic as well as MRI abnormalities. Enthesitis, tenosynovitis and dactylitis can occur with IBD just as they occur with other arthritides. It is important to differentiate IBD related arthritis from septic arthritis due to extension of an enteric fistula.
Deceased bone mineral density is a common finding in inflammatory disease. It occurs as a combination of malabsorption of Vitamin D due to intestinal involvement and the effects of therapy, particularly corticosteroids. Insufficiency fractures of the spine, sacrum and extremities can mimic the symptoms of arthritis. Finally, IBD can be associated with chronic non-bacterial osteomyelitis, although this association is relatively rare.
This review will illustrate several of the skeletal manifestations of IBD, focusing on the arthropathies.

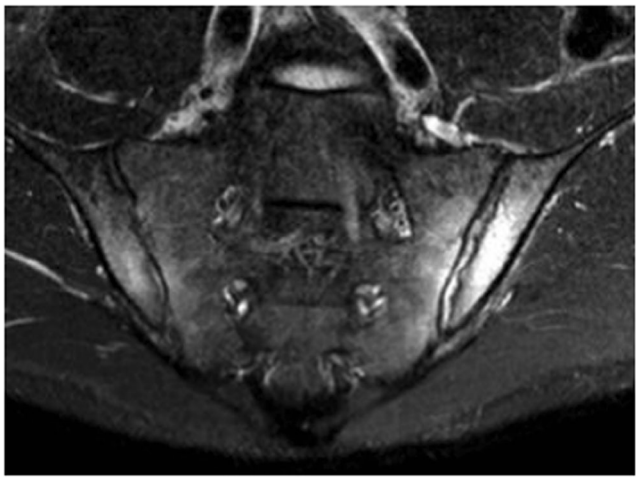

15-year-old with back pain and Crohn's disease. There is bilateral sacroiliitis

Take home points:

- Skeletal pain in patients with inflammatory disease may be due to and IBD related arthropathy, septic arthritis, or insufficiency fracture.
- IBD related arthritis is similar to other seronegative arthritides.
- There are axial manifestations as well as peripheral joint inflammatory changes.

Juvenile spondyloarthritis (JSpA)

E. von Brandis; Oslo/NO

Summary:
Juvenile idiopathic arthritis (JIA) can be defined as an arthritis of unknown cause occuring in children younger than 16 years and of at least 6 weeks duration. Juvenile spondyloarthritis (JSpA) is a subset of JIA and is characterized by enthesitis (inflammation at the attachment of tendons, ligaments and the joint capsule), arthritis and an increased risk of axial disease. There is also a strong association with human leukocyte antigen B27. JSpA accounts for approximately 10-15% of juveniles arthritis cases in Europe and is the most common form of juvenile arthritis in Asia. The condition is associated with significant long-term morbidity, high health-care costs and poorer outcomes compared with other forms of juvenile arthritis as well as its adult counterpart. Up to 40% of patients continue to be at risk of developing ankylosing spondylitis (AS) during the disease course. Recognizing spondyloarthritis (SpA) in children is challenging, particularly early in the course of disease, as the signs and symptoms at disease onset differ from those seen in adults. JSpA typically presents with hip and lower limb arthritis in conjunction with enthesitis. Inflammatory back pain as a presenting symptom is less common. As a consequence, JSpA may be missed or confused with other juvenile arthritides and patients often experience prolonged delays in diagnosis.

Classification

Currently there is no single diagnostic or classification system that is representative of the JSpA population. According to the International League of Associations for Rheumatology (ILAR) classification system, most childhood SpA's are classified as enthesitis-related arthritis (ERA), psoriatic arthritis or undifferentiated arthritis. Recent studies indicate that there are two clinical phenotypes of ERA: those with early axial disease often associated with hip arthritis in addition to peripheral arthritis; and those who follow a more peripheral disease course with arthritis and enthesitis and do not develop axial disease. The ILAR classification system places patients with both axial and peripheral involvement into the ERA subtype, and does not specifically address children who meet the criteria for AS. The correct approach to the classification of ERA is uncertain, and this issue is confusing to both pediatric and adult rheumatologists.

Clinical characteristics

Unlike other categories of juvenile arthritis, JSpA affects boys more often than girls, and peak age of onset is early adolescence. Enthesitis is a defining characteristic of JSpA. It is more common and affects more sites in the paediatric population compared with the adult one. The most commonly tender entheses are the insertions of the patellar ligament at the inferior patella, plantar fascia at the calcaneus, and the achilles tendon. Arthritis in JSpA is typically asymmetrical, oligoarticular (< 5 joints) and involves predominantely the weight-bearing joints. Isolated hip joint arthritis may be the presenting feature and predicts early axial disease. Involvement of the small toe joints is common in JSpA but rare in other forms of JIA. Midfoot arthritis and tarsitis (inflammation of the intertarsal bones, overlying tendons, entheses and soft tissue) is highly suggestive of spondyloarthritis. In adults, inflammatory back pain typically heralds the onset of sacroiliitis, whereas children seldom present with symptoms of axial disease. However, according to several studies, sacroilitis can be asymptomatic in JSpA and only detectable by imaging. Other axial manifestations in JSpA are inflammation of the lumbar apophyseal joints and interspinous ligaments, corner lesions of the spine and other sites of axial enthesitis-osteitis including the various ligamentous and muscular attachments of the pelvis. Extraarticular manifestations of JSpA are highly associated with axial disease and include acute anterior uveitis, bowel inflammation, psoriasis, and cardiac disease.

Imaging

Clinical diagnosis of JSpA can be difficult and the role of imaging may be more critical than in adult disease. The major goal of imaging in JSpA is to identify children with early signs of axial disease, as this group is at the greatest risk for progression to AS. The presence of axial disease in SpA has also major implications for treatment decisions, since traditional first-line therapies appear to have minimal effectiveness in the management of axial inflammation. In addition, recent studies in adults suggest that earlier initiation of biologic agents (anti-TNFs) may slow radiographic progression.

X-rays are not sensitive to acute inflammatory changes and will only show advanced disease in the sacroiliac joints. For these reasons plain radiographs are not useful in children or adolescents.

Ultrasound is a non-invasive, non-ionizing and relatively inexpensive technique that can be performed in a clinical setting. It is emerging as a valid diagnostic tool in SpA and can be used to visualize peripheral synovitis, tendonitis and enthesitis, but the method is heavily operator-dependent and there does not yet exist a clear definition for the diagnosis and grading of enthesitis in children. Secondary changes (calcifications, enthesophytes) have been observed much less in children compared with adults. There is a need for better consensus on abnormal ultrasonographic findings that define enthesitis lesions and standardization of methods.

Magnetic resonance imaging (MRI) is a radiation free and sensitive imaging modality for detection of synovitis as well as cartilage and bone destruction. MRI of the sacroiliac joints is increasingly obtained for early detection of inflammatory changes, as it shows active inflammatory (bone marrow edema, osteitis, enthesitis and capsulitis) and structural (erosions, subchondral sclerosis, subchondral fatty change and bony ankylosis) lesions of sacroiliitis long before radiographic changes become evident. In adults, MRI has become the gold standard imaging modality for detecting arthritis and enthesitis. Consensus definitions of lesions indicating pathology on MRI are now incorporated into diagnostic criteria for adult with SpA. In children and adolescents there is no gold standard MRI technique and it is therefore not clearly defined whether changes

seen in the sacroiliac joints are pathologic or part of normal maturation in the growing skeleton. The use of contrast enhanced imaging for the detection of active sacroiliitis on MRI in JSpA is a major controversy. Synovial enhancement can be detected without accompanying bone marrow edema in children, and it can be argued that contrast should be administered in order not to miss the diagnosis. Some authors argue that contrast administration does not change or add substantially to the MRI findings made on non-enhanced scans. Certainly, given the risks associated with gadolinium administration, contrast should be used with caution. Perhaps the use of contrast agents should be limited to selected cases when high STIR signal in the joint is the only finding in order to confirm the presence of synovitis, and when the differential diagnosis includes etiologies such as infection or tumor. The development of new MRI techniques has made it possible to perform whole body MRI scans (WBMRI) that allow assessment of the full range of affected entheses and joints. There is limited data on the utility of WBMRI in the pediatric population. It is worth noting that edema-like changes seen in the marrow of healthy children is an important potential pitfall to consider during interpretation and further studies are required in order to establish specific reference standards for MRI of the pediatric skeleton.

Diffusion-weighted imaging (DWI) offers a new approach to detect inflammation. Inflammation produces an increase in the apparent diffusion coefficient (ADC) of water molecules in affected tissues. Several studies in adults and a few recent studies in children have demonstrated that ADC is elevated in sacroilitis versus controls and that diffusion scores correlates well with STIR images. DWI is promising as a potential biomarker of disease activity in JIA and presents a novel approach to contrast– free imaging of synovitis. However, further studies are needed before it can be implemented in clinical practice.

Take home points:

JSpA is distinct from adult SpA and manifests more frequently as peripheral arthritis and enthesitis. Symptoms involving the spine and sacroiliac joints often occures later in this population. Clinical diagnosis of JspA can be difficult, and imaging therefore plays an important role in the diagnostic workup of disease. Identifying early signs of axial disease has major implications for treatment decisions and MRI of the sacroiliac joints is increasingly obtained for early detection of inflammatory changes. However, MRI criteria for sacroilitis in children are lacking. A major controversy in imaging of sacroilitis in JSpA is the use of contrast, as children can have sacroilitis without accompanying bone-marrow edema. DWI presents a novel approach to contrast-free imaging of synovitis but further studies are needed before it can be used in clinical practice.WBMRI has been shown to be more sensitive than clinical examination in the assessment of both disease activity and extent, but there is limited data on WBMRI in children. Normal variants in the growing skeleton may mimic pathologic changes and potentially cause overdiagnosing and -staging of disease**.** Hence, there is an urgent need to establish specific reference standards for MRI of the pediatric skeleton and to develop a gold standard MRI technique for the axial skeleton in children and adolescents.

Juvenile idiopathic arthritis

O. Olsen; London/UK

Summary:

Juvenile idiopathic arthritis (JIA) is common (about 1:1,000 children). Diagnosis and classification are based on clinical criteria. These criteria are in flux depending on 1) contemporaneous knowledge about aetiology and 2) available treatment options. Radiology has currently no role in establishing the diagnosis.

The clinical classification rests on whether the child has few joints affected (oligo JIA), many joints (poly JIA), has a condition similar to adult spondyloarthritis (entesitis-related arthritis) or other clinical presentations (systemic-onset JIA, psoriatic JIA, etc).

Radiology can potentially assess expressions of JIA, such as synovitis, tenosynovitis, systemic manifestations and permanent damage caused by inflammation. It is therefore thought to play a part in gauging the disease activity. The clinical care aims at optimising the child's everyday function, reducing acute symptoms (pain, swelling, joint restriction), allowing normal growth, minimising long-term sequelae (joint deformity) and minimising adverse effects of medical treatment.

Medical treatment in JIA is systemic (immuno-modulation) and local (steroid injection to joints and tendon sheaths). Both modes of therapy may to some degree be guided by imaging. However, there currently is no evidence that any form of whole-body imaging is efficacious for guiding treatment. This means that, in principle, indication for imaging should be 1) specific clinical questions, e.g. uncertainty regarding active inflammation at specific sites, or 2) a high pre-test likelihood of inflammation at a site which is difficult to assess clinically and where imaging offers reasonable accuracy. One example of the latter are the temporo-mandibular joints where destruction is frequently seen at an early stage, often without prior symptomatic warning.

There is one fundamental challenge for imaging research in JIA: what is the reference standard? For lack of anything better, a standardised clinical examination is often used as 'ground truth'. The dilemma is obvious. If clinical examination is reliable and accurate, then why bother with imaging? But we think imaging offers an improvement, then we cannot use an inferior method to set the standard. This problem is not unique to JIA. As is often the case, radiology in JIA is all about: knowing your clinicians (i.e. the pretest likelihood for disease) being technically eloquent (e.g. using high-resolution US probes, not delaying post-contrast MRI acquisitions) knowing what is normal (e.g. normal undulations in the articular surface, focal bone marrow signal variation) not being dogmatic about individual observations or measurements interpreting your findings in a clinical context

The lecture will demonstrate similarities and differences among joints and modalities in children with variable-severity JIA. The following points will be made: Focal areas in the bone marrow with high signal (T2) and corresponding enhancement are often seen in healthy children. In isolation, these do not signify active inflammation. Active synovitis in children often is not associated with (much) effusion The combination of synovial thickening with hyperaemia (US)/abnormal contrast enhancement (MRI) and surrounding soft-tissue swelling suggests active inflammation, however there is (yet) no established system for quantifying hyperaemia/enhancement Focal pits in the carpal bones do not represent erosions unless there is an associated cartilage defect Radiographs are useful for detection of destructive abnormality In MRI, scan fairly soon after injecting contrast. Gadolinium physiologically leaks into the synovial fluid making it difficult to delineate the synovium

A few differential diagnoses to keep in mind when there is mass-like swelling within or adjacent to a joint: vascular and neoplastic lesion, pigmented villonodular synovitis, synovial chondromatosis, lipoma arborescens.

Synovial inflammation is not always primary. Even when there is an established diagnosis of JIA, do consider that it may be secondary to biomechanical abnormality (erosion, osteochondral lesion, deformity).

Take home points:

Focal areas in the bone marrow with high signal (T2) and corresponding enhancement are often seen in healthy children. In isolation, these do not signify active inflammation. Active synovitis in children often is not associated with (much) effusion The combination of synovial thickening with hyperaemia (US)/abnormal contrast enhancement (MRI) and surrounding soft-tissue swelling suggests active inflammation, however there is (yet) no established system for quantifying hyperaemia/enhancement Focal pits in the carpal

bones do not represent erosions unless there is an associated cartilage defect Radiographs are useful for detection of destructive abnormality In MRI, scan fairly soon after injecting contrast. Gadolinium physiologically leaks into the synovial fluid making it difficult to delineate the synovium

Pulmonary manifestation of connective tissue disorders
C. M. Owens; London/UK

Summary:
Connective Tissue Diseases are an important cause of morbidity and mortality in children with very varied presentations. Nomenclature is confusing and a more appropriate descriptive term would be "multisystem inflammatory disorder +/- autoimmunity". It is important for the radiologist to be aware of the protean radiological appearances and clinical manifestations.

Take home points:
Different Patterns of diffuse lung disease (eg, desquamative interstitial pneumonia, non specific interstitial pneumonia, lymphocytic interstitial pneumonia, organising pneumonia, diffuse alveolar damage) may be present in several forms of collagen vascular disease, (and indeed other rheumatological conditions such as JIA) including scleroderma, Systemic lupus erythematosis, juvenile dermato and polymyositis, Sjogren's syndrome and mixed connective tissue disease.
These will be discussed in detail with illustrations for thin section high resolution CT with histopathological correlation.
The clinical presentation, prognosis and response to therapy vary depending on the histological pattern of diffuse lung disease, as well as on the underlying collagen vascular disease.

Whole body imaging in children: Sonography, CT, MRI, Nuclear Medicine - What and when?
R. A. Nievelstein; Utrecht/NL

Summary:
There are several (benign and malignant) disease processes in children that frequently involve more than one organ system or body region. Diagnostic imaging of children with such multifocal or multisystem diseases has been quite challenging, often requiring a combination of different imaging techniques for a whole body coverage. The recent technical developments in Computed Tomography (CT), Magnetic Resonance Imaging (MRI) and Nuclear Medicine (NM) have changed the role of imaging in these children revolutionary. In the past, imaging techniques have been mainly used as a tool to detect the cause of illness and to assess the extent of disease spread before, during and after therapy (i.e. structural imaging). But nowadays, it has also become possible to use imaging techniques to gain information on the biological behavior of diseases before and during therapy (i.e. functional imaging). Plain radiography, Ultrasonography (US) and Computed Tomography (CT) have been the structural imaging techniques of choice for many decades, more recently supplemented by functional imaging techniques like single-photon emission tomography (SPECT) and positron emission tomography (PET). A major disadvantage of most of these techniques is the use of ionizing radiation, which may be associated with induction of second cancers later during life. This small but not negligible health risk is of particular concern in children as their tissues are more radiosensitive than adults and they have more years ahead in which cancerous changes might occur. That is why there is an increasing interest in the use of alternative imaging techniques that do not use ionizing radiation. With MRI it is nowadays possible to acquire images with a high spatial resolution and excellent soft tissue contrast throughout the body, which makes it an ideal radiation-free tool for the detection of pathology, especially in soft tissue, parenchymal and bone marrow locations. Moreover, recent technological advances have resulted in fast diagnostic sequences for whole-body MR imaging (WB-MRI), including functional techniques such as Diffusion Weighted Imaging (DWI). As a result, WB-MRI has become a clinically feasible imaging modality for diagnosis and follow-up of multifocal and multisystem diseases in children. In this scope, the recent development of integrated PET/MRI systems is very interesting, combining the superior structural imaging of MRI with the functional (molecular) information of both imaging techniques while decreasing the radiation dose.
Traditionally, whole body imaging techniques have been mainly used for oncological indications, such as staging of malignancies, and monitoring of the effectiveness of therapy. However, whole-body imaging techniques are increasingly used for the diagnostic imaging of other benign multisystem diseases and indications, including chronic recurrent multifocal osteomyelitis (CRMO), rheumatological diseases, neuromuscular diseases, neurofibromatosis type 1, generalized vascular malformations, multifocal osteonecrosis after intensive chemotherapy, fever of unknown origin, and post-mortem imaging. Finally, these imaging techniques may be used for the screening of children with a cancer predisposition syndrome. During this lecture, imaging protocols and indications of the different whole body imaging techniques will be discussed with a focus on their clinical application in children with benign and malignant multifocal or multisystem diseases.

Suggestions for further reading: Treves ST, Falone AE, Fahey FH (2014) Pediatric nuclear medicine and radiation dose. Semin Nucl Med 44(3):202-209 Uslu L, Donig J, Link M, et al (2015) Value of 18F-FDG PET and PET/CT for evaluation of pediatric malignancies. J Nucl Med 56(2):274-286 Damasio MB, Magnaguagno F, Stagnaro G (2016) Whole-body MRI: non-oncological applications in paediatrics. Radiol Med 121:454–461 Davis JT, Kwatra N, Schooler GR (2016) Pediatric Whole-Body MRI: A Review of Current Imaging Techniques and Clinical Applications. J Magn Reson Imaging 44:783–793 Eutsler EP, Khanna G (2016) Whole-body magnetic resonance imaging in children: technique and clinical applications. Pediatr Radiol 46:858–872 Lecouvet FE (2016) Whole-Body MR Imaging: Musculoskeletal Applications. Radiology 279:345–365 Nievelstein RAJ, Littooij AS (2016) Whole-body MRI in paediatric oncology. Radiol Med 121(5):442-53

Take home points:
Whole body imaging techniques have become an integral part of the diagnostic algorithms of pediatric malignancies. Whole body imaging techniques are increasingly used for the diagnostic imaging of other benign multifocal and multisystem diseases, including rheumatologic, infectious, and congenital disorders. For many benign and malignant disease processes, structural and functional imaging techniques are combined nowadays, allowing for a better definition of anatomic localization, characterization, segmentation, and information on biological behavior in a single visit.

SESSION: TUMORS OF THE HEAD AND NECK

Soft tissue tumors and pseudotumors
T. von Kalle; Stuttgart/DE

Summary:
A number of benign and malignant tumours may occur in the extracranial head and neck. The awareness of their imaging

appearances is important for any radiologist involved in child imaging, because we have an important role in characterizing the lesions and guiding purposeful and minimally invasive but successful diagnostic procedures.

Most head and neck masses in children are benign and have an inflammatory, infective, vascular or congenital cause (cf. special presentation on vascular malformations). Malignant lesions are less common, however, early diagnosis is paramount as many of these cancers are readily treatable and often curable. Differential diagnosis is guided by patient age, clinical presentation, tumour localisation, and imaging characteristics. While some masses such as (epi-)dermoids, fibromatosis colli and swollen lymph nodes including atypical mycobacterial infections (MOTT) may be readily diagnosed by clinical inspection und ultrasound, others present special diagnostic challenges. Fibromatosis, for example, is a benign lesion with an often complex and potentially destructive local spread. Some malignant lesions tend to be localised such as the embryonal rhabdomyosarcoma, while others may be part of a systemic disease such as lymphoma and Langerhans cell histiocytosis (LCHC).

In case of a suspected malignancy, patients should be referred to a specialized centre which will be able to provide the full spectrum of multidisciplinary evaluation and treatment according to the guidelines of an international oncology study group. This is also important for image guided or surgical biopsies as long term outcome and survival of many of the young patients are directly associated with these initial diagnostic and therapeutic strategies.

With its excellent spatial resolution in the near field, ultrasound is the method of choice for all superficial masses. An experienced paediatric radiologist will be able to identify most of the benign lesions and in other cases will be able to guide further diagnostic decisions. Tumours in the midline require thorough workup to exclude an encephalocele or a dermal sinus with connection to the intracranial space. High resolution MRI is required if such an extension cannot be ruled out by ultrasound or if a tumour is larger than the transducer's scan area. Soft tissue tumours in the deeper parts of face and neck as well as tumours of osseous origin are also best delineated by MRI. In lesions adjacent to the skull base contrast enhanced and fat saturated MR images with high spatial resolution are of utmost importance to completely depict the tumour's extension through the foramina and along the meninges (Fig. 1). CT can provide additional information on the involvement of osseous structures.

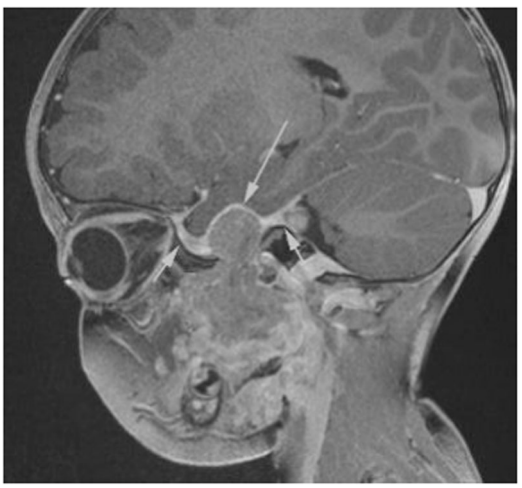

Embryonal rhabdomyosarcoma. High resolution MRI with fat saturation after contrast injection depicts the tumour's extension through the foramen ovale (long arrow) and along the meninges (short arrows).

Take home points:

- Ultrasound is the modality of choice for all small and superficial lesions
- High resolution MRI with fat saturation before and after contrast injection is essential in more complex or potentially malignant lesions
- Diagnostic work-up of suspected malignant tumours should be reserved for specialized centres

IMAGING of BONE TUMORS of the HEAD and NECK

M. Elmaleh-Bergès; Paris/FR

Summary:

Skull base and face lesions are less frequent in children than in adults. Symptoms may be subtle or unspecific. Depending on their localization, clinical findings may be common (nasal obstruction, otitis…) or more disturbing (cranial nerves palsies, exophthalmos, vision loss …).

Clinical history and physical examination findings are important to reduce the spectrum of differential diagnosis, but imaging data are the key features to determine the nature of these lesions. CT and MRI play an important role in diagnosis, treatment survey and surgery planning of skull base and face lesions.

Skull base and face bone lesions are either intrinsic lesions of the bone or secondary to soft-tissue tumors or pseudo tumors invasion. This lecture will focus on bone intrinsic lesions, and include soft-tissue and pseudo tumors only as differential diagnoses.

Computed tomography plays the role for skull base and face of plain radiograph for long bones. Therefore, the same semiology may be used to determine if the lesion is slowly or rapidly growing, aggressive or looks benign. Helical CT allows reconstructions with both soft-tissue and bone algorithms as well as multiplanar reformations. It gives a good visualization of the anatomy of the skull base and allows a good depiction of the bone architecture. CT is first used for the initial work up of the disease but also for surgery and therapeutic planning (endoscopic sinus surgery with navigation).

However, CT analysis may be challenging in children due to growth changes: normal process of pneumatization according to age, sutures not yet fused has to be recognized. Some variations in pneumatization must not be mistaken for pathology: asymmetrical pneumatization of the petrous apex and arrested pneumatization of the sphenoid mimicking intraosseous lesion are the most common.

Both CT and MR imaging are complementary: most preferably, contrast-enhanced MR is associated with non-contrast high resolution CT.

MRI allows a good delineation of bone involvement of skull base lesion due to bone marrow changes, whether CT can fail to detect subtle extension within the bone. In addition to T1 and T2 weighted sequences, the use of specific sequences and/or techniques such as fat-saturation, diffusion, dynamic-contrast-enhanced sequences, and MR angiography helps to characterize the lesions. T1 spin echo sequence is mandatory to appreciate bone marrow infiltration in adults and older children. But when red bone marrow has not yet be replaced by fatty bone marrow, in young children, this can be challenging. It is useful to know the bone marrow fatty conversion of the skull base chronology.

Cranial MR can also be associated to whole body MR to look for multifocal or metastatic disease.

Epidemiologic data concerning bone tumors of the skull base are scarce due the rarity of these lesions. They can be classified according to their location within anterior, middle or posterior cranial fossa or classified according to their origin: osteogenic (osteoblastoma, osteoma, osteosarcoma…), chondrogenic (chondroma, chondrosarcoma), fibrous (fibrous dysplasia, fibro-

osseous lesions..), notochord (chordoma), hematopoietic (leukemia, histiocytosis), vascular (hemangioma), neuro ectodermic (Ewing sarcoma) or unknown origin (aneurysmal cyst, giant cell tumor).
The aim of this presentation is to draw attention to skull base growth changes that can mimic pathology and to describe the imaging specificities of the most common bone tumors of the skull base and face in children.

Take home points:
- Chronology of skull base and face bone marrow changes and pneumatization has to be known
- Some variations in skull base maturation may mimic pathology
- CT helps to characterize bone destruction and appreciate periosteal reaction
- Bone marrow changes on MR can detect tumor extension not visible on CT

Vascular tumors and malformations of the trunk and extremities: A comprehensive review of findings and discussion of the nomenclature.
T. A. G. M. Huisman, A. Tekes; Baltimore/US

Summary:
Vascular anomalies comprise both vascular tumors and vascular malformations that can occur anywhere in the pediatric body. Because conflicted nomenclature can cause confusion, accurate diagnosis and classification of these anomalies is important for proper clinical evaluation and management. Many of these patients require multidisciplinary care, consequently the usage of a correct nomenclature across all disciplines is a sine qua non. The International Society for the Study of Vascular Anomalies (ISSVA) classification, updated in 2014, offers a comprehensive classification accepted by many subspecialities. This approach/classification has facilitated correct communication for all medical subspecialties involved in the care of these complex vascular anomalies.
Pediatric radiologists play a critical role in evaluating these patients since the majority present during childhood. In this presentation, we present a state of the art MRI imaging protocol with exemplary cases of the most common types of vascular anomalies in the pediatric trunk and extremities, using the current ISSVA classification. In addition, we discuss the common syndromes associated with vascular anomalies such as Klippel-Trenaunay and LUMBAR syndrome.

Take home points:
- Updates International Society for the Study of Vascular Anomalies nomenclature should be used
- Dynamic contrast enhanecd MRA faciliattes differentiation of pediatric trunk and extremity vascular lesions

SESSION: SYNDROMES AND GENETICS

Brain and bone: Pattern recognition approach.
T. A. G. M. Huisman[1], M. Wagner[2]; [1]Baltimore, MD/US, [2]Baltimore/US

Summary:
Genetic skeletal disorders (GSD's) are a heterogeneous group of syndromes characterized by an intrinsic abnormality in growth and (re-)modeling of cartilage and bone. A large sub-group of GSD's may have additional involvement of other structures/organs beside the skeleton, such as the central nervous system (CNS). CNS abnormalities have an important role in long-term prognosis of children with GSD's and should consequently not be missed. Sensitive and specific identification of CNS lesions while evaluating a child with a GSD requires a detailed knowledge of the possible associated CNS abnormalities. Here, we will present and discuss a pattern-recognition approach for identifying relevant neuroimaging findings in GSD's guided by the obvious skeletal manifestations of GSD. In particular, we will discuss which CNS findings should be ruled out for the various GSD. To facilitate this diagnostic approach the multiple GSD are classified based on the pattern of skeletal involvement (1. abnormal metaphysis or epiphysis, 2) abnormal size/number of bones, 3) abnormal shape of bones and joints, and 4) abnormal dynamic or structural changes). Skeletal involvement is defined in accordance with Online Mendelian Inheritance in Man. The spectrum of co-existing CNS involvement is extracted from an extensive literature search. Selected examples will be shown based on prevalence of the diseases and significance of the CNS involvement. CNS involvement is common in GSD's. A wide spectrum of morphological abnormalities is associated with GSD's. Early diagnosis of CNS involvement is important in the management of children with GSD's. This pattern-recognition approach aims to assist and guide physicians in the diagnostic work-up of CNS involvement in children with GSD's and their management.

Take home points:
- Skeletal findings related to systemic disorders may be accompanied by CNS lesions
- Pattern of skeletal findings may suggest "typical" CNS findings

SESSION: PANEL DISCUSSION

Radiologic challenge: Child abuse or genetic/metabolic disease: A case based session
T. A. G. M. Huisman; Baltimore, MD/US

Summary:
Not infrequently the correct radiological differentiation of skeletal and/or central nervous system findings secondary to non-accidental injury versus inherited genetic and/or metabolic disorders may be challenging. Imaging findings may be non-specific, can result in incorrect diagnosis and subsequently inadequate patient management or initiation of faulty treatment. The diagnostic work-up of children suspected of non-accidental injury or genetic/metabolic disorders requires a multi-disciplinary approach involving many key players including physicans of various disciplines, nurses, psychologists, social workers and many more. A proper and detailed medical history and physical examination of the patient, collection of the relevant family history, a metabolic and genetic work up, a detailed interview of care givers, friends and family are essential for the correct and comprehensive evaluation of imaging findings. In the current session, various exemplary and possibly confusing cases will be interactively discussed with the audience by a panel of experts (Susan Blaser, Thierry A.G.M. Huisman and Andrea Supert-Furga). Goal is to offer a case based approach to challenging patients with discussion of the best diagnostic approach including differential considerations.

Take home points:
- Chid abuse and genetic or metabolic disorders may have similar imaging findings
- A multidisciplinary approach is necessary to narrow down teh differential diagnosis.

Programme - 53rd Annual Meeting

Programme - 53rd Annual Meeting

Thursday, June 01, 2017

07:45-08:00 — Room 1
Opening Ceremony
G. Eich, Aarau/CH; J. Schneider, Basle/CH

08:00-09:00 — Room 1
Special Focus Session: Emerging infectious diseases: ZIKA Virus infection

Pre- and Postnatal Imaging in Zika virus: Where are we?
P. Daltro, Rio de Janeiro/BR
P. Jungmann, Recife/BR

09:00-10:00 — Room 1
ESPR meets CHOP

Applications of Susceptibility-weighted Imaging in Pediatric Neuroradiology
A. Vossough, Philadelphia/US

State of the Art Imaging of the Single Ventricle
D. Biko, Philadelphia/US

10:00-10:30 — Break

10:30-11:30 — Room 2
Task Force Session: Neuro

Neuroimaging in head trauma
M. Argyropoulou, Ioannina/GR
G. Alexiou, Ioannina/GR

10:30-11:30 — Room 3
Task Force Session: MSK - Imaging in juvenile idiopathic arthritis (JIA) - An update

Normal MR-findings mimicking pathology of the wrist
D. Avenarius, Tromsø/NO

MR-scoring of acute and permanent JIA changes of the wrist – Status
Ch. Nusman, Amsterdam/NL

A novel radiographic scoring system for permanent hip involvement
L. Tanturri de Horatio, Rome/IT

Bone age assessment – Statement from the ESPR task force
K. Rosendahl, Bergen/NO

11:30-12:30 — Room 2
Scientific Session: Neuro

Radiation-induced vascular changes in childhood medulloblastoma survivors: An MRI study
Y. Tanyildizi, Mainz/DE

Fast "black-bone" MR imaging in evaluation of craniofacial abnormalities: Comparison with high resolution CT
Z. Habib, Liverpool/UK

Vessel shape alterations of the vertebrobasilar arteries in Mucopolysaccharidosis type IVa (Morquio A) patients
Y. Tanyildizi, Mainz/DE

Intraspinal cyst presenting as a pediatric emergency: Imaging considerations
E. Vazquez, Barcelona/ES

Automated quantification of myelin in children using multiparametric quantitative MRI
H.G. Kim, Suwon/KR

Role of MR Imaging of the Orbit in Staging of Retinoblastoma: Prospective Study Correlated with Histopathological Results
A. Youssef, Cairo/EG

Patterns of the cortical watershed continuum of term gestation hypoxic ischaemic injury – the "Wish-bone sign"
S. Andronikou, Bristol/UK

Correlation of brain edema degree and biochemical parameters in pediatric posterior reversible encephalopathy syndrome with hematologic/oncologic diseases
T. Akbas, Adana /TR

T1 signal intensity changes of deep brain nuclei after multiple gadobenate dimeglumine injections: Comparison of children and adults
S. Kinner, Essen/DE

Kearns-Sayre Syndrome (KSS): Neuroimaging in 8 cases
L. Pasquini, Rome/IT

11:30-12:30 — Room 3
Scientific Session: MSK

Ultrasound for monitoring distraction of magnetically controlled growing rods (MCGR): A reproducible geometric technique
G. Poillucci, Trieste/IT

Refuting child abuse denialists – healing rickets is clearly different from child abuse metaphyseal fracture
A.E. Oestreich, Cincinnati/US

Simultaneous Multi-Slice Turbo Spin Echo: A 2-fold time-saving alternative to conventional TSE in MR imaging of the pediatric knee
S. Benali, Boston/US

MRI for sacroiliitis in children: Panel findings and inter-observer evaluation using standardised reporting
K.E. Orr, Plymouth/UK

Ultrasound-guided steroid tendon sheath injections in Juvenile Idiopathic Arthritis
S. Peters, Toronto/CA

Artificial intelligence with deep learning technique in the determination of bone age: Accuracy and feasibility study
J.R. Kim, Seoul/KR

Temporomandibular joint MRI findings in adolescents with primary disk displacement in comparison to those in juvenile idiopathic arthritis
J. Bucheli, Zurich/CH

Midterm MRI follow-up of TMJ inflammation, deformation and mandibular growth in JIA patients under systemic treatment
A. Bollhalder, Zurich/CH

12:30-13:30 — Industry sponsored symposium

13:30-14:30 — Room 2
Scientific Session: Abdominal (GI & GU) Imaging

Pediatric Ileocolic Intussusception: Symptom Duration/Time to Enema Do Not Affect Pneumatic Reduction Success
L.A. Binkovitz, Rochester/US

Evaluation of splenic stiffness measurements for the diagnosis and the follow-up of portal stenosis after paediatric liver transplantation
A. Dabadie, La Timone, Marseille/FR

Comparison between the standard gradient echo (GRE) sequence and echo planar imaging (EPI) sequences in MR Elastography in a pediatric population
C. Maya, Philadelphia/US

Contrast-enhanced Voiding Urosonography, a sensitive & radiation free technique. 6-year experience in a tertiary referral center
P.K.J. Chan, Hong Kong/HK

Percutaneous transbiliary needle or forceps biopsy in hepatic masses with biliary dilatation
A. Dabadie, La Timone, Marseille/FR

Inflammatory bowel disease in children - ultrasound vs. magnetic resonance imaging
M. Jeckovic, Novi Sad/RS

Findings in Percutaneous Transhepatic Cholecysto-Cholangiography in neonates and young infants presenting with conjugated hyperbilirubinemia
S. Peters, Toronto/CA

Role of Shear Wave Elastography in Diagnosing Biliary Atresia
R.P. Kesav, New Delhi/IN

Microlithiasis: Is it a risk factor for testicular tumor?
K. Darge, Philadelphia/US

Do ADC-values reflect renal function or obstruction in children with uretero-pelvic-junction obstruction?
P. Grehten, Zurich/CH

13:30-14:30 — Room 3
Task Force Session: CT and radiation dose

Introduction to EC Tender DRL Project with focus on CT in children
C. Owens, London/UK

Most common imaging procedures in children and their contribution to collective dose
E. Sorantin, Graz/AT

Most common interventional procedures in children
C. Granata, Genoa/IT

14:30-15:30 — Room 2
Task Force Session: Abdominal (GI & GU) Imaging

Introduction: Update Task force work and projects
M. Riccabona, Graz/AT

Contrast enhanced US in childhood – Applications in children: literature review and results from a recent questionnaire,
with special emphasis on moderate abdominal trauma & trauma follow-up
C. Bruno, Verona/IT

Imaging in IBD – Joint recommendation statement with ESGAR
F. Avni, Brussels/BE; P. Petit, Marseille/FR

New aspects to consider when giving gadolinium based contrast agents in infants and children
H-J. Mentzel, Jena/DE; M. Riccabona, Graz/AT

Procedural recommendation: how to perform pediatric gastro-intestinal US
M.L. Lobo, Lisbon/PT; M. Riccabona, Graz/AT

14:30-15:30 — Room 3
Scientific Session: CT and radiation dose

Ionizing radiation in pediatric radiology - do medical staff and parents know enough?
J. Lovrenski, Novi Sad/RS

Fluoroscopy in pediatric radiology - how important is an individual impact to radiation exposure of children?
J. Lovrenski, Novi Sad/RS

Automated tube voltage selection in combination with automated tube current modulation in pediatric non-contrast chest CT
A. Hojreh, Vienna/AT

Advantages and disadvantages of Cone Beam CT for pediatric interventions
C. Schaefer, Phoenix/US

PiDRL guidelines: A review of local DRL for pediatric fluoroscopy in a Italian referral center
A. Magistrelli, Rome/IT

PiDRL guidelines: A review of local DRL for pediatric head, thorax and abdomen CT in a Italian referral center
A. Magistrelli, Rome/IT

DRL-curve in optimization of pediatric body CT
R. SEURI, Helsinki/FI

Reduced Slice CT as a means of lowering patient Dose in Children with Diffuse Lung Disease
S. Servaes, Philadelphia/US

15:30-16:30 — Room 1
Case Report Presentation Session

Crazy paving - Pulmonary manifestation of Type b Niemann Pick Disease - An interesting Paradigm
S. Muthiyal, Doha/QA

Blast from the past: Lemierre's syndrome in adolescents with sore throat
O. Kvist, Stockholm/SE

Unicameral bone cyst associated with secondary aneurysmal bone cyst of clavicle
I. Dasic, Belgrade/RS

Imaging of glomus tumor of liver in a child (case report)
N. Tewattanarat, Khonkaen/TH

Brain MRI in a pediatric patient with linear scleroderma en coup de sabre
M. Mortilla, Florence/IT

Median Arcuate Ligament Syndrome (MALS) – A report of two cases
M. Lintrop, Tartu/EE

Cutaneous metastases of infantile choriocarcinoma can mimic infantile hemangioma both clinically and radiographically
R.B. Towbin, Phoenix/US

A rare case of Ovarian Juvenile Granulosa Cell Tumor associated with Ollier's Disease - Generalised mesodermal dysplasia
P. Joshi, Pune/IN

Role of whole-body MRI in the diagnosis of Goldbloom syndrome in paediatrics: The sock sign
M.B. Damasio, Genoa/IT

Are all hypoplastic appearing ventricles really hypoplastic?
Ö.I. Koska, Izmir/TR

Kimura disease in a thirteen year old male
K.S. Minhas, London/UK

Increased NAA: Is it surely Canavan Disease?
E. Varga, Budapest/HU

Magnetic resonance imaging findings in medium-chain acyl-coenzyme A dehydrogenase (MCAD) deficiency
D. Narese, Rome/IT

A case of a newborn with accessory scrotum associated with bifid scrotum and perineal lipoma
D. Narese, Rome/IT

"Half - moon" sign: Look for a tumor or a fracture
M. Raissaki, Heraklion/GR

15:30-16:30 — Room 2
Scientific Session: Abdominal (GI & GU) Imaging

Pediatric MR Elastography on Siemens scanners: Early experience
C. Maya, Philadelphia/US

Prone versus supine ultrasound positioning for evaluation of urinary tract dilation (UTD) in children

C. Maya, Philadelphia/US

Non-pathologic Diffusion Restriction of the Jejunum on MR Enterography

D.M. Biko, Philadelphia/US

Imaging findings in the newborn with meconium peritonitis that require surgery

P. Caro Dominguez, Cordoba/ES

Renal Diffusion Tensor Imaging (DTI): Are quantitative DTI values useful in the evaluation of children with ureteropelvic junction obstruction (UPJO)?

J. Delgado, Philadelphia/US

The potential causes of premature microbubble destruction during echo-enhanced voiding urosonography in children

D. Kljucevsek, Ljubljana/SI

MRI T1 mapping of the liver in adolescents with Fontan circulation

K.J. Thrane, Oslo/NO

Diagnostic accuracy of ultrasound, computed tomography and wedge portography in the work-up for mesenterico-rex bypass in children with extrahepatic portal hypertension

S. Toso, Geneva/CH

MRE identifies more abnormalities, but is no more likely than bowel ultrasound to impact clinical decisions in pediatric IBD as judged by a clinical consensus

J.L.J.B. Barber, London/UK

15:30-16:30 **Scientific Session: MSK** — Room 3

Sickle cell crisis in children: Analysis of Fluid signal on unenhanced fat-suppressed T1-weighted MRI on 12 patients with an acute bone crisis

T. Youssef, Leicester/UK

Role of MRI to Assess Skeletal Age in Pediatric Celiac Disease

S. Bernardo, Rome/IT

The prevalence of metaphyseal injury and its mimickers in otherwise healthy children under two years of age

P. Eide, Bergen/NO

Hand MRI and Greulich-Pyle atlas in skeletal age estimation

A. Hojreh, Vienna/AT

Metabolic Bone Disease in Preterm Infants: Assessment of the Relationship between Radiologic Grading in the Wrist and Serum Biochemical Markers

S.K. You, Daejeon/KR

Quantitative grading of TMJ synovitis in children with JIA–influence of MR-coil, timing after contrast-injection and location of measurements on joint-to-muscle enhancement ratio

A. Hamardzumyan Schmid, Zurich/CH

Clinical applications of navigational software in the Interventional Radiology suite at a Pediatric Institution

S. Shellikeri, Philadelphia/US

Spinal Ultrasound a primary screening tool in suspected abnormalities of Neonatal Spine

A.S. Karnik, Mumbai /IN

16:30-17:00 Break

17:00-17:45 **Jacques Lefèbvre Lecture** — Room 1

Hominid Evo-Devo: Reconstructing the evolution of human development

Ch. Zollikofer, Zurich/CH

Friday, June 02, 2017

07:45-08:45 **Special Focus Session: Age assessement** — Room 1

Age estimation at the end of puberty: From a hand radiograph or from mental/psychological assessment?

O. Jenni, Zurich/CH

H. Thodberg, Holte/DK

08:45-09:45 **ESPR meets CHOP** — Room 1

Innovative imaging in IR - From bubbles to beyond

A.M. Cahill, Philadelphia/US

Multimodal Assessment of Autism Spectrum Disorders using MEG, MRS and MRI - Towards Biomarkers

T. Roberts, city/country

09:45-10:15 Break

10:15-11:30 **Interventional Radiology** — Room 1

Post-Liver Transplantation Intervention

S. McGuirk, Birmingham/UK

Vascular Access

R. Gnannt, Zurich/CH

Dos and Don'ts in Image Guided Pediatric Biopsy

D. Parra, Toronto/CA

Pediatric Interventional Oncology: Big Cases in Little People

M. Heran, Vancouver/CA

Vascular Anomalies

P. Patel, London/UK

11:30-12:30 **Scientific Session: Cardiac and thoracic** — Room 2

Diagnostic Utility of MRI of Thorax in Pulmonary Tuberculosis

K.S. Sodhi, Chandigarh/IN

Cardiac MRI: Differences of myocardial strain assessed by feature tracking between pectus excavatum patients and healthy volunteers

A. Lollert, Mainz/DE

Pectus excavatum in children - variations of Haller index and single-slice CT technique

J. Lovrenski, Novi Sad/RS

Aortic tortuosity: A new finding in patients with Mucopolysaccharidosis type IVa (MPS IVa)

Y. Tanyildizi, Mainz/DE

Lung ultrasound in the diagnosis and follow-up of pneumonia in children - is it really as reliable as chest X-ray?

J. Lovrenski, Novi Sad/RS

Role of chest radiography in screening of childhood TB contacts in the UK – A migrant context

K.S. Minhas, Bristol/UK

Is there really no cardiac problem for performing sports

Ö.I. Koska, Izmir/TR

Pulmonary Langerhans Cell Histiocytosis In Children: Chest CT imaging features and proposal of a scoring system

V. Della Valle, Paris/FR

High Resolution computed tomography for chronic small airway disease in HIV infected adolescents

S. Andronikou, Bristol/UK

11:30-12:30 **Outreach in Pediatric Radiology** — Room 3

The ARABKIR Children's Hospital in Yerevan Armenia. An Outreach Project by the University Children's Hospital in Zurich

G. Eich, Aarau/CH

International collaborations helps to unravel the Zika Virus Mystery

T. Huisman, Baltimore/US

Title to be confirmed

K. Darge, Philadelphia/US

Outreach in different environments (Central Eastern Europe, Asia, Africa) – What is it good for? Helpful or contra-productive?

M. Riccabona, Graz/AT

'Spotting the difference'. Distribution and extent of CRMO lesions in children on baseline whole body MRI

T. Mendes da Costa, Bristol/UK

Hepatic Hemangiomas – Focal and Multifocal Diagnosis Predictor?

J. Brisson, Montreal/CA

Symptomatic and asymptomatic meckel's diverticulum in the pediatric population - A retrospective analysis of imaging findings with histopathologic correlation

N. Abu Ata, Jerusalem/IL

Preliminary results on DNA damage from CT irradiation in pediatric patients

E. Sorantin, Graz/AT

Emergency Room Imaging Procedures in a Tertiary Pediatric Trauma Center

E. Sorantin, Graz/AT

12:30-13:30 Industry sponsored Symposium

13:30-14:00 **Contrast media in neonates and infants: What, when and how?** — Room 1

F. Avni, Brussels/BE

14:00-15:00 **Task Force Session: Oncology and whole body imaging** — Room 2

Paediatric brain tumours: Differential diagnosis between low and high grade, from basic to advanced

L. Porto, Frankfurt/DE

Experience with central review of paediatric renal tumours

G. Khanna, Washington/US

Is there a role for DWI in nephroblastoma?

A. Littooij, Utrecht/NL

Ins and outs of PET MRI in children

J. Schaefer, Tuebingen/DE

14:00-15:00 **Scientific Session: Neuro** — Room 3

Head CT in a regional children's hospital without MRI - effective doses and justification of clinical indications

J. Lovrenski, Novi Sad/RS

Diffuse and symmetric diffusion restriction involving the white matter of the brain in patients with neonatal seizures

J.-Y. Hwang, Yangsan-si, Gyeongsangnam-do/KR

Whole Body MRI on diagnosis and follow-up of Neurofibromatosis type 1

H.M. Lederman, Sao Paulo/BR

Accuracy of non-radiologists and lay-persons for identifying children with cerebral cortical atrophy from 'Mercator map' curved reconstructions of the brain

S. Andronikou, Bristol/UK

Safety and efficacy of sphenopalatine ganglion blockade in children – initial experience

C. Schaefer, Phoenix/US

Pediatrics Orbital Masses: The value of adding Diffusion-Weighted Imaging to the conventional MRI in Lesion Categorization

A. Youssef, Cairo/EG

Utiliy of resting state fMRI in children for preoperative language mapping

L.-M. LEIBER, Angers/FR

Is Sclerotherapy an Effective Treatment Option for Ranulas or Thyroglossal Duct Cysts in Children?

R.B. Towbin, Phoenix/US

Role of the Susceptibility-weighted imaging (SWI) in the neuroimaging of term newborns

G. Rudas, Budapest/HU

Mechanical birth-related trauma: Imaging of the "accidents of birth"

J.G. Blickman, Rochester/US

15:00-16:00 **Case Report Presentation Session** — Room 1

Ewing sarcoma of tibia in an infant girl

A. Seehofnerova, Brno/CZ

Scimitar syndrome together with pulmonary sequestration and horseshoe lung: Congenital pulmonary venolobar syndrome

B.E. Derinkuyu, Ankara/TR

Congenital cervical cyst with rare association with pyriform sinus fistula in neonates: Imaging characteristics

G.Y. Lim, Seoul/KR

Congenital pulmonary venolobar syndrome in combination with multiple abnormalities in a child

B.E. Derinkuyu, Ankara/TR

Neck infection disclosing diagnosis of congenital fourth branchial arc anomaly in a girl

M. Haliloglu, Ankara/TR

Heart and hepatic faillure: Uncommun onset of Wilms' tumor

S.M.S.D. Rocha, Sao Paulo/BR

A Case of Angiomatous Fibrous Histiocytoma of the Forearm

S. Ali, Birmingham/UK

Nasopharyngeal anlage tumor in a neonate with the initial presentation of respiratory difficulty: Correlation between imaging and clinicopathologic findings

P.-S. Tsai, Taipei/TW

Sonographic Detection Of Intussception With Malrotation: Waughs Syndrome

A. Sulaiman, Chennai/IN

A rare case of epidermal naevus syndrome

P. Joshi, Pune/IN

Bilateral axillary lump in a newborn diagnosed as hematoma

M. Haliloglu, Ankara/TR

Pediatric colorectal carcinoma presenting as misleading abdominal pain: A case report

A. Cavaliere, Padua/IT

Lemierre syndrome: A diagnostic dilemma in paediatric patients

V. Bhalla, Birmingham/UK

When the Working Hypothesis of Meningitis Could Not Help

E. Kovacs, Budapest/HU

Radial pattern of femoral head edema in chronic non-bacterial osteomyelitis (CNO)

M. Raissaki, Heraklion/GR

15:00-16:00 Scientific Session: Oncology and whole body imaging — Room 2

Detection and prevalence of pulmonary nodules in young children with and without cancer
M. Verhagen, Amsterdam/NL

The acquisition of a diagnostic CT improves the diagnostic value of combined integrated FDG PET/ CT in pediatric oncology
C. Loberg, Aachen/DE

Comparison of the Detectability of UBOs in Neurofibromatosis Type I patients with Proton density-weighted and FLAIR sequences in 3T MRI
L. Porto, Frankfurt/DE

Assessment of radiation doses from diagnostic imaging in the follow-up of paediatric oncology patients
P. Logan, London/UK

MRI-based evaluation of multiorgan iron overload is a predictor of adverse outcomes in pediatric patients undergoing allogeneic hematopoietic stem cell transplantation
F. Zennaro, Nice/FR

Quantitative Diffusion weighted MR Imaging in children with Neuroblastoma
B. Ammann, Ulm/DE

Pulmonary Nodule Detection and Characterisation in Children with Wilms Tumours: Do Radiologists Agree?
S.C. Shelmerdine, London/UK

Whole-Body MRI (WB-MRI) in the diagnosis of children with fever without a focus
J. Delgado, Philadelphia/US

Subjective Differences in Solid Tumor Measurements by Pediatric Radiologists Results in Inconsistent Reporting of Tumor Burden Which Could Adversely Affect Treatment Decisions
R.B. Towbin, Phoenix/US

Quail-quantitative MRI-based evaluation of pancreatic iron overload in pediatric patients undergoing allogeneic hematopoietic stem cell transplantation
F. Zennaro, Trieste/IT

15:00-16:00 Task Force Session: Child abuse — Room 3

Welcome
A. Offiah, Sheffield/UK

The updated RCR/RCPCH Guidelines for Imaging in Suspected Physical Abuse: Revisions and Rationale
K. Halliday, Nottingham/UK

Summary of the Swedish Agency for Health Technology Assessment and Assessment of Social Services' Document on the Triad of Shaken Baby Syndrome (SBU report)
M. Raissaki, Heraklion/GR

Initial response and actions by the ESPR and SPR
A. Offiah, Sheffield/UK

Discussion, Future Plans and Proposals for Collaborative Research
A. Offiah, Sheffield/UK; M. Raissaki, Heraklion/GR

16:00-16:30 Break

16:30-17:15 jESPeR lecture — Room 1

Common artefacts in paediatric MRI – How to recognise, avoid or take advantage of them
Ch. Kellenberger, Zurich/CH

17:15-18:00 General Assembly — Room 1

Saturday, June 03, 2017

07:45-08:45 Special Focus Session: Radiology of child abuse: From head to toe — Room 1

Broken Bones & Brittle Bones: Novel Research Approaches
A. Offiah, Sheffield/UK

Neuroradiology in child abuse
N. Girard, Marseille/FR

08:45-09:00 Break

09:00-10:00 Task Force Session: Fetal and postmortem — Room 2

Advances in Post Mortem Imaging
O. Arthurs, London/UK

International PM CT protocols
Ch. Gerrard, Albuquerque/US

Post Mortem imaging research: Updates and future proposals
O. Arthurs, London/UK

09:00-10:00 Scientific Session: Cardiac and thoracic — Room 3

Comparison of Chest X-ray findings in ambulatory and hospitalised children with suspected pulmonary TB
S. Andronikou, Bristol/UK

Lung ultrasound in pediatric pneumonia - why is it necessary to use the additional trans-abdominal approach?
J. Lovrenski, Novi Sad/RS

Is thoracic ultrasound really competitive to computed tomography in children – A two-year retrospective study
J. Lovrenski, Novi Sad/RS

The value of lateral chest X-rays for the diagnosis of lymphadenopathy in children with pulmonary tuberculosis
S. Andronikou, Bristol/UK

Pitfalls encountered when setting up a 4D CT service for dynamic airway imaging in children
S. Andronikou, Bristol/UK

Assessment of airway compression on chest radiographs in children with pulmonary tuberculosis
S. Andronikou, Bristol/UK

Paediatric Ultrasound-guided Biopsies in a Tertiary Oncology Centre: Five Years Experience
M. Smedley, Oxford/UK

The role of imaging in the diagnosis of thymoma in paediatric patients with myasthenia gravis
J. Adu, London/UK

Increased Risk of Venous Thrombosis of the Arm with Multiple Peripherally Inserted Central Catheters Insertion in Paediatric patients
R. Gnannt, Zurich/CH

Diagnostic performance of lung ultrasound for the detection of community acquired pneumonia in children
J. A. M. Stadler, Paarl/ZA

10:00-11:00 Case Report Presentation Session — Room 1

'White-out' on plain chest radiograph- a late presentation of congenital diaphragmatic hernia
A. Fagan, Peterborough/UK

Ovarian tuberculosis with peritoneal dissemination mimicking ovarian tumor with peritoneal seeding
H.M. Lederman, Sao Paulo/BR

Langerhans'-cell histiocytosis with thoracic involvement in infant and young child: CT findings
S.-L. Shih, Taipei/TW

Case of fungal infection of the soft tissue in a child with acute myeloid leukemia (ultrasound aspects of diagnosis)
I. Begun, Minsk Region/BY

Unfortunate outcome of the first infantile hepatic hemangioendothelioma to be diagnosed in the district of Bethlehem due to lack of medical experience with such rare cases
R. Albad, Bethlehem/PS

Fatal Outcome of Acute Gastric Dilatation Causing Acute Abdomen Compartment Syndrome in a Child: A Case Review
C.S. Yoon, Seoul/KR

Pleuroperitoneal fistula in a pediatric patient with primary hyperoxaluria type 1
W.P. Chu, Hang Hau/HK

Osteosarcoma with Pulmonary Intra-arterial Tumor Embolism Metastasis
A. Alzaher, Dammam/SA

Endovascular embolization of left gastric artery pseudoaneurysm for acute upper gastrointestinal hemorrhage in a child with pancreatitis
J. Donnellan, Toronto/CA

A case of neonatal hemochromatosis
G. Perucca, Torino/IT

Fishing for the answer – A rare case of paediatric exogenous lipoid pneumonia secondary to fish oil aspiration
H. Moodley, Johannesburg/ZA

The possible role of visual evaluation of DWIBS in childhood renal masses based on our five cases
E. Varga, Budapest/HU

MR Urography in a 9-years-old female with unusual urinary dribbling
S. Salerno, Palermo/IT

Agenesis of the dorsal pancreas: Case report
A. Giovagnoni, Ancona/IT

10:00-11:00 Scientific Session: Fetal and postmortem — Room 2

Malformations of cortical development associated with corpus callosum dysgenesis (CCD): Diagnostic value of foetal MRI in prenatal counseling
A. Antonelli, Rome/IT

Recognition of Neonatal Lymphatic Flow Disorder: Fetal MR Findings and Postnatal Dynamic MR Lymphangiogram Correlation
D.M. Biko, Philadelphia/US

Congenital bronchopulmonary malformation: Prenatal MR and postnatal CT and histopathological correlation
M. Koci, Prague/CZ

Real Time Virtual Sonography: A new integrated approach for the evaluation of fetal cerebral pathologies?
S. Bernardo, Rome/IT

Role of foetal MRI in the evaluation of ischaemic-haemorrhagic lesions of the foetal brain
S. Bernardo, Rome/IT

The contribution of mid-trimester virtual autopsy with MR imaging
A. D'Hondt, Brussels/BE

Diffusion coefficient and perfusion fraction parameters correlate with gestational age in normal human in vivo placenta: A preliminary study
A. Antonelli, Rome/IT

Central Nervous System involvement in congenital heart diseases: Is fetal MRI mandatory?
A. Antonelli, Rome/IT

First experiences and diagnostic utility of micro-CT for fetal autopsy
J.C. Hutchinson, Newcastle upon Tyne/UK

Investigation of perinatal body organ diffusion-weighted post mortem MRI
S.C. Shelmerdine, London/UK

10:00-11:00 Scientific Session: Abdominal (GI & GU) Imaging — Room 3

Usefulness of combined grey-scale and color Doppler ultrasonography(US) findings in the evaluation of acute pyelonephritis in children
K. Lee, Anyang/KR

Colonic Strictures in Children and Young Adults with Crohn's Disease: Recognition on MRE
D.M. Biko, Philadelphia/US

Disorders of sexual differentiations in neonates: Standardized sonographic evaluation and proposal of a reading grid
H. Lerisson, Lille/FR

Hepatic Shear Wave Elastography in Children under Free-Breathing and Breath-Hold Conditions
J. Herrmann, Hamburg/DE

Hydronephrosis and crossing vessels in children: Sensitivity of Colour-Doppler Ultrasound and Magnetic Resonance Urography
M.B. Damasio, Genoa/IT

Urosonography - Nonradiant alternative for voiding cystourethrography
O.M. Fufezan, Cluj-Napoca/RO

New sonographic features useful in differentiating congenital duodenal anomalies from malrotation: Gastric and duodenal wall thickening and hyperechogenicity
P. Caro Dominguez, Cordoba/ES

A Measure of Renal Morphology as an Indicator for Potential Renal Failure
A.C. Eichenberger, Zurich/CH

Factors that can distort the DJ flexure mimicking malrotation
V. Bhalla, Stoke-on-Trent/UK

16 year experience of Native Paediatric Renal Biopsies
K.S. Minhas, London/UK

11:00-11:15 Break

11:15-12:00 Awards & Closing remarks — Room 1

G. Eich, Aarau/CH; J. Schneider, Basle/CH

12:00 Farewell & Invitation to ESPR 2018 — Room 1

Invited Abstracts - 53rd Annual Meeting
Special Focus Sessions, Task Force Sessions

Abstracts appear as submitted to the online submission system and have not been checked for correctness and completeness.

THURSDAY, JUNE 01, 2017

SESSION: SPECIAL FOCUS SESSION: EMERGING INFECTIOUS DISEASES: ZIKA VIRUS INFECTION

Pre- and Postnatal Imaging in Zika virus: Where are we?

P.A.N. Daltro, H. Werner, F. Lopes; Rio de Janeiro/BR

Summary:

INTRODUCTION: Zika virus (ZIKV) infection has been associated with several malformations of the fetal central nervous system (CNS)[1,8].The virus was first described in a Rhesus monkey in Uganda in 1947, followed by reports of the virus in East and West Africa and Southeast Asia. The ZIKV is transmitted mainly by the bite of female *Aedes aegypti* and *Aedes albopictus* mosquitoes. Other forms of transmission, including through sexual intercourse, blood transfusion, and neonatal, are currently under evaluation, although more elements are still needed to assess the real importance of these transmission routes[4].

The course of the ZIKV infection is self-limited. So far, no specific symptoms have been attributed to the disease, and a wide variety of manifestations ranging from absent to mild symptoms (in 25% of cases) have been described. When symptoms are present, they may lead to a misdiagnosis of other bacterial and viral infections, especially other arboviroses in endemic areas. The most frequently reported symptoms are mild fever, cutaneous rash, fatigue, arthralgia/myalgia, and conjunctivitis. Dizziness, malaise, edema of the extremities, anorexia, retro orbital pain, photophobia, gastrointestinal disorders, sore throat, cough, sweating, and lymphadenopathy have also been reported. Infection by the ZIKV in adults may be associated with autoimmune complications such as Guillain-Barré syndrome[9].

The laboratory diagnosis of ZIKV infection is based on the demonstration of the virus in the urine and blood using real-time reverse transcription polymerase chain reaction (RT-PCR). The main limitation of this diagnostic method is a false-negative result after the viremia is resolved. The serological diagnosis of the disease is limited due to cross-reactivity of the ZIKV with other viruses of the *Flavivirus* genus, especially those causing dengue and chikungunya. Physicians should be aware of this fact when the diagnosis of ZIKV infection relies solely on serological results. The diagnosis is also possible by IgM measurement in serum, urine, or cerebrospinal fluid using enzyme-linked immunosorbent assay (ELISA)[9].

The prevention against ZIKV infection is similar to that of other arboviroses, including vector control and mosquito bite prevention.

The first major ZIKV epidemics were reported in the French Polynesia in 2013 and 2015. At that time, some neurological changes were observed in neonates of infected pregnant women but were not associated with a maternal-fetal transmission of the virus. The growing increase in the number of cases and the severity of the infection specific to this subpopulation then led to the evidence of a congenital disease[9].

In Brazil, the situation became alarming with the report of a high number of infected individuals in the second half of 2015[2,5]. The Brazilian Ministry of Health attributed to congenital ZIKV infection the 20-fold increase in cases of neonatal microcephaly in the northeastern part of the country, particularly in the state of Pernambuco. This led the World Health Organization (WHO) to declare the ZIKV infection a "public health emergency of international concern" in February 2016[6].

The main challenge for radiologists practicing in regions of endemic ZIKV infection is to become familiarized with findings of congenital ZIKV infection in perinatal imaging studies; this is particularly important for the prenatal screening of pregnant women[3,6]. The diagnosis of ZIKV infection in the fetus by neuroimaging is based on prenatal ultrasound (US), especially in the third trimester, and complemented with magnetic resonance imaging (MRI).

Postnatal imaging was obtained by transfontanellar US, CT or MRI.

The main imaging findings on CT are microcephaly, an exuberant external occipital protuberance, rectification of the frontonasal angle, and a redundant scalp skin. Three-dimensional (3D) reconstruction of al skull permits a better evaluation of these findings and enhances the parents' understanding of the disease. Moreover, CT scan data may yield a 3D virtual physical model that can maybe obtained from CT scan data and printed onto using thermoplastic acrylonitrile butadiene styrene[7].

The aim of this study was to describe the perinatal imaging findings in cases of congenital ZIKV infection.

METHODS:

We studied 18 mothers diagnosed with ZIKV infection from October 2015 to November 2016. They had all presented a maculopapular rash and fever during the first or second trimester of pregnancy, and their neonates presented neurological defects that were attributed to intrauterine transmission of the ZIKV. The maternal diagnosis of ZIKV infection was confirmed by serology (n=4) or RT-PCR (n=14). All patients were TORCH (toxoplasma, rubella, cytomegalovirus, herpes simplex) negative. Prenatal US was performed every 3 weeks after the first imaging findings, and fetal MRI was obtained in all cases. Microcephaly was considered present when the infant's head circumference was two standard deviations below the mean value for age and sex or below the second percentile. Postnatal imaging follow-up was obtained in all cases by transfontanellar US, CT or MRI.

RESULTS:

We found several CNS malformations, including lissencephaly, pachygyria and/or polymicrogyria, cerebral atrophy (Panel 1), enlarged cisterna magna with abnormalities of the corpus callosum, ventriculomegaly, brainstem hypoplasia, malformation of the cortical development, and cortical and/or periventricular calcifications mainly in the junction between the cortical and subcortical white matter (Panel 2). The skull of the infants had a collapsed appearance, with overlapping sutures and redundant skinfolds (Panel 3). Craniofacial disproportion was easily identifiable, and arthrogryposis was identified in one case. Similar neurological findings were observed in the infected patients and seemed to differ from findings of other infectious diseases.

CONCLUSIONS:

The finding of microcephaly in neonates with congenital ZIKV infection seems to be only the tip of the iceberg, as several CNS malformations have been identified in connection with the disease. In Brazil, a spectrum of imaging findings associated with congenital ZIKV infection has been observed. Such findings are useful in helping radiologists to identify suspected cases of the disease.

References:

1) Aragao MFV, Linden V, Brainer-Lima AM, Coeli RR, Rocha MA, Silva PS, Carvalho MDCG, Linden A, Holanda AC, Valenca MM. Clinical features and neuroimaging (CT and MRI) findings in presumed Zika virus related congenital infection and microcephaly: retrospective case series study. BMJ. 2016; 353: i1901.

2) Brasil P, Pereira JP Jr, Moreira ME, et al. Zika virus infection in pregnant women in Rio de Janeiro. N Engl J Med. 2016; 375 (24): 2321–34.

3) Guillemette-Artur P, Besnard M, Eyrolle-Guignot D, Jouannic JM, Garel C. Prenatal brain MRI of fetuses with Zika virus infection. PediatrRadiol. 2016; 46: 1032–39.

4) ISUOG. ISUOG Interim Guidance on ultrasound for Zika virus infection in pregnancy: information for healthcare professionals. Ultrasound Obstet Gynecol. 2016; 47(4): 530-532.

5) Oliveira Melo AS, Malinger G, Ximenes R, Szejnfeld PO, Alves Sampaio S, Bispo de Filippis AM. Zika virus intrauterine infection causes fetal brain abnormality and microcephaly: tip of the iceberg? Ultrasound ObstetGynecol 2016; 47: 6–7.
6) Soares de Oliveira-Szejnfeld P, Levine D, Melo AS, et al. Congenital brain abnormalities and Zikavírus: What the radiologista can expect to see prenatally and postnatally. Radiology 2016; 282: 203-218.
7) Werner H, Fazecas T, Guedes B, Lopes dos Santos J, Daltro P, Tonni G, Campbell S, AraujoJúnior E. Intrauterine Zika virus infection and microcephaly: correlation of perinatal imaging and three-dimensional virtual physical models. Ultrasound Obstet Gynecol. 2016; 47(5):657-660.
8) Werner H; Sodre D, Hygino C, Guedes B, Fazecas T, Nogueira R, Daltro P, Tonni G, Lopes dos Santos J, Araujo Júnior E. FirsttrimesterIntrauterineZikavirusinfectionandbrainpathology: prenatalandpostnatalneuroimagingfindings. PrenatalDiagnosis 2016; 36: 1-5.
9) ZareMehrjardi M, Poretti A, Huisman TAGM, Werner H, Keshavarz E, AraujoJúnior E. Neuroimaging findings of congenital Zika virus infection: a pictorial essay. Jpn J Radiol. Published online January 2017.

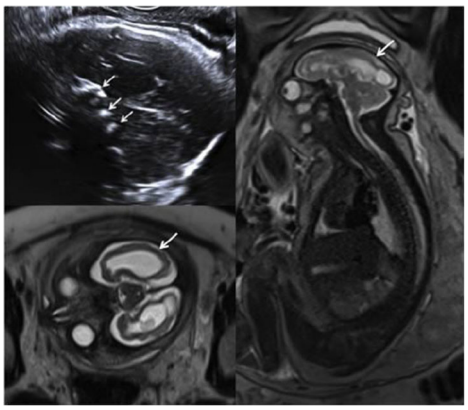

Panel 1: Prenatal ultrasound (37 weeks) shows calcifications (arrows) and microcephaly. Axial and sagittal T2 shows relative smoothness of the brain surface (arrows) and assymmetric colpocephaly.

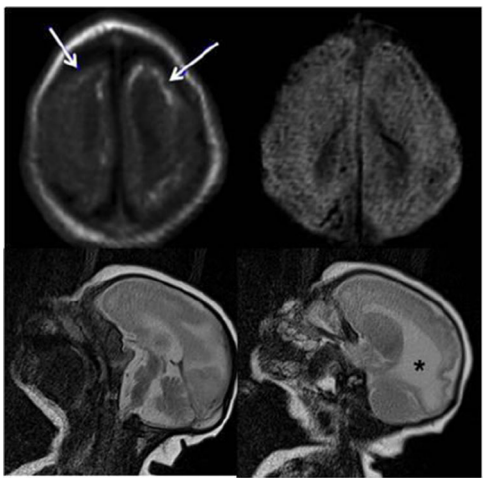

Panel 2:Ax T1-WI multiple cortical-subcortical fronto-parietal hyperintense foci (arrows) and markedly hypointense on SWI. Sagittal T2: dysgenesis of the corpus callosum, with dilation of the posterior horns of the lateral ventricles (colpocephaly).

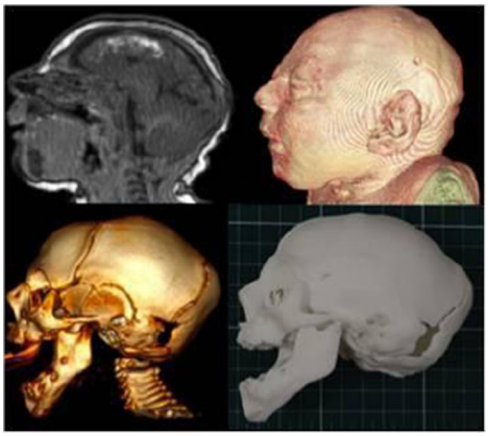

Panel 3: Sag T1-WI showing sharpenedfrontoparietal parenchyma, with poverty of sulci and gyri and extensive subcortical calcifications. 3D sagittal reconstruction obtained by MRI. 3D sagittal reconstruction from CT and corresponding 3D printing. Note

Take home points:

- Zika virus (ZIKV) infection has been associated with several malformations of the fetal central nervous system (CNS) and is transmitted mainly by the bite of female *Aedes aegypti* and *Aedes albopictus* mosquitoes.
- The course of the ZIKV infection is self-limited. The most frequently reported symptoms are mild fever, cutaneous rash, fatigue, arthralgia/myalgia, and conjunctivitis.
- The main challenge for radiologists practicing in regions of endemic ZIKV infection is to become familiarized with findings of congenital ZIKV infection in perinatal imaging studies
- The CNS malformations including lissencephaly, pachygyria and/or polymicrogyria, cerebral atrophy, enlarged cisterna magna with abnormalities of the corpus callosum, ventriculomegaly, brainstem hypoplasia, malformation of the cortical development, and cortical and/or periventricular calcifications. The skull of the infants had a collapsed appearance, with overlapping sutures and redundant skinfolds and craniofacial disproportion was easily identifiable.

Pre- and Postnatal Imaging in Zika virus: Where are we? Early insights into Zika's Microcephaly physiopathology, from the epicenter of the outbreak: a case for teratogenic apoptosis of central nervous system.

P. Jungmann; Recife/BR

Summary:
Early insights into Zika's Microcephaly physiopathology, from the epicenter of the outbreak: a case for teratogenic apoptosis of central nervous system.
In mid-October 2015, intense interaction among surgical pathology and fetal medicine specialists from University of Pernambuco was only focused on the dramatic and non explained Ultrasonographic (US) findings and hopelessness due to lack of explanations on the odd US discoveries on the first gestational cases of Zika's microcephaly. This is the field of our history of a physiopathological hypothesis on Zika virus (ZIKV) related microcephaly when it first struck Pernambuco state (PE), Northeast Brazil, the place that has been at the front line of the global response to the microcephaly and responsible for a large amount of data from affected children. The outbreak onset came with a sudden increase in microcephalic newborns being reported in PE state from August 2015 (Panel, Fig. 1).
ZIKV was previously thought to cause a relatively mild disease, but was recently accepted to lead to severe and diverse neurologic conditions in

some children born from infected mothers and in adults[1]. The scientific community is actively trying to uncover the extent of these disorders but little has been reported on the early days of the outbreak when doctors were approaching the unknown. While evidence that ZIKV is related to microcephaly in newborns is accumulating, the mechanisms of how the virus affects the fetus is still uncertain. In the outbreak onset we had to face daunting challenges to search the cause of microcephaly and the emotional toll on the families. We took a very early approach from 9 microcephalic fetuses on gestation and 46 microcephalic babies on clinical follow-up from different PE areas, evaluated between 15 October and 17 December 2015 in Oswaldo Cruz Hospital, to propose the early physiopathologic hypothesis that, a viral-related brain developmental disruption could be the basic neuropathogenesis in ZIKV babies instead of a direct injurious process due to viral insult followed by active inflammation.

The eight pregnant women were all in the 3rd gestational trimester and had had normal US follow-ups till week 20th. Crucially, we were facing a temporal-geographic association of cases presenting an unanticipated pattern of US alterations. Because of their late alarming findings they were re-examined and the US scans revealed sudden encephalic alterations after 28 th gestational week. Such devastating US clustering images were not seen here before, but are now considered as part of the "congenital ZIKA syndrome". We observed late appearing severe dysmorphic encephalic changes in 9 out of 9 fetuses, including small skull, small brain, sub arachnoidal space enlargement, ventricular dilation, brain calcifications of varied shape and distribution, inclined frontal bone, progressive decline of head growth potential, early fontanels closure and redundant scalp (Panel, Figs. 2A, 2B). We had no clues on the causes and mechanisms responsible for this phenotype of severe alterations. Thus, we had no explanation to offer to patients, in particular, or to the medical community. Both as physicians and human beings, we were committed straightaway to continue the study of these victims of an unknown medical tragedy, engaging our expertise in fetal imaging and immunopathology.

From beginning October, the first microcephalic babies were referred to the UPE Pediatric Infectology Service for initial investigation. Strikingly, the newborns exhibited "healthy" appearance, excluded the microcephaly itself and motor sequels. We then looked for CSF analysis of the microcephalic babies. For that, we obtained from Dr. Patricia Travassos, a CSF specialist at UPE, a cohort of 120 CSF samples that have been studied for signs of meningitis or encephalitis. About 87% (42 cases) of the CSF analyzed looked normal for any signs of central nervous system ongoing inflammatory responses (Panel, Fig. 3). The babies had been examined by outpatient clinic Dr Angela Rocha, from the UPE Hospital Infectology Reference Center that have stated that although small, the babies were near to full term gestation (36-39 weeks gestation), had good Apgar scores and variable degrees of microcephaly and neurologic impairments, i.e. contractures, spasms, irritability and in some retinal macular atrophy. During the follow-up, the babies were cared at home, breastfeeding, gaining weight and having routine vaccines. None of them expressed signs of ongoing inflammatory reaction in the CNS (Panel, Fig. 4) or alterations on peripheral blood count and other routine laboratory tests up to 3 months of age. Despite the striking neurological phenotype, 80% of the babies were negative for TORCH agents, no deaths were recorded. Furthermore only in January 2016, the first evidence associating ZIKV to microcephaly from RT-PCR test on amniotic fluid was reported[2].

Astonishingly, a particular kind of physiopathological process linked to fetal brain development was arising without clinical manifestation of inflammatory reactions or necrotic processes in these babies. Unfortunately, no necroscopic samples of affected brain tissues were available to us to monitor the presence of putative neural dysgenesis and the very nature of brain calcifications background offering histological support for our hypothesis. Nevertheless, with this restricted dataset we hypothesized that whatever the etiologic agent involved in these cases, its physiopathologic mechanism must trigger the cellular death program - the apoptotic process - at a particular development window on the CNS, assuming clinically that the agent was not encephaalitogenic but silently tertogenic. If not, the clinical outcome of affected babies would not be so mild as far as signs of inflammation on CNS was concerned. Consequently, the inflammation-free clinical status of patients suggested us that a massive enhanced apoptotic cell death during the window of telencephalic expansion was the most probable physiopathologic process operating this microcephaly phenotype, with no direct direct lytic brain lesion or significant necrosis due to usual injury. Furthermore, Knowles and Penn [3] stated that this window is very active to select the "fittest" neural cells by a constitutive apoptotic pathway. We so hypothetized that during this developmental time window, the "fit or not fit" status of the rapid, transient amplifying neural progenitors cells facing ZIKV, would heavily shift the selective process toward the self-elimination of virus-bearing cells through apoptotic pathways. Thus, ZIKV-enhanced constitutive apoptotic mechanisms would lead a massive loss of developing telencephalic neuronal precursors and, consequently, provoking losses of dividing cells and the arrest of further brain development. This could be particularly inferred by the absence of the characteristic morphology of late stages structures of neocortex, according with our US images of ZIKV microcephalics in gestation. Similar processo could also be inferred to neurocrest derivatives as deformities in the viscercrany always accompany the cephalic malformation.

Our initial understandings based on clinical examination on the field, when no specific laboratory test, necroscopic data or experimental evidence on the disease causality were available, conducted our physiopathological approach to the "Apoptosis Hypothesis" for Zika microcephaly that is now gaining strong support. In February, Mlarkar et al[4] showed clear connection between ZIKV and microcephaly, presenting CNS histopathologic analyses, revealing remnants of neural germinative matrix, intense gliosis, alterations in cortical ribbon, calcifications in gray and white matters without associated necrosis, encephalitis or meningitis and the presence of the virus, further supporting neurodevelopmental arrest. Similar results were showed by Driggers et al[5]. The CT scans from microcephalic babies from Hazin at al [6], have added details of brain development arrest with no radiological signs of brain destruction or active inflammation. Finally, experimental models have provided a body of evidence f or neuroprogenitors permissiveness to ZIKV and viral-induced apoptotic process. Tang et al[7] demonstrated by ICQ that the ZIKV infection of cortical neural progenitors attenuates their growth and increases Caspase-3 activation, calling for an apoptotic process. This finding was corroborated by the up regulations of Caspase-3 genes by RNA sequencing. Nowakowsky et al [8] demonstrated that ZIKV may hijack AXL protein as an entryway to infection. Interestingly, AXL is highly abundant on the surface of neural stem cells but not on differentiated neurons in the developing brain. Recently, Cugola et al [9] demonstrated that ZIKV was able to cause CNS congenital brain dysgenesis upon vertical transmission in mice. In parallel, human brain organoids infected by ZIKV show a reduction of proliferative zones and disrupted cortical layers, so targeting cortical progenitors and inducing apoptotic cell death with impaired development.

For babies born with ZIKV-related microcephaly, the many expected consequences besides the evolving congenital neurosequels, are the unanticipated pattern of persistence of ZIKV in CNS host cells, unsafe maintenance of neuron genome stability on remaining arrested populations, implying risks for brain tumors, risks for impaired adult type neuron wiring and neuron survival in an affected neuronal circuitry. In brief, evolve life with a wide vulnerable brain.

The outbreak of ZIKV in the Americas will eventually decline as herd immunity increases, but the world remains at risk of further waves of infection in affected countries and spread into new territories[1]. While experimental studies will be carried out to fully understand the pathophysiology of ZIKV infection in the developing fetus, our findings provide a coherent and testable physiopathological hypothesis for CNS teratogenic phenotype linked to ZIKV congenital infection, which may be critical for the clinical care of pregnant mothers and their babies before and after birth.

Panel: Time-line sequence on microcephaly related events in Pernembuco State, Brazil from August to December 2015, til the formulation of the apoptotic hypothesis for Zika neuropthogenesis.

References:

1. PAHO. Preliminary guidelines for the surveillance of microcephaly in newborns in settings with risk of Zika virus circulation. ISBN 9789275-11888-7 (2016).

2. Oliveira Melo, A. S. et al. Zika virus intrauterine infection causes fetal brain abnormality and microcephaly: tip of the iceberg? Ultrasound Obstet. Gynecol. ***47,*** *6–7 (2016).*

3. Knowles, J. K. & Penn, A. A. Perinatal Brain Development, Malformation, and Injury. Colloq. Ser. Dev. Brain ***2,*** *1–84 (2011).*

4. Mlakar, J. et al. Zika Virus Associated with Microcephaly. N. Engl. J. Med. ***374,*** *951–958 (2016).*

5. Driggers, R. W. et al. Zika Virus Infection with Prolonged Maternal Viremia and Fetal Brain Abnormalities. N. Engl. J. Med. ***374,*** *2142–2151 (2016).*

6. Hazin, A. N. et al. Computed Tomographic Findings in Microcephaly Associated with Zika Virus. http://dx.doi.org/10.1056/NEJMc1603617 (2016).

7. Tang, H. et al. Zika Virus Infects Human Cortical Neural Progenitors and Attenuates Their Growth. Cell Stem Cell ***18,*** *587–590 (2016).*

8. Nowakowski, T. J. et al. Expression Analysis Highlights AXL as a Candidate Zika Virus Entry Receptor in Neural Stem Cells. Cell Stem Cell ***18,*** *(2016).*

9. Cugola, F. R. et al. The Brazilian Zika virus strain causes birth defects in experimental models. Nature ***534,*** *267 (2016).*

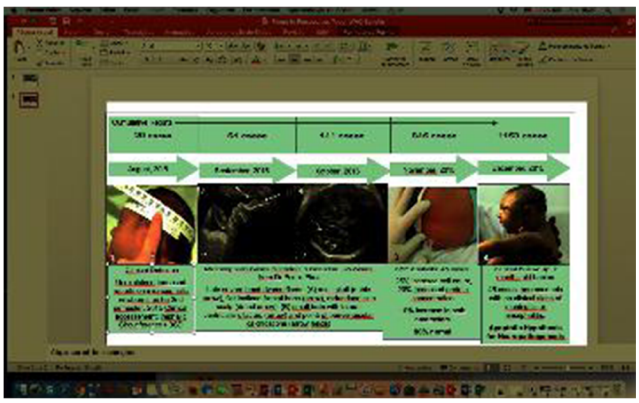

Take home points:

Fetal dysmorphisms detected by ultrassonographic and MRI images in Congenital Zika Syndrome are late findings, usually after the 20th gestational week and requires acurate analyses. Clinically, Zika's Virus Microcephaly is an infectiuos congenital condition that is not encephalitogenic but primarily teratogenic on the Nervous System. The most important process leading to Zika's Virus Microcephaly is pathologically induced apoptosis in telencephalic neuroprecursosrs cells and neurocrest precurssors cells. Viral induced autophagy and low antiviral responses during the fetal period are linked to Zika virus persistence in the central nervous system of affected new borns and babies

SESSION: ESPR MEETS CHOP

Applications of Susceptibility Weighted Imaging in Pediatric Neuroradiology

A. Vossough; *Philadelphia/US*

Summary:

Susceptibility-weighted imaging (SWI) has proven to be a valuable MR imaging sequence in a variety of applications. Pediatric imaging has also immensely benefitted from this technique. In this presentation we will review pediatric neuroimaging applications in trauma, arterial and venous vascular disorders, hypoxic-anoxic injury, congenital malformations, congenital heart disorders, neoplasms, and pediatric degenerative disease. Use of SWI in pediatrics other than demonstrating hemorrhage and calcification will be reviewed. Challenges in the clinical use of SWI in pediatrics, interpretive pitfalls, and sources of clinical misinterpretation of SWI will also be explored. We will also briefly present ongoing research and clinical use of SWI in pediatrics and potentials for future collaborative investigations.

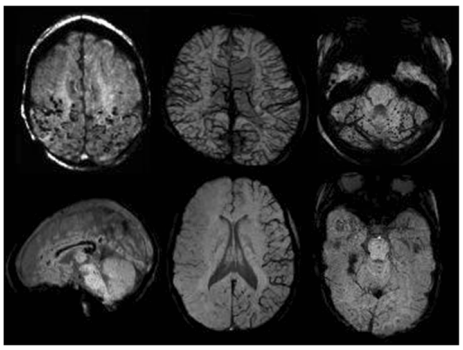

SWI in Various Disease States

Take home points:

- SWI is highly sensitive in detection of susceptibility effects on MRI.
- In many cases, but not all, SWI processing can differentiate between calcium and blood products.
- There are some pitfalls in the interpretation of SWI that can lead to misdiagnosis.
- SWI is additionally helpful in assessement of cerebrovascular hemodynamics in conjunction with other MRI sequences.
- Quantitation information can also be obtained from SWI with further processing.

State of the Art Imaging of the Single Ventricle

D.M. Biko; *Philadelphia/US*

Summary:

There are many congenital heart defects that result in a functional single ventricle. This may be functional or anatomical as a result of a dysfunctional valve or absent or ineffective pumping chamber. The repair of single ventricle physiology most often involves a staged reconstruction due to changing physiology ultimately resulting in a total cavopulomonary connection or Fontan procedure. To appropriately image the single ventricle throughout its stages of palliation, familiarity with the physiology of the various steps in surgical palliation of the single ventricle is essential

Although echocardiography is a mainstay of cardiac imaging, cross sectional imaging has a vital role in the evaluation of the single ventricle. The role of CT angiography is mostly for anatomic evaluation. Although it is fast and has high spatial resolution for evaluation of vasculature, CT has lower temporal resolution than MRI and is unable to quantify flow. Ventricular performance along with quantification of flow can be performed with MRI. Systemic to pulmonary collateral flow, which has been shown to result in adverse outcomes after Fontan, can be quantified. Valvular insufficiency and myocardial scarring can also be assessed. Additionally, high anatomic vascular detail can be obtained with MRI, particularly with the recent investigational use of the blood pool agent ferumoxytol. MRI also has the ability to assess the lymphatics either through non-contrast T2 weighted imaging and/or dynamic contrast MR lymphangiography as lymphatic pathology may play a role in post-surgical hemodynamics in single ventricle patients.

This lecture will focus on the use of CT and MRI in the evaluation of the single ventricle particularly concentrating on the developing use of MRI for anatomic and physiologic assessment.

Take home points:
In single ventricle physiology, there is only one effective pumping chamber. Familiarity with the physiology of the various steps in surgical palliation of the single ventricle is essential in imaging this disorder CT angiography provides high anatomic detail but limited in its assessment of physiology since it cannot quantify flow and has lower temporal resolution than MRI. MRI can evaluate ventricular performance, quantify flow and valvular insufficiency, and assess myocardial scarring. High anatomic vascular detail can also be obtained with MRI particularly with the emerging investigational use of ferumoxytol. With non-contrast T2 weighted MRI and/or dynamic contrast MR lymphangiography, lymphatic evaluation can be performed which may play a role in post-surgical hemodynamics in single ventricle patients.

SESSION: TASK FORCE SESSION: NEURO

Neuroimaging in Head Trauma

M. Argyropoulou, G. Alexiou; Ioannina/GR

Summary:
Objective: Head trauma in children is one of the most common reasons for visiting emergency department. However, only a small portion of patients will have a traumatic brain injury. Patients with moderate or severe head trauma should undergo CT scan, however, a debate exists for the indication and yield of neuroimaging for minor head trauma. We performed a systematic literature review on the accuracy of symptoms and signs in children with minor head trauma in order to identify those with severe intracranial injuries.
Materials: A systematic literature search of MEDLINE (2000-2016) was performed to identify studies assessing the diagnosis of intracranial injuries in children. The authors independently performed critical appraisal and data extraction.
Results: We identified studies that evaluated the performance of findings for detecting intracranial injury using the reference standard of neuroimaging or follow-up examination. Mechanism of injury, multiple vomiting episodes and decline in GCS score were more commonly associated with severe intracranial injury on CT.
Conclusion: Combinations of history and physical examination features in clinical decision rules can timely identify patients with head trauma at risk of severe intracranial injuries.

Take home points:
History and physical examination features can timely identify patients with head trauma at risk of severe intracranial injuries.

SESSION: TASK FORCE SESSION: MSK- IMAGING IN JUVENILE IDIOPATHIC ARTHRITIS (JIA) - AN UPDATE

Normal MR-findings mimicking pathology of the wrist

D. Avenarius[1], L.-S. Ording-Müller[2], K. Rosendahl[3]; [1]Tromsø/NO, [2]Oslo/NO, [3]Bergen/NO

Summary:
Normal variations in the amount of joint fluid, ganglion cysts, bone marrow edema, and bony depressions that resemble erosions are frequent in the wrists of children. The results of a follow-up of a healthy cohort aged 6-17 will be presented. The cohort was examined twice with MR of the wrist, and the second time also with a cartilage sequence for better visualization of the bony depressions. Knowledge of these normal variations is important because they can resemble disease.
Bone marrow edema, joint fluid more than 2 mm, and bony depressions that can resemble erosion are frequent findings in the normal wrist.

Take home points:
Bone marrow edema, joint fluid more than 2 mm, and bony depressions that can resemble erosion are frequent findings in the normal wrist. These findings can not be attributed to dissease without additional findings of synovitis. A cartilage sequence can be of use in the differentiation between true erosions and bony depressions.

MRI scoring of the wrist in patients with JIA-Current status and future perspectives

C. Nusman; Amsterdam/NL

Summary:
The wrist is a frequently affected joint in patients with juvenile idiopathic arthritis. Due to recent improvements in treatment strategies, permanent damage is not that common anymore. Also, imaging has been playing a key role in monitoring the disease activity in the wrist of JIA patients. The past years lots of efforts have been made to improve the assessment of acute and permanent changes of the JIA wrist. Requisites and recommendations for the MRI protocol to use for of the JIA wrist are available in literature. Currently, the features of scoring the JIA wrist are synovitis, tenosynovitis, bone marrow edema and bone erosions. The repeatability of the above-mentioned scoring features proved to be acceptable. Recent studies showed that the appearance of the wrist in healthy children can mimic pathology. Therefore, construct validity of the scoring features needs to be assessed by comparing wrists of healthy children with the wrists of JIA patients.

Take home points:
- Features of scoring the JIA wrist are synovitis, tenosynovitis, bone marrow edema and bone erosions.
- The repeatability of the above-mentioned scoring features proved to be acceptable.
- Requisites and recommendations for the MRI protocol to use for of the JIA wrist are available in literature.
- The appearance of the healthy growing wrist in children can mimic pathology.
- Construct validity of the scoring features needs to be assessed by comparing wrists of healthy children with the wrists of JIA patients

A novel radiographic scoring system for permanent hip involvement

L. Tanturri de Horatio[1], P.L. Di Paolo[1], S.C. Shelmerdine[2], P. Toma[1], K. Rosendahl[3]; [1]Rome/IT, [2]London/UK, [3]Bergen/NO

Summary:
Approximately 20-50% of children with JIA, particularly those with systemic onset disease, will have hip-involvement within 1-6 years after disease onset. As scoring systems for radiographic changes in children with hip involvement are lacking, we aimed to examine the reliability of potential markers and suggest a novel scoring system.
A set of 75 hip-radiographs from 75 children with JIA and clinical hip-involvement: 59 seen at the outpatient clinic at Great Ormond Street Hospital (GOSH), London, and 16 seen at Ospedale Pediatrico Bambino Gesù, Rome, was used. All hip radiographs were scored in a blinded fashion, once by an experienced paediatric radiologist and a paediatric radiologist with minor experience in musculo-skeletal imaging in Rome, and twice by an experienced radiologist and a research fellow in Bergen/London. Radiographic findings suggestive of 1) destructive change (bone erosion, flattening of the femoral head, squaring of the femoral head contour, presence of sclerosis, joint space height, and 2) growth abnormality (length and width of the femoral neck, varus/valgus deformity, the CCD angle and the trochanteric-femoral head height) were assessed.
Assessment of erosions of the femoral head, femoral neck and the acetabulum showed moderate to good agreement for the same reader. The inter-reader agreement was, however lower. There was a high to moderate

agreement for the assessment of femoral head flattening using the Mose' circle. The measurements of femoral neck length and width, the CCD and trochanteric-femoral head lengths were precise, with 95% limits of agreements within 10-15% of the mean.
We have identified a set of relative robust radiographic findings suggestive of growth abnormalities and destructive change in children with hip-JIA, and suggested a novel scoring system.

X-ray of a 21 years-old JIA patient with severe chronic hip involvement.

X-ray of a 6 years-old boy with growth abnormalities on hips (bilateral coxa magna).

Take home points:
In JIA hip involvement is often a predictor of a severe disease course.
Radiographic findings vary according to mode of onset and age: in younger children the initial findings may be developmental rather than destructive while children with later onset JIA may have destruction/narrowed joint space as the first feature.
Several of the commonly used radiographic findings for chronic hip-change are inaccurate.
We have identified a set of relative robust radiographic findings suggestive of growth abnormalities and destructive changes in children with hip-JIA, and suggested a novel scoring system.

Bone age assessment – Statement from the MSK task force
K. Rosendahl; Bergen/NO

Summary:
Age assessment is an important, yet complex and challenging issue that authorities may need to perform to determine whether an individual is an adult or a child in circumstances where their age is unknown. There is currently no method which can identify the exact age of an individual and there are concerns about the invasiveness and accuracy of the methods in use, namely analysis of documentary evidence, interviews, physical or other form of medical examination such as imaging.
The main imaging methods include carpal, collar bone and dental examinations. Whilst many countries make use of these methods they do not apply them in the same way and often use different combinations and/or order. One of the main reasons for this is the fact that age assessment procedures remain to a large extent determined by national legislation, with procedures evolving through national jurisprudence (Ref.: European Asylum Support Office (EASO Age Assessment Practice in Europe)). The ethical and legal aspects of using bone age to determine age will be addressed in a statement from the MSK task force.

Take home points:
The ethical and legal aspects of using bone age to determine age will be addressed in a statement from the MSK task force.

SESSION: TASK FORCE SESSION: CT AND RADIATION DOSE

Establishing European Diagnostic Reference Levels for paediatric imaging: An update on the PiDRL project - Dr. C.M. Owens on behalf of the working PiDRL group
C.M. Owens; London/UK

Summary:
Little information exists regarding Diagnostic Reference Levels (DRLs) for paediatric examinations and procedures. The main reasons for this is are

a) that the number of examinations carried out in children is lower compared to adults and
b) data need to be categorised into age or weight subgroups.

The 'European DRLs for Paediatric Imaging' project (abbreviation: PiDRL) is a European Commission project that aimed to

a) develop a methodology for establishing and using DRLs for paediatric medical imaging and b) update and extend the European DRLs. The professional organisations involved include the ESR as coordinator, as well as EFOMP, EFRS, and ESPR, covering the key European stakeholders and professional groups with relevance to radiation protection of paediatric patients.
b) The PiDRL project has very recently drafted European Guidelines on how to establish and how to use paediatric DRLs.

The main recommendations of 'PiDRL European Guidelines' are in summary:
- All examinations resulting in high collective doses should have DRLs. This can include both the most common low dose examinations and the less common high dose examinations.
- The application of DRLs should be the responsibility of all providers of x-ray imaging. This means that DRLs should also be applied to imaging performed outside the radiology department.
- The physical quantity used to establish DRLs should be an easily measurable quantity, usually directly obtainable from the x-ray equipment console, obtained either by manual recording or preferably by automatic recording and analysis. Organ doses and effective dose are not considered feasible as a DRL quantity because these cannot be easily determined.
- The values used for patient dose monitoring, at the display unit and in the DICOM header should be regularly calibrated or checked for all beam qualities used in clinical practice.
- The parameters to group the patients should be patient weights for all body examinations and patient ages for all head examinations. For body examinations, in the transition period until data from weight-based patient dose surveys becomes available, age can be used as an additional grouping parameter and for the purpose of comparing proposed new weight-based DRLs with earlier age-based DRLs (trend analysis).

- The DRLs can also be given as a DRL curve by expressing the DRL quantity as a continuous function of the grouping parameter (e.g. DLP as a function of patient weight) provided the collected data for setting of the DRLs indicates a clear relationship between patient doses and the grouping parameter.
- The DRLs should be based on sufficient patient dose data determined or collected from the records of individual paediatric patients. Using data obtained only from typical protocol data or from measurements in phantoms is not recommended.
- National DRLs (NDRLs) should be based on national patient dose surveys with a representative sample of all radiological institutions and all types of equipment and practices in the country when practical.
- For NDRLs, by definition, the 3rd quartile or the 75th percentile value of the median (the 50th percentile) values of the distributions of patient doses obtained from a representative sample of radiology departments in the country should be determined, for a defined clinical imaging task (i.e., common indication based protocol) surveyed for standardised patient groupings.
- For the setting of DRLs, statistically relevant numbers of patient dose data should be collected. From each hospital or radiology department a representative sample of at least 10 patients per procedure type and per patient group is recommended for non-complex examinations such as radiography and CT, and at least 20 patients per procedure type and per patient group for complex procedures such as fluoroscopy and fluoroscopically guided procedures.
- In collecting the patient dose data for the DRLs, likewise in daily imaging practices, there should always be a system in place to judge whether image quality is adequate for the diagnosis according to the indication of the examination. This could be based, on image quality assessment of typical test cases by several radiologists, for example. The image quality requirement should be based on clinical grounds only.
- Due to the generally large amount of data needed and the large number of potential errors when these data are to be collected during routine practice, automatic data collection is recommended wherever possible.
- Besides the actual patient dose data according to the recommended patient grouping, other data from the examination characteristics (e.g. x-ray equipment type, exposure parameters, use of AEC) should be collected for evaluation and decision making when DRLs are to be established.
- Patient dose surveys for the basis of setting the NDRLs, should be conducted by the authoritative body which sets the DRLs or by another competent institution, with the collaboration of national professional/scientific societies or at least having recognised clinical experts as consultants in the process.
- The complete history of the patient dose surveys for the setting of DRLs, including all essential dosimetric and statistical information (e.g. quantities and their collected values, coverage of institutions and practices, sample sizes) should be documented and preferably reported.

The ultimate mission of EuroSafe Imaging is to support and strengthen medical radiation protection across Europe following a holistic, inclusive approach.

Most common imaging procedures in children and their contribution to collective dose

E. Sorantin[1], C. Granata[2]; [1]Graz/AT, [2]Genova/IT

Summary:
Several countries have released „Diagnostic Reference Levels (DRL)" for imaging procedures using ionizing radiation. Unfortunately those DRL differ in types of procedures and granularity as well as information about the proportion of pediatric patients within the different examinations are sparse.
Therefore an more evidence based approach seems to be feasable - meaning releasing DRL first for frequent and radiation burdened examinations.
Therefore a survey within Europe was conducted and a questionnaire was sent to key persons of the European Society of Pediatric Radiology (www.espr.org) as well to members of a large academic, interdisciplinary, international Network within the CEEPUS programme (Central European Exchange Programm for University Studies – www.ceepus.info).
Alltogether 33 centers were contacted and an response was received from 18 (54.5.%). From one center only frequencies for Interventional Radiology was sent.
Plain films: most frequent procedures are extremities (48.5%), followed by chest films (31.4%) - both account together for more than ¾.
Flouroscopy: voding cysto urethrography (VCU) 37.2%, followed by upper gastro intestinal (GI) series with 32.1% - again representing 2/3 of those examinations.
Computed Tomography: head & neck 46.8%, chest 27.8%, abdomen 13.7% - together almost 90%.
Interventional Radiology and cardiac interventions: only limited data available and procedures quite hardly standardize and comparable. It seems adviseable, that only a few procedures are suitable for DRL like peripheral insertion of vascular lines, occlusion of Ductus Arteriosus botalli or stent implantation for coarctation.
In order to estimate the contribution to the relative collective dose all values were normalized to a chest xrays (1.0) and the following numbers could be calculated: abdominal plain film 0.1, skull 0.01, CT Head 2.6, CT chest 10.2, CT Abdomen 4.5.

Take home points:
The most frequent imaging procedures using on ionizing radiation are: in plain films extremities and chest xrays in flouroscopy VCU and upper GI series in CT head, chest and abdomen
Therefore EU wide DRL should be released for those examinations. As it could be expected chest CT is the main contributor to the collective dose.

SESSION: TASK FORCE SESSION: ABDOMINAL (GI & GU) IMAGING

Introduction: Update Task force work and projects

M. Riccabona; Graz/AT

Summary:
Since the ESPR Abdominal (GI and GU) Imaging Task Force has changed its name and agenda, extending from initially only genitourinary queries to also other abdominal imaging topics, new projects have been added such as for example imaging in anorectal and cloacal malformations, imaging in paediatric inflammatory bowel disease (IBD, a joint project with ESGAR), or paediatric abdominal CEUS applications. Results of these new projects will be presented in the upcoming talks – hoping that again (as the last procedural recommendations and proposed imaging algorithms) our proposals and recommendations will help to standardise paediatric imaging, to reduce radiation burden, and to facilitate comparable imaging data for future research. Other topics in this session are a proposal for a more standardised approach to gastrointestinal ultrasonography, and considerations on Gadolinium applications in children in the light of new observations (i.e., Gadolinium deposit in tissue even in children with normal renal function).
The work goes on – only achievable with active participation of interested and competent members. Many interesting topics for either recommendations or joint research are on the list such as addressing late decompensating PUJO or specific imaging needs in IBD in early childhood; other new ones may be proposed by any task force member. Thus all ESPR members are invited to join the group, work with us and share their expertise.

Contrast enhanced US in childhood – Applications in children: Literature review and results from the questionnaire

C. Bruno; Verona/IT

Summary:

In adults, following the characterization of focal liver lesions, several applications of contrast-enhanced ultrasound (CEUS) have emerged in the last two decades, since second-generation contrast agents have been introduced and approved for use in most European countries.

From many points of view, children represent an ideal population for CEUS, because of the absence of radiation exposure and of need of sedation. Moreover, due to the small body size many anatomical targets in children can be adequately explored with high-frequency ultrasound, obtaining images with higher spatial resolution than in adults.

However, to date comparatively few data on pediatric CEUS are available. Although very rare and usually mild, possible adverse effects of contrast agents probably limit their use in many centers. In addition, the intravenous administration of ultrasound contrast agents in children is still off-label in Europe, which makes informed consent necessary in every case. Finally, for unclear reasons information on this topic does not flow easily.

Take home points:

- The use of CEUS in the identification and characterization of expansive, inflammatory, traumatic, vascular, and malformative disease of virtually all anatomical targets accessible to ultrasound has been proposed in adults, and further indications are under investigation. Levels of recommendation for CEUS have recently been defined for a large number of such conditions.
- From the comparison between the data available, similar or better results are likely to be obtained with CEUS in children than in adults, and some specific pediatric indications might be proposed.

Imaging in IBD–Joint recommendation statement with ESGAR

F.E. Avni[1], M. Napolitano[2], P. Petit[3]; [1]Brussels/BE, [2]Milan/IT, [3]Marseille/FR

Summary:

The first joint ESGAR/ESPR consensus statement on the technical performance of cross-sectional small bowel and colonic imaging (1)

Objective: to develop guidelines describing a standardized approach to patient preparation and acquisition protocols for magnetic resonance imaging (MRI), computed tomography (CT) and ultrasound (US) of the small bowel and colon, with an emphasis on imaging inflammatory bowel disease.

Methods: An expert consensus committee of 13 members from the European Society of Gastrointestinal and Abdominal Radiology (ESGAR) and European Society of Paediatric Radiology (ESPR) undertook a six-stage modified Delphi process, including a detailed literature review, to create a series of consensus statements concerning patient preparation, imaging hardware and image acquisition protocols in pediatric and adult patients.

The Delphi process is constructed as follow: *step 1* questionnaire construction to includes all contents relevant to the guideline and set up of working groups; *step 2* questionnaire completed by all committee member, *step 3* literature search; *step 4* draft consensus produced by each WG based on the literature review and questionnaire responses; *step 5* committee members indicate agreement or otherwise for each individual draft consensus; *step 6* acceptance of agreed statements (more than 80% of members), face to face meeting to modify statements without agreement. Committee members indicate agreement or otherwise for each modified consensus statement and final consensus statements.

The questionnaire was split into four broad topics, each of them treated by a subgroup including in each of them a pediatric radiologist: (1) patient preparation for MRE/MR enteroclysis/CTE/CT enteroclysis, (2) MRE/MR enteroclysis technique and sequence selection, (3) CTE/CT enteroclysis technique, and (4) enteric US patient preparation and technique. After an extensive literature research each member were instructed to always base their statements on the retrieved literature wherever possible, and to this end graded the strength of retrieved relevant publications from I (high) to V (low) using the criteria of the Oxford Centre for Evidence Based Medicine (2) during their review process. If no relevant literature was available for a particular item, members used expert opinion to construct the consensus statements.

Results:

The pediatric guidelines were based on the opinion of 3 pediatric radiologists and 4 adult radiologists who have experience in pediatric practice.

Patient preparation MRE

- It is recommended that children aged 6-9 should not eat any solid food for 2-4h
- It is recommended that children aged 6-9 should not undergo fluid restriction
- It is recommended that children aged over 9years should not eat any solid food for 4-6h
- It is recommended that children aged over 9years should not undergo fluid restriction
- *Basic technique—MRE*
- It is recommended that the optimal volume of oral contrast for MRE or CTE is 20 ml/kg with a maximum up to 25 ml/kg
- Installation of the patient can be either supine or prone.
- It is recommended that the use of a spasmolytic agent is optional. Unlike adult practice, the use of spasmolytic prior to MRE is considered optional in paediatric patients and use is likely dependent on the age of the patient, with older children more likely to tolerate spasmolytic injection. There are data supporting the benefits of glucagon on image quality, at the expense of prolonged imaging time and precipitation of nausea in just under half of paediatric patients (3,4). However, high diagnostic accuracy can also be achieved without spasmolytic (5).
- The recommended first line spasmolytic agent is i.v. hyoscine butylbromide, if a spasmolytic is used .The recommended dose of hyoscine butylbromide is 0.5mg/kg i.v. The recommended second line agent is i.v. glucagon, if a spasmolytic agent is used. The recommended dose of glucagon in the paediatric population is 0.5mg (<24.9kg) and 1mg (>24.9kg), given as a slow infusion with i.v. saline atan infusion rate at 1ml/s
- The recommended dose of i.v. gadolinium is 0.1mmol/kg

Recommended sequences:

- It is recommend to use the following sequences:

a) Axial and coronal fast spin echo (FSE) T2W sequences without fat saturation.

b) Axial and coronal steady state free precession gradient echo (SSFP GE) sequences without fat saturation.

c) An axial or coronal FSE T2W sequence with fat saturation.

d) Non-enhanced coronal T1W sequence with fat saturation followed by contrast-enhanced coronal and axial T1W sequences with fat saturation.

e) In patients with known or suspected inflammatory bowel disease, contrast-enhanced sequences should be in the enteric (45 s) or portal venous phase (70 s).

f) In patients with suspected chronic GI bleeding contrast-enhanced sequences is should be in the arterial (30 s), enteric (45 s) or portal venous phase (70 s) phase.

- It is recommended that i.v. gadolinium is pump-injected with an infusion rate of 2 ml/s and a dosage of 0.1–0.2 mmol/kg.
- It is recommended that the maximal slice thickness for FSE T2Wand SSFP GE sequences should be 5 mm.

- It is recommended that FSE T2W sequences may be performed in either 2D or 3D, although 2D is preferred.
- It is recommended that the maximal slice thickness for axial and coronal T1W sequences, should be 3 mm.
- It is recommended that T1W sequences should be performed in 3D

Optional sequences
- Optional additional sequences include an additional FSE T2Wsequence with fat saturation, axial and coronal SSFP GE sequences with fat saturation, cine motility and diffusion weighted imaging.
- It is recommended that a free breathing technique is used if diffusion-weighted sequences are performed.
- It is recommended that diffusion-weighted sequences should include lower b values ranging from 0 or 50 and upper b values ranging from 600 to 900.
- It is recommended that the maximal slice thickness for a diffusion-weighted sequence should be 5 mm.
- It is recommended that the total scan duration should equal to or be less than 45min

Patient preparation and basic technique—CTE/CT enteroclysis
- Use of CT scanning in children should be limited to exceptional circumstances, when US and/or MRE cannot address the clinical question.
- It is recommended that if CT scanning is used, only a portal phase from the diaphragm to the pubic symphysis is acquired

Patient preparation—enteric US
- It is recommended that children aged 1-9 should not eat any solid food for 2-4h.
- It is recommended that children aged 1-9 years should be nil by mouth for carbonated and milk beverages for 2-4h. Ingestion of still water or noncarbonated fruit juice is recommended.
- It is recommended that children aged over 9years should not eat any solid food for 4-6h.
- It is recommended that children aged over 9years should be nil by mouth for carbonated and milk beverages for 4-6h. Ingestion of still water or non-carbonated fruit juice is recommended.

Basic technique—enteric US
- Use of laxative bowel preparation is not recommended.
- Additional colonic distension with a rectal water enema is not recommended.
- It is recommended that for dedicated colonic evaluation, a standard protocol without specific modification is used.
- Use of a spasmolytic agent is not recommended.

Doppler and IV contrast
- The use of i.v. US contrast is not recommended.

Scan coverage
- It is recommended that scan coverage should include an abdominal and pelvic examination, including the liver.

There are no specific recommendations as to the use of hydro US in the paediatric patient as practice is not well developed. If oral contrast is given prior to US, it would seem sensible to follow the recommendations for MRE in the paediatric population

Statements for which consensus could not be reached after attempted modification:
- It is recommended that the minimal volume of oral contrast for dedicated MRE/MR enteroclysis or CTE/CT enteroclysis is 500 ml
- Splitting the oral contrast into two loads and scanning after ingestion of each to improve small bowel distension is not recommended.
- The optimal field strength for MRE/MR enteroclysis is 1.5 T.
- It is recommended to split-the dose of spasmolytics before T2W sequences and before contrast-enhanced T1W sequences.
- It is recommended to routinely use small bowel motility sequences during MRE.
- It is recommended to routinely use an axial diffusion-weighted sequence during MRE/MR enteroclysis.
- It is recommended that if a spasmolytic is used, and hyoscine butylbromide is unavailable/contraindicated, a second-line agent is employed during CTE/CT enteroclysis.
- It is recommended to administer a spasmolytic before MRE in the paediatric population.
- It is recommended that if CT scanning is used in the paediatric population, no specific preparation is usually required although administration of positive oral contrast could be considered; for example, prior to percutaneous drainage of abscesses.

Limitations: There is little evidence in the literature to ascertain all these proposals. The recommendations were mainly based on expert opinion. No recommendations have been proposed for children before 6 years of age. Especially the benefice of MRE under sedation (6) in the younger compare to US Doppler need to be explored.

References:

1) Taylor SA, Avni F, Cronin CG, et al. The first joint ESGAR/ESPR consensus statement on the technical performance of cross-sectional small bowel and colonic imaging. Eur Radiol. 2016 Oct 18. Epub Ahead of print
2) Centre for Evidence Based Medicine, Oxford University, Oxford. http://www.cebm.net/ocebm-levels-of-evidence/
3) Dillman JR, Smith EA, Khalatbari S, Strouse PJ. I.v. glucagon use in pediatric MR enterography: effect on image quality, length of examination, and patient tolerance. AJR Am J Roentgenol 2013; 201:185–189
4) Absah I, Bruining DH, Matsumoto JM et al MR enterography in pediatric inflammatory bowel disease: retrospective assessment of patient tolerance, image quality, and initial performance estimates. AJR Am J Roentgenol 2012; 199: W367–W375
5) Maccioni F, Al Ansari N, Mazzamurro F et al. Detection of Crohn disease lesions of the small and large bowel in pediatric patients: diagnostic value of MR enterography versus reference examinations. AJR Am J Roentgenol 2014; 203: W533– W542
6) Mollard BJ, Smith EA, Lai ME et al.. MR enterography under the age of 10 years: a single institutional experience. Pediatr Radiol. 2016;46(1):43-9

Take home points:
- MRE children's protocols are specific.
- The role of CT in children's IBD is limited.
- Emergent US technics need to be validated.

Aspects to consider when giving gadolinium based contrast agents in infants and children

H.-J. Mentzel; Jena/DE

Summary:
Contrast media application is essential for a number of MRI studies in children. There is some evidence that gadolinium-based contrast agents (GBCA) are well tolerated in infants and children. The risk of adverse reaction is no higher in children than in adults. There are only few data available about pharamakokinetics in children, especially for the use of GBCA in neonates. Age-adapted reference values of the glomerular filtration rate (GFR) have to be used to identify children with a potential risk. In the past few years there was some attention toward the potential cellular toxicity of gadolinium and its role in the development of nephrogenic systemic fibrosis (NSF). There were only few children identified with proof of NSF. But, particulary renal insufficiency, poor hydration, acidosis and inflammation increase the risk for NSF. Because the cases of NSF have been observed with linear componds the guidelines

from the ESUR and the ESPR and others propose to avoid linear compounds and to prefer macrocyclic GBCA. In the past year several studies have described observations about possible gadolinium retention in the brain; hyperintense brain structures in native T1 weighted sequences were verified - globus pallidum and dentate nucleaus - also in children undergoing multiple MRI examinations with GBCA application. So, repeated MR investigations within a short time should be avoided - the cumulative dose of GBCA should be recorded. Consider all these points, the benefit of a contrast-enhanced study should be weighted against the potential risks before administering a GBCA for each child separately. But, never deny a child an indicated ceMRI study. Use single dose application (0.05-0.1 ml/kg body weight), improve renal function and hydration, balance acidosis - and ask your pediatric nephrologist if necessary.

Take home points:
Gadolinium-based contrast agents are safe. Macrocyclic compounds should be used in children. Avoid contrast media in neonates and be careful in infants. Identify risk factors. Avoid repetivite application.

Procedural recommendation: How to perform pediatric gastrointestinal US
M.L. Lobo[1], M. Riccabona[2]; [1]Lisbon/PT, [2]Graz/AT

Summary:
Ultrasound (US) is the first imaging modality applied in the investigation of abdominal complaints in children, and an increasingly valuable imaging tool in the assessment of the gastrointestinal (GI) tract in neonates, infants and children.
A comprehensive US examination is a critical first-step to optimize the potential of US diagnostic yield in many paediatric GI conditions. Using proper high resolution transducers and graded compression technique is an essential part of GI US examination. A methodical and systematic analysis is crucial to facilitate a thorough evaluation of the bowel segments as complete as possible: follow bowel in a cross section, complete by longitudinal and oblique views. For some bowel sections filling is essential – such as stomach for gastroesophageal reflux and pyloric function, and distensibility and size of the colon by enema (e.g. for query *microcolon*). Modern US methods are valuable, but not a pre-requisite. Proper documentation of abnormal size of the GI tract segments, their luminal content, peristalsis, bowel wall characteristics and its surroundings, as well as local tenderness should be noted.
A proposal for recommendation on how to perform paediatric gastrointestinal US will be presented for public discussion.

Take home points:
- Careful and dedicated US examination is crucial to obtain maximum anatomic and functional information in many gastrointestinal disorders in children.
- Systematic and methodical analysis helps to assess the bowel as complete as possible.
- Satndardization of US technique is essential to optimize US diagnostic capabilities and to allow for comparable examinations wich is essential to improve future evidence-based knowledge.

SESSION: JACQUES LEFÈBVRE LECTURE

Hominid Evo-Devo: Reconstructing the evolution of human development
C. Zollikofer; Zurich/CH

Summary:
From an evolutionary biologist's perspective, modern humans represent the only surviving species of a group of highly specialized "bipedal great apes". They evolved more than seven million years ago in Africa and managed to spread over the entire globe. In this talk, I will trace the history of our species with an emphasis on key developmental innovations that underlie major evolutionary innovations. Why are we born with brains that have the size of adult great ape brains? And why do we grow up so slowly and get so old? I will highlight how advanced biomedical imaging methods help addressing these questions, and show how combined fossil, clinical and great ape data yield surprising insights into the evolution of our development.

FRIDAY, JUNE 02, 2017

SESSION: ESPR MEETS CHOP

Innovative imaging in IR-From bubbles to beyond
A.M. Cahill; Philadelphia/US

Summary:
Purpose:
To present our experience with innovative imaging in pediatric interventional radiology.
Imaging technologies presented will include:
1. Use of bubble contrast (Lumeson) for indicatons including; complex pleural effusion and abdominal collection assessment pre and post therapy, primary G tube placement, renal perfusion pre and post rena artery angioplasty, vascular patency during central venous line placement, vascular malformation therapy and biliary tube assessment.
2. Intravascular US (IVUS) in arterial intervention pre and post angioplasty and venous thrombolysis intervention.
3. Optical Coherence Tomography pilot study assesssment for renal artery intervention - validation in normal subjects. Currently this imagng which uses laser light technology to assess vascular mural detail at the micron level, is only validated in coronary artery intervention in adults.
4. MR Overlay - a technology that fuses MR imaging with low dose fluoroscopy and can faciltate biopsy of MR positive/CT negative lesions in the IR suite. Focus will be on bone lesion biopsy and vascular malformation therapy. Critical structures to be avoided can be outlined on the MR and transposed onto the fluoroscopic image during biopsy. In our experience this technology has promise in the pediatric setting with significant dose reduction when compared to CT.
5. MR fusion and I guide fusion technology enables an MR positive/CT negative lesion that would require CT guided imaging to be biopsed, using low dose C - arm CT, with fusion of the CT and MRI images performed using landmarks, facilitating fluoroscopically guided biopsy in the IR suite. Critical landmarks/structures to be avoided can be outlined on the CT or MR and transposed onto the fluoroscopic image during biopsy path planning and orchestration. Focus will be on bone lesion biopsy.
6. Color parametric flow related imaging in vascular intervention - this software enables time to peak opacification of arterial or venous contrast to be color coded in time and can provide adjunctive information for assessent of perfusion change during vascular intervention such as renal artery angioplasty, dialysis access intervention and cerebral embolization.
7. MR guided intervention - this focus will be on the initial development of an MR interventional program and our initial experience with MR arthrography. Discussion will also involve the use of this modality for vascular malformation sclerotherapy and other MSK interventions such as biopsy and nerve injections.
8. High frequency US imaging- focus will be on the use of a 40mHz US probe in the IR suite for various indications including visualization of smaller targets such as neonatal central venous access, superficial vascular malformation therapy and thyroid fine needle biopsy.

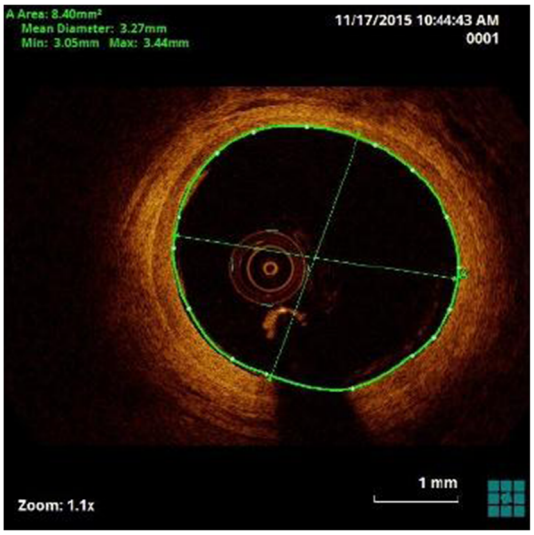

OCT of the normal pediatric renal artery

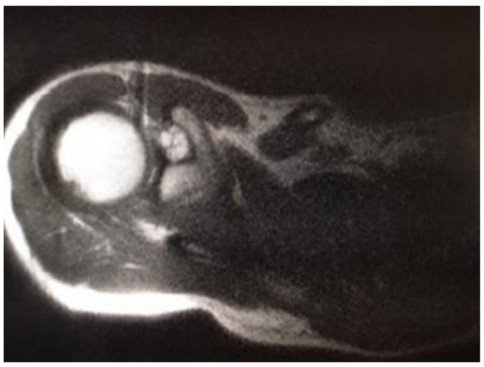

MR shoulder arthography

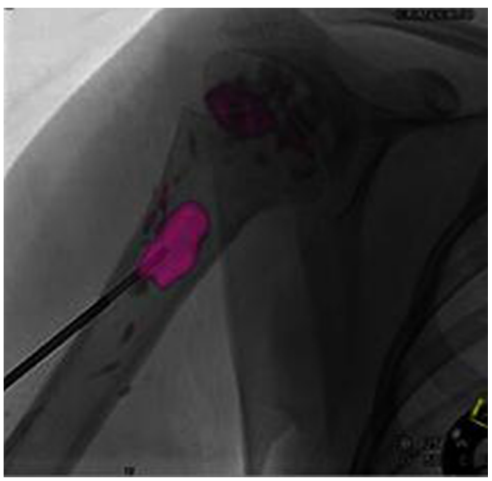

MR Overlay biopsy right humeral lesion

Take home points:
Objectives of this presentation:

1. Participants will become more familiar with exisitng and emerging innovative imaging technologies for pediatric intervention.
2. Participants will learn about the various indications and limitations of these technologies.
3. Participants will gain insight into the process of introducing new imaging modalities into their pediatric interventional practice.

Multimodal Assessment of Autism Spectrum Disorders using MEG, MRS and MRI-Towards Biomarkers
T. Roberts; Philadelphia/US

Summary:
Increasing evidence supports the notion that Autism Spectrum Disorder is associated with anomalies of brain function and connectivity. It is also evident that there are atypicalities in development/maturation of brain systems. Particular promise arises from findings of atypical electrophysiology - indexing brain neuronal activity in real time. In particular, this talk will address a characteristic electrophsyiologic signature of delayed auditory evoked response latency (at ~100ms). This, and related timing anomalies, have been proposed as biomarkers for ASD - with candidate use for diagnosis, prognosis, stratification and therapy monitoring. Progress along each of these axes will be discussed. However, to justify the term "biomarker", we demonstrate converging evidence from spectrally-edited (MEGAPRESS) MRS and diffusion-MRI. MRS offers insights into neurotransmitter levels, especially GABA and glutamate, imbalance of which may be associated with anomalous electrophysiologic oscillations in the gamma band. Diffusion offers insights into the white matter of the brain (auditory pathway will be illustrated) and an interpretation of diffusion parameters as an index of central conduction velocity will be offered. Combining these mechanistic measures with the spectro-spatio-temporal capabilities of magnetoencephalography (MEG), this talk will present a state of the art review of multimodal biomarker development in ASD.

Take home points:
MEG captures brain activity in space and time as well as showing sensitivity to activity at different frequencies (where, when and what)
Delays in cortical neuronal response latency are evidence in ASD
Atypical coupling between diffusion evidence of conduction velocity and timing of cortical responses in shown in ASD
Oscillatory activity is atypical in ASD (elevated "noise", decreased "synchrony")
Diminished inhibitory neurotransmitter (GABA) levels are shown in ASD
Disturbance of teh typical coupling between GABA and gamma-band oscillations in development leads to anomalous adult oscillatory activity (taken to index local circuit function).
Multimodal and longitudinal approaches may be required to tackjle the complex and heterogeneous landscape of ASD

SESSION: INTERVENTIONAL RADIOLOGY

Vascular Access in Paediatric Patients
R. Gnannt; Zurich/CH

Summary:
The paediatric radiologist can play an important role in establishing vascular access in paediatric patients ranging from neonates to teenagers. A breadth of knowledge and skills are needed to deal with changing body morphology and varied pathology in this age range. Some of the skills particular to performing and managing vascular access in children will be discussed. Different devices which can be placed, their indications, advantages and disadvantages will be reviewed. Choice of access vessel is important in children, because there are known long term complication such as central venous stenosis and thrombosis, which can have a huge impact for future venous procedures or potential creation of an arteriovenous fistula of the arm for dialysis. Preserving venous access sites is a

key responsibility especially in children with complex medical and surgical co-morbidities. Because vascular access in children has associated morbidity it's important to manage and maintain devices that are placed. The risk of infection when repairing or exchanging a broken line will be highlighted.

Take home points:
- Indications of different venous access devices
- Short- and long-term advantages and disadvantages of accessed venous vessels
- How to manage an externally broken line

Dos and Don'ts in Image Guided Pediatric Biopsy
D.A. Parra; Toronto/CA

Summary:
Image guided biopsy is a very frequent procedure in pediatric patients. They range from random organ parenchyma for the diagnosis of medical disease up to tumor biopsies for histopathology analysis.
Different imaging modalities can be used for guidance as well as different biopsy devices and needles. Ultrasound guidance is the most common modality used for this purpose in the pediatric population.
The success of this procedure depends on multiple factors: from pain control up to choosing the correct device and area to sample. The radiologist performing the procedure also needs to be familiar with the potential complications of the intervention, how to prevent them and how to manage them. The intention is to perform the safer procedure as possible, obtaining the best quality of sample.
The goal of this lecture is to present in a didactic way technical tips to perform safe and effective image guided pediatric biopsies, which may be applicable to different groups of operators, ranging from general pediatric radiologists performing occasional biopsies up to pediatric interventional radiologists. The objectives will be: to identify the safest approach to different types of biopsies; to describe ways to obtain the better quality of sample as possible; to demonstrate the use of different approaches in challenging clinical scenarios; to illustrate new devices currently used in specific applications; to discuss potential complications and its management and to show imaging modality integration applied to biopsy planning an performance.

Take home points:
Image guided biopsy is a frequent procedure in pediatric patients.
A pre-procedure planning is fundamental in the success of the intervention.
The operator must be aware of the aims of the biopsy and based on this choose the best approach, device and site for sampling.
Preparation and competency to manage complications is mandatory.

Pediatric Interventional Oncology: Big Cases in Little People
M. Heran; Vancouver/CA

Summary: The pediatric patient presents unique challenges in diagnosis and management of oncologic disorders. Interventional Radiology (IR) has a prominent role in the care of these children, with improvements in imaging and equipment offering better and safer options to traditional diagnostic and therapeutic procedures. As cancer can involve any organ system, consultations to the IR service can involve any part of the body, and can be non-vascular and vascular, simple and complex. The most common IR procedures in the pediatric oncology patient are enteric tube placement/change, vascular access, and percutaneous image-guided tissue/organ biopsy. However, with the explosion of Interventional Oncology in the adult setting, the variety and complexity of IR in pediatric oncology has begun to increase as well. IR techniques, such as thermal ablation, transarterial pharmacotherapy, and preoperative embolization, are now increasingly discussed in multi-disciplinary conferences as complementary or primary modes of treatment of oncologic disorders or related diseases/complications. However, although the principles of these diagnostic and therapeutic IR procedures remain essentially the same in their translation from adults to children, well recognized differences in pediatric physiology and metabolism, as well as the range in weight, size, and age of children, result in a practical question of "how do we do this?" The aim of this presentation is to provide an overview of the role of IR in the pediatric oncology patient, and to highlight areas of research and innovation.

Take home points:
- IR plays a very significant role in the care of the pediatric oncology patient.
- There has been tremendous growth in the field of Interventional Oncology, with greater and greater recognition of the role that IR has in this arena.
- Innovation and collaboration allow for the development of new and novel techniques in pediatric IO.

Vascular Anomalies: how Pediatric Interventional Radiology can help
P. Patel; London/UK

Summary:
Vascular anomalies encompass a spectrum of disorders including vascular tumours and vascular malformations. Incorrect nomenclature and misdiagnoses resulting in inappropriate treatment are commonly experienced by patients with vascular anomalies. The currently accepted method for classification of vascular anomalies is straightforward and clinically relevant. Vascular malformations can be divided into high flow lesions such as arteriovenous malformation or low flow lesions such as venous or lymphatic malformations. In children, a diagnosis can often be made with the history, examination and ultrasound. The classification of vascular anomalies will be briefly reviewed with examples of commonly encountered pathologies. A multidisciplinary team approach to the management of these conditions is vital. Paediatric radiologists can play a key role not only in diagnosis but also in management, principally by injection sclerotherapy of low flow lesions and embolization of the much rarer arteriovenous malformation. Many sclerotherapy agents are available with sodium tetradecyl sulphate the most commonly used for venous malformations and doxycycline for lymphatic malformations. Different sclerotherapy agents have different characteristics and uses which will be covered. Symptomatic relief is often achieved with treatment but multiple treatment episodes may be needed to achieve the desired outcome. Ensuring the child and family understand this is vital to ensure they are satisfied with the management of the condition.

Take home points:
- A multi-disciplinary team approach to vascular anomalies is essential.
- Venous malformations and lymphatic malformations can be non-invasively treated by image guided sclerotherapy.
- There are many agents which can be used for sclerotherapy, including sodium tetradecyl sulphate, doxycycline & bleomycin and each has advantages and disadvantages.

SESSION: CONTRAST MEDIA IN NEONATES AND INFANTS: WHAT, WHEN AND HOW?

Contrast media in neonates and infants: What, when and how?
F.E. Avni; Brussels/BE

Summary:
Contrast media is commonly used during imaging in children whatever their age and whatever the pathologic conditions. Still, youngest patients are vulnerable and unstable. Therefore, in neonates and infants the use of

contrast media should be carefully evaluated and customized putting in balance the risk versus the benefit of its use.

When using ***contrast media in neonates and infants***, several features should be highlighted:

- Prematures and neonates have rather immature kidneys and some contrast media might be difficult harmful
- The thyroid gland in prematures may be (transitorily) depressed by iodinated contrast media
- The use of high osmolar contrast may induce a fluid shift and dehydration especially in premature and neonates
- Most contrast media are used off label; almost none has obtained the authorization to be used in neonates.
- There are very few studies evaluating the short and long term adverse reactions in neonates and infants below the age of two. Fortunately these reactions seem very rare in these age groups.
- Using contrast extends the duration of the examination and the need for sedation

Different ***types of techniques*** will potentially need ingestion, instillation or injection of contrast media:

1) Opacification of the entire GI tract pre- and post-operatively
2) Retrograde uretro-cystography
3) Contrast enhanced CT
4) Contrast enhanced MR imaging
5) Contrast enhanced US
6) Angiography

Furthermore, different ***types of contrast media*** can be used to achieve these purposes

1) Barium (sulfate)
2) Iodinated water-soluble contrast media (hyper-, iso- or hypo-osmolar)
3) Chelates of Gadolinium
4) US contrast micro-bubbles
5) Air

Remarks regarding ***opacification of the upper GI tract***:

- The upper or lower GI tract should be opacified using water soluble contrast in the immediate postoperative period or whenever a bowel perforation is suspected.
- Air can be used to confirm esophageal atresia and duodenal atresia
- Barium should be preferred in case of T-E fistula
- Either barium or water soluble iodinate contrast can be used in order to opacify (sub)obstructed upper GI tract

Remarks regarding the ***opacification of the lower GI tract***

- Iodinated iso/hypo osmolar contrast should be used to opacify the colon in case of obstruction
- A higher osmolarity iodinated contrast can be used in case of suspected meconium ileus or plug; still this contrast should be used diluted and under close clinical surveillance and adequate hydration.
- In some more specific cases, for instance whenever Hirschprung disease or a stenosis post nectotizing enterocolitis are suspected, barium enema can be used

Remarks regarding ***CT scan***

- Contrast enhancement may help for the global assessment of various pathologies especially in case of cardio-vascular malformations or for the evaluation of abdominal masses. Any iodinate contrast among those available is acceptable in neonates. Higher osmolality contrast allows to inject a lower volume
- Injected volumes of 1.5 mL/Kg seem adequate using 22-24 gauge needles
- Power injectors are acceptable as long as adequate catheters can be used
- Allergic or side effects are very rare and should be managed similarly to adults.

Remarks regarding ***MR imaging***

- The use of Gd chelates in neonates remains controversial as there is no data available on the long term effects of Gd injected so early in life
- Gd should be used only when enhancement may provide additional information compared to the non-enhanced study (CNS infections, tumors, cardiovascular imaging, abdominal tumors, uro- MR imaging...)
- Only Gd with low NSF risk should be used
- Gd should not be used in children with renal failure

Remarks regarding ***Contrast enhanced US***

- Little is known about the use of CE-US in neonates
- Indications seem equal to older children
- There are very few side or allergic effects
- Doses suggested are 0.1 mL/year of age

References:

1) Carroll AG & al Comparative effectiveness of imaging modalities for the diagnosis of intestinal obstruction in neonates and infants Acad Radiol 2016; 23:559-568

2) Callahan MJ & al Selecting appropriate gastro-enteric contrast media for diagnostic fluoroscopic imaging in infants and children: a practical approach Pediatr Radiol 2016 Published online 10 oct 2016

3) Sundgren PC & al Is administration of Gd-based contrast media to pregnant woman and small children justified JMRI 2011; 34: 750-757

4) Emond S & al Gd-DOTA administration at MRI in children younger than 18 months of age: immediate adverse reaction Pediatr Radiol 2011; 41: 1401-1406

5) Rangamani S & al Safety of cardiac MR and contrast angiography in neonates and small infants: a 10 year single institution experience Pediatr Radiol 2012; 42: 1339-1346

6) Callahan MJ & al Practice patterns fort he use of iodinated i.v. contrast media for pediatric CT studies: a survey of the SPR AJR Amer J reontgenol 2014; 202: 872-879

7) Stenzel M & al US elastography and CE-US in infants, children and adolescents Eur J Radiol 2014; 83: 1560-1569

Take home points:

- The use of contrast media should be carefully evaluated in neonates and infants.
- Whenever possible, its use should be avoided.
- Whenever needed, its use should be customized and optimized

SESSION: TASK FORCE SESSION: ONCOLOGY AND WHOLE BODY IMAGING

Paediatric brain tumours: Differential diagnosis between low and high grade, from basic to advanced

L. Porto; Frankfurt/DE

Summary:

Children present varied histological types of brain tumours. It's now possible to combine different information and image techniques to improve the diagnosis of paediatric brain tumours. The multimodal approach has increased the diagnostic specificity and permits, in most cases, the pre-operative differentiation between low and grade tumours. Children with low grade lesions, and in particular the less accessible tumours, would benefit the most from avoiding biopsy. In addition, *pre*-operative spinal MRI evaluation to rule out drop metastases should be performed in patients with suspected high grade tumours.

In general paediatric brain tumours are less necrotic, i.e. aggressive tumours in paediatric patients tend to be more hypercellular and homogeneous. Because of its ready availability and speed, *computed tomography*

(CT) is the first investigation generally performed for a suspected brain tumour. CT can rule out haemorrhage or calcifications, but can also be used to evaluate tumour cellularity. A hyperdense tumour on CT reflects hypercellularity and is very often high grade. Medulloblastoma are, for example, typically hyperdense on CT scans and paediatric low-grade astrocytomas are almost always hypodense.
MRI plays a major role in the evaluation of brain tumours. In *conventional MRI*, the "general aspect" is the single most important parameter in predicting high-grade tumours in children. The same does not hold true for low-grade tumours, of which only 67% can be predicted using the general aspect. In our previous study, hyperintensity on T2-w and the lack of diffusion changes were the most important single parameters with 83% positive prediction.
Embryonic tumours, such as medulloblastoma or PNET have high tumour cellularity with consequent very low ADC and hypo/isointense T2 compared to the cortex. *ADC values* derived from DWI have been shown to be decrease in highly cellular tumours. ADC values cannot reliably be used in individual cases due to the substantial overlap between tumour types previously described in the literature. Nevertheless, ADC has a higher predictive value in children and increases the accuracy of preoperative differentiation between low grade and high grade paediatric tumours. The cut-off values for differentiating between low and high grade paediatric brain tumours are 0.7 x $10^3 mm^2/s$ and 1.0 x $10^3 mm^2/s$ for minimum ADC and average ADC values, respectively.
Perfusion with relative cerebral blood volume (rCBV) is considered a marker of angiogenesis and is helpful in distinguishing high and low grade tumours. However, perfusion can be difficult to perform in small children; small catheters with manual injection are therefore used in such cases (or, as an alternative, arterial labelling). It should however be taken into account that choroid plexus tumours can have high rCBVs resulting from highly leaky capillaries.
MR spectroscopy (MRS) shows the metabolic profile of the tumour. High grade tumours show elevated choline (Cho) - reflecting increase in cell membrane turnover - and decreased N-acetylaspartate (NAA), which represents a neuronal marker. The absolute values of the MRS peaks are not used by us; we favour to normalize the signal intensities of metabolites to their values in contralateral brain tissue. MRS is helpful not only as guidance for stereotactic biopsy (Cho Hot Spot) but also for determining whether the tumour is high or low grade. As a rule of thumb, a 200% increase of Cho when compared to the contralateral brain tissue is highly suggestive of a high-grade tumour. However, in children, increased Cho levels can also be found in pilocytic astrocytoma; in this case the typical aspect with cystic component and location can suggest the diagnosis, despite the MRS result. Therefore, in children, high Cho levels do not necessarily imply the presence of a malignant tumour.
Task based *functional MRI* (fMRI) can be used for pre-operative localization of the eloquent cortex together with the identification of the language and somatomotor function. In the future, small children who are unable to cooperate will probably profit from resting-state fMRI.
PET MRI has the advantage of integrating structural MR imaging with physiologic PET.

Take home points:
Take home points Although the histology of paediatric brain tumours is diverse, their general morphological aspect on MRI has a very high diagnostic reliability. Unlike adult grade IV brain tumours, malignant paediatric brain tumours are less necrotic, but are highly cellular with high nuclear-to-cytoplasmic ratios. Adding information on signal intensities on T2w and DWI further increases the diagnostic accuracy of conventional MRI. The solid areas of high-grade tumours are iso- or hypointense on T2w and hyperintense on DWI, whereas low-grade tumours show inverse signal characteristics. Advanced MR techniques (perfusion and spectroscopy) provide important biological information which can be used to correctly identify grading (high vs. low) and to guide biopsy. In children high Cho levels, although suggestive, do not necessarily mean a malignant tumour.

Experience with central review of paediatric renal tumours
G. Khanna; St Louis/US

Summary:
Central imaging review of pediatric renal tumors has been performed in Children's Oncology Group since 2006. To date, more than 5500 cases of pediatric renal tumors have been centrally reviewed real time by the study radiologists. The mean time for central review was <8 days. Discrepancies between local and central risk stratification were identified for detection of bilateral disease and pulmonary metastasis. In addition, central archiving of images has created a rich repository of cases for future research.
The role of imaging in detection of key diagnostic features in pediatric renal tumors will be reviewed. The diagnostic performance of imaging for staging, detection of vascular invasion and tumor rupture will be discussed.

Take home points:
Real time central review of imaging is feasible in pediatric oncology Wilms tumor remains the most common pediatric renal malignancy, followed by renal cell carcinoma Cystic nephroma typically presents as a Bosniak 3 lesion, and has high association with DICER-1 mutations

Is there a role for DWI in nephroblastoma?
A.*S. Littooij; Utrecht/NL*

Summary:
Wilms tumour or nephroblastoma is the most common malignant renal tumour in children. Ultrasound is usually the first line investigation. MRI of the abdomen is often performed to further delineate the tumor and its surroundings. The addition of diffusion-weighted imaging (DWI) to the standard MRI protocol may enable subtype characterisation and allows assessing treatment response beyond necrosis and volume change. Overall, the survival rate in patients with nephroblastoma is relatively good and the current focus is on finding biomarkers to further improve outcomes while reducing therapy-related side effects in these children. Therefore, identifying low- or high-risk type nephroblastoma might be relevant for treatment planning. Diffuse anaplastic nephroblastoma and extensive blastema in residual tumour after preoperative chemotherapy may require more intensive treatment. The limited available literature suggest a linear relation between ADC values and subtypes nephroblastoma at histopathology. Furthermore, the addition of DWI to the standard MRI protocol may detect lesions (e.g. nephrogenic rests of nephroblastomatosis) that remain undetected at post contrast T1-weighted images.
Unfortunately, there is a considerable heterogeneity in acquisition techniques and methods of ADC measurements. Nephroblastoma often contains areas of necrosis and/or hemorrhage that can demonstrate very low ADC values and consequently mimic highly cellular portions of tumours. Therefore these areas should be excluded from further analysis.
This lecture will highlight the potential additional benefit and limitations of DWI in children presenting with renal tumour.

Take home points:
- Whole-tumour ADC measurements with exclusion of poorly or non-enhancing parts is the preferred method
- Three components of response to treatment can be measured with MRI: change in size, necrosis and shift in ADC
- Further research is needed to validate the potential additional role of ADC measurements in identiftying high or low risk nephroblastoma

Ins and outs of PET MRI in children
J.F. Schäfer; Tübingen/DE

Summary:
In theory, the combination of PET and MRI might be the best modality for paediatric cancer imaging. The rationales for this hypothesis are: (a) the

significantly lower radiation exposure even in comparison to low-dose PET/CT, (b) the higher diagnostic accuracy as compared to PET/CT even when using diagnostic contrast-enhanced CT, (c) the unique possibility to combine distinct MR-inherent contrasts (e.g. DWI) with specific PET-tracers (e.g. 64Cu-labeled antibody imaging) for the evaluation of novel targeted therapies, and (d) the opportunity to stage local and systemic tumour burden within a single and highly resolved examination.
On the other hand, many circumstances are challenging the extensive use of PET/MRI in children. In general, the availability of PET/MRI systems is low, particularly for children. Thus, only a few sites in Europe have experience with this technique in children, and therefore the generated scientific evidence is limited. Moreover, whole-body-MRI is still not a broadly adopted method for the combined assessment of local disease extent and whole-body staging, potentially replacing other whole-body modalities like the bone scan. In this context, especially the detection of pulmonary metastases is biased also against PET/MRI. Finally harmonized sequence protocols and specific recommendations for trace dosage are not available for PET/MRI.

Take home points:
In conclusion, further efforts are needed to keep the promises of PET-MRI in the daily practice.

SESSION: JESPER LECTURE

Common artefacts in paediatric MRI–How to recognise, avoid or take advantage of them

C. Kellenberger; Zurich/CH

Summary:
While MRI is a robust and radiation free imaging technique for assessing anatomy and pathology of most tissues and organs throughout the body, it is inherently prone to artefacts as no other imaging modality is. MRI artefacts may impair image quality potentially leading to difficulties or errors in interpretation, but in some instances can contribute diagnostic information. Main sources of image degradation are motion, disturbances of the local magnetic field and other factors inherent to image acquisition. Strategies to reduce effects from various kinds of motion and adjustment of sequence parameters for eliminating artefacts will be discussed.

Take home points:
- Understanding the origin and effects of artefacts encountered in paediatric MRI is essential for modification of MRI protocols, so that artefacts and associated errors can be avoided.
- For safely and successfully imaging children with implants and devices, the composition, location and functionality of the foreign body needs to be known.

SATURDAY, JUNE 03, 2017

SESSION: SPECIAL FOCUS SESSION: RADIOLOGY OF CHILD ABUSE: FROM HEAD TO TOE

Neuroradiology in child abuse

N. Girard; Marseille/FR

Summary:
Injuries to the central nervous system in abusive head trauma are responsible for the primary cause of morbidity and mortality in infants. Neuroradiology has an important role in diagnosis but also in depicting injury and extent of brain damage of poor outcome. Computerized Tomography (CT) and Magnetic Resonance Imaging (MRI) are the primary imaging techniques. CT is usually performed in the acute phase while MRI is performed the following days after injury. Some injuries are better identified on MRI such as diffuse axonal injury and cerebral edema with susceptibility and diffusion weighted images.

Introduction
Abusive head trauma (AHT) is the primary cause of morbidity and mortality in infancy, especially during the first year of life. AHT is clinically characterized by a triad consisting of subdural hematoma, retinal hemorrhage and encephalopathy caused by brain swelling (1). The most common mechanism responsible for brain damage is thought to be caused by whiplash shaking injury explaining that abusive head trauma is also referred as shaken baby syndrome. Impaction, compression and penetrating injury are also possible mechanisms as well as strangulation. However because of the variability of types and severity of injury, clinical symptoms vary from subtle to severe such as alteration of consciousness or coma (2). The most common symptoms include vomiting, seizure, lethargy, poor feeding and apnea of which vomiting and respiratory pauses are non-specific (3). Poor feeding, irritability or lethargy is also non-specific signs. However apnea and/or retinal hemorrhages seen in children with brain injury are strongly associated with inflicted trauma (4). In contrast to acute injury some children may manifest with increased head circumference related to chronic subdural hematomas. Neuroimaging is therefore playing a crucial role to assess infants and children with a suspicion of abusive head trauma. Computerized tomography (CT) and magnetic resonance imaging (MRI) are the primary imaging techniques. CT is performed for the initial evaluation in cases with acute symptoms to look for hemorrhagic intracranial injury as subdural hematoma. MRI is more often performed in the following days to further evaluate brain injury and to look for spine and spinal cord damage (5, 6) or in the presence of normal or equivocal CT findings (7). However brain MRI may be the first option in children presenting with increased head circumference. Recently the study from Flom et al showed the high sensitivity of MRI for intracranial hemorrhage in well appearing infants at risk for abusive head trauma suggesting MRI as a screening tool with 3 pulse sequences (axial T2, axial gradient recalled echo and coronal T1 weighted inversion recovery) (8).

CT and MRI
CT is generally performed without intravenous contrast injection with 3D volume rendering (VR) reconstructions for identification of fractures. In some cases postcontrast images are also obtained specially to rule out deep venous thrombosis especially when children present with nonspecific clinical symptoms. MRI protocol should include axial T2, T2* or susceptibility weighted images, coronal T1 images, diffusion or diffusion tensor images, and postcontrast 3DT1 images including MIP reconstructions to evaluate the venous structures. MR venography can also be performed. Susceptibility-weighted images are usually preferred because they allow the depiction of smaller hemorrhagic DAI lesions and greater number of lesions compared to GRE T2 (9). It was also reported by Colbert et al (10) that the presence of micro-hemorrhages alone was useful for outcome prediction in abusive head trauma with significant poor long-term outcome. The sensitivity and specificity of micro-hemorrhages was also higher than the other clinical (such as retinal hemorrhages and glasgow coma scale score) and other imaging findings for prediction of outcome. Diffusion Tensor Imaging (DTI) measurements were reported in abusive head trauma by Imagawa et al: decreased axial diffusivity related to axonal injury with consequent reduced mean diffusivity did correlate with poor outcomes (11). Magnetic resonance spectroscopy (MRS) is usually not part of the standard protocol. However Aaen et al (12) showed that N-acetylaspartate/creatine and/or N-acetylaspartate/choline ratios were decreased significantly in the corpus callosum, frontal white matter, parieto-occipital white matter, and parieto-occipital gray matter in children with poor outcomes. This study mentioned above also reported that the prediction of outcome was accurate in 100% of patients by using a logistic regression model that include age, initial glasgow coma scale score, presence of retinal hemorrhage, lactate on MRS, and mean total N-acetylaspartate/creatine. Functional MRI,

volumetry may be performed in long-term follow up of victims of child abuse. Physical abuse is associated with altered emotion with greater activation in the salience network in response to negative stimuli, that includes amygdala, thalamus, putamen and anterior insula (13). Increased responsiveness of the right amygdala to fearful and angry faces (negative stimuli) and structural changes as reduced hippocampal volume, are reported by Dannlowski et al (14). Impaired attention was also reported in patients with childhood abuse (15) with reduced activation during attention tasks in the left hemispheric ventral and dorsolateral prefrontal regions.

Intracranial injury

Intracranial injuries include extracerebral hemorrhages and parenchymal damage as brain swelling and ischemia, venous infarction, diffuse axonal injury, contusions and intraparenchymal hematomas (7, 16).

Extracerebral hemorrhages

Subdural hematoma is a characteristic finding of inflicted traumatic brain injury, is generally multifocal and most commonly seen along the posterior interhemispheric scissure, over de convexities at the vertex level and/or in the posterior fossa (17-19). Subdural hematomas are most likely bilateral but may be unilateral. All locations are related to disruption of bridging veins. The identification of bridging vein rupture allows the diagnosis of traumatism in relation to acceleration/deceleration, rotational and shearing forces due to violent shaking (20). A mixed density appearance of subdural hematomas is frequent but is also seen in accidental traumatic brain injury (21-23). Indeed this feature is often present in the very early hours following trauma and is thought to be secondary to early sedimentation of blood clots and supernatant serum.

Tubular high density is often seen on non-contrast CT over the convexities in abusive head trauma. This CT feature is related to a clot secondary to venous disruption (24, 25) that can end up in thrombophlebitis. This tubular high density was reported more recently as tadpole sign (26) and lollipop sign (27) respectively seen in 40 and 44% of abusive head trauma. This appearance is strongly associated to inflicted trauma and much less frequent in accidental trauma (3 out of 83 cases (3,6%) of accidental trauma in our experience). Associated venous infarction is reported in 12% of cases of abusive head trauma (24) and often located in the parieto-occipital region, unilaterally at the site of venous disruption of bridging veins.

Subdural hemorrhages, when multiple, in the convexity and interhemispheric, or in the posterior fossa were found significantly associated with abusive head trauma in the meta- analysis reported by Kemp et al (28). In addition subdural hematoma, cerebral ischemia, skull fracture, retinal hemorrhage and intracranial injury were significantly associated with abusive head trauma in the review from Piteau et al (29).

Subarachnoid hemorrhages (SAH) and epidural hematomas are also found in inflicted trauma and are not considered discriminant-imaging features. However epidural hemorrhages, isolated skull fracture and scalp swelling were reported as significantly associated with accidental traumatic brain injury (29). SAH in shaking injury is usually caused by tears of the vessels within the pia and arachnoid predominantly in the interhemispheric fissure and high convexity (7).

Parenchymal injury

Parenchymal injury include brain swelling and ischemia, venous infarction (discussed above), diffuse axonal injury related to rotationally-induced shear-strain injury with different inertia for grey and white matter due to their different specific gravities, contusions seen in deceleration trauma with friction between the skull and brain, and in blunt trauma and intraparenchymal hematomas related to lacerated vessels.

Brain swelling/ischemia may be related to increased blood volume (congestive swelling), increased presence of water in the nervous tissue, and the combination of both. Increased water in the nervous tissue may manifest as vasogenic edema located in the white matter due to extravasation of plasma like fluid related to incompetent blood-brain-barrier and as cytotoxic edema located in the grey matter, related to ionic imbalance. Cerebral edema can be recognize on CT within the 12 hours following injury as loss of gray-white matter differentiation and decreased attenuation of grey and white matter. Cytotoxic and vasogenic edema are better characterized on MRI with diffusion-weighted imaging. Brain swelling and edema occur early after trauma with consequent underestimation of subdural hematoma. Therefore imaging should be repeated (CT or MRI) especially when neurologic symptoms change rapidly. Brain swelling/edema may also involve the posterior fossa and is better identified on brain MRI. Two frequent patterns have been reported in abusive head trauma (24). Diffuse supratentorial brain swelling (infarction) involving the cortex and white matter was reported in 39% of cases and is considered as severe hypoxic-ischemic injury with poor outcome (30). Watershed infarction was reported in 36% of cases and considered a less severe form of hypoxia-ischemia. Apparent diffusion coefficient (ADC) values are strongly associated with poor neurodevelopmental outcomes in the acute phase (within 4 days) especially basal ganglia, thalamus, brainstem, cerebral cortex, cerebellar vermis, cerebellar cortex and mean total brain (31). During the early phase up to 1 month ADC values in fewer regions (basal ganglia, thalamus, brainstem and corpus callosum) were associated with poor outcome. When patients with and without parenchymal lesions are compared, the detection of diffuse lesions during the first 3 months as well as beyond 3 months is significantly associated with severe developmental outcome (32). Late MRI (beyond 3 months after injury) also showed that recovery depends on the extent of brain damage. Patients with diffuse lesions show more severe motor and intellectual impairments and are more likely to have blindness and epilepsy than patients with focal or hemispheric lesions (32).

Diffuse axonal injury (DAI) is related to shear-strain injury of small medullary veins and was reported in 6% of cases of abusive head trauma (24). It is encountered in trauma with sudden acceleration-deceleration associated with rotational angular forces and in shaking-impact trauma. The lesions may be hemorrhagic or non hemorrhagic (related to axonal swelling). DAI is most often located in the subcortical white matter at the gray-white matter junction, corpus callosum, basal ganglia, brainstem and internal capsule. If the lesions are large enough and hemorrhagic DAI may be seen on CT. However DAI is usually better identified on MRI with susceptibility and diffusion weighted images. The detection of changes in the basal ganglia or brainstem during the first 3 days as well as during the first month after injury is significantly associated with poor long-term outcome in survivors (30). The presence of intraparenchymal brain micro-haemorrhages detected on SWI in children with abusive head trauma correlates with significantly poor long-term neurologic outcome (10)

Contusion is also reported in abusive head trauma and is seen in blunt trauma with impact with or without contrecoup contusion. Contusions are located at the surface of the brain (crest of gyri) and may be pial and haemorrhagic (disruption of cortical arteries). They are also found in the frontal and temporal regions related to impact of the brain on the roof of the orbit, middle cranial fossa and sphenoid wing. White matter tears are also seen in the frontal and temporal area related to the vulnerability of unmyelinated and soft white matter in infants.

Skull fractures

Skull fractures are seen in blunt impact and are less frequent than long bones and rib fractures in non-accidental trauma. The most common site is the parietal bone (because of bulging of parietal bones below 1 year of age). The fracture may be linear as in accidental trauma. Radiologic features significant for inflicted trauma are multiple fractures, bilateral fractures and fractures that cross suture lines (28, 33). Focal underlying brain damage can be seen such as subdural hematoma and hemorrhagic contusion.

Vascular injury

Hypoxic-ischemic encephalopathy is seen in strangulation injury with involvement of the territories of the internal carotid artery related to their anatomic vulnerability.

Conclusions

Neuroradiology (CT and MR) is crucial for the diagnosis of trauma, to predict outcome when showing edema and hypoxic-ischemic injury.

References:
Guthkelch AN. Infantile subdural haematoma and its relationship to whiplash injuries. Br Med J. 1971;2(5759):430-1. Chiesa A, Duhaime AC. Abusive head trauma. Pediatr Clin North Am. 2009;56(2):317-31. Laurent-Vannier A, Nathanson M, Quiriau F, Briand-Huchet E, Cook J, Billette de Villemeur T, et al. A public hearing "Shaken baby syndrome: guidelines on establishing a robust diagnosis and the procedures to be adopted by healthcare and social services staff". Guidelines issued by the Hearing Commission. Ann Phys Rehabil Med. 2011;54(9-10):600-25. Maguire S, Pickerd N, Farewell D, Mann M, Tempest V, Kemp AM. Which clinical features distinguish inflicted from non-inflicted brain injury? A systematic review. Arch Dis Child. 2009;94(11):860-7. Adamsbaum C, Husson B. [Shaken baby syndrome: which lesions in imaging ?]. Arch Pediatr. 2012;19(9):1002-7. Kadom N, Khademian Z, Vezina G, Shalaby-Rana E, Rice A, Hinds T. Usefulness of MRI detection of cervical spine and brain injuries in the evaluation of abusive head trauma. Pediatr Radiol. 2014;44(7):839-48. Hsieh KL, Zimmerman RA, Kao HW, Chen CY. Revisiting neuroimaging of abusive head trauma in infants and young children. AJR Am J Roentgenol. 2015;204(5):944-52. Flom L, Fromkin J, Panigrahy A, Tyler-Kabara E, Berger RP. Development of a screening MRI for infants at risk for abusive head trauma. Pediatr Radiol. 2016;46(4):519-26. Tong KA, Ashwal S, Holshouser BA, Shutter LA, Herigault G, Haacke EM, et al. Hemorrhagic shearing lesions in children and adolescents with posttraumatic diffuse axonal injury: improved detection and initial results. Radiology. 2003;227(2):332-9. Colbert CA, Holshouser BA, Aaen GS, Sheridan C, Oyoyo U, Kido D, et al. Value of cerebral microhemorrhages detected with susceptibility-weighted MR Imaging for prediction of long-term outcome in children with nonaccidental trauma. Radiology. 2010;256(3):898-905. Imagawa KK, Hamilton A, Ceschin R, Tokar E, Pham P, Bluml S, et al. Characterization of microstructural injury: a novel approach in infant abusive head trauma-initial experience. J Neurotrauma. 2014;31(19):1632-8. Aaen GS, Holshouser BA, Sheridan C, Colbert C, McKenney M, Kido D, et al. Magnetic resonance spectroscopy predicts outcomes for children with nonaccidental trauma. Pediatrics. 2010;125(2):295-303. Seeley WW, Menon V, Schatzberg AF, Keller J, Glover GH, Kenna H, et al. Dissociable intrinsic connectivity networks for salience processing and executive control. J Neurosci. 2007;27(9):2349-56. Dannlowski U, Stuhrmann A, Beutelmann V, Zwanzger P, Lenzen T, Grotegerd D, et al. Limbic scars: long-term consequences of childhood maltreatment revealed by functional and structural magnetic resonance imaging. Biol Psychiatry. 2012;71(4):286-93. Lim L, Hart H, Mehta MA, Simmons A, Mirza K, Rubia K. Neurofunctional Abnormalities during Sustained Attention in Severe Childhood Abuse. PLoS One. 2016;11(11):e0165547. Chen CY, Zimmerman RA, Rorke LB. Neuroimaging in child abuse: a mechanism-based approach. Neuroradiology. 1999;41(10):711-22. Cohen RA, Kaufman RA, Myers PA, Towbin RB. Cranial computed tomography in the abused child with head injury. AJR Am J Roentgenol. 1986;146:97-102. Zimmerman RA, Bilaniuk LT, Bruce D, Schut L, Uzzell B, Goldberg HI. Interhemispheric acute subdural hematoma: a computed tomographic manifestation of child abuse by shaking. Neuroradiology. 1978;16:39-40. Hymel KP, Rumack CM, Hay TC, Strain JD, Jenny C. Comparison of intracranial computed tomographic (CT) findings in pediatric abusive and accidental head trauma. Pediatr Radiol. 1997;27(9):743-7. Rambaud C. Bridging veins and autopsy findings in abusive head trauma. Pediatr Radiol. 2015;45(8):1126-31. Vinchon M, Noule N, Tchofo PJ, Soto-Ares G, Fourier C, Dhellemmes P. Imaging of head injuries in infants: temporal correlates and forensic implications for the diagnosis of child abuse. J Neurosurg. 2004;101(1 Suppl):44-52. Tung GA, Kumar M, Richardson RC, Jenny C, Brown WD. Comparison of accidental and nonaccidental traumatic head injury in children on noncontrast computed tomography. Pediatrics. 2006;118(2):626-33. Kemp AM. Abusive head trauma: recognition and the essential investigation. Arch Dis Child Educ Pract Ed. 2011;96(6):202-8. Zimmerman RA, Bilaniuk LT, Farina L. Nonaccidental brain trauma in infants: diffusion imaging, contributions to understanding the injury process. J Neuroradiol. 2007;34(2):109-14. Adamsbaum C, Rambaud C. Abusive head trauma: don't overlook bridging vein thrombosis. Pediatr Radiol. 2012;42(11):1298-300. Hahnemann ML, Kinner S, Schweiger B, Bajanowski T, Karger B, Pfeiffer H, et al. Imaging of bridging vein thrombosis in infants with abusive head trauma: the "Tadpole Sign". Eur Radiol. 2015;25(2):299-305. Choudhary AK, Bradford R, Dias MS, Thamburaj K, Boal DK. Venous injury in abusive head trauma. Pediatr Radiol. 2015;45(12):1803-13. Kemp AM, Jaspan T, Griffiths J, Stoodley N, Mann MK, Tempest V, et al. Neuroimaging: what neuroradiological features distinguish abusive from non-abusive head trauma? A systematic review. Arch Dis Child. 2011;96(12):1103-12. Piteau SJ, Ward MG, Barrowman NJ, Plint AC. Clinical and radiographic characteristics associated with abusive and nonabusive head trauma: a systematic review. Pediatrics. 2012;130(2):315-23. Tanoue K, Matsui K, Nozawa K, Aida N. Predictive value of early radiological findings in inflicted traumatic brain injury. Acta Paediatr. 2012;101(6):614-7. Tanoue K, Aida N, Matsui K. Apparent diffusion coefficient values predict outcomes of abusive head trauma. Acta Paediatr. 2013;102(8):805-8. Bonnier C, Nassogne MC, Saint-Martin C, Mesples B, Kadhim H, Sebire G. Neuroimaging of intraparenchymal lesions predicts outcome in shaken baby syndrome. Pediatrics. 2003;112(4):808-14. Meservy CJ, Towbin R, McLaurin RL, Myers PA, Ball W. Radiographic characteristics of skull fractures resulting from child abuse. AJR Am J Roentgenol. 1987;149(1):173-5.

SESSION: TASK FORCE SESSION: FETAL AND POSTMORTEM

Advances in Post Mortem Imaging

O.J. Arthurs; *London/UK*

Summary:
This presentation will present an update on post mortem MRI (PMMR) with relevance to clinical developments over the last 2 years. In particular, reference will be made to diagnostic accuracy of PMMR across different body parts, the current limitations of post mortem MR, and protocol development at different field strengths. Imaging correlates of post mortem interval are also being investigated. Maceration (autolysis within intrauterine fluid) and perimortem hypoxic brain changes caused difficulties in image interpretation, which more advanced and quantitative techniques may be able to address. Jawad N, et al., Bodyweight limits of fetal post mortem MRI at 1.5T" Ultrasound Obstet Gynecol (2016) 48: 92-97 Kang X, et al. Post-mortem whole-body MRI of human fetuses: a comparison of 3-T vs. 1.5-T MR imaging with classical autopsy. *European Radiology* (2017) in press Papadopoulou I, et al., Diffusion-weighted post-mortem MRI of the human fetal brain in situ" *European Journal of Radiology* (2016) 85:1167-117 Montaldo P et al., Quantification of maceration changes using post mortem MRI in fetuses"*BMC Med Imaging* (2016); 16: 34

Take home points:
Below 500g, 1.5-T PMMR shows a significant reduction in diagnostic yield, compared with conventional autopsy, and therefore its clinical usefulness in this setting will depend on individual circumstances.
3T PMMR performs better than 1.5 T particularly <20 weeks gestation, and particularly for the chest, heart and abdomen.
Diffusion characteristics in different fetal brain areas are multifactorial, with maceration the strongest predictor in most areas.

International PM CT protocols

C.Y. Gerrard[1], O.J. Arthurs[2]; [1]*Albuquerque, NM/US,* [2]*London/UK*

Summary:
The European Society of Pediatric Radiology (ESPR) Taskforce and the International Society of Forensic Radiology and Imaging (ISFRI) Pediatric Working Group have combined efforts to establish best practice standards for performing perinatal and pediatric post mortem computed tomography (PMCT) examinations. Use of PMCT in the investigation of pediatric death has increased significantly in the past decade. Due to quick acquisition times and the ability to acquire thin slice, high detailed images of the whole body,

many hospitals and forensic institutes have implemented PMCT into daily practice. However, there lack an overall standardization of how cases are triaged and the acquisition methods when comparing institutes using PMCT. In an effort to address inconsistencies in acquisition parameters, post processing, and case selection, PMCT protocols were compiled from international institutes and centres currently performing pediatric imaging. This paper will describe both the uniform and divergent elements of image acquisition and procedural uses identified among the participating centres. The outcome is to provide a single source of information that can guide already established and new centres on the best practice standards for implementing pediatric PMCT.

Take home points:
Describe how pediatric post mortem computed tomography (PMCT) has increased in utility over the past decade. Identify the differences in acquisition methods for clinical computed tomography versus post mortem computed tomography. Discuss the overall consensus of case triage and scan acquisitions when comparing institutes in aggregate. Provide comprehensive statement of best practice standards for pediatric PMCT.

Post Mortem imaging research: Updates and future proposals
O.J. Arthurs; London/UK

Summary:
Paediatric and perinatal post mortem imaging is a new and rapidly growing field, and the Post Mortem Imaging Taskforce was founded in Graz at ESPR 2015. The PMI Taskforce aims to help reach consensus and guidance regarding imaging protocols and the potential yield of post mortem ultrasound, CT and MR. The key priorities are the themes of collaboration, image acquisition, best practice guidelines, training and education, raising awareness and access to imaging.
This presentation will give updates on the latest developments in perinatal and paediatric imaging, with particular focus on where the PMI taskforce can help. In particular, protocol development is underway, and the ESPR meeting acts as an opportunity for collaborative working and network development, to facilitate best clinical practice and welcome new members.
Arthurs OJ et al., ESPR Post mortem imaging task force: where we begin. Pediatr Radiol (2016); 46: 1363 – 1369

Take home points:
Post mortem imaging is an exciting sub-specialty which requires a combination of in depth fetal medicine, perinatal autopsy and pediatric imaging knowledge to help shape and grow the clinical and research arena.
Dedicated personnel have an opportunity to create the evidence-based behind a growing clinical service, with clear benefits to patients, families and referring clinicians.

Submitted Abstracts -53rd Annual Meeting
Scientific Sessions & Case Report Presentation Sessions
Abstracts appear as submitted to the online submission system and have not been checked for correctness and completeness.

THURSDAY, JUNE 01, 2017

SESSION: SCIENTIFIC SESSION: NEURO

Radiation-induced vascular changes in childhood medulloblastoma survivors: An MRI study
Y. Tanyildizi, S. Keweloh, M. Neu, A. Russo, A. Wingerter, J. Faber, M.A. Brockmann; Mainz/DE

Objective:
Black blood sequences with high (≤ 0.4 x 0.4 mm) in-plane resolution and low slice thickness (≤ 0.5 mm), so called Vessel Wall Imaging (VWI) - sequences, are an emerging tool for evaluating intracranial vessel disease. Improved survival due to emended treatment protocols results in an increasing number of long-term medulloblastoma survivors who experience delayed treatment effects. Microbleedings, developement of cavernomas, vasculitis and atherosclerotic lesions are cerebrovascular structures affecting sequelae of the applied radiochemotherapy. This study evaluates radiation-induced intracranial vascular changes.

Materials:
Twenty-two long-term pediatric medulloblastoma survivors (mean age 25.8 years, range 10-53 years; mean years after primary radiochemotherapy 16.3 years, range 1-45 years) underwent MRI. The scan protocol included precontrast 3-dimensional time of flight (TOF) – magnetic resonance angiography (MRA), precontrast 2D T1- and 2D T2-VWI-sequences and postcontrast 2D T1-VWI-sequences of the medium and large intracranial arteries. Vessel wall thickening, contrast enhancement and luminal narrowing were analyzed. Additionally precontrast T1-, T2-SWI and T1-weighted images of the supra- and infratentorial brain were acquired.

Results:
VWI- sequences: Vessel wall changes could be found in 12 (54%) and 14 patients (63%) of the right and left ICA, respectively. For the BA 4 (18%) patients revealed vessel wall changes; for the left and right VA 2 (9%) patients were detected with vessel wall changes, respectively. In the TOF angiography no alteration of the ICA, BA or VAs could be identified. In total vessel wall changes for the vertebrobasilar system and the ICAs could be found in 16 (72%) patients.
SWI- sequences: All patients (100%) revealed SWI lesions, the smallest lesion measuring less than 2 mm, the biggest up to 5 mm. Sixteen patients (72%) were presented with lesions > 4 mm, suspicious for cavernomas.

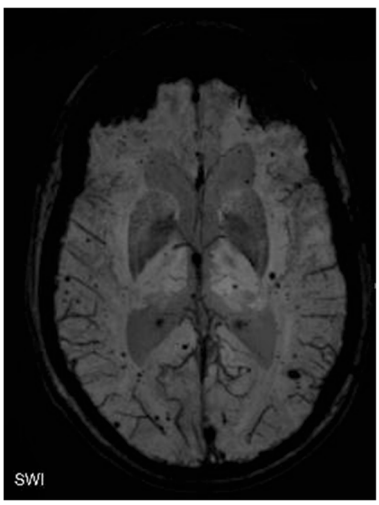

SWI-sequence; revealing multiple SWI lesions

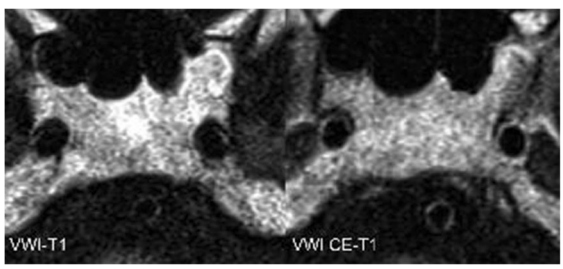

precontrast T1 VWI and postcontrast T1; revealing vessel wall contrast enhancement in both ACI and in the BA

Conclusion:
To ensure quality of life in long term childhood medulloblastoma survivors, monitoring of long-term effects, like vascular changes after RCT is gaining in importance. High resolution MRI, including SWI and VWI-sequences could be used here for. This study images, asymptomatic vessel wall alterations in former childhood medulloblastoma patients through VWI sequences and micro bleedings through SWI sequences. Vessel wall alterations, revealing RCT induced arteriosclerosis, can lead to symptomatic intracranial stenosis which is associated with ischemia, furthermore micro bleedings and cavernomas can lead to intracranial hemorrhage. However further studies are needed to standardize MRI sequence protocols to ensure a high standard follow up protocol, detecting clinically still asymptomatic vascular changes.

Fast "black-bone" MR imaging in evaluation of craniofacial abnormalities: Comparison with high resolution CT
Z. Habib, A. Talib, C. Parks, S. Avula, L.J. Abernethy; Liverpool/UK

Objective:
To evaluate the feasibility and diagnostic value of a fast field echo, "black bone" MRI sequence in children with craniofacial abnormalities.

Materials:
A fast "black bone" MRI sequence has been used in addition to standard brain MRI in 16 children (mean age 17 months, age range 3 months to 5 years and 5 months) referred to the Supra-regional Craniofacial Surgery Unit at Alder Hey Children's Hospital, Liverpool, UK. A subgroup of 10 of these patients with complex craniofacial abnormalities additionally had high resolution volume CT performed at the same visit.
"Black bone" MR imaging was performed on Philips Ingenia 3T and 1.5T scanners, using a 3D Fast Field Echo sequence (TR=8.3 ms, TE=4.6 ms, Flip Angle 5^0). This sequence can be performed with an acquisition time of less than 2 minutes. The "black bone" sequences were assessed for accuracy in evaluating the patency of the sagittal, coronal and lambdoid sutures, and, where applicable, were compared with high resolution CT.

Results:
The fast "black bone" MRI sequence was shown to be technically feasible in all cases. The resultant images successfully demonstrated both patent sutures, which were confidently seen, and prematurely fused sutures which were confidently not seen. Visualisation of patent sutures was found to be further enhanced by the use of minimum intensity projection. In the subgroup of patients with complex craniofacial abnormalities, comparison with high resolution volume CT confirmed good sensitivity for patency of cranial sutures. There was complete agreement in 50 out of 50 sutures assessed.
The "black bone" MR images were also found to produce good-quality surface-rendered images and were also suitable for 3-D printing of models for pre-operative planning.

Conclusion:
Fast "black-bone" MRI has proven to be technically feasible and to demonstrate cranial suture patency with good agreement with high resolution CT. Additionally "black-bone" MRI can be used to produce good quality surface-rendered images and 3-D printed models for surgical planning.

Vessel shape alterations of the vertebrobasilar arteries in Mucopolysaccharidosis type IVa (Morquio A) patients
Y. Tanyildizi, S. Gökce, J. Hennermann, M.A. Brockmann; Mainz/DE

Objective:
Main symptom of mucopolysaccharidosis type IVa (MPS IVa) is progressive systemic skeletal dysplasia. This is routinely monitored by cerebral and spinal MRI. The vascular system is generally not in the primary focus of interest. In our population of MPS IVa patients we observed vessel shape alterations of the vertebrobasilar arteries, which has not been described before

Materials:
MRI-datasets of 26 patients with MPS IVa acquired between 2008 and 2015 were eligible for retrospective analysis of the vertebrobasilar arteries. The vessel length and angle of the basilar artery (BA) and both vertebral arteries (VA) were analyzed. A deflection angle between 90° and 130° in the vessel course was defined as tortuosity, less than 90° as kinking. The results were compared to an matched control group of 23 patients not suffering from MPS.

Results:
The deflection angle [°] of the VA and BA was significantly decreased in the majority (85%) of MPS IVa patients (Fig. 1) compared to the control group: BA 132±24 vs. 177±6, BA/VA transition 113±21 vs. 152±13, right VA 108±23 vs. 156±13, left VA 110± 22 vs. 157±14 (all $p<0.005$). Likewise, vessels of MPS IVa patients were significantly longer compared to the control group: BA 27±4 vs. 21±2, right VA 20±6 vs. 10±1, left VA 18±5 vs. 11±2 (all $p<0.005$).

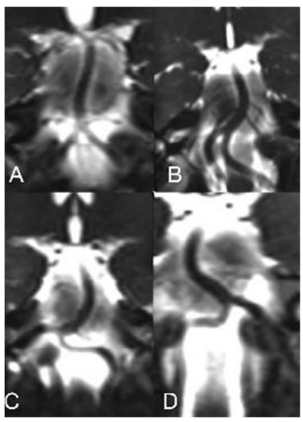

Fig. 1 Coronal view MRI of the vertebrobasilar arteries in four patients suffering from MPS IVa A) normal course, B) tortuosity C) kinking D) kinking

Conclusion:
MPS IVa is associated with significantly increased tortuosity of vertebrobasilar arteries. Therefore the vascular system of MPS IVa patients should be monitored on routinely basis, as vessel shape alterations had been associated with dissections, leading to a higher risk of cerebrovascular events.

Intraspinal cyst presenting as a pediatric emergency: Imaging considerations
E. Vazquez, I. Delgado, A. Sanchez-Montañez, P. Cano, A. Macaya, M.A. Poca; Barcelona/ES

Objective:
In the pediatric population, intraspinal cysts (arachnoid or neurenteric cysts) are rare lesions mainly located in the thoracic region, whose acute onset is not well described in the literature.

We present a series of four children seen in the last two years as spinal cord emergencies and discuss the clinical aspects, imaging diagnosis, and management approaches, particularly in the emergency setting. A comparison of our cases with those reported in the literature is also provided.
As in other types of spinal cord lesions, MR imaging is the diagnostic procedure of choice, because of its potential to demonstrate the exact location and extent of the cyst and its relationship to the spinal cord, valuable information for planning surgical treatment.

Materials:
This is a retrospective review of 4 cases of pediatric intraspinal cyst occurring in 4 boys and 1 girl, aged 2 to 6 years, treated at our institution between 2014 and 2016. Onset was sudden in all cases and mimicked transverse myelitis or infarction.
All our affected patients had no preceding history of trauma and presented with signs of spinal cord compression—back pain and less commonly abdominal pain—followed by weakness.
All patients underwent emergent MR imaging, including T1, T2, T2*, 3D CISS, diffusion imaging and enhanced T1 sequences, mainly in the sagittal and axial planes.

Results:
In each sequence, MR imaging showed a well-defined cystic lesion with signal intensity similar to cerebrospinal fluid, and secondary spinal cord compression that was severe in most cases. Blood remnants were not visualized within or around the arachnoid cyst in any patient, which correlated with the absence of trauma antecedents.
Three of the four cysts were located in an anterior position relative to the spinal cord, and only one was located posteriorly; this latter had an associated subdural effusion. None of our patients had an associated neural tube defect.
All patients were urgently treated with cyst wall fenestration or resection. The symptoms improved in all except one patient, whose symptoms did not abate, but ceased to progress.

3 year boy presented in March 2015 with abdominal pain, followed by loss of strength in the lower left extremity. MR imaging in T2 sagittal plane shows an intraspinal cystic lesion anterior to the cord at D4-D5 level with severe mass effect.

2 year old girl presented in November 2015 with weakness of the lower limbs of left predominance. MR imaging on T2 sagittal plane demonstrates a cystic lesion at D4-D6 level, dorsal to the spinal cord, with associated subdural effusion.

6 year old boy presented in October 2016 with progressive paraparesis and sphincter dysfunction, without previous trauma. MRI sagittal T2WI shows an intraspinal cyst, anterior to the spinal cord, at C7-D3, with significant compression of the cord.

Conclusion:
A prompt emergent diagnosis with MR imaging is important, as the symptoms can resolve if surgical treatment is performed before the spinal cord becomes irreversibly damaged.
Urgent surgery is essential in these cases, particularly if progressive neurological dysfunction develops over the course of spinal cord compression.
The outcome following surgical fenestration or excision is excellent in most cases.
Nevertheless, a long-term imaging follow-up is recommended to detect possible recurrence.

Automated quantification of myelin in children using multiparametric quantitative MRI

H.G. Kim[1], J.W. Choi[1], S.-M. Gho[2], Y. Lee[2]; [1]Suwon/KR, [2]Seoul/KR

Objective:

The objective of this study was to evaluate the usefulness of multiparametric quantitative MRI model for myelination quantification in children.

Materials:

Twenty-two children (age range: 9-5,400 days) were scanned with multiparametric quantitative MRI. Total volume of myelin water fraction (MWF) (Msum), the percentage of Msum within the whole brain parenchyma (Mbpv), and the percentage of Msum within intracranial volume (Micv) were obtained. MWF values of brain regions were acquired by drawing regions of interests. The values were fitted to representative models of myelin maturation. Spatiotemporal pattern of MWF mapping was visually assessed.

Results:

Values of Msum, Mbpv, and Micv well fitted to a developmental model of myelination. MWF of brain regions well fitted to a developmental model with high R^2 values: pons (R^2=74.6), middle cerebeller peduncle (R^2=75.5), genu of corpus callosum (R^2=93.6), splenium of corpus callosum (R^2=79.7), thalamus (R^2=85.8), frontal white matter (WM) (R^2=95.7), parietal WM (R^2=95.1), temporal WM (R^2=93.7), occipital WM (R^2=94.5), and centrum semiovale (R^2=82.1). MWF mapping followed the known spatiotemporal pattern of myelination.

Conclusion:

Multiparametric quantitative MRI is a useful tool for MWF quantification in children.

Role of MR Imaging of the Orbit in Staging of Retinoblastoma: Prospective Study Correlated with Histopathological Results

A. Youssef, Y. Sameh, H.E. El Zomer, H. Taha, H. El Kiki; Cairo/EG

Objective:

Retinoblastoma is the most common intraocular tumour of childhood. It is a highly malignant. Retinoblastoma is curable. If detected while still confined to the globe and if there are no metastatic risk factors, the child will nearly always survive following appropriate treatment. Our aim is to assess diagnostic accuracy of preoperatively performed magnetic resonance (MR) imaging for detection of tumor extent in patients with histopathologically proved retinoblastoma.

Materials:

Local ethics committee approval and informed consent were required for reviewing of patients' images and records. Fifty-eight eyes in 30 girls and 27 boys with retinoblastoma (mean age at diagnosis was 23 months ±18.9) were reviewed on unenhanced T1wi, T2wi, and gadolinium-enhanced T1-weighted MRI with and without fat suppression. MRI parameters such as anterior chamber hyperintensity, involvement of choroid, ciliary body, optic nerve, sclera, orbital fat, and pineal gland were determined. Maximum tumor diameter was measured and correlated to metastatic risk factors. Imaging and pathologic findings were compared.

Results:

Choroidal invasion was suspected with MR imaging in 47/58 eyes; findings were false-positive in 6 eyes and false-negative in two (accuracy, 86.2%; sensitivity, 95.3%; specificity, 60%). MR imaging findings were true-positive in 10 of 17 eyes with proved prelaminar optic nerve invasion (60% sensitivity) and false-positive in 7 (82.9% specificity, 75.8% accuracy). Postlaminar optic nerve invasion was correctly detected in 23 eyes; 4 eyes were false positive, in other 4 eyes, this metastatic risk factor was missed (accuracy, 86.2%; sensitivity, 85.2%; specificity, 87%). Of nine eyes with histologically proven scleral invasion, 5 eyes were true positive . In the other 4 eyes, scleral involvement was missed on MRI (accuracy, 93%; sensitivity, 55.6%; specificity, 100%).Extraocular fat invasion was suspected on MRI in 5/58 eyes. Of these, findings were truly positive in 4 eyes (80%) and in 1 eye (20%) was incorrect (false positive) (accuracy, 98.3%; sensitivity, 100%; specificity, 98%).Anterior chamber hyperintensity on T1-weighted MR images obtained after contrast agent administration correlated well with main MRI and histolopathology findings. Tumor size (assessed in our study by the maximum diameter in mm) was statistically associated with postlaminar optic nerve invasion (ρ=.002) and choroidal invasion (ρ=.007).

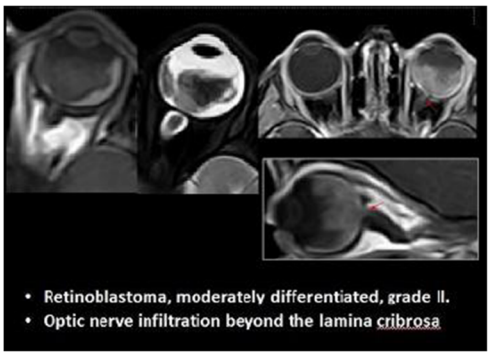

Conclusion:

MR imaging shows promising role for tumor staging and detection of metastatic risk factors. Tumor diameter, measured with MR imaging, is associated with postlaminar optic nerve and choroidal involvement.

Patterns of the cortical watershed continuum of term gestation hypoxic ischaemic injury – the "Wish-bone sign"

A. Chacko[1], S. Andronikou[2], S. Vedajallam[1], J. Thai[2]; [1]East London/ZA, [2]Bristol/UK

Objective:

Background

Partial-prolonged term hypoxic ischaemic injury (HII) involves the cortical and subcortical watershed zones of the brain, which are visually difficult to conceive. New innovative methods of demonstrating watershed cortical atrophy using flattened maps of the brain surface gives added insight into distribution of the watershed zone by demonstrating the entire brain surface.

Aim

Determining and validating patterns of HII sustained at birth in term infants using cross-sectional MRI and the innovative Mercator and scroll map views of cortical surface anatomy, to define the distribution of the watershed zones in children with partial-prolonged injury.

Materials:

One hundred paediatric MRI brain scans with an MRI and clinical diagnosis of chronic term hypoxic injury were read by 3 radiologists independently. All sites of abnormality were recorded and patterns classified.

Patients with partial-prolonged and combined patterns were evaluated using Mercator and scroll map reconstructions, generating schematics of the watershed zone.

Results:
Predominant patterns of disease were partial-prolonged and acute-profound types. The watershed zone was demonstrated, on the derived maps, representing a continuum of involvement in the shape of a 'wish-bone' extending bilateral from frontal lobes to posterior parietal lobes in band-like fashion along the para-falcine cortex and intersected by another band of atrophy in the peri-Rolandic regions extending along peri-Sylvian cortices. This is defined in schematics as a visual aid.

Conclusion:
Predominant patterns of injury in term hypoxic ischaemic injury are described and quantified, with the 'wish-bone sign' introduced to describe the typical distribution pattern of partial-prolonged HII in the watershed zone.

Correlation of brain edema degree and biochemical parameters in pediatric posterior reversible encephalopathy syndrome with hematologic/oncologic diseases

T. Akbas[1], S. Ulus[2], B. Karagun[1], T. Arpaci[1], C. Kalayci[2], B. Antmen[1]; [1]Adana/TR, [2]Istanbul/TR

Objective:
Posterior reversible encephalopathy syndrome (PRES) often associated with hypertension is characterized by typical transient parieto-occipital predominantly brain edema on magnetic resonance imaging (MRI) with neurological symptoms such as seizures, headache and visual disturbances. Even if endothelial dysfunction, increased blood- brain barrier permeability and hyper- hypoperfusion remain as controversial mechanisms to explain, the pathophysiology of PRES is unremain. The aim of our study was to investigate the correlation between brain edema degree on MRI and serum biochemical parameters such as lactate dehydrogenase (LDH), albumin (ALB), creatinine, uric acid (UA) and urea.

Materials:
A total of 27 pediatric hematology and oncology patients (19 male, 8 female, aged 3-17, mean age: 11 years 6 months) diagnosed with PRES during treatment and after hematopoietic stem cell transplantation (HSCT) were included in this retrospective study. Underlying diseases were beta thalassemia (n:14), aplastic anemia (n:4), acute lymphoblastic leukemia (n:4), acute myeloid leukemia (n:3), lymphoid leukemia (n:1) and Burkitt's lymphoma (n:1). PRES was seen after undergoing HSCT in 21 patients. The brain edema degree according to specified anatomical regions on fluid attenuation inversion recovery (FLAIR) MRI sequence was scored by two radiologists blinded to patients' records. The levels of serum biochemical parameters at onset of symptoms were correlated with score of brain edema degree on MRI.

Results:
Serum LDH concentration was statistically correlated with the score of brain edema degree (Spearman's rho correlation, r=0.459, P=0.016). No relationship was found between other biochemical parameters and the score of brain edema degree.

Conclusion:
Our results suggest that increased serum LDH as a marker of endothelial dysfunction is the main biomarker for development of brain edema in pediatric PRES patients under treatment and after HSCT with underlying hematologic and oncologic diseases.

T1 signal intensity changes of deep brain nuclei after multiple gadobenate dimeglumine injections: Comparison of children and adults

S. Kinner[1], T. Schubert[2], S. Rebsamen[2], S. Reeder[2], H. Rowley[2]; [1]Essen/DE, [2]Madison/US

Objective:
Gadolinium based contrast agents (GBCAs) have been associated with increasing signal intensities in deep brain nuclei on unenhanced T1-weighted brain imaging. Until now, most studies have been performed in adults, while results on pediatric patients are sparse. Therefore, the aim of this study was to evaluate if there is any difference between signs of gadolinium retention in pediatric and adult patients.

Materials:
In this IRB-approved, single center retrospective study, we extracted all patients with at least 5 contrast-enhanced MRIs archived on PACS between 2009-16. All patients with gadobenate dimeglumine only enhanced MRIs were reviewed. Seventy-six pediatric patients with the most injections and 86 adult patients with the most injections were included in the final evaluation. Therapies were documented. T1 signal intensity measurements for the initial and last unenhanced brain MRIs were performed for dentate nucleus, pons, globus pallidus and thalamus. Signal intensity ratios for dentate-to-pons (DNP) and globus pallidus-to-thalamus (GPT) were calculated and correlated with number of injections and time interval as well as therapy. Differences between adults and pediatrics were assessed.

Results:
Mean age for the pediatric group was 9.3 years compared to 47.7 years in the adults. No significant difference was found for gender distribution (47 vs. 43% females) and follow up time (3.1 vs. 3 years). There was no difference concerning the signal intensities on first and last MRI in children and adults (p=0.81/0.84, respectively). For each additional year of follow-up the change in ratio increases by 0.016 for adults but only 0.002 for peds (p=0.002). Comparing therapies, in children a statistically significant difference between patients with and without former radiation was found (p<0.001) while there was no difference in adult patients with and without therapy (p=0.65).

Conclusion:
Children and adults show a similar increase in T1 signal in deep brain nuclei ascribed to gadolinium deposition. In children, radiation and chemotherapy) seem to have a higher influence on gadolinium deposition. This correlation cannot be found in our adult cohort, indicating therapies have no (additional) influence.

Kearns-Sayre Syndrome (KSS): Neuroimaging in 8 cases

L. Pasquini[1], D. Narese[2], M.C. Rossi Espagnet[1], S. Stagliano`[1], A. Napolitano[1], D. Longo[1]; [1]Rome/IT, [2]Palermo/IT

Objective:
Kearns–Sayre syndrome (KSS) is a rare mitochondrial DNA-deletion syndrome characterized by early onset (<20 years), progressive external ophthalmoplegia and pigmentary retinopathy, often associated with cerebellar ataxia, muscle weakness, bilateral sensorineural hearing loss and cardiomyopathy.
Pyramidal symptoms may be present in KSS, but they are poorly reported in the literature.
Through this case series, we aim to evaluate the concordance with the imaging patterns proposed by literature, correlating them with clinical and laboratory data, and to investigate possible microstructural damage with diffusion tensor imaging (DTI) and magnetic resonance spectroscopy (MRS).

Materials:
We evaluated eight patients (8-19 years of age) with genetically confirmed diagnosis of KSS.
All Pts. were studied with 3T/1.5T MRI.
In 5/8 Pts. the study was completed by MRS and in 7/8 by DTI imaging with reconstruction of cortico-spinal tracts (CST) using a 2-ROIs approach.
A t-test comparative study between mean fractional anisotropy (FA) of CST in the 7 KSS patients with DTI and a group of 4 healthy controls was performed.

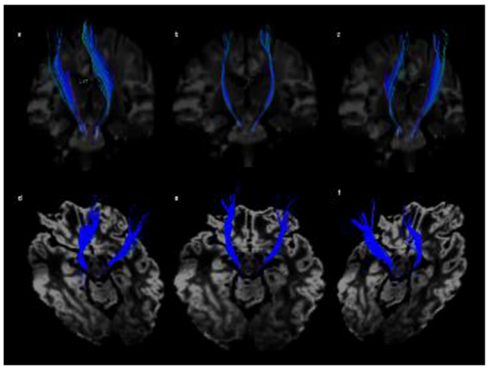

CST reconstruction in a patient suffering from KSS (images a-c), compared to an healthy control (images d-f). The DTI study showed significantly reduced FA values, pointing out a possible microstructural damage.

Results:
The disease showed an MR pattern of mixed white and gray matter signal abnormality, with periventricular and/or subcortical white matter hyperintense lesions, which in 1/8 Patient presented a "tigroid pattern" (Fig.2)
Three Patients displayed a disease extension to the cervical spinal cord. (Fig.2)
DWI images demonstrated restricted diffusivity in almost all lesions (Fig.3), with persistence of low ADC values.
MRS study documented a high lactate peak in 2/8 Pts. and a NAA reduction in 5/8 Pts; an increment of GSH was noted in one Patient (Fig.3).
The t-test comparative study of CST showed a significant reduction of mean FA value in KSS patients compared to healthy controls (P= 0,004).

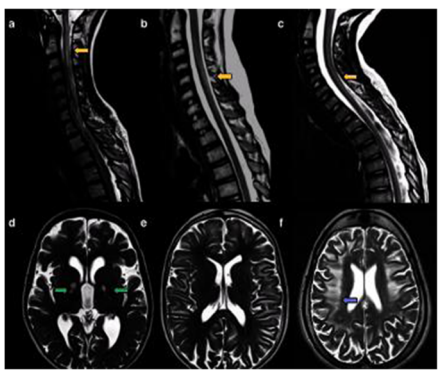

Involvement of the spinal cord (a-c, yellow arrows). Comorbidity was suspected in "a" (myelitis). Below (d-f): pale nuclei (d, green arrows) and subcortical white matter (e) alterations. Right image displays the "tigroid pattern" (purple arrow).

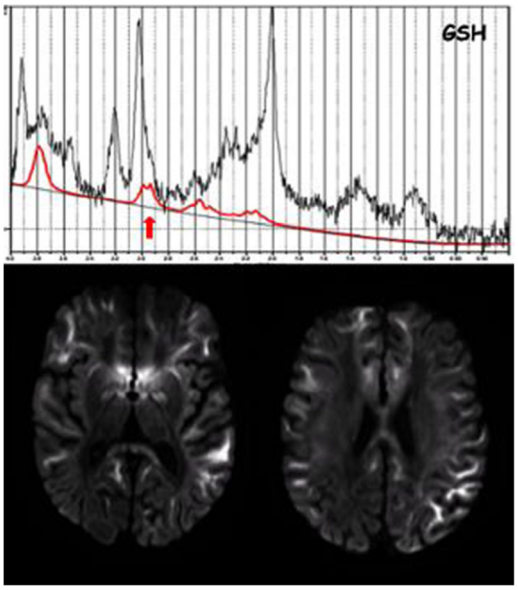

MRS showing the presence of a GSH peak, which may suggest an augmented antioxidative activity within the encephalic tissue. Below: DWI hyperintensity in many regions of the brain in Patients suffering from KSS, due to diffusion resctriction.

Conclusion:
The integration of neuroimaging with clinical data can implement the diagnosis of mitochondrial diseases such as KSS.
According to our experience, comorbidities can delay the achievement of a correct diagnosis.
The finding of an altered signal in the spinal cord of 2/8 Pts. may suggest a new possible localization of the disease, while in one Patient was referable to myelitis (Fig.2, a)
The evidence of a "tigroid patter" in should be taken in count in the differential diagnosis with lysosomal disorders.
The presence of a prominent GSH peak may represent an augmented antioxidant activity, which may correlate with a more favorable outcome.
An involvment of CST can be speculated even if pyramidal symptoms are poorly represented in KSS.

SESSION: SCIENTIFIC SESSION: MSK

Ultrasound for monitoring distraction of magnetically controlled growing rods (MCGR): A reproducible geometric technique

G. Poillucci[1], P. Guastalla[1], A. Pellegrin[1], F. Vittoria[1], E. Cattaruzzi[2]; [1]Trieste/IT, [2]Muggia/IT

Objective:
Remotely distractible, magnetically controlled growing rod (MCGR, Fig. 1) system has been developed to allow for gradual lengthening on an outpatient basis. This allows for safe spinal lengthening with continuous neurologic monitoring and real-time feedback by the patient. This study aims to evaluate retrospectively our ultrasound (US) geometric method and his accuracy compared with the plain radiograph (gold standard) for assessing MCGR distractions.

Materials:
This is a retrospective study that includes patients with early-onset scoliosis undergoing multiple consecutive distractions after MCGR implant. The rods length was measured for with US, for each distraction (3-months interval), and compared with plain radiograph follow-up (1-year interval). All patients included were treated with dual-rod systems. Distraction length was monitored by a senior radiologist with US at each visit, one rod at a

time, before and after magnetic lengthening, with our geometric measurement method (Fig.2). Low-dose upright two-projections radiograph were taken immediately after surgery and at 1-year intervals and measured by two radiologists (1 and 10 years of experience respectfully)(Fig.3). We compared measurements with the Wilcoxon signed-rank test.

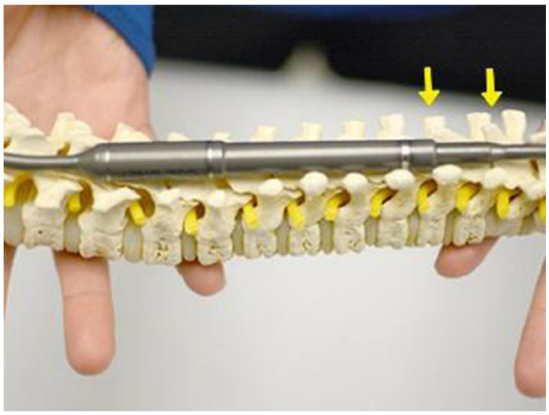

Fig. 1: MAGEC® system. The yellow arrows point to the segment object of this study

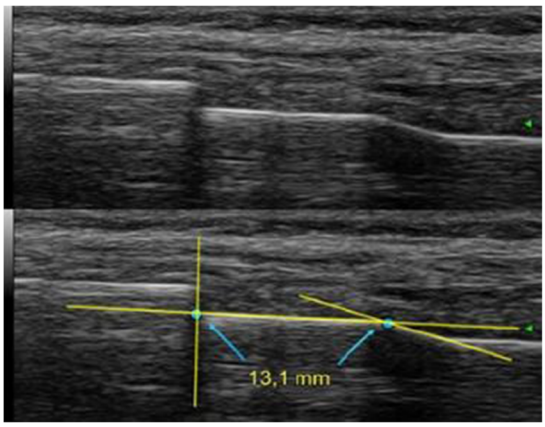

Fig.2: 11 yrs old female. The figure shows the same image - a magnetic expandible rod- without and with graphics. Please note the three-line method used in our institute to standardize measurements and increase accuracy.

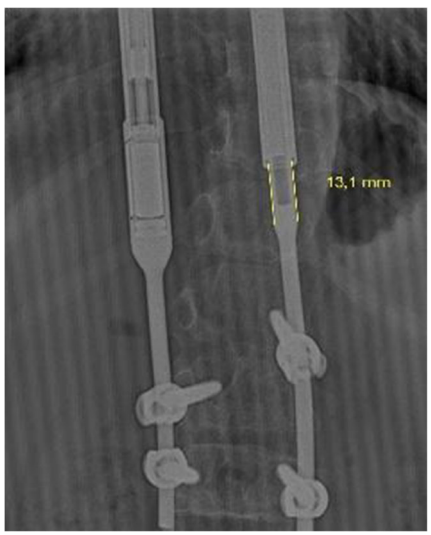

Fig.3: Plain radiograph (AP projection) of the same patient as in Fig.1, at the same time. The corresponding measured segment is highlighted by the yellow line.

Results:
From January 2014 to October 2016, a total of 5 patients (4 females and 1 male), which diagnoses included mitochondrial encephalopathy syndrome (n=1), spina bifida (n=1), ataxia of unknown cause (n=1), juvenile idiopathic scoliosis (n=1) and Trisomy 8 (n=1), with a mean of 10 distractions per patient (standard deviation [SD] ±1,2), were recruited. Fifty distractions for each system (95 measurements in total) were performed, targeting different lengths of distraction (from -2.0 mm to +4.6 mm) on each occasion. A total of 21 sets of plain radiographs were taken. From these, 18 sets of data points were used for correlation analysis. The mean distracted length per year on plain radiographs was 10,1 mm (SD ± 3,8 mm) and the mean distracted length on US per 6-months interval was 4,5 mm (SD ± 2,9 mm). Excellent correlation was observed between radiographic and ultrasound measurements. In particular, correlation between RX measurements and ultrasound was excellent both for junior ($0.001<p<0.005$, W=70) and senior radiologist ($p<0.001$, W=28,5). There were no rod's breaches identified neither in ultrasound or radiographs in this series.

Conclusion:
The measured changes in rod length between the two imaging modalities were highly correlated. Thus, ultrasonography is at least as accurate as radiographs in measuring changes in rod length. Our geometric measurement method adds reproducibility to an effective, non-ionizing and low-cost procedure for monitoring distraction of MCGR in children population.

Refuting child abuse denialists – healing rickets is clearly different from child abuse metaphyseal fracture
A.E. Oestreich; Cincinnati/US

Objective:
Child abuse denialists, who testify against the diagnosis of child abuse, often claim that radiographic findings generally recognized by pediatric radiologists as likely due to abusive trauma are instead a consequence of rickets, including healing rickets. In particular, bucket handle transverse bony density at metaphyses are declared by some denialists to be identical to the pattern of healing rickets. I demonstrate by reviewing the details of these different patterns that this is an incorrect declaration. Additionally, concave distal ulna margins alone are not a sign of rickets. Rickets is radiologically distinct from classic metaphyseal fractures.

Materials:
I reviewed medicolegal documents and published articles by several well known physicians who claim that certain children suspected of having suffered child abuse instead demonstrate rachitic bone disease. Their statements and images in support of their opinions are critically reviewed and contrasted with known examples of rickets, including healing rickets.

Results:
At the physeal region of long bones in rickets, the zone of provisional calcification (ZPC) is not calcified and the normal metaphyseal collar shaftward from that zone is not maintained. In metaphyseal fractures from abuse, the ZPC and collar are maintained. In early healing rickets, the zone of provisional calcification calcifies first, giving a transverse calcification separated from the already ossified metaphysis. This calcification is different from a bucket handle fracture pattern without signs of rickets. Moreover, concave distal margin of the ulna without other signs of rickets is seen in about 20% of normal infants. Repeatedly, denialists have testified against the diagnosis of child abuse, claiming rickets in the absence of radiographic evidence – I critique one well known "Commentary" article by two of them (all 4 cases show normal ZPC and intact metaphyseal collar) and I show other denialists quoting incorrect examples of rickets. I contrast the specific patterns of bucket handle metaphyseal fracture and healing rickets. Moreover, rickets is systemic and affects all enchondral growth zones, while abuse fractures are limited to individual sites.

Conclusion:
Child abuse is a serious diagnosis – claiming by denialists of an alternate diagnosis, such as rickets, when radiographically no rickets is present, should be refuted. A clear understanding of the differences between abuse fractures and rickets is obligatory. When no rickets is seen at other growth sites, including seeing the presence of zones of provisional calcification, rickets is not present.

Simultaneous Multi-Slice Turbo Spin Echo: A 2-fold time-saving alternative to conventional TSE in MR imaging of the pediatric knee
S. Benali, A. Gholipour, P.R. Johnston, S.D. Bixby; Boston/US

Objective:
Simultaneous multi-slice (SMS) is a novel iteration of parallel imaging in MRI that reduces acquisition time at least two-fold over conventional turbo spin echo (TSE) acquisitions. The aim of this study is to determine whether 2-dimensional (2D) SMS TSE can replace conventional 2D TSE in imaging of the knee in pediatric patients without compromising diagnostic quality.

Materials:
This was an IRB-approved retrospective study. Subjects included all pediatric patients referred for routine 3-Tesla MRI of the knee between October through December 2016. MRI examination consisted of institutional basic protocol with both traditional T2 TSE and SMS T2 TSE in axial and sagittal planes with fat suppression. Two anonymized study folders were created for each subject, one containing all basic sequences (basic exam), and one in which T2 TSE sequences were substituted with T2 SMS sequences (SMS exam). Two pediatric radiologists independently and blindly reviewed each study and noted presence or absence of 15 pre-determined abnormalities (Table 1). Discrepancies between radiologists were settled by consensus. Qualitative assessment was performed using a Likert scale to evaluate edge blurring, contrast resolution, image noise, and flow artifact.

Results:
Thirty-five subjects comprised the study population (mean age 14.6 years, range 8-20, 26 female, 9 male). Diagnostic performance was assessed by comparing findings (Table 1) from basic exam to SMS exam based on absolute agreement and Cohen's kappa statistic. For all findings, the proportion of absolute agreements between basic and SMS exam was >0.96 for Reader 1, > 0.88 for Reader 2, and 1.00 for consensus between readers. Kappas for consensus reads were 1.00 on all 15 structures ($p<$ 0.001, lower 95% confidence limit >0.97). For Reader 1, kappas were 1.00 for 14/15 structures ($p<$ 0.001) and 0.00 for PCL. For Reader 2, kappas were 1.00 for 14/15 structures ($p<$ 0.001) and 0.45 for cartilage defects. Paired t-test was used to compare mean Likert scores for image quality characteristics. For both readers, SMS was preferred for flow artifacts whereas TSE was preferred for the three remaining image quality characteristics ($p<$ 0.05).

Imaging findings (n=35 patients)	
Abnormalities	**Number of abnormalities**
Medial meniscus tear	3
Lateral meniscus tear	6
Discoid meniscus	5
Anterior cruciate ligament tear/sprain	7
Posterior cruciate ligament tear/sprain	1
Medial collateral ligament tear/sprain	5
Lateral collateral ligament tear/sprain	1
Cartilage defect	6
Osteochondral defect	3
Free body	3
Bone contusion	10
Fracture	5
Bone lesion	5
Patellar retinaculum tear/sprain	2
Extensor tendon tear/sprain	4
	Total abnormalities = 66

Table 1: Imaging findings in the study population

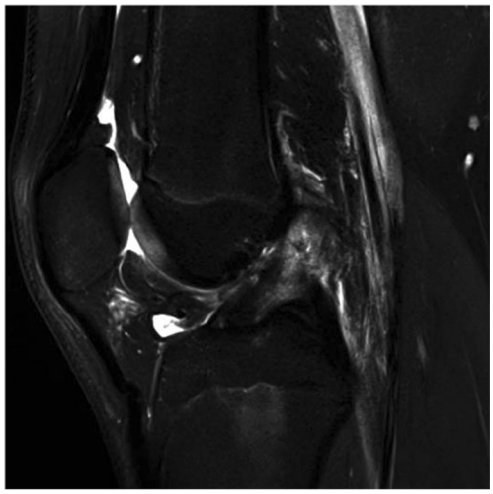

Image 1: Sagittal T2 TSE in a 13 year-old female showing complete tear of the anterior cruciate ligament (ACL)

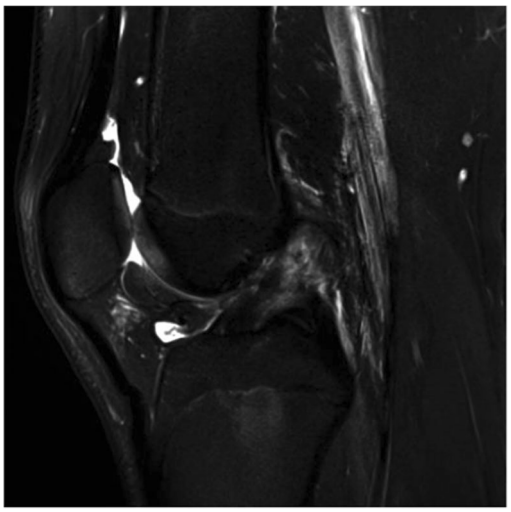

Image 2: Sagittal T2 SMS TSE in the same patient showing complete tear of the ACL

Conclusion:
Our primary assessment suggests that SMS T2 TSE is comparable to standard TSE in terms of diagnostic performance in the evaluation of the pediatric knee despite modest decrease in overall image quality. The 2-fold decreased acquisition time of SMS is a significant advantage which is felt to offset the mild decrease in image quality, particularly as it increases the likelihood that children will tolerate the examination without motion.

MRI for sacroiliitis in children: Panel findings and inter-observer evaluation using standardised reporting
K.E. Orr[1], M.J. Bramham[1], S. Andronikou[2]; [1]Plymouth/UK, [2]Bristol/UK

Objective:
There is little evidence regarding MRI for diagnosing sacroiliitis in children with Juvenile Idiopathic Arthritis (JIA). The limited literature presents varied opinions but no published recommendations for standardisation of reporting. Axial disease in JIA responds poorly to conventional first-line treatments but identifying these children using history and examination findings is unreliable. Standardised MRI reporting

may improve diagnosis and selection of patients in whom newer biologic treatments are indicated.
The aim was to use a standardised reporting proforma based on published definitions for recording MRI findings in suspected sacroiliitis to evaluate inter-observer agreement and determine the reliability of findings according to specific sequences.

Materials:
Ninety-nine sacroiliac joint MRIs (198 joints) were included, 80 were initial examinations and 19 were follow-up MRIs. The age range was between 6.6 and 20.3 years (mean age 15.4 years).
Three readers retrospectively reported all 99 MRIs using the standardised proforma. 'Reader 1' was the study group panel while readers 2 and 3 were specialist paediatric radiology consultants working in the United Kingdom. Readers were blinded to additional clinical information and other imaging.
Inter-reader variation was evaluated for the presence of bone marrow oedema, erosions, effusions, ankylosis, sclerosis and enhancement, as well as the presence or absence of sacroiliitis.
The quality of MRI examinations was evaluated, including presence and adequacy of sequences performed and alignment of the coronal/oblique studies.
MRI findings were correlated with clinical details and final diagnosis.

Results:
Sequences included in the 99 MRIs were: T2/STIR (99/99, 100%); T1 without fat suppression (90/99, 91%); contrast-enhanced T1 (76/99, 77%); and DWI (80/99, 81%). Of note, 45/99 MRI examinations (45%) had suboptimal coronal/oblique alignment.
The panel deemed 12 MRI scans (12%) positive for sacroiliitis (2 bilateral, 5 left-sided and 5 right-sided). Oedema was present in 8 (8%), joint effusions in 4 (4%), erosions in 8 (8%), abnormal enhancement in 3 (3%), and sclerosis in 6 (6%). All cases with abnormal enhancement had other features of sacroiliitis.
Inter-reader agreement and clinical correlation are pending.

Conclusion:
There is significant variability in sacroiliac joint MRI protocols. Refinement of these to include only necessary sequences based on inter-reader reliability and reinforcement of good positioning will improve reporting and result in universal standardisation.
There is inconsistency in current reporting practice of sacroiliac joint MRI in children but increasingly, clinicians rely on imaging to select patients with sacroiliitis and guide appropriate treatment. Using a standardised reporting proforma may improve the quality and consistency of reporting.

Ultrasound-guided steroid tendon sheath injections in Juvenile Idiopathic Arthritis

S. Peters, D.A. Parra; Toronto/CA

Objective:
Juvenile Idiopathic Arthritis (JIA) is the most common chronic rheumatic disease in childhood. Tenosynovitis is one of the manifestations of JIA, which can explain the absence of response to treatment when adjacent joints are injected. Steroid injection is one of the treatment options for tenosynovitis and it has been shown to be effective in the literature. Utilizing Ultrasound (US) guidance for injections into tendon sheaths has shown clinical advantage to conventional blind injections in the adult rheumatoid arthritis population. The aims of this study are to: (a) Identify tendon sheaths most commonly treated in our patient population with JIA referred for steroid injections; (b) Describe technical aspects of the procedure; (c) Characterize sonographic appearance of tenosynovitis in JIA; (d) Assess agreement between clinical request and sites injected.

Materials:
This was a 10 year single-center retrospective study (May 2006-April 2016) in which we recruited patients with JIA referred by Rheumatology for US-guided tendon sheath injections. We collected patient demographics, clinical assessment information, sonographic appearance of the tendons and technical aspects of the intervention from the procedure records.

Results:
We collected data from 308 visits of 244 patients (75% female, mean age 9 years 8 months) with a total of 926 injections. The ankle region was most commonly injected (85%), specifically the tendon sheaths of tibialis posterior (22%), peroneus longus (20%) and brevis (20%). 63% of the procedures were performed under general anesthesia and triamcinolone hexacetonide was used in 97% of the injections. An "out of plane" approach was used in 86% of the interventions and the 15 MHz "hockey stick" US probe was preferred for guidance (86%). We found 2 minor intra-procedure complications without sequelae. The majority of treated sites (92%) showed peritendinous fluid and sheath thickening on US. Other findings were increased color-Doppler signal and echogenic peritendinous fluid. A strong agreement between clinical request and sites injected was observed and most patients required one visit (78%).

Conclusion:
US-guided tendon sheath injections are used frequently to treat patients with JIA. It is a safe intervention with a high technical success rate. The ankle region, specifically the medial compartment, is the area most commonly injected in this cohort of patients. The most common sonographic finding is peritendinous fluid and sheath thickening. These findings might assist radiologists and rheumatologists to characterize and more effectively manage tenosynovitis in patients with JIA.

Artificial intelligence with deep learning technique in the determination of bone age: Accuracy and feasibility study

J.R. Kim, H.M. Yoon, J.S. Lee, Y.A. Cho, A.Y. Jung; Seoul/KR

Objective:
To evaluate the accuracy of the software for automatic bone age (BA) estimation based on deep learning technique, and to validate the feasibility of this system in clinical practice.

Materials:
The software for automatic BA estimation was developed based on deep learning technique using 18,940 left hand radiographs and estimated BA of each radiograph based on Greulich-Pyle method. BA estimation was done for left hand radiographs of 100 consecutive patients (9 months – 17 years; 42 boys and 58 girls) in three methods: (1) AI bone age (assessed by the software), (2) AI-assisted BA (assessed by two radiologists with the assistance of the software), (3) GP atlas-assisted BA (assessed by two radiologists with only GP atlas but the software). The reference BA was determined by two radiologists by consensus. The accuracy of the estimated BA by each method was assessed using concordance rate (%), Pearson's correlation analysis, the root mean square error (RMSE), and Bland-Altman plot. Reading time for BA estimation by each method was evaluated.

Results:
AI bone age showed 61% of concordance rate, and a significant correlation with reference BA (r2=0.986, $P<0.05$). The Bland-Altman plot of agreement between the reference BA and AI bone age showed the mean difference of - 0.20 years (95% limit of agreement, ±1.22 years). RMSE was 0.42 years.
In reviewer 1, concordance rates were same between both GP atlas-assisted BA and AI-assisted BA (72%), and RMSE of AI-assisted BA (0.20) was slightly lower than that of GP atlas-assisted BA

(0.23). In reviewer 2, concordance rate was slightly higher in AI-assisted BA (60%) than GP atlas-assisted BA (58%), and RMSE was almost the same (0.54 in AI-assisted BA, 0.55 in GP atlas-assisted BA). The reading time was reduced 20.0% in reviewer 1 and 62.7% in reviewer 2.

Conclusion:
The software for automatic BA estimation based on deep learning technique showed high accuracy and may enhance work efficiency in BA estimation by allowing radiologists to save reading time and to improve accuracy.

Temporomandibular joint MRI findings in adolescents with primary disk displacement in comparison to those in juvenile idiopathic arthritis

J. Bucheli, D. Ettlin, C. Kellenberger; Zurich/CH

Objective:
To investigate potential differences of morphology and degree of inflammation in temporomandibular joints (TMJs) affected by primary anterior disk displacement (ADD) and juvenile idiopathic arthritis (JIA).

Materials:
In 18 adolescents (15 female, age 15 ± 2 y), contrast enhanced magnetic resonance images (Fig. A) of TMJs with ADD were retrospectively compared to those of age- and gender-matched controls with JIA. Morphology of articular disk and bony structures were described. Osseous deformity and inflammation were qualitatively scored with progressive 4-grade scales and compared between groups with Mann-Whitney-U test. Mandibular ramus length, measured on gradient echo minimum intensity projection images (Fig. B), was compared between groups and to normal values with independent samples t-test.

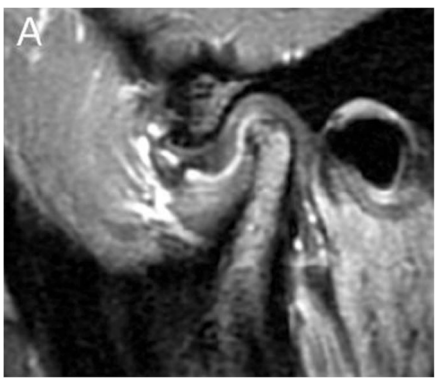

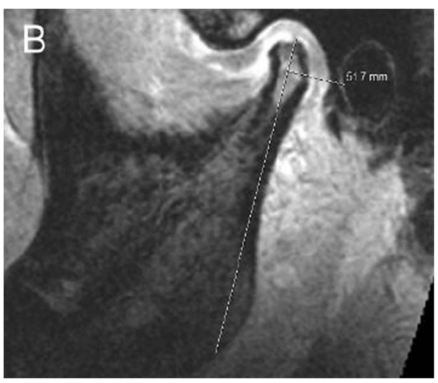

Results:
In the ADD-group, 31/36 disks were dislocated anteriorly and showed thickening of the posterior band (27/31). In contrast, TMJ disks of JIA patients were mainly flattened (n=23) and/or centrally perforated (n=12) and rarely dislocated (n=1). TMJs with ADD showed similar overall grades of inflammation (p=0.39) and osseous deformation (p=0.53) as TMJs in the JIA group. While erosions were frequent in both groups (ADD 25/31; JIA 32/36, p=0.55), the mandibular condyle (p<0.001) and glenoid fossa (p<0.001) were less flattened in TMJs with ADD. In ADD TMJs, bone marrow oedema was less frequent (p=0.001) and grades of joint enhancement slightly lower (p=0.03), but presence of synovial thickening (p=0.43) and degree of effusion (p=0.87) were not significantly different between groups. Mandibular ramus length was not significantly different (p=0.72) between groups, but in both groups clearly decreased compared to mean normal values (p<0.0001).

Conclusion:
Articular disks in TMJs affected by JIA are rarely dislocated. Surprisingly, TMJs with primary ADD show considerable inflammatory change including condylar erosions. Still, chronic systemic inflammation in JIA joints results in considerable higher deformity of the mandibular condyle and the temporal joint surface. Observation of the mostly preserved normal shape of the temporal bone may help differentiating primary ADD from JIA.

Midterm MRI follow-up of TMJ inflammation, deformation and mandibular growth in JIA patients under systemic treatment

A. Bollhalder, R. Patcas, M. Eichenberger, L. Müller, S. Schroeder, R. Saurenmann, C. Kellenberger; Zurich/CH

Objective:
To investigate the course of temporomandibular joint (TMJ) inflammation, osseous deformation and mandibular ramus growth in patients with juvenile idiopathic arthritis (JIA) not treated with articular corticosteroid injections (CSI).

Materials:
Retrospective magnetic resonance imaging (MRI) study of 49 consecutive JIA patients (35 female, median age 14 y) with at least two consecutive TMJ MRI examinations ≥ 2y apart and no CSI. Degree of TMJ inflammation was determined on T2-weighted and contrast-enhanced T1-weighted fast spin echo images (Fig. A), and degree of osseous deformity on gradient echo images (Fig. B) by progressive 4-grade scales (0–3). Change of respective grades was assessed with Wilcoxon test. Mandibular growth was determined by ramus length change and compared to normal values.

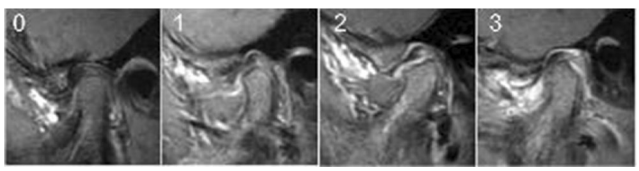

Figure A Contrast-enhanced T1-weighted images showing inflammatory grades 0-3 (normal, mild, moderate, severe)

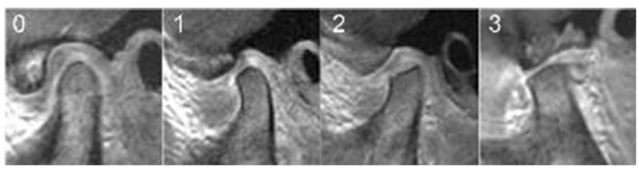

Figure B Gradient echo images showing osseous deformity grades 0-3 (normal, mild, moderate, severe)

Results:
Over a median period of 3.4 y (interquartile range, 2.4 – 4.6 y), degree of TMJ inflammation improved ($p<0.001$) with decrease in frequency of grade 3 (4.1% to 0%) and grade 2 (19.4% to 4.1%). Inflammatory grades improved both in patients with ($n=39$, $p=0.007$) and without ($n=10$, $p=0.02$) systemic disease modifying medication. The degree of osseous deformation slightly improved ($p=0.04$), with decrease in frequency of grade 3 (5.1% to 3.1%) and grade 2 (9.2% to 6.1%), and increase of grade 0 (48% to 54.1%). Overall growth rates of mandibular ramus (median, 1.3 mm/y) were not significantly different from normal growth rates ($p=0.27$) (Fig. C). Growth rates of TMJs from patients only receiving non-steroidal anti-inflammatory drugs (median, 1.25mm/y) were not significantly different ($p=0.9$) compared to patients treated with systemic disease modifying drugs (median, 1.35mm/y).

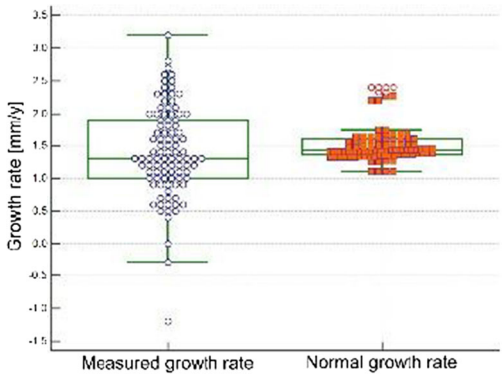

Figure C Boxplots comparing the measured growth rates to age- and gender-matched normal mean values

Conclusion:
In patients with systemic treatment of JIA, both the degree of TMJ inflammation and osseous deformity as seen on MRI improved at midterm follow-up. Normal growth of the mandibular ramus was maintained. These results are in contrast to those from an earlier cohort treated with CSI, in which on average deformities deteriorated and growth was impaired.

SESSION: SCIENTIFIC SESSION: ABDOMINAL (GI & GU) IMAGING

Pediatric Ileocolic Intussusception: Symptom Duration/Time to Enema Do Not Affect Pneumatic Reduction Success

L.A. Binkovitz[1], A. Kolbe[1], P. Thapa[1], C. Moir[1], P. Thacker[2]; [1]Rochester/US, [2]Charleston/US

Objective:
Objective: Pediatric Ileocolic Intussusception, ICI, is a common abdominal condition for which pediatric radiologists are asked to attempt emergency pneumatic reduction. Because of the high success and low complication rates of pneumatic reductions, radiologists are able to make several attempts at reduction in stable patients if the initial enema attempt is unsuccessful. We have observed patients with successful reductions with rather long periods between initial symptoms of ICI and performance of the air enema. We hypothesize that successful pneumatic reduction rates are independent of length of symptoms and in stable patients, repeated reduction attempts can be performed with the expectation of successful reduction.

Materials:
We performed an IRB-approved retrospective review of all ICI with a pneumatic reduction attempt between 2008-2016 at XXX. Clinical, imaging and surgical data was reviewed. Time to enema was defined as the time from first symptom to first air enema attempt. Linear and second order polynomial statistical analysis was performed to assess the relationship between time to enema and enema outcome.

Results:
Results: 66 ICI were identified in 61 patients. Air enema was successful in 46 ICI, 77%. The mean time to enema was 37.5 hours, range 4-168 hours with SD of 42.2 hours for successfully reduced ICI and 35.1 hours, range 2-336 hours with SD of 53.9 hours for unsuccessfully reduced ICI. Surgical resection was required in 4 patients with ischemic bowel including one with an irreducible Meckel's diverticulum as lead point. There was no correlation between time to enema and successful reduction, Fig 1. No patient with a successful pneumatic reduction of a ICI required subsequent bowel resection.

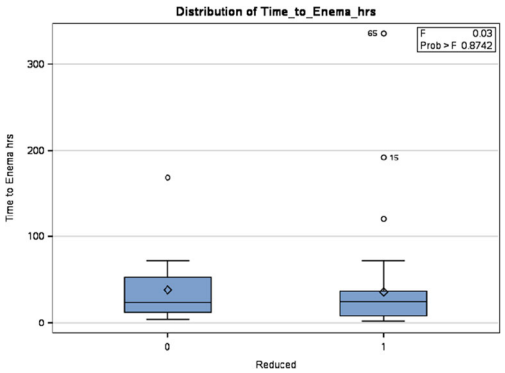

Pneumatic Reduction Success vs Time to Enema

Conclusion:
Conclusions: Air enema for ICI can be safely performed despite prolonged time to enema with the anticipation of a successful reduction. The lack of correlation of pneumatic reducibility and time to enema suggests that in surgically cleared patients with ICI, the pneumatic reduction attempt may not be a true emergency and that repeated attempts at reduction are safe. Additionally, though our numbers are small, they suggest that an ICI is reducible or not from the beginning and do not "become irreducible" with prolongation of the time to enema.

Evaluation of splenic stiffness measurements for the diagnosis and the follow-up of portal stenosis after paediatric liver transplantation

C. Escalard[1], A. Dabadie[2], S. Chapeliere[1], D. Pariente[1], C. Adamsbaum[1], S. Franchi[1]; [1]Le Kremlin-Bicêtre, Paris/FR, [2]La Timone, Marseille/FR

Objective:
To report our preliminary findings about the role of splenic and hepatic supersonic shear-wave elastography (SSWE) in the diagnosis and follow-up after treatment of portal stenosis in paediatric liver graft recipients.

Materials:
All paediatric liver recipients with portal stenosis treated by the interventional radiology procedure, and who underwent splenic and hepatic SSWE pre and post interventional procedures, were retrospectively reviewed. Demographics, data about the portal stenosis (delay post transplantation, clinical presentation, initial radiological findings, hemoglobin and platelet counts), IR procedure performed, clinical and ultrasonographic follow-up and spleen stiffness pre and post IR procedure were collected.

Results:
Four patients were included, median age 6,5 years (range 0,9 months to 8 years) and median delay post transplantation 3,9 years (range 1 month to 4.5 years). Two patients presented with anemia, associated in one case with progressive splenomegaly. One patient had liver test abnormalities, and one had decreased portal flow found on systematic Doppler follow-up. Spleen stiffness was elevated pre-procedure in all 4 patients, from 36 to 65 kPa (normal <20 kPa), and liver stiffness was normal or mildly elevated in all. Portal stenosis was successfully treated by IR in 3 patients.

Spleen stiffness decreased rapidly, ranging from 38 to 53% (Figure 1). However, the size of the spleen remained unchanged. In the last patient, angioplasty of the portal stenosis failed leading to portal thrombosis. Spleen stiffness increased on the subsequent ultrasound (Figure 2).

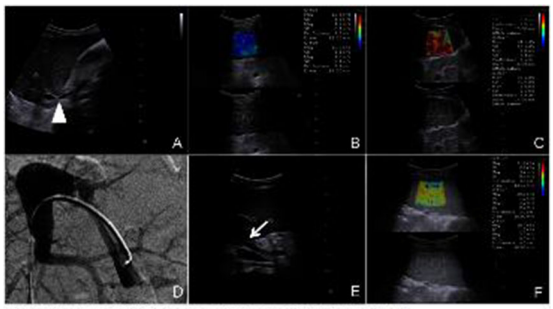

8 year-old male, liver test abnormalities at 4.5 years post liver transplantation.
A. Severe stenosis of the portal anastomosis (arrowhead) was diagnosed on ultrasound and confirmed on CT.
B. Pre-procedure liver stiffness was mildly elevated (mean 10.5 kPa, normal liver stiffness <8 kPa).
C. Pre-procedure spleen stiffness was highly elevated (mean 58.8 kPa, normal spleen stiffness <20 kPa).
D. Balloon dilatation of the stenosis was performed, with resolution of the stricture on control.
E. The follow-up ultrasound confirmed the absence of residual stricture.
F. Post-procedure spleen stiffness decreased significantly (mean: 25.2 kPa).

Figure 1

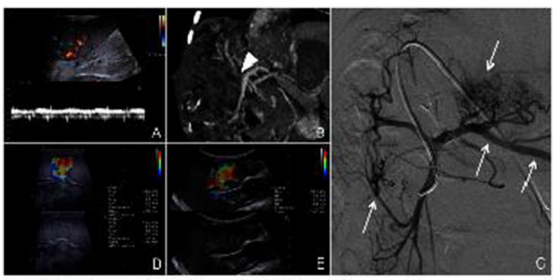

9 month-old female, one month post liver transplantation for biliary atresia.
A. Decreased intrahepatic portal flow velocity was demonstrated on a follow-up ultrasound, with no associated clinical symptoms noted.
B. Severe stenosis of the portal anastomosis was confirmed on angio-CT (arrowhead).
C. Attempts were made to perform an angioplasty of the anastomosis, with no opacification of the intrahepatic portal vein seen on the control post balloon dilatation and reflux into the splenic vein, left gastric veins and mesenteric varices (arrows). The ultrasound performed post-procedure confirmed intra-hepatic portal thrombosis.
D. Pre-procedure spleen stiffness was moderately elevated (mean 35.3 kPa).
E. Spleen stiffness slightly increased after the procedure (mean 40.9 kPa).

Figure 2

Conclusion:
Spleen stiffness increases in case of portal stenosis and decreases when the obstacle is relieved. Combining spleen and liver stiffness could help finding the etiology of portal hypertension after liver transplantation, by distinguishing patients with pre-hepatic obstacle from patients with intra or post-hepatic causes. Spleen stiffness could be useful for systematic follow-up post liver transplantation and follow-up after treatment of portal stenosis.

Comparison between the standard gradient echo (GRE) sequence and echo planar imaging (EPI) sequences in MR Elastography in a pediatric population

C. Maya, E.A. Hartung, R.H. Carson, K. Darge, S. Anupindi; Philadelphia/US

Objective:
MR Elastography (MRE) is a novel imaging technique that provides a non-invasive evaluation of liver fibrosis. The standard sequence used for this purpose on a Siemens scanner has been gradient echo (GRE). We also implemented echo planar imaging (EPI) available as a work-in-progress (WIP). Our aim is to compare the liver elastogram values between GRE and EPI in children.

Materials:
After consent from both research and referred clinical subjects, a dedicated MRE of the liver was performed on a 3T MR scanner (MAGNETOM® Skyra, Siemens) with a pediatric mechanical driver over the right upper quadrant. An axial T2 BLADE with fat saturation, coronal T1 VIBE Dixon and axial diffusion weighted imaging (DWI) were obtained. Elastograms were obtained using both standard GRE and EPI, in the axial plane. For the GRE sequence, 5 different slices were selected and each scanned sequentially. The EPI sequence incorporated 5 different slices in just one series. Images were post-processed placing regions-of-interest (ROI) and measuring the stiffness in kilopascals (kPa). For each sequence and each slice the mean stiffness and then the average of the means was calculated. A spleen elastogram was simultaneously generated, without changing the mechanical driver location, and the mean stiffness was also calculated. Increased stiffness was defined as >2.9 kPa in the liver and >3.6 kPa in the spleen. We focused on a technical comparison between the sequences without clinical or histological correlation of findings.

Results:
We included 15 subjects that had elastogram measurements of liver and 11 of them spleen stiffness on both GRE and EPI sequences. Mean liver stiffness on GRE was 2.4 (SD+/- 0.71) and on EPI was 2.8 (SD+/-1.04), with a Pearson's correlation of R= 0.92 (p<0.001). Increased liver stiffness was found in 4/15 (26.6%) of the cases in GRE and 9/15 (60%) of the cases in EPI. Mean spleen stiffness on GRE was 3.9 (SD+/- 1.39) and on EPI was 4.8 (SD +/- 1.45) with a Pearson's correlation of R=0.69 (p= 0.01). EPI reported consistently higher values than GRE in both liver and spleen stiffness.

Conclusion:
Our preliminary data shows a moderate to high correlation between GRE and EPI sequences; however, the EPI values were higher in both liver and spleen. In the future, larger studies are needed to validate these thresholds and patterns among different sequences.

Contrast-enhanced Voiding Urosonography, a sensitive & radiation free technique. 6-year experience in a tertiary referral center

P.K.J. K.C. Chan, K.-S. Tse, W.S. Fok, J.C.Y. Lee, L. Wong; Hong Kong/HK

Objective:
Contrast-enhanced Voiding Urosonography (ceVUS) is a sonographic technique developed in the recent decade to diagnose vesicoureteric reflux in children. This technique enables real time continuous observation of the urinary system during both filling and voiding phases. It has the advantage of obviating radiation exposure over traditional Micturating Cystourethrogram (MCU). In this study, we retrospectively evaluate the test characteristics, patient outcomes and complication rate of all ceVUS studies since its introduction at our institution.

Examples of positive & negative VUS findings

Materials:
All the ceVUS cases performed at our tertiary referral center from September 2010 to March 2016 were included in this study. The demographic data of patients, indication for study, VUS & MCU findings & discrepancies were reviewed. Results of MAG-3, DMSA & MRU studies

were also reviewed if done. Patient's medical & surgical treatment, and clinical progress were also reviewed. Active telephone follow-up 3 days after ceVUS was performed.

Results:
120 patients giving a total of 240 pelviureteric units were referred for VUS study during the study period, with age ranging from 1 month to 7 years old. No contrast-related complication was encountered. Except 2 cases with failed catheterization, 108 were investigations of urinary tract infection (UTI), antenatal hydronephrosis and congenital anomalies etc., and remaining 10 were follow up studies of known reflux. Of all cases of UTI, 36 refluxing units were picked up by VUS, ranging from Grade I to V. Of the 36 refluxing units diagnosed by ceVUS, 17 were missed on MCU, among which 12 were high grade refluxes (grade III to V) requiring treatment; whereas ceVUS only missed one Grade I refluxing unit detected by MCU. Besides, one grade IV refluxing unit identified on VUS was under graded by MCU to Grade I.
Regarding patient outcomes, one patient with MCU-missed refluxing unit presented with breakthrough UTI on follow up. Two refluxing units that were missed on MCU but detected on ceVUS demonstrated scarring on DMSA.

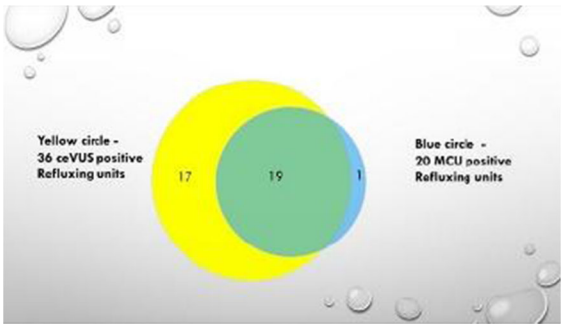

Chart showing positive cases on VUS & MCU

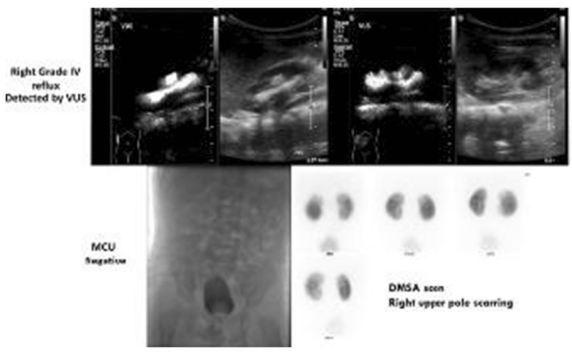

Case showing MCU missed, VUS diagnosed Grade IV reflux showing DMSA scarring

Conclusion:
ceVUS is shown to be more sensitive in detecting vesicoureteric reflux than MCU. The fact that MCU-missed refluxes detected by ceVUS were associated with breakthrough urinary tract infection and scarring on DMSA indicated that the extra sensitivity brought by ceVUS did translate to clinical significance. Difficulty in visualizing low-grade reflux is a potential limitation of this technique.
With favourable diagnostic performance and safety profile, ceVUS can be further applied in this community in the era of radiation reduction.

Percutaneous transbiliary needle or forceps biopsy in hepatic masses with biliary dilatation

A. Dabadie[1], S. Franchi[2], D. Pariente[2]; [1]La Timone, Marseille/FR, [2]Le Kremlin-Bicêtre, Paris/FR

Objective:
Hepatic masses with biliary dilatation are rare in children and mainly include rhabdomyosarcoma of the biliary ducts, but also other masses or pseudo-masses compressing the hepatic hilum. In these patients histological diagnosis of the lesion as well as temporary biliary drainage are warranted. The objective of this study is to report our experience in percutaneous transbiliary biopsy performed simultaneously and using the same access as the percutaneous biliary drainage in children with hepatic mass obstructing the biliary ducts.

Materials:
Children presenting with a hepatic mass causing biliary obstruction, with need for biliary drainage, were considered candidates for percutaneous transbiliary biopsy of the lesion performed at the same time. The biopsy was performed under ultrasound guidance, through a sheath introduced in the dilated biliary system, using a semi-automatic 16 gauge needle or the Transluminal Biliary Biopsy Forceps Set (Cook Medical, Bloomington, USA).

Results:
Between 2009 and 2016, four patients were included, three females and one male, median age 5.5 years (range 2.5-11.5). All presented with jaundice and were diagnosed with a hepatic mass with secondary biliary obstruction. Percutaneous transbiliary biopsy was performed in all 4 patients using the 16 gauge needle. In one patient, the biopsy did not demonstrate any tumoral cells and a second biopsy was performed using the forceps device through the same biliary access. The samples deemed adequate for analysis by the Pathology department in all patients, however the samples were larger when using the needle. No immediate or delayed complication in relation to the transbiliary biopsy occurred in either patient. Final diagnoses were rhabdomyosarcoma of the biliary ducts (2 patients), fibrolamellar hepatocarcinoma (1 patient) (Figure 1) and invasive fungal infection (Exophiala dermatitidis) in a patient with CARD9 immunodeficiency (Figure 2).

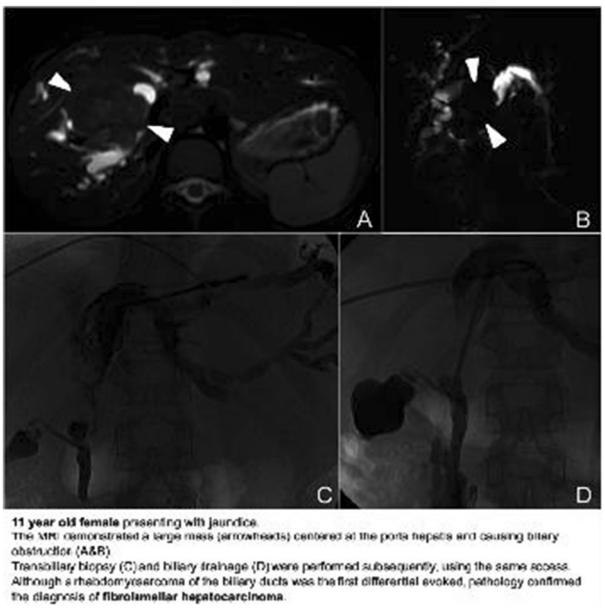

Figure 1

6 year old female presenting with jaundice and hyper eosinophilia.
The CT (A) and MRI (B) showed unrelated diffuse biliary dilatation, with possible ill-defined mass centered at the porta hepatis.
Transbiliary biopsy (C) and biliary drainage (D) were performed subsequently, using the same access.
Pathology confirmed the diagnosis of pseudo mass secondary to fungal infection (Exophiala dermatitidis).
Further analysis showed an associated CARD9 immunodeficiency.

Figure 2

Conclusion:
Percutaneous transbiliary biopsy in children with masses involving the porta hepatis causing biliary obstruction is an interesting technique allowing to perform both the biliary drainage and the biopsy of the lesion using the same access, therefore reducing the risk of choleperitoneum.

Inflammatory bowel disease in children - ultrasound vs. magnetic resonance imaging
M. Jeckovic, V. Vucaj Cirilovic, M. Stojšic, I. Varga, D. Tomić; Novi Sad/RS

Objective:
To compare the accuracy and reliability of ultrasound (US) and magnetic resonance imaging (MRI) as diagnostic methods in inflammatory bowel disease (IBD).

Materials:
A retrospective - prospective study included 62 patients of both sexes (13,72 +/- 3,17 y), in a two-year span. Patients were divided into two groups according to the used diagnostic method (positive – group A on US and A1 on MRI, with intestine mural thickness above 3mm, and negative – group B on US and B1 on MRI, with mural thickness below 3mm). Overall sensitivity and specificity of US and MRI in diagnosing IBD was calculated in comparison to pathohistological (PH) findings.

Results:
US examination showed an average intestinal mural thickness of 4.93 ±1.39mm and 2.7+0.18mm in group A (28 patients) and group B (34 patients) respectively. MRI examination showed an average intestinal mural thickness of 6.50±1.45mm and 2,8+0,16mm in group A1 (27 patients) and group B1 (35 patients) respectively. Out of 28 patients from group A, 15 (52%) had irregular mural architecture, contrary to group B in which mural architecture irregularities have not been observed. In groups A1 and B1 14 (51.9%) and 2 (5.7%) patients had irregular mural architecture respectively. Average length of affected intestinal segment on US and MRI was 103mm and 105mm respectively. Five patients from group A and four from group A1 had signs of fibrosis. Color Doppler showed hyperemia in 17 and 22 patients of group A and A1 respectively. Transmural signs of inflammation were found in 59% of patients on US, and 61.3% of patients on MRI. Average longer diameter of mesentery lymph nodes measured by US and MRI was 13.29 ±3.74mm and 12.7±5.68mm, respectively. Overall sensitivity of US and MRI was 88.4% and 92.31% respectively. Both US and MRI showed a specificity of 88%.

Conclusion:
US and MRI are reliable and compatible methods in diagnosing IBD, with MRI being slightly more accurate. US is an extremely valuable and widely available imaging modality in every-day clinical work, both in diagnosing and follow-up of therapy effects in children with IBD.

Findings in Percutaneous Transhepatic Cholecysto-Cholangiography in neonates and young infants presenting with conjugated hyperbilirubinemia
D.A. Parra, S. Peters, J. Amaral; Toronto/CA

Objective:
Conjugated hyperbilirubinemia is a concerning finding in neonates and young infants, biliary atresia (BA) being one of the main diagnostic considerations. BA is a rare disease characterized by fibrosis of the biliary tree. The obliteration of the biliary system leads to cholestasis and ultimately liver parenchymal injury, cirrhosis and death. An early diagnosis of BA along with a Kasai portoenterostomy operation significantly improves the long-term prognosis. Percutaneous Transhepatic Cholecysto-Cholangiography (PTCC) is one of the options described in the diagnostic algorithm of BA.
The aims of this study are to: (a) Describe PTCC findings in patients with conjugated hyperbilirubinemia; (b) Identify the abnormal patterns encountered that justify further investigations; (c) Analyze technical aspects of the procedure.

Materials:
This is a 16 year single-center retrospective study (2000-2016) in which we recruited patients with the diagnosis of cholestasis (less than 6 months old) referred for PTCC. We collected patient demographics, clinical information, findings in PTCC, post-procedure management and long term clinical outcome.

Results:
Eigthy-nine patients were referred for PTCC in the study period. The procedure was technically feasible and successfully performed in 73 patients (68% male, mean age 2.2 months). Forty-one had a pre-procedure HIDA scan suggestive of BA. Fifty-nine patients had an ultrasound-guided biopsy in conjunction with the PTCC and in all of them the cholangiography was performed through a needle placed using ultrasound guidance in the gallbladder. 53% (39) of the patients had a normal PTCC. Abnormal patterns encountered were: 1) Variable degrees of hypoplastic bile ducts seen in 25%; 2) Atretic gallbladder without demonstration of communication with bile ducts seen in 18%; and 3) Gallbladder communication with a cystic structure not communicated with the biliary ducts (cystic biliary atresia) seen in 4%. The most common diagnosis in the abnormal group was BA (71%). Alagille's syndrome, Alpha-1 antitrypsin deficiency and Progressive Familial Intrahepatic Cholestasis were other diagnoses in this group. No complications related to the procedure were observed.

Conclusion:
PTCC is a safe and effective option in the diagnostic algorithm of patients presenting with cholestasis early in life. Visualization of the gallbladder is fundamental to perform the procedure. The majority of studies were normal in our patient population preventing further invasive investigations. Three types of abnormal PTCC patters were encountered, with BA being the most common diagnosis in this group of patients.

Role of Shear Wave Elastography in Diagnosing Biliary Atresia

R.P. Kesav, M. Jana, R. Sharma, A.K. Gupta, D. Kandasamy, V. Bhatnagar, S. Agarwala, R. Malik, S.D. Gupta, P. Das; New Delhi/IN

Objective:
To evaluate the additive role of shear wave elastography in the sonographic distinction of biliary atresia from other causes of neonatal/infantile cholestatic liver disease.

Materials:
Neonates and infants with clinical and biochemical diagnosis of cholestatic jaundice were enrolled in our study after obtaining informed written consent from the parents. Grey scale, Doppler and shear wave elastographic findings were recorded after 4 hours of fasting using Aixplorer® ultrasound system (SuperSonic Imagine, Aix en Provence, France). Sedation was not needed during the study. For obtaining elastographic values, linear transducer (4-15Hz) was used and after image stabilization a Q-Box measuring 3mm was placed in the most homogenous vessel free area. The mean of three elastographic values were recorded. HIDA scan, liver biopsy, intra-operative cholangiogram and histopathological evaluation of resected specimens was done wherever feasible and clinically indicated. The prospectively obtained elastographic values were retrospectively evaluated.

Results:
Eleven of 25 patients included in our study were proven to be biliary atresia (BA) by intra operative cholangiogram and histopathological reports. The diagnosis in the remaining 14 patients included other causes of infantile cholestatic jaundice like infantile choledochal cyst, neonatal idiopathic hepatitis, progressive familial intrahepatic cholestasis, Abernathy malformation, CMV hepatitis etc. The elastographic values of BA and non-BA patients were compared. Six of 25 infants were younger than 60 days which included four patients with BA and their elastographic values (18.75±2.9kPa) were significantly different from that of non-biliary atresia (7±1kPa) in the same age group (p value <0.05). Similarly, for patients aged >60 days also we had a significant difference (p value <0.05) in elastographic stiffness between BA (45.7±11kPa; n=7) and non-BA (19.4±3.6kPa; n=12) groups.
The mean echogenic area anterior to right portal vein (EARPV) was 4.45 ±0.84mm in BA and 1.47±0.36mm in non-BA group (p value <0.05). The mean gall bladder (GB) length was 1.82±0.26 mm in biliary atresia group in contrast to 3.2±0.26mm in the rest (p value <0.05). The ROC plot for EARPV and GB length gave a Youden Index cut off value of >2.7mm (Sensitivity 72.7 & Specificity 71.4%) and <3.32 cm (Sensitivity 100 & Specificity 42.9%) respectively.

Conclusion:
Infants with biliary atresia have a significantly higher elastographic value when compared to age matched patients with other causes of neonatal cholestasis. We expect to validate the findings in our ongoing study with a larger sample size.

Microlithiasis: Is it a risk factor for testicular tumor?

A.T. Trout[1], J.S. Chow[2], E.R. McNamara[2], K. Darge[3], R. Ramirez[3], M.M. Munden[4], S.M. Rothan[4], O.M. Navarro Kunstmann[3], M. Tijerin Bueno[6], K.E. Bove[1], K. Chikwava[3], A. Heider[7], J. Hicks[4], G.R. Somers[5], B. Zhang[1], J.R. Dillman[1]; [1]Cincinnati/US, [2]Boston/US, [3]Philadelphia/US, [4]Houston/US, [5]Toronto/CA, [6]Toronto/US, [7]Michigan/US

Objective:
To retrospectively define in a large pediatric population the association between testicular microlithiasis and testicular neoplasia.

Materials:
Retrospective multicenter study of scrotal ultrasounds performed between January 2000 and April 2014 in subjects <18 years of age. All unique subject scrotal ultrasound reports from each institution were reviewed for mention of microlithiasis. For subjects with serial exams, the most recent exam performed was included in the analysis. All exams mentioning microlithiasis were reviewed by site-specific investigators to confirm the presence of ≥5 punctate calcifications in the testicle on a single image. The presence of testicular germ cell and stromal tumors were determined for subjects with and without microlithiasis through review of institutional pathology and imaging databases. The risk of testicular neoplasia in the context of microlithiasis was expressed in terms of odds ratios with (A-OR) and without adjustment (U-OR) for fixed study site (institution) effects by logistic regression.

Results:
The study population included 37,863 unique subjects with confirmed microlithiasis in 1,097 (2.9%). Mean subject age was 11.1±4.7 years for subjects with microlithiasis and 9.1±5.9 years for subjects without (p<0.0001). One hundred thirty-nine subjects (0.37%) had germ cell tumors (86 malignant, 63 benign) and 34 subjects (0.09%) had stromal tumors. Malignant germ cell tumors were present in 2.8% of subjects with microlithiasis and 0.12% without for an A-OR of 22.37 (95%CI: 13.35-37.49) and an U-OR=17.26 (95%CI: 11.8-25.25), p<0.0001. Benign germ cell tumors were present in 1.4% of subjects with microlithiasis and 0.13% without for an A-OR of 10.97 (95%CI: 5.74-20.99) and an U-OR=10.61 (95%CI: 5.7-19.72), p<0.0001. Stromal tumors were observed in 0.46% of subjects with microlithiasis and 0.079% without for an A-OR=6.39 (95%CI: 2.21-18.44) and an U-OR of 5.8 (95%CI: 2.1-16), p<0.01.

Conclusion:
This large, multicenter study confirms that there is a significant, strong association between testicular microlithiasis and testicular neoplasia, particularly malignant germ cell tumors. Children with microlithiasis have approximately 22X greater odds of having a malignant germ cell tumor than children without microlithiasis. This reinforces the need for a large prospective study assessing the risk of developing testicular neoplasia in children with incidentally identified diffuse microlithiasis.

Do ADC-values reflect renal function or obstruction in children with uretero-pelvic-junction obstruction?

P. Grehten, A.C. Eichenberger, C. Kellenberger; Zurich/CH

Objective:
The use of diffusion weighted imaging (DWI) in renal MRI is increasing. In adults as well as in infants a positive linear correlation between ADC-values and glomerular filtration rate has been demonstrated. The aim of our study was to assess whether renal DWI can provide information on the grade of urinary tract obstruction or renal function in children with uretero-pelvic-junction (UPJ)-obstruction.

Materials:
Retrospective analysis of 19 children (age 3.1+/-4.5y) with unilateral UPJ-obstruction who underwent pre- and postoperative MRI at 1.5T and 6 normal controls (age 6.6+/-4.0y). Functional MR-Urography and multiple b-value DWI were part of the MR-protocol. Renal ADC-values were correlated to measures of obstruction and function, and compared between obstructed and non-obstructed kidneys and between pre- and postoperative studies.

Results:
No correlation was found between mean parenchymal, cortical or medullary ADC-values and calyceal transit time (CTT), renal transit time (RTT) and measures of differential renal function (%parenchymal

volume, vDRF, pDRF). There was moderate correlation with absolute parenchymal volume and total kidney volume, and low correlation with pelvic volume. ADC-values showed high correlation with age and patient's weight. ADC-values normalized for age or weight showed low correlation with RTT and CTT, but no correlation with functional measures. ADC-values were not significantly different between obstructed and contralateral normal kidneys (p=0.2-0.9) or between pre- and post-operative studies (p=0.3-1).

Conclusion:
Renal ADC is dependent on age and weight in young children and does not correlate with differential renal function. For assessing urinary tract obstruction with ADC normative values need to be established.

SESSION: SCIENTIFIC SESSION: CT AND RADIATION DOSE

Ionizing radiation in pediatric radiology - do medical staff and parents know enough?

J. Lovrenski, M. Strahinić, S. Zahorjanski, I. Varga; Novi Sad/RS

Objective:
To determine the level of knowledge and awareness of medical staff, medical students and parents concerning possible risks associated with ionizing radiation.

Materials:
A prospective study has been conducted at Children's hospital, Center for adult's radiology, and Medical faculty, by filling out two anonymous questionnaires (questionnaire 1 – medical staff and medical students, questionnaire 2 – parents of the children exposed to X-ray based procedures), and it included 254 participants. Statistical analysis was performed using the SPSS 21.0.

Results:
The majority of examinees assessed their knowledge about ionizing radiation as moderate. Knowledge level was statistically significantly higher only in the group of medical students who passed the course of radiology, in comparison to the group of those who have not attended the course yet. Only 45% of radiologists and up to 37.5% of pediatricians, pediatric surgeons and anesthesiologists are informed about “Image gently” campaign. Up to 80% of radiologists, and up to 22% of clinicians, both specialists and residents, are aware of ALARA principle. Over 60% of medical doctors think that diagnostic radiology procedures are very often performed unnecessarily among children, while only 12.5% of parents share this opinion. Most of the radiologists and clinicians consider it necessary to inform parents about potentially harmful effects of ionizing radiation, but even though 60-80% of clinicians claim they do inform parents in every-day clinical practice, over 70% of parents affirm that they had never been informed about effects of ionizing radiation before diagnostic procedures were performed on their children. Only 26% of pediatric surgeons and pediatricians, but 72.7% of radiologist and 60% of anesthesiologists are concerned that informing parents about ionizing radiation would cause problems in every-day work. Nearly 71% of parents claimed that they would not refuse to expose their child to X-ray based diagnostic procedure, after the given information about potential harmful effects. Over 70% of radiologists and less than 50% of pediatric surgeons and pediatricians support the initiative to calculate the total effective dose child was exposed to during hospitalization, and place it on the discharge list. Between 50% and 85% of pediatricians and pediatric surgeons greatly underestimated the effective doses in CT and fluoroscopy procedures. There are 58-100% of clinicians who are aware that CT increases the risk of carcinoma development.

Conclusion:
This study showed that general knowledge about ionizing radiation, potential risks and effective doses in pediatric population is poor, and that organized education is required.

Fluoroscopy in pediatric radiology - how important is an individual impact to radiation exposure of children?

J. Lovrenski, I. Varga; Novi Sad/RS

Objective:
To determine whether there are differences between different pediatric radiologists and radiology residents in exposure of pediatric population to ionizing radiation during fluoroscopy procedures.

Materials:
A retrospective study has been conducted at the regional children's hospital, and included all the diagnostic fluoroscopy examinations performed within a one-year period. The fluoroscopic data along with the names of pediatric radiologists/radiology residents performing these examinations were retrieved from the evidentiary notebooks, and included: dose-area product (DAP), skin dose, and fluoroscopy time. There were 4 radiologists (R1-R4), and 4 radiology residents (R5-R8) involved in fluoroscopic examinations. We found all the fluoroscopic findings in the hospital's data base, which enabled a differentiation between positive and negative findings. Statistical analysis was performed using the SPSS 21.0. A P-value less than 0.05 was considered statistically significant.

Results:
A total of 191 fluoroscopy procedures in children (mean age 4,5y, 107 males and 84 females) have been performed within a one-year period, most of which were voiding cystourethrograms (VCUG) - 93, and an upper gastrointestinal (GI) series - 79 examinations. Radiology residents and radiologists carried out 82 and 109 examinations respectively. Duration of fluoroscopy procedures performed by residents (av. 32.5s) was statistically significantly shorter in comparison with duration of fluoroscopy examinations performed by radiologists (av. 53s). DAP and skin dose did not show statistically significant difference between these two groups, as well as the number of positive and negative fluoroscopic findings in groups of examinations performed by radiologists and radiology residents. Mean DAP value ranged from 0.82μGym^2 (R2) to 7.5μGym^2 (R7) when performing VCUGs, and from 1.35μGym^2 (R2) to 4.79μGym^2 (R1) for upper GI series. Mean skin dose ranged from 14.33mGy (R2) to 151.48mGy (R3) for VCUGs, and from 28.66mGy (R2) to 120.54mGy (R4) for upper GI series. Mean fluoroscopy time ranged from 11.76s (R2) to 48.5s (R3) for VCUG, and from 26.22s (R2) to 125.75s (R3) for upper GI series. Statistically significant difference was shown only between radiologists R2 and R3 for DAP and skin dose values in performing VCUG, and for fluoroscopy time in performing an upper GI series. For all examinations DAP and skin dose were statistically significantly higher in the group of positive fluoroscopic findings.

Conclusion:
This study has shown that exposure of children to ionizing radiation during fluoroscopy procedures significantly depends on radiologist/radiology resident and the nature of fluoroscopic finding.

Automated tube voltage selection in combination with automated tube current modulation in pediatric non-contrast chest CT

A. Hojreh, P. Homolka, J. Gamper, S. Unterhumer, D. Kienzl-Palma, C. Balassy, H. Prosch; Vienna/AT

Objective:
To evaluate image quality and radiation exposure of non-contrast pediatric chest CT with automated tube voltage selection (ATVS), in combination with automated tube current modulation (ATCM).

Materials:
Non-contrast chest CT scans of 160 children (91 male and 69 female; mean age, 8.7 ± 5.4 years) were analysed retrospectively with regard to radiation exposure and image quality before and after the implementation of an automated tube voltage selection. Correlations of volume CT Dose index ($CTDI_{vol}$) and the effective diameter (EDM), before and after the implementation of ATVS were compared, and confidence intervals related to the change in correlations with and without ATVS were determined using Fisher's z-transformation. Image quality was assessed by mean signal-difference-to-noise ratios (SNRs) in the aorta and in the left principal bronchus with the independent samples t-test. Subjective image quality was rated by two pediatric radiologists and a general radiologist on a 10-point scale. Agreement between the readers was assessed using weighted kappa coefficients. A $p<0.05$ were considered significant.

Results:
$CTDI_{vol}$ correlation with EDM was r=0.62 before and r=0.80 after ATVS (CI: -0.04 to -0.60; p=0.025). Mean SNR was 10.88 without and 10.03 with ATVS (p=0.0089). Readers' agreement improved with ATVS (weighted kappa between pediatric radiologists from 0.1 (0.03-0.16) to 0.27 (0.09-0.45) with ATVS; between general and each pediatric radiologist from 0.1 (0.06-0.14) to 0.12 (0.05-0.20), and from 0.22 (0.11-0.34) to 0.36 (0.24-0.49)).

Conclusion:
Automated tube voltage selection, in combination with an automated tube current modulation, resulted in optimization of scan protocols, homogeneity of image quality, and reduction of radiation exposure for pediatric patients.

Advantages and disadvantages of Cone Beam CT for pediatric interventions
L. Dance, R.B. Towbin, D. Aria, C. Schaefer, R. Kaye; Phoenix/US

Objective:
Illustrate the advantages and disadvantages of cone beam CT (CBCT) as an alternative to conventional CT guidance and an adjunct to angiography.

Materials:
There is a steep learning curve to optimize utilization of CBCT. We found that CBCT reliably identifies high-contrast lesions. However, the lower dose and decreased penetration of CBCT resulted in poorer visualization of low-contrast lesions. Also CBCT can be degraded by streak artifact from hardware or dense contrast. The relatively narrow field of view can be restrictive for peripherally located lesions in larger patients. However, the anatomic display is adequate for guidance in most instances.

Results:
These findings are illustrated in a series of CBCT-guided cases including pulmonary nodule localization, osteoid osteoma ablation, ABC sclerotherapy, renal AV fistula embolization, and liver lesion biopsy.

Conclusion:
The advent of CBCT as an adjunct modality in the IR suite has significantly decreased the use of conventional CT guidance and significantly decreased the radiation dose in children. We have found CBCT to be a practice changer.

PiDRL guidelines: A review of local DRL for pediatric fluoroscopy in a Italian referral center
A. Magistrelli, V. Cannatà, E. Genovese, P.M.S. Schingo, M. Cirillo, P. Toma; Rome/IT

Objective:
The aim of this study is to review our local DRL in pediatric fluoroscopy and to compare them to values proposed by PiDRL guidelines and recent international litterature.

Materials:
Data were prospectively collected on consecutive procedures (750 total) performed from January 2016 to December 2016 on 2 different fluoroscopy units (Siemens Iconos R200, Luminos dRF). Of each procedure patients data (name, weight and birth date), examination-data (kind of procedure, date, DAP [cGy*cm2], total fluoroscopy time, number of images) were recorded.
Data from micturating-cystourethrography(MCU), barium meal/swallow(BS) and most commonly performed procedures were divided into 4 weight-groups (<10Kg,10-15Kg,15-30Kg,30-60Kg) and of each one 75th-percentile was calculated. Data were compared to EuropeanDRL and recent literature data (by age:newborn,1-,5-,10-years old). Weight-groups are considered a representative sample if at least 20-patients per procedure-type and per patient-group are included.

Results:
Our local-DRL for MCU are 7(<10Kg), 10(10-15Kg), 24(15-30Kg) and 57(30-60Kg). They results to be lower than PiDRLs values (30, 70, 80, 75) but higher if compared to a previous local survey of 2014 (4, 9, 18, 29). BS data are 9(<10Kg), 32(10-15Kg), 28(15-30Kg); these data are lower than that of a previous local survey of 2014 (23, 34, 68).

Conclusion:
The update of local-DRL is helpful in daily practice to identify (and solve) critical issues such as incorrect technique or poor practice with new flat-panel equipment.

PiDRL guidelines: A review of local DRL for pediatric head, thorax and abdomen CT in a Italian referral center
A. Magistrelli, V. Cannatà, E. Genovese, M. Cirillo, R. Lombardi, P. Toma; Rome/IT

Objective:
The aim of this study is to review our local DRL in pediatric CT and to compare them to values proposed by PiDRL guidelines and recent international litterature.

Materials:
Data were prospectively collected on consecutive procedures (347 total) performed from January 2016 to June 2016 on a Somatom Definition FLASH Siemens. Of each procedure patients data (name, weight and birth date), examination-data (kind of procedure, clincal question, date, CTDIvol16/32 and DLP16/32) were recorded.
CTDIvo/DLP16 from head CT were divided into 4 age-groups (<4weeks,4weeks-1y,1-6y,≥6y) and of each one 75th-percentile was calculated. CTDIvol/DLP32 from thorax (chest, cardiovascular CT angiography) and abdomen+pelvis CT examination were divided into 5 weight-groups (<10Kg,10-15Kg,15-30Kg,30-60Kg,>60Kg) and of each one 75th-percentile was calculated. Data were compared to EuropeanDRL and recent literature data.
Weight-groups are considered a representative sample if at least 20-patients per procedure-type and per patient-group are included.

Results:
Our local DRL are substantially lower than that proposed by PiDRL guidelines. Specifically CTDIvol/DLP32 for chest CT are 1/22(<5Kg), 1,52/42(5-15Kg), 1,83/56(15-30Kg), 2,99/113(30-60Kg), 6,07/239(>60Kg) respectively. For cardiovascular CT angiography are 0,71/15(<5Kg), 1,01/21(5-15Kg), 2,44/36(15-30Kg), 2,87/90(30-60Kg), 13,72/311(>60Kg). While for abdomen+pelvis CT are 1,9/47(<5Kg), 2,68/83(5-15Kg), 3,25/131(15-30Kg), 7,77/320(30-60Kg), 11,21/532(>60Kg). Data for trunk sere not collected. For head CT local DRL are higher in age-group 0 and 1 but lower in other age-group if compared to routine head CT PiDRL ones.

Conclusion:
The update of local-DRL allowed us to identify (and solve) some critical issues such as incorrect technique.

DRL-curve in optimization of pediatric body CT
R. Seuri[1], P. Laarne[2], A. Nikkola-Sihto[3], K. Nygaard Bolstad[4], M.S. Perhomaa[5], A. Thilander Klang[6], K. Rosendahl[4], J. Ruohonen[3], E. Tyrvainen[7]; [1]Helsinki/FI, [2]Tampere/FI, [3]Seinäjoki/FI, [4]Bergen/NO, [5]Oulu/FI, [6]Gothenburg/SE, [7]Kuopio/FI

Objective:
Diagnostic reference levels (DRLs) in medical imaging represent valuable tools to study dose optimization in clinical practice. This is particularly important in pediatric computed tomography (CT) as the number of the examinations in many institutions is low. DRLs are typically given as a percentile point, usually as 75% or 3rd quartile of the observed distribution of patient dose. In pediatric practice DRLs are often given for each age- or weight group separately. We present continuous DRL-curve as a feasible way to compare dose levels in pediatric body CT.

Materials:
During 2016-2017 a selected group of Nordic hospitals collected dose values (CT Dose Index by volume, $CTDI_{vol}$, and Dose-Length Product, DLP) from pediatric body CT examinations on children aged 5-16 years. The dose values were imported into a dynamic Excel table, previously established by the Radiation and Nuclear Safety Authority in Finland, STUK (Fig 1). The STUK-table includes a graphic presentation of a continuous DRL-curve presented as a function of body weight, and the program automatically calculates a dose curve and compares it to the established reference level (Fig 2).

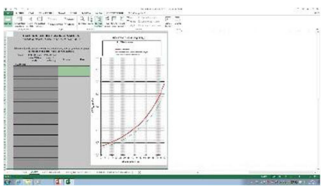

Fig 1.

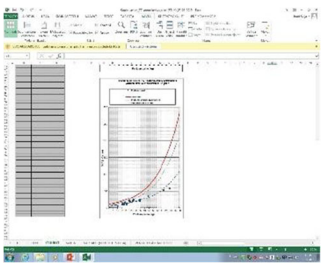

Fig 2.

Results:
The dose values were easily exported to the Excel tables, and the graphic presentation and comparison with an established DRL-curve was clear and readily understandable for both radiologists and radiographers. In some of the institutions included in the present study, the weight of the patient was not recorded routinely. This represents a challenge for the use of the DRL-curves provided by STUK.

Conclusion:
The DRL-curves provided by STUK were feasible for clinical practice. The automatic calculation of the dose curve and graphic presentation were helpful to interpret the results. The DRL-curve also allows relevant comparison even with a smaller number of patients.

Reduced Slice CT as a means of lowering patient Dose in Children with Diffuse Lung Disease
S. Servaes, C. Maya, T. Presenza, D.A. Mong, X. Zhu, M. Ortiz, A. White; Philadelphia/US

Objective:
Develop a strategy to reduce radiation dose without compromising the diagnostic accuracy of chest CT scans in diffuse lung disease.

Materials:
Fifty randomly selected CT chest studies performed over 10 years to assess diffuse lung disease were included in the study sample (25 females, 25 males; mean age 9.9 years + 6.6 years), comprising 9 disorders. Two pediatric radiologists and a pediatric radiology fellow blinded to the results of the CTs evaluated four subsets of complete chest CTs (3 slices, every third slice, every other slice, and all images below the thyroid) and compared the subsets with the entire chest CT, interpreted as the control. Accuracy of evaluating the primary diagnosis and determination if significant diagnoses were missed in the reduced slice CT subsets were rendered. We assume linear distribution of dose across the anatomy to estimate dose reduction on reduced slice subsets.

Results:
Most significant findings were present on all reduced slice CT subsets. All relevant findings were present in 100% of subthyroid, 96% of every other slice, 86% of every 3rd slice, and 50% of 3 regional slice subsets respectively. Excluded findings included small foci of ground glass opacity, consolidation, focal mosaic attenuation, and linear parenchymal bands; peribronchial thickening, dextrocardia vs dextropositioning, tree-in-bud opacities, extent of mild bronchiectasis. With the exception of consolidation in 1 of the studies, these findings were not thought to inhibit diagnostic assessment. The underlying diagnosis was correctly identified in most of the subsets: 100% subthyroid and every other slice, 90% every 3rd slice, and 80% of 3 regional slice subsets. Dose is significantly decreased by using any of these methods.

Conclusion:
While some findings are excluded with increasing gaps between slices, equivalent diagnostic information can be provided on reduced slice CT and can serve as a viable strategy to reduce lifetime radiation dose to children and young adults with diffuse lung disease imaged for routine follow-up. As findings are missed with larger gaps, this strategy should be used with caution in patients presenting with acute symptoms

SESSION: CASE REPORT PRESENTATION SESSION

Crazy paving - Pulmonary manifestation of Type b Niemann Pick Disease - An interesting Paradigm
S. Muthiyal, V. Kini, V. Mathew; Doha/QA

Objective:

1. To highlight the exiguous prevalence of the pulmonary manifestation of type b Niemann Pick disease
2. To enumerate the pulmonary manifestations of type b Niemann Pick disease.
3. To extrapolate the significance of early diagnosis which will compliment to Treatment planning and management.

Case presentation:
Types A and B Niemann-Pick disease are lysosomal storage disorders that result from deficient Acid Sphingomyelinase activity and lead to the accumulation of sphingomyelin, primarily in tissues of the reticuloendothelial system. Type B Niemann- Pick disease manifestations are hepatosplenomegaly, excess bleeding and bruising, growth retardation, and recurrent respiratory infections. Features of HRCT include thickened peribronchovascular and interlobular septal thickening, ground-glass opacities. The intermixed regions could be characterized as showing crazy paving, although this is not the predominant pattern. Type B Niemann-Pick disease should be added to the list of clinical entities that can demonstrate crazy paving. Our patient is a seven-year old girl, presented with dry cough and fever. Physical examination revealed hepato splenomegaly. Radiological work up included abdominal ultrasound examination, which showed mild hepatosplenomegaly. Chest radiography revealed diffuse reticulonodular infiltration in both lungs. Chest HRCT was done for more comprehensive evaluation which showed multilobar bilateral peribronchovascular interstitial thickening and interlobular septal thickening with ground-glass opacities and crazy paving appearance. No honeycomb pattern was seen. No sizable pulmonary nodule or sizable mediastinal lymphadenopathy was seen. No pleural effusion was seen. Finding were indicating extensive pulmonary intestitial disease. A corroborative analysis along with lab tests and genetic studies revealed the diagnosis of type b Niemann Pick disease.

Fig No : 1

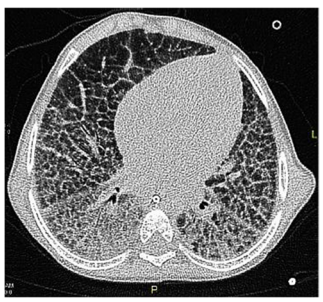

Fig No:2

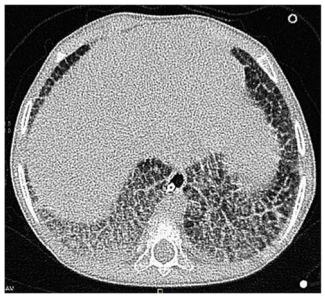

Fig No: 3

Unique teaching points:

1. Type b Neimann Pick disease with pulmonary manifestation has exiguous prevalence.
2. The spectra of HRCT features including crazy paving pattern may be encountered; though not frequent. Hence should be included in the differential diagnosis of crazy paving pattern.
3. HRCT chest is a valuable adjunct for proper treatment planning and management and should be included in the diagnostic armamentarium.

Blast from the past: Lemierre's syndrome in adolescents with sore throat

O. Kvist; Stockholm/SE

Objective:
A minor ailment such as a sore throat could prove to be a severe disorder known as Lemierre's syndrome. This syndrome mostly affects previously healthy adolescents and young adults and in its classical form should meet four diagnostic criteria; primary infection of the oropharynx, septicemia, clinical- or radiographic evidence of thrombosis of the internal jugular vein (IJV) plus secondary metastatic abscesses. The infection is caused by Fusobacterium necrophorum, a species of obligate anaerobe bacteria forming part of the normal human flora. The syndrome should be suspected in any patient with pharyngitis, cervicalgia and pulmonary symptoms.
The incidence of Lemierre's syndrome decreased dramatically after the introduction of antibiotics but has, of unknown reasons, increased over the past 15 years.

Case presentation:
We will present four patients diagnosed with Lemierre's syndrome in our department during the last 8 years. The purpose of this case report is to raise awareness of this "forgotten disease".
Of the four patients diagnosed with Lemierre's syndrome two fulfilled all 4 criteria while two fulfilled 3 out of 4. (Table 1). The first two presented at the emergency department with one week's history of a sore throat, left sided cervical lymphadenopathy, erythematous tonsils, leukocytosis and elevated CRP. In both cases the clinical condition deteriorated and they were referred to the ICU. One developed ARDS and required initiation of ECMO. In both patients, chest CT revealed multiple pulmonary consolidations with cavitations, findings consistent with septic emboli (Image 1,2 and 3). Incidentally CT-neck revealed thrombosis in the left EJV and IJV (Image 4). Ultrasound of the neck veins confirmed the finding (Image 5 and 6). Blood cultures taken on admission later proved positive to F. necrophorum. The third and fourth case, with similar clinical histories but with a less aggressive development, had positive blood cultures but no thrombosis and vice versa. (Table 1 and 2) According to the literature approximately two thirds of documented cases with Lemierre's syndrome have thrombosis of the IJV.

All four patients recovered and could be discharged with oral antibiotics and anticoagulants.

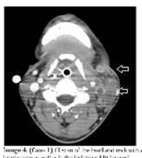

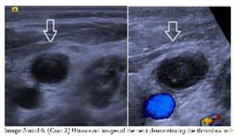

Neck images

Case	Age	Sex		Primary infection of the oropharynx	Metastatic focus in lung	Positive blood culture	Jugular vein thrombosis	CRP day 1	CRP day 7
			African					396	350
1	16	male		Yes	Yes	Yes	Yes	mg/l	mg/l
			Caucasian					161	195
2	17	female		Yes	Yes	Yes	Yes	mg/L	mg/L
			Caucasian					171	65
3	14	male		Yes	Yes	Yes	No	mg/L	mg/L
			Caucasian					395	242
4	17	female		Yes	Yes	No	Yes	mg/L	mg/L

Table 1.

Time between onset of symptoms and:	antibiotic treatment commenced	The patient sought at the A&E department
Case 1	14 days	14 days
Case 2	7 days	7 days
Case 3	2 days	2 days
Case 4	5 days	9 days

Table 2.

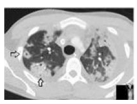

Thorax images

Unique teaching points:

In conclusion, Lemierre's syndrome is less common today thanks to antibiotics but may still occur in previously healthy adolescents and may lead to a fatal outcome. The pediatric radiologist should be aware of typical findings like septic emboli in the lungs and thrombosis in the IJV.

Unicameral bone cyst associated with secondary aneurysmal bone cyst of clavicle

I. Dasic, G.J. Djuricic, S. Ducic; Belgrade/RS

Objective:

Aneurysmal bone cyst (ABC) accounts for 2,5 % of all bone tumors. They are benign but locally destructive lesion of the bone characterized by presence of spongy or multiloculated cystic tissue filled with blood. ABCs are metaphyseal, excentric, bulging, fluid-filled and multicameral, and may develop in all bones of the skeleton. Most common locations include the proximal humerus, distal femur, proximal tibia, and spine. Clavicle is a very rare site for aneurysmal bone cyst with only few cases reported in literature.

Case presentation:

A 10-year-old boy reported to the University Children's Hospital for detailed examination of swelling of right shoulder. 2-3 days before admission parents noticed tumefaction of right shoulder. There was no history of trauma or fever. Physical examination revealed tumefaction of the right shoulder, in projection of acromial end of clavicle, measuring approximately 8x8cm, which was tender and fixed. The swelling was not hot to the touch, and there was no skin discoloration over that area. Regional lymph nodes were not palpable. (Fig. 1a) X-ray revealed osteolytic, expansible lesion in the lateral end of clavicle and there was no pathological fracture. (Fig. 1b) Laboratory analyzes were within normal limits. Blood cultures remained sterile. Chest X ray and abdominal ultrasound were normal. Computed tomography (CT) revealed a thin-walled multiloculate lesion in lateral end of right clavicle. (Fig. 2a) There was no extension in the soft tissues on Magnetic Resonance Imaging (MRI). MRI shows the multiloculate cavities and fluid levels. (Fig. 2b). The open biopsy was done. Histopathological examination confirmed the secondary aneurysmal bone cyst on the field of simple bone cyst of clavicle.

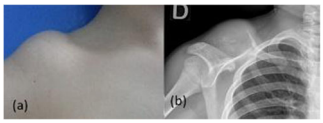

Fig. 1. (a) Preoperative clinical photograph showing a large swelling in the right clavicular region. (b) radiograph showing a lesion involving the medial aspect of the right clavicle with marked expansion of the cortex

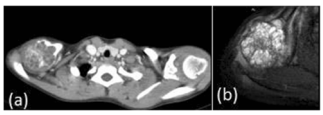

Fig. 2. (a) CT scan shows expansion of the bone and thinning of the cortex with multiple loculations. (b) Magnetic resonance image shows multiple septations with multiple fluid levels, but without soft tissues extension

Unique teaching points:

The clavicle is an uncommon site for bone tumors. Review of literature shows clavicle accounts for less than 1 % of all bone tumors.

The patient with an aneurysmal bone cyst generally presents with pain and swelling, which may vary in duration from weeks to several years.

Up to 8 % of bone tumors occur in less than 20 years of age with peak incidence in second decade.

Radiologically, lesion is lytic and may have a soap-bubble appearance with ballooned distension of the periosteum.

The differential diagnosis for aneurysmal bone cyst include giant cell tumor, chondromyxoid fibroma and telangiectatic osteosarcoma.

Distinction from telangiectatic osteosarcoma is difficult because the conditions have overlapping clinical and radiologic features. The differentiation is made from the histologic features.

Imaging of glomus tumor of liver in a child (case report)

N. Tewattanarat, J. Srinakarind, J. Wongwiwatchai, P. Komvilaisak, S. Areemit, P. Ungarereevittaya, P. Intarawichian; Khonkaen/TH

Objective:

Glomus tumors occur preferentially in subcutaneous tissue of fingers and toes, but extremely rare in visceral organs. Most cases of the tumors are diagnosed in adults. Several cases of glomus tumors in liver have been reported in adults. A literature review, no case of glomus tumor in liver in children was published. Therefore, we present clinical, imaging findings of the first case of pediatric patient with glomus tumor in liver and also histopathological features.

Case presentation:

A previously healthy 11 year-old-girl was admitted with a two-week history of progressive dyspnea on exertion and vomiting. Family history was unremarkable. Physical examination revealed hypertension and smooth and firm mass at epigastrium. Systolic apical murmur on heart examination was noted. Liver function test

showed elevated cholesterol (396 mg/dl). Other laboratory tests (complete blood count, blood chemistry, renal and liver function test, coagulation test, hepatitis profiles and alpha-fetoprotein) were within normal limits. Echocardiogram found mitral and tricuspid regurgitation and poor left ventricular systolic dysfunction. Abdominal MRI demonstrated a 12-cm well-defined exophytic hypervascular mass with intratumoral hemorrhage at segment 3/4b of the liver. There were no other suspicious lesions in other organs. The biopsy was done and revealed glomus tumor. Patient underwent preoperative embolization and the liver mass revealed decreased size to 8-cm after 1-month follow up with ultrasound. After that, exploratory laparotomy with left lateral segmentectomy was performed.
The pathological results showed dilated vascular channels surrounded by uniform neoplastic cells, uniform with round nuclei, fine chromatin, inconspicuous nucleoli, and pale eosinophilic cytoplasm, and well-defined cytoplasmic border. No mitotic figures and necrosis are identified.
Immunohistochemical (IHC) staining of tumor was positive for CD34, smooth muscle actin (SMA) and h-Caldesmon. Others IHC including AE1/AE3, Heppar1, CD31, desmin and myogenin were negative. From these findings, the tumor was finally diagnosed as glomus tumor of uncertain malignant potential due to deep location and large size.

Unique teaching points:
Primary glomus tumor is a rare entity of liver tumor diagnosed in children. However, it should be considered in the differential diagnosis of a hypervascular liver mass. Most of these tumors are benign, however tumor in liver have malignant potential due to deep seated position. Therefore, tumor removal with pre-operative embolization should be considered.

Brain MRI in a pediatric patient with linear scleroderma en coup de sabre

M. Mortilla, A. Rosati, E. Canale, C. Filippi; Florence/IT

Objective:
Linear scleroderma "en coup de sabre" (ECDS) is a rare subset of localized scleroderma. Affected individuals typically have a characteristic atrophic skin lesion involving the fronto-parietal scalp. The disease usually has a benign course but rare neurologic symptoms can be seen associated: the most common described is epilepsy.
Intracranial MRI findings described in the literature include: focal brain atrophy, calcifications and T2-hyperintense white matter lesions that may demonstrate contrast enhancement. White matter lesions and calcifications are found in the cerebral hemisphere ipsilateral to the skin abnormality.
In the literature only a few pediatric cases have been described.

Case presentation:
A 4yrs. old girl was hospitalized at our institution for evaluation of a lesion of the frontal skin associated to a history of febrile seizures and MRI alterations.
She presented febrile seizures at the age of 2 on April 2013. On January 2014 parents noted a frontal cutaneous lesion that was defined as "linear scleroderma, port-wine stain type". On November 2014 she performed an MRI at another institution showing a diffuse white matter alteration in the left emisphere with focal lesions with high susceptibility and mild contrast enhancement.
She was addressed to immunosuppresive therapy with steroids and methotrexate, with steroids stopped after 6 months. A clinical cutaneous improvement was noted. On July 2016 a second MRI showed a worsening of the findings.
She continued the therapy with methotrexate.
She has never presented neurologic symptoms. She performed a 3T MRI on September 2016 showing a mild progression of the WM lesions. No alterations of circle of Willis. MR Spectroscopy showed reduced NAA/Cr ratio and presence of lactate on the lesion.

Unique teaching points:
We describe a case of a little girl with ECDS with no neurologic deficits or symptoms that shows extensive and progressive neuroradiologic alterations.
Only a few pediatric cases have been described, but it has to be known that also in absence of symptoms, patients with linear scleroderma should be screened with MRI to look for CNS involvement in this immune disease. Brain MRI can also be used to monitor the progression of the disease and the response to therapy.

Median Arcuate Ligament Syndrome (MALS) – A report of two cases

M. Lintrop, M. Murruste, O. Uibo; Tartu/EE

Objective:
MALS is a vascular compression syndrome which symptoms can overlap chronic functional abdominal pain. In MALS the proximal part of the celiac artery is compressed by the too low located median arcuate ligament during expiration resulting in hemodynamically significant symptoms.
We report two cases with MALS diagnosed primarily by ultrasonography.

Case presentation:
Case 1
18-year-old girl was admitted to Tartu University Children's Clinic (TUCC) due to recurrent acute epigastric pain episodes with nausea and loss of appetite during 7 years. Previous analyses were normal, abdominal USs and gastroscopy did not show any abnormalities.
She was referred to Paediatric Radiology department for Doppler US (DUS) which showed narrowed proximal celiac artery (CA) with turbulent flow, increased peak-systolic and end-diastolic velocities on deep inspiration and expiration, and positive CA deflexion angle on expiration. Superior mesenteric artery (SMA) was markedly widened, indicating possible collateral blood-supply due to severe CA stenosis. According US findings MALS was suspected.
Abdominal MRA showed proximal CA kinking, stenosis and post-stenotic dilatation and confirmed diagnosis. During DSA collateral blood-supply from SMA via pancreaticoduodenale arcade (PDA) was seen.
Laparoscopic release of MAL resulted in relief of patient's symptoms, she has been pain-free for two years.
Case 2
16-year-old girl applied to TUCC due to recurrent abdominal pain episodes for 2-3 years. Usually, pain occurred 2-3 times per week about 15 minutes after the start of intense cycling training or competitions, and passed about 5 minutes resting in squat position. Mild mid-epigastric bruit was audible at physical examination.
DUS showed two-fold increase in expiratory peak-systolic and end-diastolic blood flow velocities compared to inspiratory velocities which indicated to the hemodynamically significant worsening of CA compression by MAL during expiration.
MRA showed proximal CA compression, upward angulation and post-stenotic dilatation. Preoperative CT-angiography depicted collateral supply via PDA.
During laparoscopic surgery CA was released by transecting MAL and surrounding fibrous tissue. After surgery the girl has been pain-free for one year except single pain episode during intense competition.

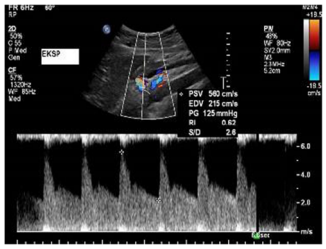

Doppler spectral images of 18 y/o girl of the proximal celiac trunk during end-expiration. Peak systolic and end diastolic velocities were markedly elevated (560/215 cm/s).

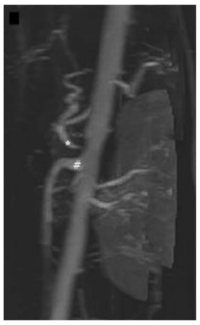

Sagittal MIP 3D SENSE MRA of 18 y/o girl showed the proximal celiac artery (*) with acute upward angulation, stenosis and poststenotic dilatation and widened superior mesenteric artery (#).

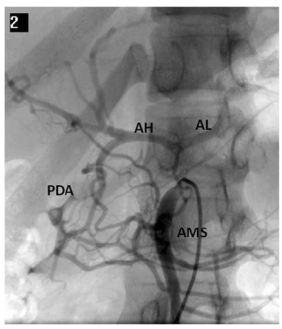

DSA of 18 y/o girl showed preocclusive compression of celiac trunk and supply from superior mesenteric artery (SMA) via pancreaticoduodenal arcade (PDA) to hepatic artery (HA) and splenic artery (LA).

Unique teaching points:

The diagnosis of median arcuate ligament syndrome should be considered in patients with postprandial abdominal pain that does not have other clearly established etiology.

Colour Doppler US should be the first choice imaging method. To confirm diagnosis in pediatric patients abdominal MRA is preferred in our institution, but as MRA may still have a tendency to movement artifacts and inadequate spatial resolution for smaller blood vessels, in these two cases MRA was followed by CTA or DSA.

Cutaneous metastases of infantile choriocarcinoma can mimic infantile hemangioma both clinically and radiographically

L. Dance, R.B. Towbin, M. Patel; Phoenix/US

Objective:

Understand the clinical and radiographic challenge of distinguishing between a common infantile hemangioma and much less common solitary cutaneous metastasis.

Understand the time-critical nature of accurate diagnosis of infantile choriocarcinoma which is usually fatal within 3 weeks of presentation if left untreated.

Understand the unique predilection of infantile malignancies to metastasize and present as skin-based masses, most commonly lymphoma/leukemia.

Case presentation:

An otherwise healthy 37 day old male presented to dermatology with a pedunculated, friable red glabellar mass (centered between the eyes). First noticed as a flat, bluish lesion at 10 days, its subsequent rapid growth led to an emergency department visit where dermatology diagnosed a hemangioma and initiated propranolol treatment. Despite this, the mass continued to grow rapidly, encroaching upon the patient's right eye. The patient was admitted for further workup.

An elevated beta hCG, anemia (7.4 mg/dL), and thrombocytopenia (92,000) suggested an alternate diagnosis. An MRI and ultrasound led to a percutaneous biopsy; pathology was consistent with choriocarcinoma. PET CT found FDG-avid glabellar, liver and lung lesions. Maternal and placental testing was negative for choriocarcinoma.

Ultrasound demonstrates a hypoechoic hypervascular mass. MRI brain demonstrates cutaneous confinement of the solid avidly enhancing glabellar mass. CT shows a peripherally enhancing liver mass with a mass-like area of consolidation in the right lung. Initial PET/CT demonstrated FDG avid liver and lung metastases with a small focus of residual activity at the glabella consistent with incomplete resection.

Follow-up PET/CT showed astoundingly rapid re-growth of the glabellar mass and enlargement of the hepatic and pulmonary masses just 12 days later demonstrating the extremely aggressive nature of this cancer. 3-month follow-up PET/CT showed significantly decreased size and activity of the metastases consistent with a treatment response.

In a series of 208 infants with cutaneous metastases, the following diseases presented with cutaneous involvement (ordered most to least common): leukemia, Langerhans cell histiocytosis, neuroblastoma, rhabdoid tumor, rhabdomyosarcoma, primitive neuroectodermal tumor, **choriocarcinoma**, and adrenocortical carcinoma.

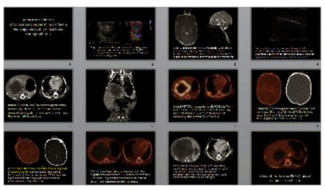

Summary of Imaging

Clinical Photos

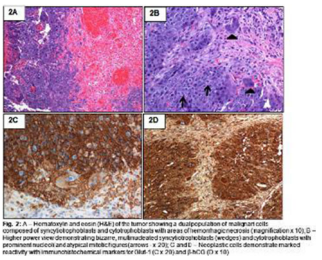

Pathology Slides

Unique teaching points:
Considered one of the fastest growing tumors, infantile choriocarcinoma classically presents with hepatomegaly, anemia, failure to thrive, and precocious puberty between 0 days and 5 months of life. Left untreated, the disease is usually fatal within 3 weeks of presentation.
A solitary cutaneous metastasis can be mistaken for infantile hemangioma both clinically and radiographically. Atypical MRI appearance is one important clue that can suggest an alternative diagnosis. PET/CT may be useful for staging and follow-up.

A rare case of Ovarian Juvenile Granulosa Cell Tumor associated with Ollier's Disease - Generalised mesodermal dysplasia
P. Joshi; Pune/IN

Objective:
To demonstrate a rare case of mesodermal dysplasia - association of ovarian granulosa cell tumour with enchondromatosis

Case presentation:
Two year 8 month old girl presented with precocious puberty i.e thelarche.
Left hand radiograph showed the radiological age corresponding to chronological age, suggestive of peripheral precious puberty.
The patient subsequently underwent a sonography which revealed a pelvic mass probably arising from the right ovary ? sex cord stromal tumour. A MRI of the abdomen and pelvis confirmed the pelvic mass and revealed multiple bone lesions in the right hemipelvis - on the side of the tumour
She was later operated.
HPE of pelvis mass revealed juvenile granulosa cell tumour.
HPE of the bone lesions revealed multiple enchondromas

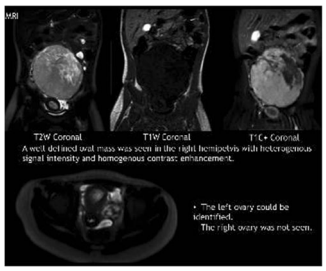

MRI pelvis confirms the findings - legend is explanatory


Ultrasound pelvis images reveal a solid pelvic mass, probably ovarian in etiology

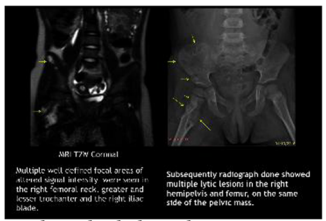

MRI pelvis also reveals multiple bone lesions

Unique teaching points:
The aim of the poster is to create awareness about this association.
The bone lesions should not be mistaken for metastasis
Juvenile granulosa cell tumour of the ovary (JGCT) is a well-known sex-cord stromal ovarian neoplasm.
OLLIER'S DISEASE is a rare, non hereditary mesosermal dysplasia consisting of multiple enchondromas.
The association of granulosa call tumour with asymmetric ipsilateral hemiskeletal distribution may indicate generalised mesodermal dysplasia as there is also association of JGCT with Maffucci's syndrome, other dysplastic conditions such as microcephaly, facial asymmetry,' and Potter's syndrome.
Review of literature showed 11 previous cases of juvenile granulosa cell tumor associated with enchondromatosis, three associated with Maffucci's syndrome, and the rest with Ollier's disease

Role of whole-body MRI in the diagnosis of Goldbloom syndrome in paediatrics: The sock sign
M.B. Damasio[1], G. Stagnaro[1], E. Aldi[2], F. Sertorio[1], G. Magnano[1]; [1]Genoa/IT, [2]Siena/IT

Objective:
WBMR has an increasing diagnostic role in systemic inflammatory diseases. Goldbloom's syndrome is a paediatric idiopathic disease characterized by transient bone marrow oedema with recurrent crisis of bone pain, periosteal hyperostosis, fever, increased inflammatory markers and dysproteinaemia.
A case series of WBMR studies in Goldbloom's syndrome is reported and differential diagnosis discussed.

Case presentation:
A 9-year-old female girl was admitted to our paediatric department because of daily crisis of bone pain of the lower limbs, associated with fever spikes, limping and nocturnal awakenings. No history of trauma was reported.
Laboratory tests showed mild anaemia (Hb 8.2 g/dl), thrombocytosis (PLT 680000/mmc), increased inflammatory markers (ERS 75 mm/h, CRP 7 mg/dl), high streptolysine O and DNase-B antibody levels (ASO 4280 IU/ml and ADN-B 6310 UI/ml, respectively). Throat swab was positive for group A β-haemolytic streptococcus (GAS). Unusual dysproteinaemia, characterized by hypoalbuminemia (2.8 g/dl) with increased a1, a2 and g globulinaemia, was noted. X-ray examinations of both legs resulted normal.
WBMRI showed markedly delineated, high and homogeneous hyper-hypointensity respectively in STIR/T1 of the distal tibial-peroneal meta-diaphysis of both legs (fig1a,b). Distal metaphysis of femur, humerus, radius-ulna and proximal tibia were also homogeneously mildly hyperintense on STIR sequences bilaterally (fig1a). Bone biopsy revealed signs of chronic inflammation. Infectious and neoplastic diseases were ruled out and the diagnosis of GS with dysproteinaemia seemed conceivable. Steroid treatment was started in association with indomethacin, leading to a prompt resolution of the clinical picture within a few days. The follow-up STIR total body MRI, performed after 10 months, showed the complete resolution of bone oedema. (fig2 a,b)

Unique teaching points:
The sock sign is a pathognomonic whole-body magnetic resonance imaging (WBMRI) feature of Goldbloom's syndrome (GS).It is a well marked, symmetric, homogeneous and high bone marrow hyperintensity, localized both at the distal tibial and peroneal meta-diaphysis, which looks like a pair of socks.

Are all hypoplastic appearing ventricles really hypoplastic?
Ö.İ. Koska, P. Bayindir, H. Alper; Izmir/TR

Objective:
Left ventricle hypoplasia is generally thought as a part of hypoplastic left ventricle syndrome or aortic hypoplasia. It is estimated that about 15-20 ml/m2 left ventricle volume is needed in order to support systemic circulation. Less than that volume generally precludes biventricular repair. However conditions associated with severe preload decrease such as total anomolous pulmonary venous return (TAPVR) should be considered in the differential diagnosis. TAPVR presenting as hypoplastic left ventricle syndrome is presented in this study.

Case presentation:
Six month old female patient admitted to emergency service with symptoms of fever, dyspnea and coughing. Emergency staff started intravenous antibiotic theraphy and from medical records learned that she has been followed for partial anomolous pulmonary venous return (PAPVR) and atrial septal defect (ASD). Lung X-rays revealed pulmonary edema. Echocardiography was performed and revealed very small left ventricle, PAPVR and 13 mm wide ASD. ECG gated cardiac CT was requested with the prediagnosis of hypoplastic left ventricle syndrome.
CT images revealed dilated right cavities, very small left ventricle, pulmonary edema, TAPVD and peritoneal fluid plus hepatomegaly.
We then retrospectively searched our archive and found she was diagnosed as PAPVR when she was 10 days old. All the cavities that time, were normal sized. According to these we confirmed our diagnosis as TAPVR and hypoplastic appearing cavities due to reduced preload and right chamber dilatation due pulmonary overcirculation.
Surgical team decided to perform corrective operation and they confirmed our diagnosis

Unique teaching points:
Small left ventricle cavity in an infant need not to be due to intrinsic hypoplasia. Whenever we experience such a situtation we should search for other reasons of pseudohypoplasia in order to give a chance for corrective surgery instead of palliative procesures.

Kimura disease in a thirteen year old male
K.S. Minhas, A. Parthipun, P. Patel, S. Stuart, S. Chippington, A. Barnacle, D. Roebuck; London/UK

Objective:
We present a case report of Kimura disease, a rare benign chronic inflammatory disease that involves the deep subcutaneous tissues and lymph nodes of the head and neck.

Case presentation:
We report the case of a thirteen year old male who presented with a right sided facial mass which had been present for two years but had enlarged rapidly in the preceding three months. US and MR were interpreted locally as an arteriovenous malformation. Review of these examinations and catheter angiography performed at this quaternary referral centre favoured a vascular tumour. Subsequent percutaneous biopsy demonstrated angiolymphoid hyperplasia with eosinophilia and blood tests showed a serum eosinophilia, consistent with Kimura disease.

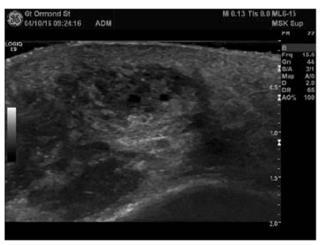

US shows a mass consisting of scattered heterogenous foci within the fat with multiple large feeding vessels.

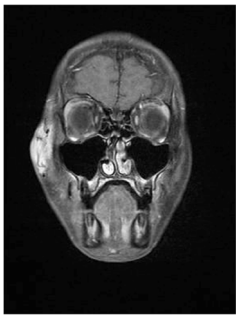

Contrast enhanced MRI demonstrated a solid, homogenously enhancing, mass with multiple vascular flow voids from the right external carotid artery branches.

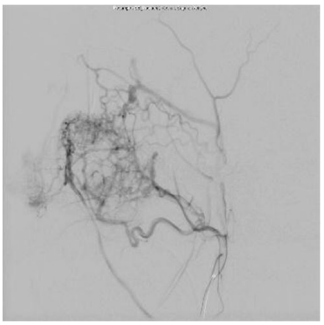

Catheter angiography showed tumour blood supply from branches of the right transverse facial artery and distal right IMA. The dominant supply arose superficially from the transverse facial artery.

Unique teaching points:
Kimura disease is a rare chronic inflammatory disorder of unknown aetiology that involves the deep subcutaneous tissues and lymph nodes of the head and neck region, most common in Asian men in the third decade and sporadic in the non-Asian population. The histopathological and biochemical characteristics are eosinophilic lymphfolliculoid granuloma, increased eosinophils in the peripheral blood and increased IgE levels. Whilst ultrasound and MRI are effective imaging modalities, imaging alone does not allow confident differentiation from malignant lesions and biopsy is necessitated. Kimura disease has a benign indolent course with an excellent prognosis following surgical excision although local recurrence has been reported.

Increased NAA: Is it surely Canavan Disease?
E. Varga, P. Barsi, G. Rudas; Budapest/HU

Objective:
Leukodystrophies are a group of rare genetic, metabolic diseases that affect the central nervous system, mainly the brain. Each type of them is caused by a specific gene abnormality that leads to abnormal development or destruction of the white matter of the brain. The differential diagnosis are made on the basis of clinical and neuroradiological signs. There are some diseases which show typical changes on MR spectroscopy.

Case presentation:
We present a case of a 12 year-old boy, who has been investigated due to somatomental retardation and muscle dystrophy since his six months of age. His perinatal period was normal except of a nystagmus visible from his birth. The child has muscle dystrophy, spastic quadriparesis, contractures, scoliosis, truncal hypotonia and ataxia and mental retardation. We started examinations to find out the background pathology of his idiopathic encephalo-myopathy. The brain MRI showed a bilateral, symmetrical white matter signal alteration, which referred to some kind of metabolic

disease. The MR spectroscopy revealed decreased cholin and increased NAA levels, which are typical of Canavan disease. Despite of this, the clinical aspects and the location of the involved brain areas were more typical of Pelizaeus-Merzbacher disease (PMD). The PMD is a genetic disorder, which is originated of the mutation of the proteolipid protein gene (PLP1) located on long arm of X-chromosome (Xq21-22). This gene has an impact on growth of the myelin sheath. Various types of mutations (deletion, duplication, point mutation, insertion) of PLP1 gene lead to various severity of clinical picture. All form of mutations show decreased NAA level on spectroscopy, except the duplication of PLP1 gene.

Unique teaching points:
In connection with our case, we present briefly the clinical and neuroradiological differences between the two entities.

Magnetic resonance imaging findings in medium-chain acyl-coenzyme A dehydrogenase (MCAD) deficiency
L. Talamanca, D. Narese, M.C. Rossi Espagnet, L. Pasquini, D. Longo; Rome/IT

Objective:
We report serial brain Magnetic Resonance (MRI) in a patient with Medium-chain acyl-coenzyme A dehydrogenase (MCAD) deficiency who developed acute encephalopathy.

Case presentation:
A 12-months-old girl was admitted in the emergency department of our hospital with sudden onset of acute encephalopathy with drowsiness. Baseline laboratory investigations revealed severe hypoglycemia, hyperammonemia, hyperchloremic metabolic acidosis and hyperuricemia. The patient was treated with glucose solution infusion that resulted in a gradual resolution of symptoms.
The first brain MRI, performed within 6 hours of onset of symptoms showed bilateral symmetric restricted diffusion on diffusion-weighted imaging (DWI) in the middle cerebellar peduncle, nucleus caudatus, putamen and periventricular white matter; the ADC map showed reduced diffusivity (Fig 1).
The second MRI, at 72 hours after the onset, revealed bilateral and symmetric hyperintensity on T2-weighted images in the middle cerebellar peduncle, nucleus caudatus, putamen and periventricular white matter. DWI showed restricted diffusion in both globus pallidus (Fig 2). A single voxel H-MRS study performed by placing a ROI in the right nucleus lenticularis revealed increased values of GABA and glutamine (Fig 3).
A further MRI was performed 4 weeks after the first neuroimaging and indicated widespread atrophy and the appearance of a hyperintense signal in T2-WI in both globus pallidus while DWI did not reveal any remarkable signal abnormality. Single-voxel MRS of the same region showed a normalization of GABA and glutamine values.

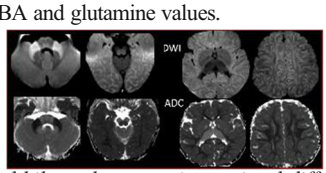

Brain MRI showed bilateral symmetric restricted diffusion on diffusion-weighted imaging (DWI) in the middle cerebellar peduncle, nucleus caudatus, putamen and periventricular white matter; the ADC map showed reduced diffusivity

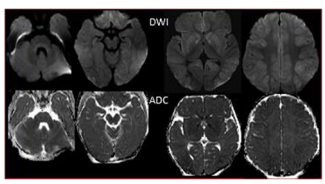

The second MRI, at 72 hours after the onset, revealed bilateral symmetric restricted diffusion on diffusion-weighted imaging (DWI) in both globus pallidus.

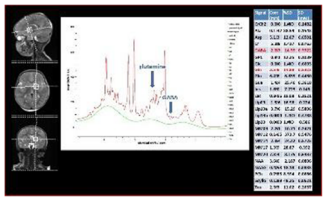

A single voxel H-MRS study performed by placing a ROI in the right nucleus lenticularis revealed increased values of GABA and glutamine.

Unique teaching points:
MCAD is an enzyme of the mitochondrial b-oxidation of fatty acids, an essential source of energy for cells during stress. MCAD deficiency is the most common genetic disorder of fatty acid oxidation.
The clinical manifestation of the disorder is typically precipitated by stress due to fasting, vomiting, fever or muscular exertion and occurs in the majority of cases before the age of 2 with the onset of acute hypoketotic hypoglycemia. Clinical features of this decompensated state include seizures and lethargy proceeding to coma and death in the absence of prompt treatment with intravenous dextrose infusion.
MCAD deficiency usually appears in an acute form and has high morbidity and mortality rates; early diagnosis is therefore extremely important in order to promptly begin treatment and obtain a complete recovery from symptoms. MR can play a significant role in the early diagnosis of the decompensated state of the disease; in our case DWI revealed the presence of lesions with a bilateral symmetric topographic distribution that strongly suggested a metabolic disease leading to acute encephalopathy.

A case of a newborn with accessory scrotum associated with bifid scrotum and perineal lipoma
E. Rossi[1], M. Basile[2], A.M. Buccoliero[2], C. Caporalini[2], A.M. Cangelosi[2], D. Narese[1], C. Defilippi[2]; [1]Rome/IT, [2]Florence/IT

Objective:
Neonatal perineal masses are very unusual. We report a rare case of accessory scrotum (AS) with peduncular lipoma.

Case presentation:
A full-term male neonate (3 days old) with external perineal anomalies was referred to our Hospital.
The physical perineal examination revealed a bifid scrotum containing palpable testis and a normal configured penis located at the bottom of the bifid scrotum. Two soft masses of 3 and 2 cm respectively, divided from a cutaneous notch, were located below the bifid scrotum and on the right of the midline. The rear biggest mass was normal epithelized, instead the other one was a rugged pigmented mass, which resembled the scrotum (Figure 1). There were no additional abnormalities of the external genitalia. The other peduncolar mass, located between the right scrotum and the posterior mass, had fluid content. A mild hydrocele in the right scrotum and a sliding testis on the left side were also revealed.
US examination showed a hyperechoic solid tissue, corresponding to the rear biggest perineal mass. The other peduncolar mass, located between the right scrotum and the posterior mass, had fluid content (Figure 2). A mild hydrocele in the right scrotum and a sliding testis on the left side were also revealed.
MRI also confirmed two perineal peduncolar masses: the biggest and posterior one, was made up by homogeneous fatty matter without contrast-enhancement after intravenous gadolinium injection (Figure 3).
The patient underwent excision of perineal masses and no complications occurred in the surgery.
The histopathological examination of the perineal masses revealed two areas with different histological features: the first one was characterized by the presence of smooth muscle bundles dispersed in the dermal collagen, instead the other contiguous area showed abundant mature adipose tissue in the deep dermis and hypodermis (Figure 5).

At last the rugged swelling mass was definitively diagnosed as AS without testis tissue inside, and the rear mass was diagnosed as lipoma.

The physical perineal examination revealed a bifid scrotum containing palpable testis. Two soft masses of 3 and 2 cm respectively, divided from a cutaneous notch, were located below the bifid scrotum.

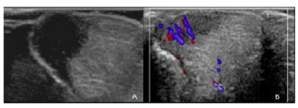

US examination showed a hyperechoic solid tissue, corresponding to the rear biggest perineal mass. The other peduncolar mass, located between the right scrotum and the posterior mass, had fluid content

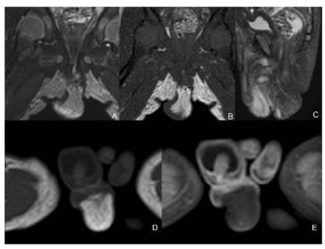

MRI confirmed the presence of two perineal peduncolar masses: the biggest and posterior one, was made up by homogeneous fatty matter without contrast-enhancement after intravenous gadolinium injection.

Unique teaching points:
Neonates presenting with perineal masses are uncommon.
These anomalies can occur isolated or more rarely in combination with other abnormalities such as uro-genital or ano-rectal anomalies or with contiguous subcutaneous tumors.
When perineal masses are found, with prenatal diagnosis or during a newborn physical examination, it is important to look for any associated congenital anomalies or subcutaneous tumors by using imaging.

"Half - moon" sign: Look for a tumor or a fracture
M. Raissaki, K. Spanakis, M. Velivassakis, E. Papadopoulou, A.H. Karantanas; Heraklion/GR

Objective:
To describe and emphasize the significance of the "half-moon" sign in pelvic MRI.

Case presentation:
A 13-year-old adolescent, karate athlete, was submitted with left hip pain, decreased range of movement and asymmetry in thigh circumference. Markers for infection or inflammation were negative. Frog-leg radiograph was negative for hip effusion, slipped epiphysis and equivocal for a left trochanteric abnormality. MRI demonstrated a half-moon pattern of bone marrow edema at the left intertrochanteric area and at the major trochanter, surrounding an apophyseal low-intensity lesion. AP radiograph and limited CT confirmed the presence of a lytic lesion with sclerotic margins, containing calcified chondroid matrix. Chondroblastoma was histologically confirmed following excision.

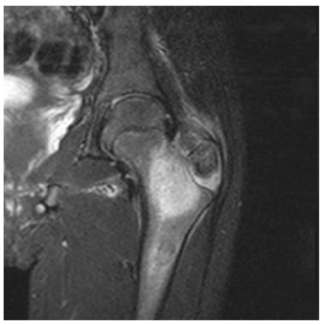

MRI, coronal STIR sequence, demonstrates semilunar-shaped hyperintense area abutting the growth plate and the cortex of the femoral neck, consistent with the half-moon sign. Note edema surrounding an apophyseal low-intensity lesion and soft-tissue edema.

CT confirms a typical apophyseal lesion with sclerotic margins containing chondroid matrix.

Unique teaching points:
"Half-moon" sign refers to a semilunar shape of bone marrow edema at the intertrochanteric area of the hip with its base located at the cortex of the femoral neck. This distribution differs from the distribution of edema in metaphyseal and metaphyseal-equivalent osteomyelitis. "Half-moon" sign has been described in patients with stress fractures and osteoid osteomas. To our knowledge, this is the first case of chondroblastoma exhibiting this sign.
Whenever the "half-moon" pattern of edema is identified at pelvic MRI scans, a thorough search for an occult fracture line or a nidus corresponding to an osteoid osteoma or a chondroblastoma is mandatory.

SESSION: SCIENTIFIC SESSION: ABDOMINAL (GI & GU) IMAGING

Pediatric MR Elastography on Siemens scanners: Early experience
C. Maya, E.A. Hartung, R.H. Carson, E.B. Rand, J. Rychik, D.J. Goldberg, K. Darge, S. Anupindi; Philadelphia/US

Objective:
MR Elastography (MRE) is a noninvasive imaging technique that quantitatively measures liver stiffness and provides an estimate of the degree of fibrosis. Our aim was to evaluate the feasibility of performing MRE using both gradient echo (GRE) and echo planar (EPI) sequences on Siemens scanners.

Materials:
A dedicated MRE of the liver was performed on a 3T MR scanner (MAGNETOM® Skyra, Siemens) with a pediatric mechanical

driver (courtesy of Mayo Clinic) over the right upper quadrant. An axial T2 BLADE with fat saturation, a coronal T1 VIBE Dixon and axial diffusion weighted imaging (DWI) were obtained. Elastograms were obtained using both an axial standard GRE and a works in-progress (WIP) EPI sequence. For the GRE sequence, 5 different slices were selected and each scanned sequentially. The EPI sequence incorporated 5 different slices in just one series. Images were post-processed placing regions-of-interest (ROI) and measuring the stiffness in kilopascals (kPa). For each sequence and each slice the stiffness mean was measured and then the average of the means was obtained. A spleen elastogram was simultaneously generated, without changing the mechanical driver location, and mean stiffness was also calculated. Based on cutoffs in the literature, values were considered abnormal if liver stiffness >2.9 kPa and spleen stiffness >3.6 kPa.

Results:
Twenty MRE exams were performed on 15 patients (7 female, 8 male) with a mean age of 16.4 years. Indications for MRE included: post Fontan (n=15), Wilson disease (n=1), non-alcoholic steatohepatitis (n=1), chemotherapy hepatotoxicity (n=1), and Tetralogy of Fallot (n=1). Increased liver stiffness was found in 11/20 (55%) on GRE and in 10/20 (50%) on EPI. Median liver stiffness values were 3.72kPa (range: 2.4-6.9 kPa) on GRE and 3.51 kPa (range: 2.2-4.6 kPa) on EPI sequences. Median spleen stiffness values were 3.85 kPa (range: 2.3-7.1 kPa) on GRE and 4.5 kPa (range: 2.7-7.1 kPa) on EPI sequences. Initially, liver stiffness could not be measured in 4/20 (20%) of GRE and 5/20 (25%) of EPI sequences, and spleen stiffness could not be measured in 6/20 (30%) of GRE and 10/20 (50%) of EPI sequences. Over time this challenge was overcome and now all measurements are obtained in each patient.

Conclusion:
Our initial experience shows that MRE is feasible on Siemens scanners using both GRE and EPI sequences. EPI sequences are a promising addition to standard GRE.

Prone versus supine ultrasound positioning for evaluation of urinary tract dilation (UTD) in children

C. Maya[1], Y. Gorfu[2], E. Dunn[1], K. Darge[1], S. Back[1]; [1]Philadelphia/US, [2]Addis Ababa/ET

Objective:
Ultrasound (US) is used in the initial evaluation and surveillance of UTD in children. UTD classification systems, including the 2014 multidisciplinary consensus, assess anterior-posterior renal pelvic diameter (APRPD) and calyceal dilation. There is currently no consensus regarding optimal patient positioning—prone versus supine—during US assessment of UTD. This study was performed to determine if there is a significant difference in the measurement of the APRPD, presence of calyceal dilation, or resulting UTD consensus score obtained between supine and prone positions.

Materials:
Two raters retrospectively reviewed renal bladder ultrasounds of patients with UTD of one or both kidneys. Technically adequate ultrasound examinations of orthotopic kidneys that were imaged in both supine and prone positions were included. Those with renal anomalies or prior surgery were excluded. APRPD measurements, as well as central and peripheral calyceal dilation, were documented in both prone and supine positions. A postnatal UTD consensus score was assigned to each kidney based only on these features.

Results:
146 kidneys (77 left) in 89 subjects had UTD in either the supine or prone position. Mean age was 0.41 years (range: 0.01 – 1.97 y). Female to male ratio was 1:3 (21/68). The interclass correlation (ICC) of the APRPD between raters was 0.88 and 0.87 in the supine and prone positions respectively (ps<0.001). Central calyceal dilation was found in 97/146 supine kidneys and 102/146 prone kidneys by rater 1 and 94/146 supine and 99/146 prone kidneys by rater 2 (Kappa 0.92). Peripheral calyceal dilation was found in 54/146 supine kidneys and 65/146 prone kidneys by rater 1 and 50/146 supine kidneys and 62/146 prone kidneys by rater 2 (Kappa 0.89). As such the results are presented as one. The APRPD tended to be greater when prone with a strong correlation between prone and supine measurements (0.92, $p<0.001$). The mean difference between supine and prone APRPD was 1.1 mm ($p< 2.2$). In 15 kidneys, calyceal dilation was seen in the prone position and not supine while 1 kidney had central calyceal dilation only when supine. The UTD score differed between supine and prone in 13/149 kidneys, with all but one higher when prone. In 10 other kidneys, the APRPD differed between positions however concurrent calyceal dilation resulted in no change in UTD class.

Conclusion:
As a screening tool, performing ultrasounds in the prone position may help identify more kidneys with UTD. Further research is needed to determine if these differences are clinically significant.

Non-pathologic Diffusion Restriction of the Jejunum on MR Enterography

D.M. Biko, J.B. Rapp, C. Maya, S.A. Anupindi; Philadelphia/US

Objective:
During the evaluation of magnetic resonance enterography (MRE), diffusion restriction (DR) has been utilized as a marker for bowel inflammation, but in our practice we commonly see DR in otherwise normal segments of jejunum. The purpose of this article is to assess the DR in normal loops of jejunum on MRE and to determine if there is a correlation between DR and luminal distention, age, magnet field strength, and bowel segment location.

Materials:
A retrospective analysis of subjects with a normal MRE and normal clinical work up (based on available clinical history, endoscopy reports, serum white blood cell count and inflammatory markers, and stool samples) was performed. The abdomen was divided into 4 quadrants. If available, 2 loops of jejunum were randomly chosen in each quadrant. Two radiologists independently evaluated these same loops of jejunum for the following: luminal distension, wall thickness, and enhancement pattern. Additionally, the loops were then evaluated for the presence or absence of DR. Inter-rater reliability was determined. Disagreement was resolved by consensus. Presence or absence of DR was correlated with luminal distension, age, magnet field strength (1.5 versus 3 Tesla), and abdominal quadrant.

Results:
One hundred ninety-seven loops of jejunum were evaluated in 39 patients. Not all subjects had jejunal loops in all quadrants. Sixteen subjects (41%) had jejunal loops with DR for a total of 29 loops. One loop had increased wall thickness and another increased enhancement but both did not demonstrate DR. No other loops demonstrate increased enhancement or wall thickening. For the presence or absence of DR, inter-rater reliability was fair (kappa=0.39). There was no correlation between the presence/absence of DR in relation to luminal distension, age, magnet field strength, or quadrant location. Of the 16 subjects who had a single loop with DR, a 2nd loop with DR was found in 50%.

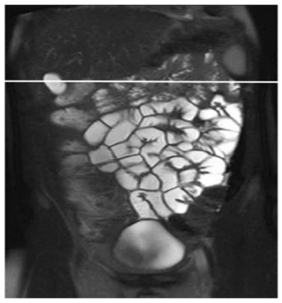

14 year old who presented with nausea. MR enterography demonstrates no bowel thickening or abnormal enhancement. a. Coronal HASTE demonstrates the craniocaudal position of the axial diffusion sequence for reference (line).

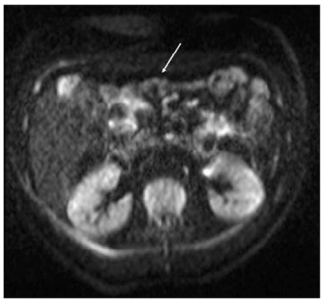

14 year old who presented with nausea. MR enterography demonstrates no bowel thickening or abnormal enhancement. b. Axial diffusion weighted seqeunce (b=800) shows diffusion restriction within loops of jejunum (arrow) within the anterior abdomen.

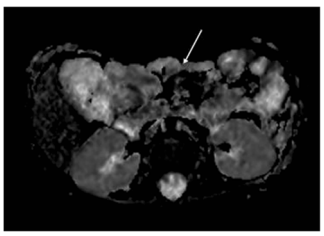

14 year old who presented with nausea. MR enterography demonstrates no bowel thickening or abnormal enhancement. c. Corresponding ADC map demonstrates low signal within the jejunal wall consistent with diffusion restriction (arrow).

Conclusion:
Diffusion restriction in normal loops of jejunum on MRE was present in 41% of patients. If DR is seen in an otherwise normal segment of jejunum, this can be considered non-pathologic. A patient with a loop of jejunum with DR is likely to have an additional loop of jejunum demonstrating DR. There is no correlation with DR of normal jejunum with luminal distension, magnet field strength, or patient age. Our data may help reduce overestimation of disease burden when clinically applied.

Imaging findings in the newborn with meconium peritonitis that require surgery

P. Caro Dominguez[1], A. Zani[2], A. Daneman[2]; [1]Cordoba/ES, [2]Toronto/CA

Objective:
Meconium peritonitis is a rare condition caused by an *in-utero* bowel perforation resulting in spillage of meconium into the peritoneal cavity and subsequent calcification. The role of prenatal and postnatal imaging is to identify infants who require surgery. The aim of this study was to evaluate the role of postnatal imaging in meconium peritonitis and to correlate the radiologic and sonographic patterns with the need for surgery.

Materials:
Imaging studies in infants with meconium peritonitis performed between 1999 and 2014 at our institution were reviewed separately by a pediatric radiologist, a pediatric radiology fellow and a pediatric surgeon. Patients were divided in a surgical and a non-surgical group. Clinical, surgical and pathology reports were reviewed to validate the diagnosis. Statistical analysis: comparisons between sonographic and radiographic findings and patterns in the surgical and non-surgical groups were performed using unpaired t-test and chi-square.

Results:
During the study period, there were 37 infants with meconium peritonitis managed at our institution. In the 23 (62%) who needed surgery, the most frequent surgical findings were idiopathic perforation, jejunal and ileal atresia. Ultrasound identified more cases with hepatic calcifications, meconium pseudocyst, ascites and pneumoperitoneum than radiography and radiography more cases of small bowel obstruction. Ascites identified with ultrasound (p=0.01) [Fig 1] and bowel obstruction [Fig 2] diagnosed either with ultrasound (p=0.04) or radiography (p=0.01) were associated with the need for surgical intervention. One third of children with meconium pseudocysts (4/12) [Fig 3], did not require surgery. Diffuse peritoneal or hepatic calcifications as an isolated postnatal finding were not associated with the need for surgery.

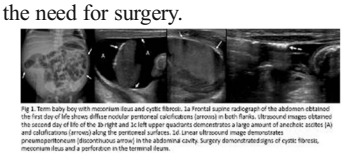

Fig 1. Term baby boy with meconium ileus and cystic fibrosis. 1a Frontal supine radiograph of the abdomen obtained the first day of life shows diffuse nodular pertioneal calcifications (arrows) in both flanks. Ultrasound images obtained the second day of life of the 2b right and 2c left upper quadrants demonstratas a large amount of anechoic ascites (A) and calcifications (arrows) along the peritoneal surfaces. 2d Linear ultrasound image demonstrates pneumoperitoneum (discontinuous arrow) in the abdominal cavity. Surgery demonstratedsigns of cystic fibrosis, meconium ileus and a perforation in the terminal ileum.

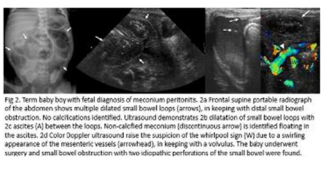

Fig 2. Term baby boy with fetal diagnosis of meconium peritonitis. 2a Frontal supine portable radiograph of the abdomen shows multiple dilated small bowel loops (arrows), in keeping with distal small bowel obstruction. No calcifications identified. Ultrasound demonstrates 2b dilatation of small bowel loops with 2c ascites (A) between the loops. Non-calcified meconium (discontinuous arrow) is identified floating in the ascites. 2d Color Doppler ultrasound raise the suspicion of the whirlpool sign (W) due to a swirling appearance of the mesenteric vessels (arrowhead), in keeping with a volvulus. The baby underwent surgery and small bowel obstruction with two idiopathic perforations of the small bowel were found.

Fig 3. Preterm twin baby girl with fetal diagnosis of meconium peritonitis. 3a Lateral portable cross table radiograph of the abdomen demonstrates a round, peripherally calcified mass in the mid abdomen (arrows), in keeping with meconium pseudocyst. 3b Linear ultrasound and 3c Doppler ultrasound images show calcification of the periphery of the mass (arrows), with twinkling artefact on color Doppler (discontinuous arrow), and heterogeneous contents. This patient was asymptomatic regarding the gastrointestinal tract, was treated conservatively and remains asymptomatic four years later.

Conclusion:
Both radiography and ultrasonography give valuable information to the surgeon to take the decision for surgery. Dilatation of bowel loops and ascites detected postnatally with radiography and/or ultrasound require surgical intervention in children with meconium peritonitis. Interestingly, a large proportion of infants with meconium peritonitis can be managed conservatively.

Renal Diffusion Tensor Imaging (DTI): Are quantitative DTI values useful in the evaluation of children with ureteropelvic junction obstruction (UPJO)?

J. Delgado, J. Berman, C. Maya, R.H. Carson, S. Back, K. Darge; Philadelphia/US

Objective:
Evaluate the value of Diffusion Tensor Imaging (DTI) quantitative parameters as biomarkers for children with UPJO.

Materials:
We retrospectively analyzed functional MR Urogram (fMRU) with renal DTI performed at 1.5T of 30 kidneys in 16 children (12 male), mean age

5.9 years (range: 0.17 – 17.4). Those included had complete fMRU analysis, DTI (b=0 and b=400, 20 directions), and UPJO configuration in at least 1 kidney. Cases with motion artifact (n=9), post-pyeloplasty (n=3) or duplex collecting systems (n=3) were excluded. Pelvicalyceal dilation grade (PCD), corticomedullary differentiation (CMD), and functional parameters were included. Pyeloplasty following fMRU was recorded. DTI tractography was reconstructed using a fractional anisotropy (FA) and an angle threshold of 0.10 and 55°, respectively **(Figure 1)**. User-defined regions-of-interest (ROI) of the renal parenchyma, excluding the collecting system, were drawn to quantify DTI parameters: mean FA, apparent diffusion coefficient (ADC), tract length and tract volume. The relationships between DTI quantitative parameters and fMRU parameters were analyzed.

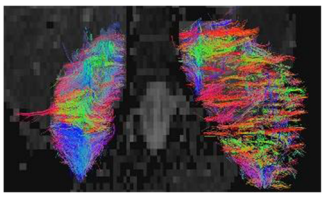

Figure 1. Diffusion tensor imaging in a 6.6 year-old male with left kidney UPJO. Note the differences in the tractography pattern between the right (normal) and left (pelvic and central/peripheral calyceal dilation) kidneys.

Results:
Age and ADC (ROI) ($p<0.01$, $R^2=0.36$), tract volume ($p<0.01$, $R^2=0.77$) and tract length ($p<0.01$, $R^2=0.60$) were positively correlated. Age and FA (ROI) ($p<0.01$, $R^2=0.46$) were negatively correlated. There was a correlation between fMRU parenchymal volume and tract volume ($p<0.01$, $R^2=0.80$), but median volumes were higher on DTI (tractography=98.5 cm^3 vs. fMRU=60.52 cm^3; $p<0.01$). Of the 16 children, 12 had pyeloplasty, 1 had nephrectomy, 2 were managed conservatively and 1 was lost to follow-up. FA was significantly lower in kidneys that went on to have pyeloplasty in comparison to those without pyeloplasty, but the 95%CI and the IQR overlapped **(Table 1)**. The ADC, tract length and tract volume were similar between these groups **(Table 1)**. There was no difference between the ADC of FA values in kidneys with and without PCD or CMD (p>0.11). Linear hierarchical regressions controlling the age did not show a significant relation between ADC and cortical or renal transit times (p>0.68), but lower FA values were related to a higher renal transit time ($p<0.01$, $R^2=0.103$).

Median (IQR)	Pre-pyeloplasty (n=12)	No pyeloplasty=(n=16)	p-value
ADC (mm^2/s)	0.0021 (0.0020 – 0.0024)	0.0020 (0.0018 – 0.0022)	0.082
FA	0.18 (0.17 – 0.20)	0.21 (0.18 – 0.23)	0.037*
Tract length (mm)	11.5 (9.6 – 13.1)	12.8 (9.3 – 15.6)	0.397
Tract Volume (cm^3)	114.0 (55.2 – 157.6)	87.4 (39.3 – 135.7)	0.397

Table 1. Quantitative DTI parameters between kidneys with and without pyeloplasty following fMRU.

Conclusion:
Renal ADC, FA, tract volume and tract length change with age but tractography overestimates renal parenchymal volume. There was a tendency towards a lower FA in kidneys that went on to pyeloplasty. Otherwise, none of the quantitative parameters evaluated in this study differentiated degrees of UPJO.

The potential causes of premature microbubble destruction during echo-enhanced voiding urosonography in children
D. Kljucevsek, O. Pecanac, M. Tomažič, M. Glušič; Ljubljana/SI

Objective:
Echo-enhanced voiding urosonography (eeVUS) has become an important imaging tool in urodiagnostics; however, it has been observed that during eeVUS the premature destruction of ultrasound contrast agent microbubbles might occur. The purpose of this study was to evaluate the possible causes of contrast vanishing during investigations and propose the protocol to avoid false negative results.

Materials:
EeVUS was performed in 163 children from April to December 2016. SonoVue mixed with saline solution in a plastic bottle is applied by continuous flow through the urine catheter. The collected data according to the protocol in this prospective study was completed in 105 children, aged from 2 weeks to 10.25 years. The protocol included general patient information, indication for eeVUS, duration of eeVUS in minutes, and the presence of vesicoureteric reflux. Extensive data about SonoVue were recorded: charge number, expiration date, time since opening, amount of initially administered contrast (ml SonoVue/ml saline solution), grading of the initial contrast opacification of the bladder, the need for immediate readministration of contrast (dose), grading of contrast opacification during examination, and the need for readministration of contrast later in the course of the examination (dose). In addition, the data regarding bladder (ratio real/predicted bladder volume, wall thickness, ureter dilatation), saline solution, the size of urine catheter (French), and the type of antibiotic prophylaxis were collected. Child observation included grading of crying and muscle stiffness.

Results:
Normal contrast opacification of urinary tract during examination was found in 87/105 children, while in 18/105 (17.2%) the contrast opacification was insufficient. In 12/18 (72.2%) microbubble destruction occurred during the first minute, in 4 (22.2%) in 5 minutes, and in 1 in 13 minutes after the beginning of contrast administration. The reason for unsatisfactory contrast opacification at the beginning of the eeVUS is probably due to small urine catheter size (25% of children with Fr6 catheter had insufficient opacification compared to 13.3% with Fr8 in whole cohort), time since the contrast is opened (more than 3 hours in 4 children), and insufficient bladder emptying at the beginning of the procedure. The reason for microbubble destruction later in the course of the examination is bladder overfilling in combination with increased muscle stiffness and strong crying, which led to increased bladder pressure. There was no correlation between the type of antibiotics and microbubble destruction.

Conclusion:
We should be aware of possible false negative VUR results during eeVUS caused by premature microbubble destruction.

MRI T1 mapping of the liver in adolescents with Fontan circulation
K.J. Thrane, K. Thomassen, K. Rydén Suther, O. Geier, B. Nguyen, A. Tomterstad, E. Thaulow, R. Almaas, L.-S. Ording-Müller, T. Möller, C. de Lange; Oslo/NO

Objective:
Patients with Fontan-type palliation of univentricular congenital heart disease have elevated central venous pressure due to their passive pulmonary flow. The altered circulation has a negative impact on several visceral organs, and these patients have chronic liver congestion. They are at risk of developing hepatic fibrosis and cirrhosis with potential malignant transformation. These changes can occur from only a few years after Fontan palliation, making early detection and grading of major importance. The patchy pattern of hepatic changes makes liver biopsy an unreliable diagnostic tool. Magnetic Resonance Imaging (MRI) T1 mapping has been suggested as a technique for non-invasive assessment and quantification of hepatic fibrosis/cirrhosis.
The aim of this study was to compare two different T1 mapping sequences of the liver in adolescents with Fontan palliation, and in healthy controls.

Materials:
15 adolescents (15-17 y) with Fontan circulation and 7 young healthy adults (18-24 y) were included as a part of an ongoing national population-based study. All underwent MRI (1.5 Tesla) pre- and post-Gadolinium contrast, including two types of T1 mapping of the liver. A 3D T1 volumetric interpolated breath-hold examination (3D VIBE) sequence with dual flips with B1 correction and a modified Look-Locker inversion recovery (MOLLI) sequence. T1 relaxation times (ms) were measured by placing five standardized circular regions of interest (ROI) in the mid- section of the liver and one in the spleen (fig 1). Statistical analysis was performed comparing measurements pre-and post-contrast, between sequences, and patients and controls.

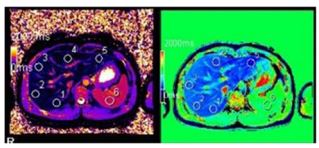

Results:
There was a significant difference in the measurements between MOLLI and 3D VIBE with increased values for the latter. Within each sequence there were small, but significant regional differences in relaxation times (table 1). The same pattern was seen in pre- and post-contrast images in both groups. There were significantly increased native T1 times on both sequences in all regions in the Fontan group as compared to the controls, but not post contrast.

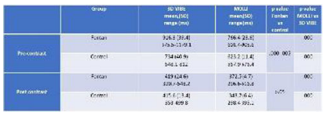

Conclusion:
T1 relaxation times differ between the T1 mapping sequences, MOLLI and 3D VIBE, pre- and post-contrast. T1 mapping of the liver revealed significantly increased native T1 times in adolescents with Fontan palliation compared to healthy slightly older controls. These findings suggest hepatic fibrosis/cirrhosis, but may also represent a component of congestion.

Diagnostic accuracy of ultrasound, computed tomography and wedge portography in the work-up for mesenterico-rex bypass in children with extrahepatic portal hypertension
S. Toso, R. Breguet, M. Annoshiravani, S. Terraz; Geneva/CH

Objective:
To identify the diagnostic accuracy of ultrasound (US), computed tomography (CT) scan and portography (wedge hepatic vein portography or direct portography) in the pre-operative work-up of mesenterico-rex bypass performed for extrahepatic portal hypertension in children.

Materials:
We conducted a retrospective analysis of pre-operative imaging for mesenterico-rex bypass in our tertiary hospital over the last 12 years. We analyzed all patients between the ages of 0-16 years, with extrahepatic portal hypertension necessitating surgical treatment that underwent US, CT and portography.
Three reviewers independently analysed the patency of the left portal vein, mesenteric vein, splenic vein and the presence of communication between the left and right portal vein on preoperative imaging with correlation to surgical findings. Statistical analysis of diagnostic accuracy was performed.

Results:
Eleven patients underwent mesenterico-rex bypass for portal hypertension secondary to portal vein thrombosis. Two patients had partial liver transplant. CT with ultrasound correlation was sufficient in responding to the preoperative criteria in 72% (8/11) cases. Portography was useful in the 27% (3/11) cases where CT could not respond to preoperative criteria, in particular the presence of left-right communication.
There was good inter-rater correlation for each modality and good correlation of findings between modalities.

Conclusion:
In the majority of cases the use of ultrasound and CT is sufficient for preoperative planning for mesentrico-rex bypass. Portography is mandatory in cases with large intra-hepatic cavernoma, where the left-right communication could not be confirmed on CT.

MRE identifies more abnormalities, but is no more likely than bowel ultrasound to impact clinical decisions in pediatric IBD as judged by a clinical consensus
J.L.J.B. Barber, A. Zambrano Perez, N. Shah, T.A. Watson; London/UK

Objective:
Assess the diagnostic agreement of MRE versus bowel US in pediatric IBD Assess the diagnostic accuracy of MRE and bowel US with reference to a clinical consensus gold standard Determine whether MRE or bowel US change patient management decisions

Materials:
Retrospective review of pediatric IBD patients from September 2014 to August 2016 who had undergone both MRE and bowel ultrasound within 30 days. MRE and US were graded independently by two radiologists. Contemporaneous clinical data was reviewed where available, and a clinical decision on disease severity and activity on a Likert scale made with and without imaging.

Results:
Fifty-three patients underwent MRE and bowel US in the specified timeframe (29 male; median age 13.02 years, range 4-16 years). Twenty patients had sufficient contemporaneous clinical information to be analysed.
Inter-observer variability for the imaging scores was assessed using Bland-Altman plots. Where variability was beyond pre-determined limits, the studies were consensus reviewed. Mean scores were used for the studies within accepted limits of variability.
There was no significant difference between total MRE and US scores (Wilcoxon signed-rank test z=1.13, p=0.26). At the bowel segment level, there was no significant difference between the MRE and US segment scores for the ileum and terminal ileum (Wilcoxon-signed rank test, z=0.72, p= 0.472), but significant differences were present between the imaging scores for other bowel segments, with MRE identifying more abnormalities.
There is a significant positive correlation between MRE and clinical consensus scores (Spearman's rho=0.598, p=0.0053) and between US and clinical consensus scores (Spearman's rho =0.657, p=0.0016). Imaging caused a refinement to the original clinical assessment in 8 of the 20 cases, with jejunal and ileal disease the most common reason for 'upgrading' a score and absence of any detectable abnormality on US and MRE the most common reason for 'downgrading' a score.

Conclusion:
We found good agreement between MRE and US for total patient imaging scores, ileal and terminal ileal scores. Both MRE and US scores correlated well with the gold standard clinical consensus, with imaging altering the original clinical decision in 40% of cases.
Although US detected fewer abnormalities than MR, it correlates marginally better with the clinical consensus, suggesting it is at least equally clinically valuable.

SESSION: SCIENTIFIC SESSION: MSK

Sickle cell crisis in children: Analysis of Fluid signal on unenhanced fat-suppressed T1-weighted MRI on 12 patients with an acute bone crisis

T. Youssef[1], J. Carmichael[2], A. Youssef[3], M. Kokkinakis[2]; [1]Leicester/UK, [2]London/UK, [3]Toronto/CA

Objective:

Background: Differentiating between acute osteomyelitis **(OM)** and acute bone infarct **(BI)** in children with sickle cell disease **(SCD)** is a challenge for clinicians and radiologists, particularly when blood cultures are negative. Although bone aspiration is the gold standard test for **OM** diagnosis, it is an invasive procedure and infrequently performed. Magnetic Resonance Imaging **(MRI)** has shown a potential role in differentiating between acute **BI** and acute **OM.**

Objective:

The goal of this case series is to evaluate the utility of fluid signal on unenhanced fat-suppressed (FS) T1-weighted MR sequence in distinguishing acute **BI** and **OM** in children with SCD.

Materials:

Methods: We reviewed a total of 22 children with SCD admitted with long bone pain during the one -year study period 2015-2016 attributed to either an acute **BI** or an acute **OM**. Twelve of 22 patients with available bone aspiration, blood culture, and MRI data were evaluated for fluid signal, marrow signal and other criteria.

Results:

Of 12 patients, nine patients were diagnosed as acute **BI** and two patients had acute **OM** and one with coexisting **BI** and **OM**. The diagnosis was based on the fluid signal on T1 unenhanced T1 FS MR images as compared to aspiration cytology in which eight of nine patients with **BI** had hyperintense fluid signal on non-contrast T1 FS MR images while one of two patients with **OM** demonstrated hypointense fluid signal. The last patient was diagnosed as a probable coexisting lesion (**OM&BI**) based on a giant well demarcated hypointense marrow signal with an extra-osseous hyperintense fluid signal.

Conclusion:

In acute **BI**, an abnormal hyperintense subperiosteal or paraosteal fluid signal is frequently observed on unenhanced T1-FS weighted images. This finding was present in the majority of cases in our study population regardless of age, sex or site in the appendicular skeleton. MRI fluid signal characteristic on unenhanced T1 FS shows promise as a criterion to differentiate between acute **BI** and **OM**.

Role of MRI to Assess Skeletal Age in Pediatric Celiac Disease

S. Bernardo, M. Martino, A. Laghi, E. Tomei; Rome/IT

Objective:

Coeliac children are often subject to weight loss and lower somatic growth rate, compared to healthy children of the same age. The purpose of this study was to asses the feasibility of magnetic resonance imaging (MRI) of the hand and the wrist to assess skeletal age and growth delay.

Materials:

We enrolled in our study 39 coeliac children (13 males and 26 females) affected by histological proven coeliac disease, with a chronological age ranged between 5 years and 1 month and 16 years and 4 months (mean age of 10years, +/3 years and 8 months standard deviation). A single MRI sequence (T13D SE, acquisition time: 1 minute 31 seconds) of the hand and wrist in coronal plane was performed of each patient to estimate the skeletal age. Patients' data were compared with a population of normal subjects.

Results:

The preliminary results showed a delay in skeletal age in children affected by coeliac disease in 85,7% of the simple study, with a delay of maturity of 0.83 years (+/- 2,2 years of SD). Only 3 children showed advance MRI skeletal age when compared to normal subjects.

Conclusion:

MRI of hand/wrist to assess skeletal age may be considered as a reliable indicator of somatic growth. MRI, without radiation exposure, can be an used as a diagnostic tool in skeletal delay. It could play an important role in the follow up of coeliac children, after glutenfree diet.

The prevalence of metaphyseal injury and its mimickers in otherwise healthy children under two years of age

P. Eide, Å. Djuve, R.E. Gjøscæter, K.F. Forseth, A. Nøttveit, C. Brudvik, K. Rosendahl; Bergen/NO

Objective:

Metaphyseal lesions in infants and toddlers are believed to have a high specificity for inflicted injury, however, normal metaphyseal irregularities may mimic pathology and lead to overdiagnosis.

Materials:

During the period 2010-2015 all children between 0 and 2 years, seen at the A&E department in Bergen (Bergen Legevakt) due to an injury, and who had radiographs taken, were included. Data on previous injury, age, sex and injury mechanism were drawn from the medical notes and PACS archive. All radiographs were reviewed by two researchers and an experienced paediatric radiologist, registering the following: number, site and type of fractures, signs of healing (yes, no), bone structure (normal, pathological) and metaphyseal appearances (shape (normal, metaphyseal collar, metaphyseal irregularity), injury). The study was approved by the institutional review board.

Results:

Six hundred one children (293 girls) between 2 and 24 months of age (mean 17.8 months) were included, of whom 218 (109 girls) had a total of 275 fractures. One hundred eight of the fractures (39.3%) involved the forearm, followed by leg-fractures (59/275, 21.5%) and fractures to the clavicle (37/275, 13.5%). One epiphyseal separation and one metaphyseal lesion (without a history of trauma) were seen. One thousand three hundred twenty metaphysis were analysed, of which 212 (16.1 %) were defined as either irregular (105/1320, 8.0 %) or demonstrating a metaphyseal collar (107/1320, 8.1 %).

Conclusion:

Metaphyseal lesions with a history of trauma did not occur in otherwise healthy neonates and infants under 2 years of age, indicating that this type of fracture has a particular mechanism. Metaphyseal irregularities are frequent, particularly around the knee, and should not be mistaken for CLMs

Hand MRI and Greulich-Pyle atlas in skeletal age estimation

A. Hojreh, J. Gamper, M.T. Schmook, M. Weber, D. Prayer, C. Herold, I.-M. Noebauer-Huhmann; Vienna/AT

Objective:

To evaluate whether MRI might be used for age estimation, based on Greulich-Pyle (GP) atlas criteria.

Materials:

1.5Tesla MRI of the left hand was conducted in 60 adolescents, and subjectively evaluated by two blinded radiologists. For sequence optimization, coronal MRI sequences (T1 TIRM, T1 VIBE-3D-WE, and T1 SE) and a left hand X-ray were compared in ten patients (eight male, two female; mean age, 13.5 years). The ages of 50 healthy volunteers (17

male, 33 female; mean age, 15 years) were assessed from coronal T1 VIBE-3D-WE. Bland-Altman plots, intraclass correlation coefficients (ICC), and logistic regression models were calculated.

Results:
Coronal T1 VIBE-3D-WE achieved the best image quality. The correlation between estimated patients' ages on X-ray and MRI was high. ICC showed high inter-observer agreement (0.95 for X-ray, 0.97 for MRI). The estimated age of the healthy volunteers tended to be older than their chronological age. The probability of overestimation was higher in girls than in boys.

Conclusion:
Coronal T1 VIBE-3D-WE of the left hand is feasible for skeletal age estimation by GP criteria with a high readers' agreement. The likelihood of overestimation of healthy children makes it necessary to develop a new hand atlas representing changes since the 1950s.

Metabolic Bone Disease in Preterm Infants: Assessment of the Relationship between Radiologic Grading in the Wrist and Serum Biochemical Markers

S.K. You[1], S.M. Lee[2], H.-H. Cho[3]; [1]Daejeon/KR, [2]Daegu/KR, [3]Seoul/KR

Objective:
To assess the relationship between the radiographic findings of metabolic bone disease (MBD) and serum biochemical markers in preterm infants.

Materials:
Preterm infants in our neonatal intensive care unit between January 2014 and September 2016 were included. Two readers retrospectively reviewed the wrist radiography for grading according to MBD severity. We recorded the levels of alkaline phosphatase (ALP) and phosphorous (P) immediately after birth, on the same day of the first wrist radiography (ALP-s, P-s), the highest ALP levels before the first wrist radiography (ALP-hb) and during follow-up (ALP-h), and the lowest P levels before the first wrist radiography (P-lb) and during follow-up (P-l). Patients were subdivided into four groups according to MBD severity determined by wrist radiography for the first analysis, and were divided into two groups according to MBD presence for the second analysis. One-way analysis of variance with a Tukey multiple comparison and the Student's *t*-test were used for statistical comparisons in the two analyses, respectively. A receiver operator characteristic (ROC) curve was constructed to determine the optimal cut-off values of the biochemical markers for the radiological prediction of MBD.

Results:
Of the 159 patients, 94, 39, 19, and 7 infants were classified into grades 0 1, 2, and 3, respectively. In the first analysis, ALP-s, ALP-hb, and ALP-h were significantly different between grades 0–1 and 2–3 (all $p<0.001$). P-lb was significantly different between grades 0 and 2 (p=0.001) and P-l was significantly different between grades 0 and 2 or 3 ($p<0.001$ or p=0.001). In the second analysis, ALP-s, ALP-hb, ALP-h, P-s, P-lb, and P-l were all significantly different between the two groups ($p<0.001$). The ROC curve of ALP-h showed the largest area under the curve values (0.752, 95% confidence interval=0.676–0.828; p=0.039) for detection of a radiographic change. The optimal cut-off value of ALP-h was 473.5 U/L, and the sensitivity and specificity were 81.5% and 47.9%, respectively. The first wrist radiography was obtained at 8.3 ± 5.1 weeks after birth, and ALP-h was measured at 6.9 ± 5.3 weeks after birth.

Conclusion:
The cut-off value of ALP for the prediction of abnormal radiological changes in wrist radiography was determined to be was 473.5 U/L. Our findings indicate that the highest ALP level at around 6.9 weeks after birth could be a valuable predictor of radiological MBD in preterm infants, including those with very low and extremely low birth weights.

Quantitative grading of TMJ synovitis in children with JIA–influence of MR-coil, timing after contrast-injection and location of measurements on joint-to-muscle enhancement ratio

A. Hamardzumyan Schmid, C. Kellenberger; Zurich/CH

Objective:
Assessment of signal intensity ratio between joint space and longus capitis muscle on contrast-enhanced MRI has been proposed as reliable method across different MR-scanners and protocols for grading temporomandibular joint (TMJ) arthritis in juvenile idiopathic arthritis (JIA) with a cut-off of 1.55 for diagnosing synovitis. The aim of this study was to investigate potential influences on such enhancement ratios (ER).

Materials:
Retrospective evaluation of 14 contrast-enhanced MR-studies of 28 TMJs in 7 girls with JIA (age 11.3±4.3y) obtained at two occasions with two different coils on a 1.5T scanner. Joint-to-muscle ER were calculated from signal intensity measurements in different joint compartments, muscles and sequences obtained with varying delay after contrast-injection, and compared with paired sample t-test. ER of TMJs without synovitis (n=10) and TMJs with synovitis (n=18), determined by qualitative criteria, were compared to ER reported in the literature.

Results:
Superior and inferior joint space to longus capitis muscle ER for normal TMJs (2.2±0.9; 2.6±0.7 respectively) exceeded 1.55 in all but one case (Figure) and for TMJs with synovitis (3.3±1.1, 3.8 ±1.1) were significantly higher than in 211 cases with synovitis from the literature (2.5±0.8, P≤0001). The same ER were higher when obtained with dual-ring coil (3.7±1.1; 4.1±0.9) than with multichannel surface coil (2.2±0.7; 2.6±0.8; P≤0.0002). While ER to longus capitis muscle were higher than those to pterygoideus muscle for both coils (P≤0.008), ER to pterygoideus muscle did not differ between coils (P>0.2). Not considering the timing of the scan, ER to pterygoideus muscle were highest in the inferior joint space (1.65 ±0.63), followed by the anterior joint recess (1.52±0.44) and superior joint space (1.49±0.62). Comparing images acquired immediately after contrast injection to later images (median delay 11min, range 5–15min), pterygoideus muscle ER in the superior (1.2±0.4 to 1.8 ±0.7) and inferior (1.2±0.3 to 2.0±0.6) joint space increased substantially ($P<0.0001$), while ER in anterior recess showed no significant increase (1.5±0.4 to 1.6±0.5, P=0.18).

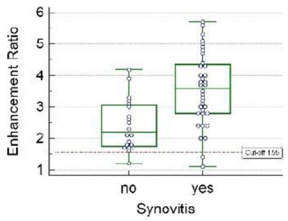

Superior joint compartment and inferior joint compartment to longus capitis muscle enhancement ratios in 28 temporomandibular joints

Conclusion:
Joint-to-muscle ER are clearly dependent on 1) the signal profile of the MR coil with muscles located further away from the coil providing higher ER, 2) the time of image acquisition after contrast-injection with later obtained images providing higher ER, and 3) where the joint signal intensity is measured. As these factors need to be accounted for, the described normal and pathologic ranges of joint to longus capitis muscle ER cannot be generalised for every MR-system and imaging protocol.

Clinical applications of navigational software in the Interventional Radiology suite at a Pediatric Institution

S. Shellikeri[1], A. Srinivasan[1], R. Setser[2], S. Vatsky[1], G. Krishnamurthy[1], M.S. Keller[1], A.M. Cahill[1]; [1]Philadelphia/US, [2]Cleveland/US

Objective:

Integration of 3D C-arm CT images with navigational software provides real-time fluoroscopic guidance during percutaneous interventions in the Interventional Radiology (IR) suite. A trajectory, drawn from skin entry point to the target lesion on the 3D C-arm CT data, is overlaid on intraprocedural fluoroscopy for real-time needle guidance. This study describes our experience with *syngo* iGuide (Siemens) needle guidance software in a range of clinical applications in the pediatric IR suite, including technical success, radiation dose and procedure time.

Materials:

In this IRB approved study, all percutaneous interventions performed in the IR suite using *syngo* iGuide over a 3-year period were included. Cases were classified by procedure type; for each type, mean effective radiation dose (mSv) was estimated using PCXMC program (v2.0.1.3, STUK) and procedure times were evaluated.

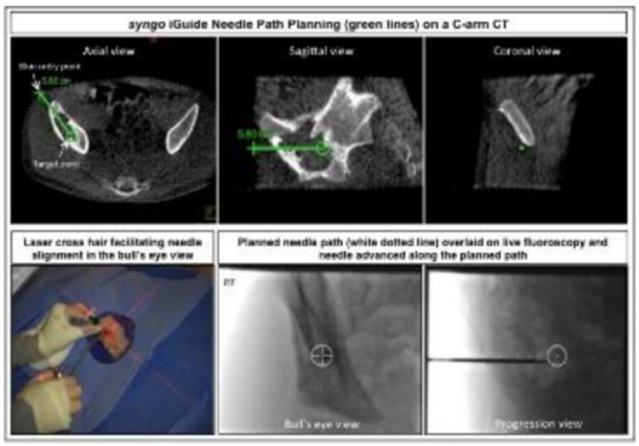

Figure 1. Needle path planning on a C-arm CT

Results:

Forty-five patients (25 male, 20 female; mean age: 11±6 years) underwent iGuide-assisted interventions including: bone biopsies - 35/45 (22 pelvic, 7 lumbar, and 6 lower extremity), intra-articular steroid injections - 5/45 (4 sacroiliac, and 1 temporomandibular joint), lumbar punctures - 2/45, percutaneous catheter placements - 2/45 (cecostomy, and chest tube placement) and bone biopsy with radiofrequency (RF) ablation - 1/45. iGuide was used in particular for the cecostomy procedure due to high sub-hepatic cecal pole position, and in the chest tube procedure due to the presence of loculated pneumothoraces.

All procedures were technically successful. The diagnostic bone biopsy rate was 97.7%. The mean estimated dose and procedure times for each procedure type are listed in Table 1.

Table 1: Mean estimated dose and procedure time by procedure type

Procedure type	N	Age (years)	Mean Effective Radiation Dose (mSv)	Procedure time (min)
Bone biopsy	35	11.5±6.2	4.1±5.8	91±84
Intra-articular Steroid Injection	5	12.2±6.2	0.7±0.9	52±25
Lumbar puncture	2	12.2±5.2	1.2±0.6	81±3
Cecostomy tube placement	1	9.0	1.8	90
Chest tube placement	1	1.5	0.5	25
Bone biopsy with RF ablation	1	12.3	1.9	101

Table 1: Mean estimated dose and procedure time by procedure type

Conclusion:

In our experience, *syngo* iGuide is a promising and feasible technique that provides high technical success and good diagnostic accuracy in various clinical applications in the IR suite.

Spinal Ultrasound a primary screening tool in suspected abnormalities of Neonatal Spine

A.S. Karnik, A. Karnik; Mumbai/IN

Objective:

Sonography of neonatal spine (SUS) is a simple, non–invasive, quick, relatively inexpensive method to evaluate lumbar spine anomalies in infants less than 4 months of age. Unossified posterior neural arches allow beam penetration to obtain high-resolution images of the intra-spinal contents. SUS is carried out at the bedside, does not utilize radiation & requires no sedation. Linear array transducers with extended field-of-view permit diagnostic sensitivity equal to MRI. Factors affecting MRI resolution like patient movement, pulsation & vascular flow do not affect SUS.

Materials:

We use SUS as first-line screening test in neonates with lumbosacral cutaneous stigmata & spinal dysraphism (SD) associated syndromes. SUS was also routinely done in all cases with DDH and talipes Equino varus deformities. SUS helps identify & characterize spinal abnormalities & guide timing of further imaging & intervention

Posterior sagittal & coronal scans are obtained in a prone position. A hypoechoic tubular structure with an echogenic central canal, the cord is positioned half-way between the anterior and posterior walls of spinal canal. The cord tapers to the conus medullaris, which continues as an echogenic cord-like filum terminale. Normal filum is 2 mm thick & surrounded by echogenic nerve roots. On Real-time imaging oscillation of cauda equina nerve roots & movement of the cord are seen on flexion extension of the spine.

Results:

SUS was able to rule out spinal abnormality in neonates with lumbosacral cutaneous stigmata where further imaging was not required. SUS helped to accurately identify those neonates with significant abnormality which needed further evaluation with MRI . In most patients SUS findings coorelated well with MRI findings.Several cases of skin-covered SD were identified & their US features are discussed. Tethered cord , Diastomatomyelia , meningocele, myelomeningocele , myelomeningocele, Spinal lipomas both intradural, extradural, & Caudal Regression Syndrome are well seen on SUS

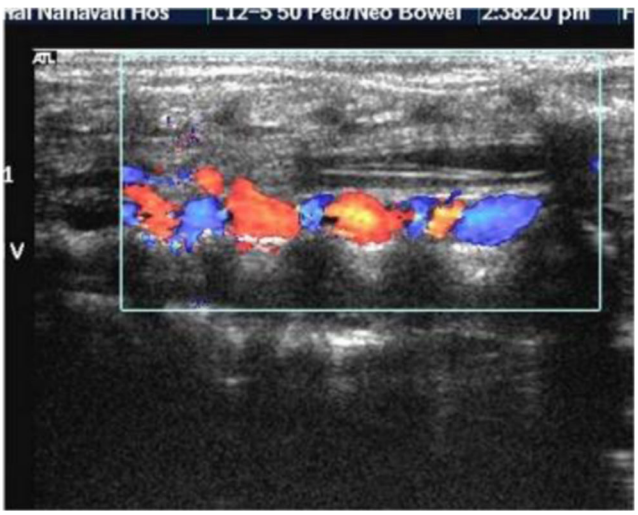

Vascular malformation

Lipomeningcoele

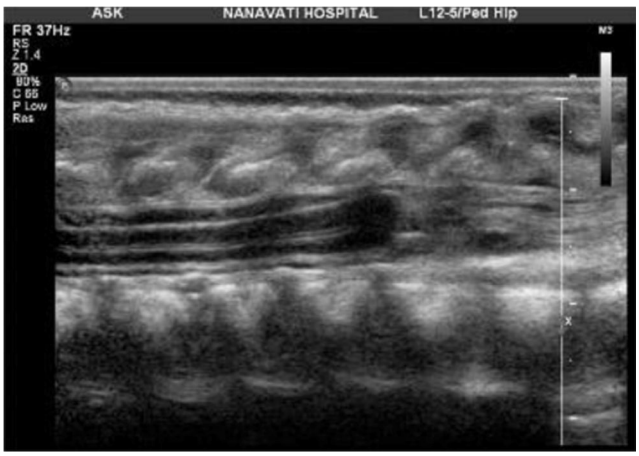

Caudal regression

Conclusion:
SUS is a simple readily available, non–invasive, quick, relatively inexpensive method to evaluate lumbar spine anomalies in upto 4 months of age. SUS should be the primary screening tool in suspected abnormalities of neonatal spine in neonates with lumbosacral cutaneous stigmata & spinal dysraphism (SD) associated syndromes saving MRI for those cases with equivocal or positive findings

FRIDAY, JUNE 02, 2017

SESSION: SCIENTIFIC SESSION: CARDIAC AND THORACIC

Diagnostic Utility of MRI of Thorax in Pulmonary Tuberculosis
K.S. Sodhi, A. Saxena, N. Khandelwal, M. Sharma, J. Mathew, M. Singh; Chandigarh/IN

Objective:
To evaluate the diagnostic utility of MRI of thorax in detection of various thoracic abnormalities in children with clinically suspected and complicated pulmonary tuberculosis (TB).

Materials:
This was a prospective study approved by the institutional ethics committee. Thirty five children (age range of 5 to 15 years) with clinically suspected and complicated pulmonary TB were enrolled in the study. Lung MRI and CT scan was performed in all the patients. The sensitivity, specificity, positive predictive value (PPV), and negative predictive value (NPV) of lung MRI in detection of radiological findings that were considered highly suggestive or diagnostic for TB, were calculated, with CT as the standard of reference.

Results:
Lung MRI performed equivalent to CT in detection of pleural effusion, mediastinal/hilar lymphadenopathy and lung cavitation with sensitivity and specificity of 100%. Agreement between CT and MRI in detection of each finding was almost perfect (k: 0.8-1).

Conclusion:
Lung MRI was found to be comparable to CT scan for detecting various radiological abnormalities which were highly suggestive for tuberculosis. Being a radiation free imaging modality, it has the potential, particularly in children, to replace chest radiographs and CT scan in the coming years.

Cardiac MRI: Differences of myocardial strain assessed by feature tracking between pectus excavatum patients and healthy volunteers
A. Lollert[1], G. Staatz[1], T. Emrich[1], S. Turial[2], C. Düber[1], K.-F. Kreitner[1]; [1]Mainz/DE, [2]Wiesbaden/DE

Objective:
To evaluate differences of myocardial strain assessed by feature tracking using SSFP cardiac MRI sequences between pectus excavatum (PE) patients and healthy volunteers.

Materials:
In this prospective study, cardiac MRI was performed in 10 PE patients (with a pathologic Haller-Index above 3.25) and 10 healthy volunteers (5 males and females, respectively; age range 13-30 years) including short- and long-axis cine-SSFP sequences on a 3T scanner. Post-examination analysis included standard cardiac volumetry with measurements of the biventricular ejection fractions (EF). Additionally, manual biventricular contouring by an experienced radiologist, and subsequent automated strain assessment using dedicated software (Circle cvi^{42}®) was performed. Longitudinal, radial, and circumferential peak systolic strain and strain rates were analyzed for both ventricles.

Results:
Left-ventricular EF was normal in all patients. Five PE patients had a normal right-ventricular EF, in 5 PE patients RVEF was slightly impaired (40-44%), all healthy volunteers had a normal RVEF. Compared with healthy volunteers, PE patients showed a significantly higher apical left-ventricular strain (radial: 53±16.8 vs. 26±8%, P<0.001; circumferential: -23.7±4.8 vs. -15.3±3%, P=0.001) and strain rate (radial: 3.76±1.05 vs 1.71±0.33s^{-1}, P<0.001; circumferential: -1.92±0.51 vs. -1.08±0.48s^{-1}, P=0.002). Mid right-ventricular strain (radial: 14.4±6.5 vs. 8.2±2.6%, P=0.019; circumferential: -9.7±3.3 vs. -6.4±1.5%, P=0.019) and strain rate (radial: 1.07±0.45 vs. 0.63±0.24s^{-1}, P=0.015; circumferential: -0.79±0.27 vs. -0.5 ±0.14s^{-1}, P=0.011), as well as apical right-ventricular strain (radial: 25.6±8.6 vs. 16.5±8.6%, P=0.009; circumferential: -15.9±3.8 vs. -11.1±4%, P=0.019) and circumferential strain rate (-1±0.26 vs. -0.72±0.24s^{-1}, P=0.029) were also significantly higher in PE patients than in healthy volunteers. Left- and especially right-ventricular radial and circumferential strain and strain rate increased from the bases to apices in PE patients. Longitudinal strain and strain rate did not differ significantly between PE patients and healthy volunteers.

Conclusion:
Myocardial strain assessed by cardiac MRI differs significantly between PE patients and healthy volunteers. As the chest wall deformity usually leads to a compression of the basal parts of the ventricles, higher values of myocardial strain in the mid and apical ventricles in PE patients might indicate a compensation mechanism to enhance especially right ventricular output against sternal compression.

Pectus excavatum in children - variations of Haller index and single-slice CT technique

R. Jokić, J. Lovrenski, M. Pajić, I. Varga, J. Antić, M. Đermanov; Novi Sad/RS

Objective:

To determine the normal range of the Haller index (HI) value, and its dependence on the age, sex, and respiratory phase. Evaluate the possibility of reduction of the effective dose (ED) of ionizing radiation using a single-slice CT scan technique.

Materials:

The retrospective-prospective study included 165 patients (av. 12y, SD 5y). It consisted of 3 parts. The prospective study included evaluation of CT scans performed by single-slice technique in 30 patients with pectus excavatum both in inspiratory and expiratory phase, without topogram. HI was measured in each patient in both respiratory phases. In retrospective study, 100 CT scans of the chest in children without pectus excavatum were analyzed to determine normal range of HI values depending on the age (0-5y, 5-10y, 10-15y, 15-18y) and gender. The retrospective study also included the analysis of another 30 CT scans in patients who were operated or diagnosed with pectus excavatum. In the latter group of patients the average value of ED of ionizing radiation was calculated, and the values were compared with the average ED obtained using low-dose CT examinations applied in the new protocol (single-slice technique).

Results:

The normal value of HI was 2.23±0.32. A significant positive correlation between age and value of HI was found. Older patients had higher HI (0-5y: 2.01±0.29, 15-18y: 2.35±0.33). Results of Mann-Whitney test did not demonstrate any difference between gender in the observed group, however girls had generally higher HI in all age groups. In the group of patients who were operated/diagnosed with pectus excavatum, HI was 3.34±0.88. The average value of HI in inspirium in children with diagnosed deformity was 2.69±0.76, while in expirium it was 3.49±1.19. Only 3/32 (9%) patients had HI value over 3.25 (a boundary value for surgical treatment) during inspirium, while 13/32 (41%) patients had it in expirium, which showed statistically significant difference (p=0.012). Single-slice CT technique during the inspiratory and expiratory phase showed average ED of 0.02mSv, which is an equivalent of 1 chest X-ray. It reduced ED more than 20 times in comparison with low-dose whole chest CT.

Conclusion:

The value of Haller index increases with the age and in expiratory phase. We propose the single-slice CT technique without topogram in expiratory phase, as a sufficient and reliable technique in evaluation of Haller index and preoperative preparation.

Aortic tortuosity: A new finding in patients with Mucopolysaccharidosis type IVa (MPS IVa)

Y. Tanyildizi, S. Gökce, J. Hennermann, M.A. Brockmann; Mainz/DE

Objective:

MPS IVa is a lysosomal storage disorder caused by a deficiency of N-acetylgalactosamine-sulfatase. Main symptom is a systemic skeletal dysplasia. Affection of the vascular system has not been described yet. Our goal is the analysis of the vascular system in patients with MPS IVa, based on the example of the aorta.

Materials:

In a retrospective study, 32 patients with MPS IVa were included. The aorta in its course from 4th thoracic vertebrae to 10th was analyzed on the basis of 49 craniospinal MR and 4 CT examinations. To describe the course of the aorta, the area around the vertebral body was devided into 5 equal parts (Fig.1). High buckled arteries in relation to the length of the affected aortal part were indicated as aortal kinking, and a moderate twist in relation to the length of the affected aortal part as aortal tortuosity.

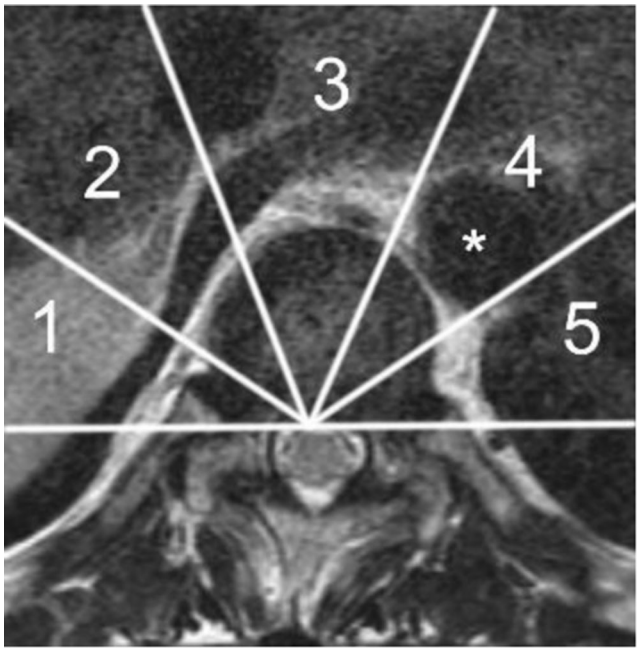

axial segments

Results:

Twelve of 32 patients had an aortal kinking, 10 of 32 patients an aortal tortuosity, 4 of these had moderate and 3 strongly tortuous aortae. Seven patients had a normal aortal course, 4 couldn't be analyzed. One patient revealed both, aortal kinking and tortuosity.

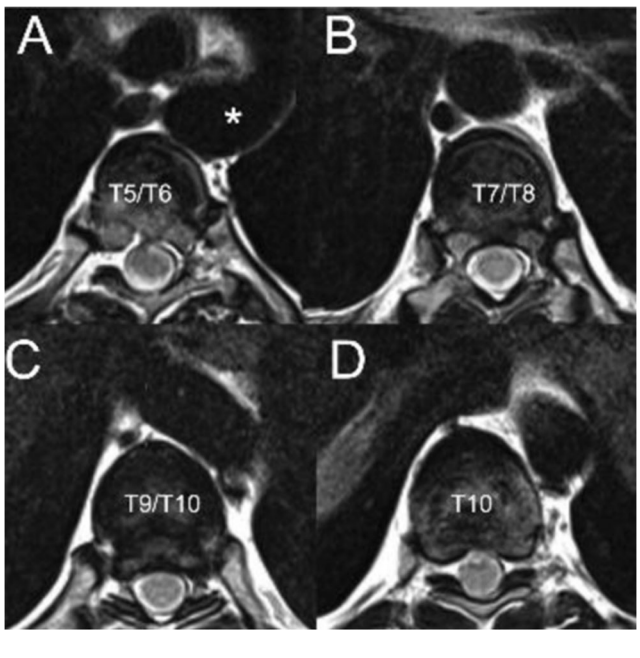

axial view of the aortal course

Conclusion:

This study reveals the occurrence of aortic tortuosity in patients with MPS IVa. We suggest that this complication could be due to glycosaminoglycane deposition in the aortic intima, which may be

associated with an increased vulnerability of the vascular wall. We conclude that the examination of the vascular system should be included in regular follow-up protocols.

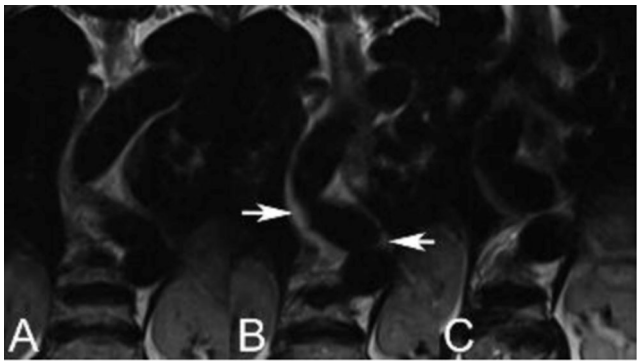

cornar view of the kinking aorta

Lung ultrasound in the diagnosis and follow-up of pneumonia in children - is it really as reliable as chest X-ray?

S. Balj-Barbir, J. Lovrenski, S. Petrović; Novi Sad/RS

Objective:

To investigate the role of lung ultrasound (LUS) both in the diagnosis and follow-up of pneumonia in children.

Materials:

A prospective study was carried out in the regional children's hospital, and included 130 children (av. 2.9y, SD 2.93y) with clinically suspected pneumonia, in whom initial LUS and subsequent chest X-ray (CXR) were performed within 24h. The final diagnosis of pneumonia at discharge was used as a reference test to determine the reliability of LUS, CXR, clinical and laboratory findings in the diagnosis of pneumonia. Children with pneumonia formed a study group, while the control group consisted of children without diagnosed pneumonia. LUS finding of subpleural lung consolidation was considered a diagnostic sign for pneumonia. The children with LUS signs of pneumonia were followed-up until complete resolution of the LUS findings. There were from one to five follow-up LUS examinations performed.

Results:

A final diagnosis of pneumonia was confirmed in 105/130 (80.8%) patients, and 77/105 (73.33%) were hospitalized (av. 10.84, SD 6.19 hospital days). In diagnosis of pneumonia LUS, CXR, auscultation, elevated CRP, and tachypnea showed sensitivity of 94.3%, 93.3%, 79%, 80% and 32.38%, and specificity of 100%, 92%, 56%, 48% and 100% respectively. LUS detected lung consolidations in 99 of 105 children with final diagnosis of pneumonia, and in 84/99 patients LUS showed air-bronchogram (Figures 1, 2). LUS was superior to CXR in the detection of lung consolidations smaller than 15mm. Interstitial lung changes were detected by LUS in 50/105 (47.62%) patients, and by CXR in 21/105 (20%). LUS and CXR detected pleural effusion in 24/105 (22.86%) and 14/105 (13.33%) patients respectively. McNemar's test showed no statistically significant difference, and Cohen's kappa coefficient showed almost perfect agreement (0.864) between US diagnosis of pneumonia and final diagnosis of pneumonia. During the follow-ups, moderate to substantial agreement between LUS and clinical evaluation of the course of the disease was obtained (k=0.406-0.621). In children with complete clinical and incomplete US regression of pneumonia, consolidations of less than 15mm were the most prevalent finding. The average time period until complete resolution of the LUS findings was 16.3±10.24 days. Children with US detected pulmonary consolidations larger than 50mm were statistically significantly longer hospitalized than others.

Fig. 1. Extensive right-sided lung consolidation with branching air-bronchogram and fluid-bronchogram (arrow) representing pneumonia visualized by trans-thoracic lung ultrasound (left image), and confirmed by chest X-ray (right image).

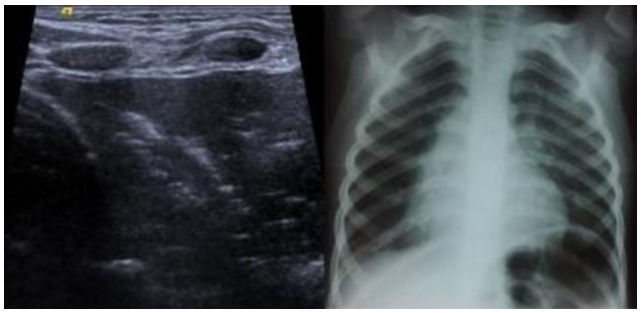

Fig. 2. Paracardiac right-sided pneumonic lung consolidation with moderate air-bronchogram showed by lung ultrasound (left image), confirmed later by chest X-ray (right image).

Conclusion:

Lung ultrasound in the diagnosis of pneumonia in children is just as reliable as radiography, and should be included in the standard diagnostic protocol.

Role of chest radiography in screening of childhood TB contacts in the UK – A migrant context

K.S. Minhas, S. Andronikou, J. Bernatoniene, D. Grier, A. Sarra, M. Roderick; Bristol/UK

Objective:

The latest UK NICE guidelines for childhood TB contact screening require that a chest X-ray (CXR) be requested only when Mantoux or IGRA testing is positive or if there is a documented reason e.g. clinical concern. NICE clarifies the role of CXR in determining treatment choice. We aimed to review CXR referral and treatment in the current climate of European migrant screening.

Materials:

Retrospective review of 148 paediatric referrals to the Infectious Diseases clinic for TB contact screening of whom 125 had CXRs, from October 2009 to August 2015 and correlation with the medical notes. A panel of 3 paediatric radiologists independently interpreted radiographs in the clinical context of TB contact screening and a majority decision was reached.

Results:

Of 148 patients referred to the Infectious Diseases Unit, 125 underwent CXR in addition to a Mantoux and IGRA test. Of those 125 CXR's, 20 were reported as having features of pulmonary TB but only 16/20 (80%) were treated as active TB. Eighteen of the 105 (17%) CXR's which were reported as having no features of pulmonary TB, were treated as active TB. Of those 18, only 6/18 (33.3%) had a clearly documented reason. Review of the 125 radiographs (mean age 14 years) by the panel of radiologists noted that all were of readable quality, 20 radiographs were in keeping with a diagnosis of TB, 6 were inconclusive and 99 were normal. The diagnosis of TB was based on lymphadenopathy in 19 and

milliary nodules in 1. Parenchymal abnormality was seen in 8 patients [one was the milliary] and effusion was seen in 3. This correlated well with the initial radiology reports of duty radiologists.
Of the 125 who underwent CXR, referral information was available in 120.109 (90.8%) of these had been appropriately referred because of a +ve Mantoux/IGRA. Only 8 out of 11 (72.7%) of those who had CXR despite a -ve Mantoux or IGRA, had a documented reason.

Conclusion:
According to NICE guidelines, 20% of CXR reported positive for TB were not treated for active TB. This may represent a lack of clarity regarding the definition of 'latent TB'. Furthermore, only a third of the 17% of patients who received treatment despite negative radiographs had a documented reason. The current migrant crisis requires clarity of X-ray definitions of latent TB to avoid the 20% under-treatment and 17% over-treatment identified in our population.

Is there really no cardiac problem for performing sports
Ö.İ. Koska, P. Bayindir, H. Alper; Izmir/TR

Objective:
Sudden death in young is a rare condition excluding known anomalies and sudden infant death sydrome; but its consequences are devastating because they are so unexpected. %25 of them occur in a context of sports event.
Everyday parents of millions of children admit hospitals in order to get permission for participating in sports events. And after physical examination and ECG, physicians are expected to decide such an important issue. However there are a number of silent reasons that may lead to child to sudden death. Altough we don't perform CT scans for such indications, we have encountered several cases with abnormalities that can lead to sudden child death and while reporting an examination, awareness of these devastating conditions may be usefull.

Materials:
We searched our database from 01.01.2016 to 01.01.2017 in order to see how often we diagnosed such a silent reason from the CT images that are performed for some reasons. As our center is a tertiary center we have performed 452 cardiac CT examinations in that period that are mainly for excluding or defining complex cardiac anomalies. In order to prepare a pictorial review of unexpected but CT detectable sudden cardiac death reasons, we excluded congenital heart diseases (namely obstructive, shunting or complex anomalies) and ECG detectable arrhytmic diseases.

Results:
The non arrhytmic, non traumatic reasons for sudden cardiac death excluding congenital heart diseases in the papers are: Hypertrophic cardiomyopathy (CMP) (%36), some coronary artery path and origin anomalies (mainly abnormal left coronary artery from pulmonary artery (ALCAPA), and interarterial path)(%24), increased cardiac mass (%10), dilated CMP (%9), Marfan disease (%6), myocarditis (%3), ischemic heart disease (%2).
We detected 18 examinations according to our inclusion criteria and selected one cases of each; RCA path anomaly, ALCAPA, dilated CMP, hypertrophic CMP, subaortic discrete membrane and increased cardiac mass for presentation

Conclusion:
Although sudden cardiac death is rare in young children it is a so devastating condition that it must be taken into account for every situation. Awareness of silent conditions and active search of them may protect professionals from medicolegal issues and unpleasent results.

Pulmonary Langerhans Cell Histiocytosis In Children: Chest CT imaging features and proposal of a scoring system
V. della Valle, C. Sileo, M. Lenoir, J. Donadieu, H. Ducou Le Pointe; Paris/FR

Objective:
To describe the spectrum of chest CT scan findings of pulmonary involvement in childhood Langerhans cell histiocytosis (LCH) and propose a simple scoring system to evaluate the profusion and distribution of the main lung lesions.

Materials:
One hundred forty-six chest CT scans of the 48 pediatric patients with Pulmonary LCH enrolled in the French National database for LCH until April 2016, could be retrospectively and independently reviewed by 3 pediatric radiologists. For each CT scan a semi-quantitative analysis was performed for nodular opacities and cystic abnormalities. The chest was divided in 6 fields (upper, medium and lower field of the left and the right lung) and for each field, both for the nodules and the cysts the score was 0=no lesion, 1= lesions involving up to 25% of the parenchyma, 2=25-50%, 3= 50-75% and 4=more than 75%.

Results:
Of 29 patients evaluated at diagnosis, 18 patients (62%) presented with nodules, 13 patients (45%) presented with cysts and 6 patients (21%) presented a combination of both nodular and cystic lesions. On the initial CT scan, median nodules total score was 1 and median cysts total score was 0. During subsequent CT scans almost the same percentage of patients with nodules (30 patients, 62 %) was found but we observed an increase number of patients with cysts (30 patients, 62 %), median nodules total score was 1 and median cysts total score was 2. The distribution of nodules and cysts was symmetric in the upper, medium and lower fields with an involvement of costo-phrenic angles in 68% of the cases.
Patients with pneumothorax (13 patients, 27%) had a higher cysts median score (10) than patients without pneumothorax (1).
We found alveolar condensation in 12 patients (25%). None of them showed signs of infection at BAL examination or any improvement after a treatment with a standard antibiotic therapy while they did show regression under the LCH standard regimen of chemotherapy.

Conclusion:
We proposed a score for semiquantitative analysis of distribution and profusion of nodular and cystic lesions on chest CT scans that can be a useful tool in pediatric population to monitor lung involvement. We found a significant correlation between pneumothorax and a high cysts median score. Alveolar condensation could be considered as a possible manifestation of PLCH in children. Lung bases involvement was found in 68% of the cases, representing an important different imaging feature from adult PLCH.

High Resolution computed tomography for chronic small airway disease in HIV infected adolescents
A.-M. Du Plessis[1], S. Andronikou[2], H. Zar[1]; [1]Cape Town/ZA, [2]Bristol/UK

Objective:
Early treatment with antiretroviral therapy (ART) and decline in infected infants due to prevention of mother-to-child transmission has resulted in an increase in the population of HIV-infected adolescents. Pulmonary disease is common among them. CXR is considered insensitive and terminology inconsistent. Therefore, despite concerns related to radiation dose in paediatric patients, high resolution computed tomography (HRCT) is the modality of choice for the evaluation of small and large airway pathology, prominent in chronic pulmonary disease. HRCT findings are used for prognosis, treatment decisions and defining anatomic extent of bronchiectasis for surgical intervention. The aim of this paper is to demonstrate the spectrum, frequency and extent of airway pathology in HIV-infected adolescents using HRCT.

Materials:
A nested sub study was undertaken within the Cape Town Adolescent Antiretroviral Cohort (CTAAC); a prospective, descriptive cohort study of 520 HIV-infected adolescents on ART and 120 age matched HIV-

negative controls. HRCT was performed on 100 patients who demonstrated abnormal lung function (defined by forced expiratory volume in 1 second (FEV1) of <85% and/or low lung diffusion capacity (DLCO)). Single phase, contrasted multi-detector volume acquisitions were performed from the thoracic inlet to the diaphragms at full inspiration and image data post-processed to yield thin (0,6mm) and thicker slice images (5mm). Three 1mm slices at 3 cm intervals were performed in full expiration. Three radiologists interpreted the C T scans independently, with strict imaging definitions, and a majority decision was generated for each finding.

Results:
Ages of patients ranged from between 10 to 17 years with a mean of 14,2. There were 53 females and 47 males with a ratio of 1:0,8. Bronchiolitis Obliterans was seen in 70% of patients and bronchiectasis was demonstrated in 39%, 12% of which was classified as severe (involving either an entire lobe or more than 50% of at least 2 lobes). There was an absence of lymphadenopathy (a sign of primary tuberculosis (TB)), lymphocytic interstitial pneumonitis (LIP) and post tuberculous apical architechtural distortion. Miliary TB was identified in a single patient. Ground glass was seen in 10% and consolidation in 13%.

Conclusion:
The majority of HIV infected adolescents with poor lung function demonstrated bronchiolitis obliterans strongly emphasizing the use of HRCT for confirming small airways disease. HRCT was also useful for demonstrating extent of associated bronchiectasis in 39%. HRCT allows classification of patients into those with diffuse small airways disease requiring medical management and those with local disease requiring surgery.

SESSION: OUTREACH IN PEDIATRIC RADIOLOGY

'Spotting the difference'. Distribution and extent of CRMO lesions in children on baseline whole body MRI

T.O.B. Mendes Da Costa, A. Ramanan, M. Hussien, S. Andronikou; Bristol/UK

Objective:
Background: Chronic recurrent multifocal osteomyelitis (CRMO) is an autoinflammatory paediatric non-infectious bone disease. Presenting symptoms are non-specific, prolonging diagnosis, and leading to deformity, morbidity and unnecessary procedures. Imaging is critical to diagnosis, with whole-body MRI (WBMRI) commonly used in all stages of care. In our institution, a baseline whole-body coronal STIR sequence is routinely obtained.
Aim: To determine lesion distribution and extent on baseline WBMRI via retrospective panel review of all patients clinically diagnosed with CRMO, and to determine any patterns of involvement that could facilitate earlier radiological diagnosis.

Materials:
Method: All patients diagnosed with CRMO since December 2009 using published Bristol criteria were identified and baseline whole body MRIs reviewed. The reviewing radiologists were blinded to the original report and previous investigations. Each MRI was reviewed for focal lesions consistent with CRMO. The extent of metaphyseal and epiphyseal lesions was categorized into involvement of thirds of the width of the structure.

Results:
The WBMRI of forty children (28 girls, 12 boys), averaging 12 years (2-18) were reviewed by the panel using a majority decision rule. Three hundred three lesions were recorded, averaging 7.6 lesions (0-26). The tibia was most affected (83 lesions), most commonly the distal tibial metaphysis (25 lesions in 16 patients, 9 bilateral). Rib, metatarsals and distal femoral epiphyseals lesions were common. Humeral, hand and skull lesions were few. Complete metaphyseal involvement, the 'smouldering physis', was most prevalent within the proximal and distal tibial metaphyses.

Although ranked seventh, the reportedly more common clavicular lesions were the site of the most florid lesions, demonstrating bone expansion and periosteal reactions. Two clear patterns of involvement emerged. In patients with clavicular lesions, fewer overall lesions were observed (average 6.4), mainly affecting the axial skeleton and feet. Patients with tibial involvement had a higher number of overall lesions (average 9.3), but few lesions outside the lower limbs. Only four patients had a both clavicular and tibial lesions. Twelve vertebral lesions and four cases of spodylo-discitis were identified; two at T5/6 level, one at T6/7 level, and one involving both T5/6 and T6/7.

Conclusion:
Our series of 40 cases of CRMO with baseline WBMRI, one of the largest in the published literature, identifies the common sites that should be interrogated for involvement. This study also demonstrates potential as-yet undescribed patterns of skeletal involvement that can be used to aid radiological diagnosis and highlights a non-infective cause for spondylo-discitis.

Hepatic Hemangiomas – Focal and Multifocal Diagnosis Predictor?

J. Brisson, F. Rypens, S. Waelti, M. David, J. Powell, C. Lapierre, J. Dubois; Montreal/CA

Objective:
Hepatic hemangiomas (HH) are the most common benign vascular tumors encountered in the pediatric population. Two main types have been described – congenital and infantile, which both display distinct clinical courses and biological features. Hemangioendothelioma in differential diagnosis of HH is controversy. Recent literature suggests that congenital hepatic hemangiomas present in a focal form, whereas infantile hepatic hemangiomas present in either a multifocal or diffuse form. The goal of this study is to evaluate the features associated with focal and multifocal HH.

Materials:
The records of 45 patients diagnosed with a hepatic hemangioma at a tertiary pediatric hospital from 1994 to 2015 were reviewed. We divided our series into 2 groups: focal or multifocal including diffuse form. Clinical endpoints are: age of diagnosis, presence of cutaneous hemangioma, alpha-fetoprotein, thrombocytopenia, cardiac insufficiency. Imaging endpoints were echogenicity on US (hypoechoic, hyperechoic or mixed), vessels density on color Doppler (<2; 2-5, >5 cm^2). Presence of calcifications, venous lakes, visible vessels and aortic tapering were assessed on US, CT-scan, MR and angio. Treatment and outcome were analyzed. Univariate and bivariate analysis were done.

Results:
This study included 24 focal (9M, 15F) and 21 multifocal (17M, 28F) HH. Antenatal diagnosis was done in 6 focal and 1 multifocal HH. Focal lesions were associated with the presence of cutaneous hemangiomas ($p<0.001$) and calcifications ($p<0.05$). No other variable was significant. Conservative management was decided in 12 focal and 11 multifocal HH. Steroids (focal: 6, multifocal: 3), steroid-interferon (focal: 1, multifocal: 3), propranolol-steroid (focal:4, multifocal: 4) and surgery in one focal form. Complete regression was observed in most lesions (focal: n=19, multifocal n=20), whereas incomplete regression <50% was observed in 4 patients (focal: n=3, multifocal: n=1) and 3 patients in the focal group with the pathology diagnosis of hemangioendothelioma.

Conclusion:
Hepatic hemangiomas demonstrate a wide range of radiological features, with important overlaps in focal, multifocal or diffuse forms. Focal and multifocal HH can be seen in congenital hemangioma, infantile hemangioma or hemangioendothelioma. The association of cutaneous infantile hemangioma in the focal group confirmed that the focal lesion can be seen in infantile hemangioma. However, calcifications are more frequent in focal HH which is described in congenital hemangioma or hemangioendothelioma.

Symptomatic and asymptomatic meckel's diverticulum in the pediatric population - A retrospective analysis of imaging findings with histopathologic correlation

N. Abu Ata, R. Cytter-Kuint, J. Bar-Ziv, I. Hadas-Halpern; Jerusalem/IL

Objective:

Though Meckel's Diverticulum (MD) is a relatively common gastrointestinal anomaly, many of the symptomatic and most of the asymptomatic MD's are often missed on abdominal imaging. Our purpose is to describe the radiologic appearance of symptomatic and asymptomatic MD in the pediatric population and to correlate the radiologic findings with histopathology.

Materials:

A retrospective analysis of all children diagnosed with MD between 1/2004-10/2016 and had relevant imaging (n=38) was done. Imaging studies- ultrasound (US), computed tomography (CT) and magnetic resonance imaging (MRI) were retrospectively reviewed and evaluated for visualization of MD in symptomatic and asymptomatic patients. Findings were compared with the preoperative radiology report and the pathology specimen.

Results:

Symptomatic group (n=24): mean age 8.6±6 years, nineteen males. MD presented with abdominal pain in 9 patients, small bowel obstruction (SBO) in 6 patients, gastrointestinal bleeding or anemia in 5 patients and intussusception in 2 cases. MD was identified in 13 preoperative reports (54.16%) and retrospectively identified in 4 more cases (overall 17 patients, 70.1%). In 7 cases, an inflamed or perforated MD were found. In 4 cases, mucosal lining resembling gastric folds was seen. Inverted Meckel and prominent tissue surrounding the diverticula were seen in 2 patients. In a single case MD was misdiagnosed as a duplication cyst. Asymptomatic group (n=14): mean age 10.9±6, eight males. MD was not mentioned in any of the original reports and only 3 MD's were identified retrospectively (21.4%). No mucosal abnormality or irregularity were noted.

Histopathology: ectopic gastric mucosa was found in 16/24 (66.67%) of the symptomatic patients vs. 2/14 (14.29%) in the asymptomatic group. All 4 patients with sonographic appearance of gastric mucosa had gastric mucosa in pathology (specificity- 100%, positive predictive value- 100%).

Conclusion:

MD has a variety of radiologic appearances. It can be detected in most of the symptomatic patients but is almost undetectable in asymptomatic patients. Heterotopic gastric mucosa is more common in the symptomatic group. Inflamed gastric mucosa may have a typical appearance resembling a small stomach, a sign that was not described before and has both high specificity and high positive predictive value for gastric mucosa within a Meckel diverticulum.

Preliminary results on DNA damage from CT irradiation in pediatric patients

I. Dilevska, E. Nagy, W. Schwinger, E. Sorantin; Graz/AT

Objective:

The increased radiation sensitivity in children, compared to adults, is a well-recognised fact in the pediatric radiology community. The high-dose irradiation induced DNA damage has been well established, however the dosages that are clinically used in everyday CT procedures are so low, that it remains unclear how this severely affects the DNA and can induce cancer in the long run. The aim of this study is to assess the effects of low-dose ionizing radiation from CT in children by establishing a standardization curve ranging from the high to the low, medically significant CTDI values. This is done by measuring the phosphorylation of the H2AX histone (γH2AX), which is considered a biomarker for quantification of radiation induced DNA Double-Strand Breaks (DDSBs).

Materials:

The detection of the γH2AX histone was done by two methods: Immunofluorescence Microscopy (IM), which is an established method for detection and quantification of this histone and the new, promising Flow cytometry technique (FACS). For this study, 35 leucocyte samples ("buffy coats") were provided by the local transfusion department and these samples were irradiated with a clinical CT scanner (AqilionONE, TMSE) with values ranging from 2153,6 to 0,16 mGy CTDI. Afterwards the samples were processed with both methods. For the Immunofluorescence, two-step immunostaining was used with two different antibodies and the cell and foci counting were done on an OLYMPUS XC10 Microscope, while the FACS staining was done with a one-step antibody and the samples were measured on a Navios Flow cytometer (Beckman Coulter).

Results:

Comparable results were detected with both methods, with a good correlation between the FACS and IM, with a linear incline (R^2>0.95) in the high and in the low dosages from 0,16 to 5.0 mGy CTDI. However, in the samples irradiated with doses below 5.0 mGy CTDI, there seems to be less phosphorylated H2AX than in the native samples. Two possible explanations arise: a) low dose irradiation initiates repair that extends to DDSBs occurring naturally or b) low dose irradiation doesn´t cause phosphorylation of this histone, but affects other DNA damage and repair pathways.

Conclusion:

The preliminary findings show that the FACS analysis can be used as a valid replacement method for the labor-intensive IF method in the higher dosages. However more analysis should be done to establish its accuracy in the lower regions since underlying mechanisms are not clear yet.

Emergency Room Imaging Procedures in a Tertiary Pediatric Trauma Center

A. Turkaj[1], G. Cicero[2], E. Sorantin[1], R. Coroiu[3]; [1]Graz/AT, [2]Mesina/IT, [3]Cluj-Napoca/RO

Objective:

There is only little information available regarding imaging procedures in the trauma setting of pediatric patients. Such data can serve as a rational basis for running pediatric trauma units.

The purpose of the paper is to investigate the number, types and distribution of imaging procedures in a tertiary pediatric trauma center serving children of about 1.2 million inhabitants with approximately 225.000 children.

Materials:

All trauma-caused admission to the emergency room and their imaging procedures were analyzed retrospectively occurring within a period of 15 months. A cohort of 263 patients (m:f=1.9:1) were analyzed. Patients were grouped according to age into the following categories: n*eonates, infants, middle childhood, early adolescence, late adolescence*. *Imaging procedures were classified into plain films, US, CT and MRI.* Furthermore, the time of admission was noted and categorized in time slots 07:00-15:00, 15:00-20:00, 20:00-24:00 and 24:00-07:00. Referral cause was divided in d*omestic accidents, motor-scooter-bicycle accidents, car accidents, sport injuries, falls from height and others.*

Results:

The average age was 9.5 ± 5.4 years, aligned in the following age-groups neonates 13 (5%), infants 68 (26%), middle childhood 42 (16%), early adolescence 58 (22%), late adolescence 82 (31%).

A total of 364 imaging procedures were performed, of which 210 plain films (58%), US 81 (22%), CT 69 (19%) and MRI 4 (1%). There was a statistically significant difference of imaging procedures due to age in particular in US and CT.

Regarding the timeslots: 07:00-15:00 ;111 patients (42%), 15:00-20:00; 118 patients (45%), 20:00-00:00; 31 patients (12%), 00:00-07:00;3 patients (1%). Domestic accidents were the leading referral cause with 82 cases (31%) prevailed age groups were infants and middle childhoods corresponding for more than 75%. Motorscooter/bicycle accidents accounted for 51 cases (19%) of which most were early and late adolescence (more than 85%),

sport's accidents 38 (14.4%) equally shared among middle childhood, early and late adolescences. Car accidents 37 (14.0%) cases and Fall from height 22 (8,3%) did not show any prevalence according to the age groups.

Conclusion:
For the first time detailed data about imaging procedures at the emergency room for pediatric patients are now available. Over half of the admissions (55%) occur outside regular work hours thus representing a challenge for the staff in duty and this fact should be considered in working schedules. Due to strict interdisciplinary developed diagnostic pathways the number of CT examinations was reasonable low.

SESSION: SCIENTIFIC SESSION: NEURO

Head CT in a regional children's hospital without MRI - effective doses and justification of clinical indications
J. Lovrenski, N. Milenković; Novi Sad/RS

Objective:
To calculate effective doses (ED) for pediatric head computed tomography (CT), to determine the most common referral diagnoses, and the share of normal and pathological CT findings.

Materials:
A retrospective – prospective study comprised all the children with performed CT examination (16-slice scanner) within a one-year period. Pediatric CT protocols were used. The values of ED for head CTs were calculated based on the two different models (Shrimpton's and ICRP Publication 103). Average ED for different age groups was expressed as the number of chest X-rays (CXRs) (1CXR 0.02mSv). The most common non-traumatic referral diagnoses for head CTs were determined, as well as percentage and type of pathological CT findings. A share of pathological CT findings was also determined for trauma as a referral diagnosis.

Results:
Head CTs were represented with 649 (71%) in total number of 924 CT examinations within a one-year period. The different calculation models have shown the difference in ED values of up to 20.5%. EDs for head CTs were equivalent of 66 (15 years of age and older) to 140 (younger than 3 months of age) CXRs for one sequence of scanning. The most common non-traumatic referral diagnoses for head CTs were: loss of consciousness, epilepsy, headache, convulsions, and vertigo. In this group of 273 patients, 86% of completely normal CT findings were found. Pathological findings in this group consisted of the patients with the most common non-traumatic referral diagnoses were as follows: cortical atrophy (15 patients), arachnoid cyst (10), ischemia (6), porencephalic cyst (3), agenesis of the corpus callosum (1), Chiari malformation - type I (1), open-lip schizencephaly (1), and tumor of the posterior cranial fossa (1). Most common incidental, extracerebral pathology discovered included sinusitis and otomastoiditis. In patients with trauma as referral diagnosis, the share of pathological CT findings was 59.5%.

Conclusion:
It is necessary to get clinicians familiar with the extent of ionizing radiation that children are exposed to during the head CT examinations. A more careful selection of children for head CTs is necessary in an every-day clinical practice, especially for patients with non-traumatic referral diagnoses.

Diffuse and symmetric diffusion restriction involving the white matter of the brain in patients with neonatal seizures
J.-Y. Hwang[1], Y.J. Lee[2], Y.-W. Kim[2]; [1]Yangsan-si, Gyeongsangnam-do/KR, [2]Yangsan-si/KR

Objective:
This study aimed to evaluate magnetic resonance (MR) imaging findings in patients with neonatal seizures focused on the diffuse white matter lesions on diffusion weighted image (DWI) in addition to clinical manifestations.

Materials:
A total of 55 neonates aged less than 1-week old underwent brain MR imaging for evaluation of neonatal seizures between November 2008 and December 2016. Among them, 12 patients showed diffuse and symmetric pattern of high signal intensity on DWI. Clinical, laboratory, and MR images were analyzed retrospectively.

Results:
Nine patients were males and three patients were females. Patient age was 5.2 ± 0.8 days (range, 3-6 days). All the patients were born at full term. The most frequent month of the hospital visit was March (n=4) and January (n=3). Eight patients showed generalized clonic seizure and four patients showed partial clonic seizure. Stool viral test was performed in nine patients. Among them, five patients were positive for the rotavirus and one patient was positive for the astrovirus. Nine patients underwent cerebrospinal fluid analysis, however, all showed negative results.
MR imaging was performed at 2.2 ± 1.6 days after onset of seizures. Diffuse and symmetric diffusion restriction were distributed along the cerebral white matter tracts and both thalami (Fig 1) accompanied with high signal intensity on either T2-weighted images or on the fluid-attenuated inversion recovery (FLAIR) sequence. Multiple foci of high signal intensity on T1-weighted images at the centrum semiovale that was affected on DWI were also observed. Follow-up period was 11.3 ± 9.6 months (range, 1.8 – 30.9 months) and developmental delay was encountered in three patients. Six patients underwent follow-up MR imaging at the age of 8.4 ± 4.2 months (median, 8.5 months; range, 3.7–13 months). Five patients showed volume loss in cerebral white matter on both sides of the brain and four patients showed high signal intensity of the periventricular white matter on either T2-weighted images or FLAIR sequences (Fig 2). Myelination delay was not observed in follow-up MR images.

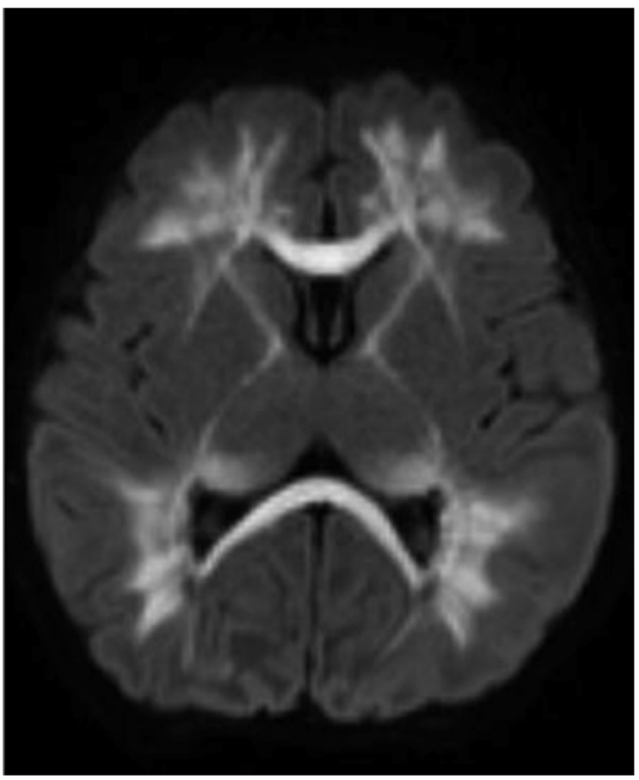

Fig 1a. Diffusion weighted image (b-value=1000) showing diffuse and symmetric diffusion restriction involving the white matter tracts and both thalami

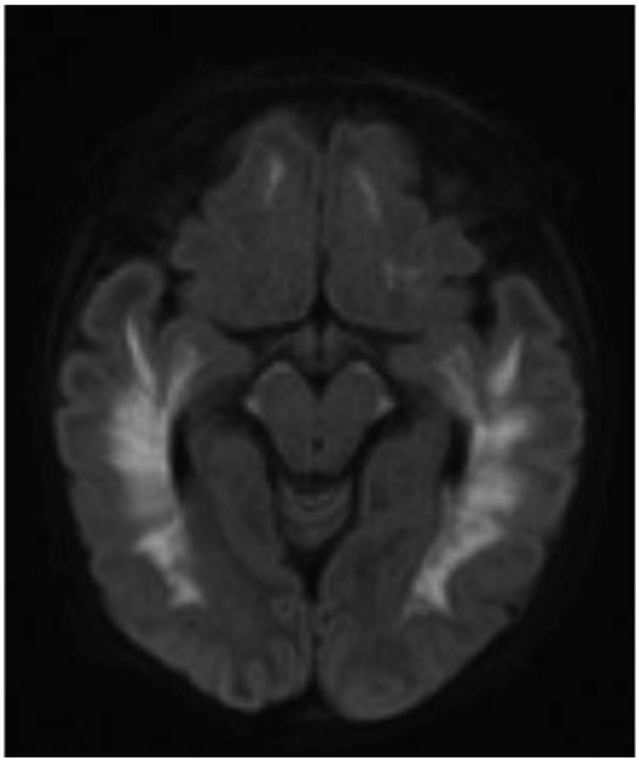

Fig 1a. Diffusion weighted image (b-value=1000) showing diffuse and symmetric diffusion restriction involving the white matter tracts and both thalami

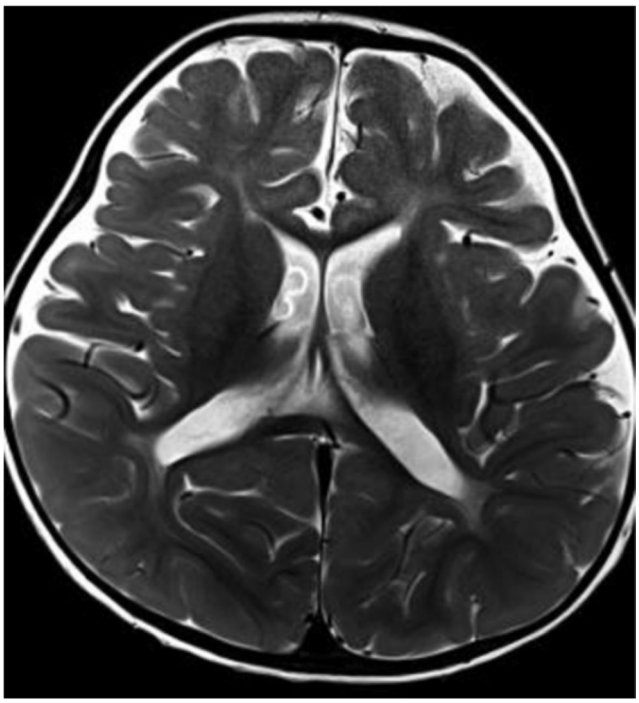

Fig 2. Follow-up MRI revealing volume loss in both cerebral white matters.

Conclusion:
Diffuse and symmetric diffusion restriction involving the cerebral white matters can be seen in patients with neonatal seizures on MR imaging. Our study shows that rotavirus is commonly encountered, but not exclusively detected in these patients. Nevertheless, viral infection-associated encephalopathy should be considered when a patient is presented with characteristic clinical and MR findings.

Whole Body MRI on diagnosis and follow-up of Neurofibromatosis type 1
D. Grassi, V. Tostes, E. Caran, H.M. Lederman; Sao Paulo/BR

Objective:
Demonstrate that whole body MRI is effective on showing neurofibromatosis type 1 involvement of different regions of the body not known by the clinicians.

Materials:
Review of 41 patients with Neurofibromatosis type 1 (NF1) who underwent whole body MRI throughout their follow-up with the majority of them had only brain and spine imaging studies.

Results:
It was possible to demonstrate that whole body MRI provides an overview of NF1 systemic manifestations and neurofibroma's extension beyond the clinic expectation. Despite being rare, sarcomatous degeneration was suspected when there was any difference on the characteristics of the neurofibromas.

Whole body overview where its possible to see the neurofibroma's extension in right cervical region, scoliosis and multiple plexiform neurofibromas.

Only the biggest neurofibroma was detected by clinical exam. However it is possible to identify two others neurofibromas.

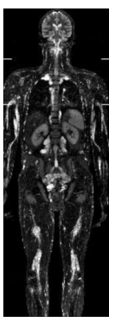

Whole body view of multiple plexiform neurofibromas.

Conclusion:
Whole body MRI is a radiation-free exam and it is useful on the diagnosis of NF1 and on patient's follow-up. It provides an overview of the systemic

involvement and neurofibroma's extension beyond the clinical expectation. During patients follow up, it could also show tumor's characteristics modification, which was considered as a possible sarcomatous degeneration.

Accuracy of non-radiologists and lay-persons for identifying children with cerebral cortical atrophy from 'Mercator map' curved reconstructions of the brain

S. Vedajallam[1], A. Chacko[1], S. Andronikou[2], E. Simpson[2], J. Thai[2]; [1]East London/ZA, [2]Bristol/UK

Objective:

Background: Communication of cortical brain atrophy in children with term hypoxic ischaemic injury (HII) to parents and the legal fraternity contesting compensation rights can be very difficult using text and standard cross-sectional images. When demonstrating the cortex in HII, a single image of the brain surface, much like the way a map of the earth is derived from a globe, can be generated from curved reconstruction of coronal magnetic resonance imaging (MRI) scans i.e. a Mercator map. Lay people's ability to identify abnormal scans from such maps without prior training requires evaluation before routine use.

Aim: To determine the sensitivity and specificity of lay people in detecting abnormal brain scans through review of Mercator flat-earth maps of the brain, without prior training.

Materials:

Ten Mercator map images were provided to 100 participants with a distribution of 5 HII, 1 cortical dysplasia and 4 reported normal. Participants were required to identify abnormal scans. Sensitivity and specificity overall and for sub-groups were derived by averaging true positives and negatives; false positives and negatives.

Results:

The results show a strong ability for lay-people to identify normal versus abnormal MRI brain studies using Mercator maps. The sensitivity and specificity in this group is 67% and 73% respectively. Non-radiologist physicians and radiographers performed slightly better than lay people as expected. Radiologists of course had very high sensitivity and specificity of 86% and 100%.

Conclusion:

The Mercator map is therefore a viable tool in the communication of complex MR imaging to the lay-person.

Safety and efficacy of sphenopalatine ganglion blockade in children – initial experience

L. Dance, C. Schaefer, D. Aria, R. Kaye, R.B. Towbin; Phoenix/US

Objective:

Sphenopalatine Ganglion (SPG) blockade is known to be a safe and effective migraine headache treatment among adults. This paper will report the initial experience in the pediatric population with SPG blockade.

Materials:

One hundred thirty-three procedures were performed in 85 patients ages 7 to 18 from February through November 2015. Pre-intervention headache scores were recorded on a scale of 1 to 10. The procedure was performed supine with neck in hyperextension. Anesthesia of the bilateral nares was accomplished with lidocaine spray and gel. Contrast was injected using a SphenoCath confirming catheter position. 4% lidocaine was injected. Patients remained supine with neck in hyperextension for 10 minutes. Post-intervention headache scores were recorded.

Results:

Mean pre-treatment score of 5.55 decreased to 3.28 post-treatment (Δ2.27, 95% CI 1.34-3.20, p<0.0001). There were no complications.

Conclusion:

SPG blockade is a safe and effective treatment for migraine headaches in children which results in decreased reliance on intravenous drug therapy.

Pediatrics Orbital Masses: The value of adding Diffusion-Weighted Imaging to the conventional MRI in Lesion Categorization

A. Youssef, A.M. Aly, D. El Galaly, M. Ali, H. Taha, H.E. El Zomer; Cairo/EG

Objective:

Orbital masses represent a spectrum of benign and malignant lesions in children that can be challenging to diagnose and treat. Imaging plays an important role in diagnosis, due to a potentially limited clinical examination and risks associated with biopsy. MR imaging is a powerful tool for imaging the orbit, due to the excellent tissue contrast it provides. Yet conventional MRI has a limitation in discriminate the benign from malignant lesions.

Diffusion-weighted imaging (DWI) is non-invasive rapid technique uses the water diffusibility to produce contrast among different kinds of tissues. Our propose was to assess the role of DWI and calculated apparent diffusion coefficient (ADC) values in characterization of the pediatric orbital masses regarding benignancy or malignancy.

Materials:

One hundred and thirty patients with recently diagnosed orbital masses and who underwent preoperative conventional MRI and DWI were included in this study. The orbit was divided into six compartments: the eye globe, retroocular fat, optic nerve, lacrimal system, bony boundaries and extra-ocular muscles. The average ADC obtained from each tumor was compared with the histopathological diagnosis determined from subsequent surgical sample.

Results:

Seventy girls and sixty boys with orbital masses were included in this study. Their age was ranged from 1 month to 18 years. The globe is the seat of lesions in 43/130 cases, optic nerve in 27/130 case. Seven cases have lesions in the lacrimal gland. Forty-five of cases was diagnosed as having benign masses & 85 of cases have malignant lesions. There is a statistically significant difference between the mean ADC value of the benign lesions ($1.39\pm0.52 \times 10^{-3}$ mm^2/s) and the mean ADC value of the malignant lesions ($0.69\pm0.22 \times 10^{-3}$ mm^2/s) (P<0.001). The optimal ADC cutoff value that was determined for discrimination between these lesions is: 1.075×10^{-3} mm^2/s), with sensitivity of 97.14% and specificity of 75%. Using conventional MRI alone in predicting benign and malignant lesions has the sensitivity of 76% and specificity of 91% with 94% positive predictive value and 67% negative predicative value.

Combining DWI and conventional MRI has increased accuracy, as the sensitivity and specificity were 95%, 86% respectively with 93% positive predictive value and 90% negative predicative value.

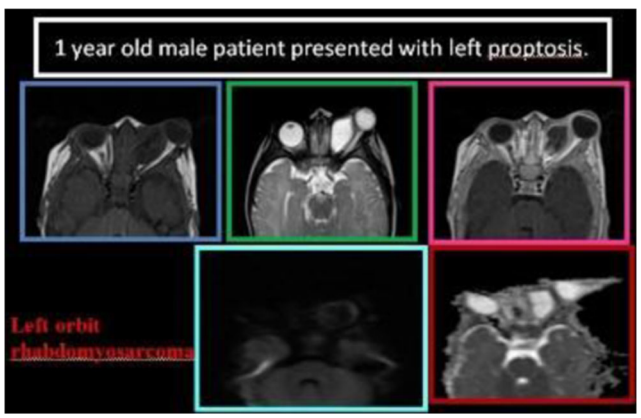

Conclusion:
ADC values provide an accurate, sensitive, fast, and non-invasive mean of characterization of pediatric orbital tumors. A priori tumor characterization is useful in timing and treatment planning for orbital tumors.

Utiliy of resting state fMRI in children for preoperative language mapping
L.-M. Leiber, M. Delion, A. Ter Minassian; Angers/FR

Objective:
To assess if resting state fMRI is able to detect language eloquent areas in childrens.

Materials:
Six children, from 8 to 15 years old suffering from brain lesions were enrolled in this study. They underwent MRI with one 3DT1 morphology session and three 10 minutes fMRI sessions, including one resting state fMRI and two language task induced activity fMRI sessions. Analysis was performed using a generalized linear model for the first one and a spatial independent component analysis approach for the two others.
Language maps were compared with cortical mapping obtained by intraoperative direct stimulation.

Results:
Language network was identified systematically by resting state session but not by task induced activity sessions. Moreover, in two of the six patients, resting state fMRI was able to detect eloquent areas found during intraoperative cortical mapping that were not present in task induced activity sessions.

Conclusion:
Resting state fMRI appears superior to task induced activity fMRI in detecting language eloquent areas.

Is Sclerotherapy an Effective Treatment Option for Ranulas or Thyroglossal Duct Cysts in Children?
D. Aria, L. Dance, C. Schaefer, R. Kaye, R.B. Towbin; Phoenix/US

Objective:
To assess the utility of sclerotherapy in the treatment of ranulas and thyroglossal duct cysts

Materials:
From 2015-2016, 8 patients varying in age from 16 months to 32 years were referred to the IR department for sclerotherapy. Of the 8 patients, 6 had a diagnosis of ranula while 2 had the diagnosis of thyroglossal duct cyst by either MR, CT, or US. Sclerotherapy treatments were performed with standard sclerosing agents, i.e. sotradecol 3% foam, absolute ethanol, and bleomycin. In the subset of patients with ranulas, sclerotherapy was commonly performed in accordance with salivary (submandibular and/or sublingual) gland botox injection or ethanol ablation. 22-gauge or 5F sheathed needles were used for US-guided access to the lesions, with ranula sclerotherapy being performed after placement of side-hole drainage catheters (5-10F) due to their increased viscosity. The preferred sclerosing agent was injected with dwell times ranging from 15 mins to 3 hours. Salivary gland injection/ablation was performed under US-guidance using a 22-gauge needle with volume injection targeted centrally within the gland or in the portion of the gland abutting the ranula. After treatment, all patients were scheduled for follow-up ultrasounds at a minimum of 8 weeks to assess lesion response or residual disease.

Results:
A total of 23 sclerotherapy treatments were performed. Of the 8 patients, 2 were lost to follow-up after single sessions for ranula and thyroglossal duct cyst. The other 6 patients all had follow-up ultrasounds after each of the remaining 21 sclerotherapy sessions. Four of these patients showed initial improvement with either decreased size of lesion or lesion resolution while the other 2 showed no improvement with either stable or increased size on initial follow-up. The 4 patients who initially showed promising response unfortunately had recurrence on follow-up imaging and ultimately, demonstrated no favorable response to sclerotherapy after subsequent treatments regardless of whether treatment was combined with ethanol/botox salivary gland injection. In summary, all 6 patients who were successfully followed show no appreciable response to treatment for ranula or thyroglossal duct cyst.

Conclusion:
Despite the emergence of clinical requests for sclerotherapy of ranulas and thyroglossal duct cysts, in our case series, sclerotherapy has not proven to be an effective treatment option using our current drug regimen.

Role of the Susceptibility-weighted imaging (SWI) in the neuroimaging of term newborns
G. Rudas, E. Varga, P. Barsi, L. Kozák, Ü. Méder; Budapest/HU

Objective:
Susceptibility-weighted imaging (SWI) was introduced in the neonatal neuroimaging only a few years ago. We can find only a few publications about its advantages and disadvantages. According to our experience, SWI is extremely useful not only for detecting bleedings but for the diagnosis of other diseases as well.

Materials:
During the last year we had 164 MRI examinations on term newborns (0-14 days of life) and the SWI gave additional information in 54 cases. We used a 3T Philips Insignia scanner.

Results:
In the case of the questionable **hypoxic-ischemic-encephalopathy** (19 cases) and the **metabolic diseases** (5 cases) we could find increased signal intensity in the cortex; in the case of **stroke** we could find the thrombus itself in 6 cases; the **AVM** were much clearer using the SWI in 3 cases; at the **PVL** in 3 cases we could visualize the cysts better using SWI; in the case of **congenital heart disease** (11 cases) and in the case of **sinus thrombosis** (4) we could find microbleedings and/or dilated veins; in 3 cases the position of the **lateral ventricle drain or shunt** was much clearer using the SWI. The SWI gave important additional information in 54/164 (33%).

Conclusion:
The SWI is a strongly recommended new sequence at the MRI examination of the term newborns' brain. A disadvantage of SWI is that it requires ca. Three minutes examination time (in contrast to T2* which is only 1 minute long).

Mechanical birth-related trauma: Imaging of the "accidents of birth"
A. Chaturvedi, J.G. Blickman; Rochester/US
Objective:

1. To discuss definition, incidence and risk factors leading to "mechanical birth-related trauma" and compare these with existing literature.
2. Offer an organ-system based classification scheme encompassing the varied manifestations of birth-related trauma and describing the implications on care decisions.

3. Discuss clinical presentation, course and complications, optimum imaging techniques and imaging findings for individual entities.

Materials: The hospital Imaging department database was searched for neonates who presented with history of difficult/traumatic birth at our obstetric center between January 1, 2013-June 30, 2016. Search software used was Primordial Customised Radiology Solutions, San Mateo, CA. The search terms used were "macrosomia", "shoulder dystocia", "instrumental delivery", "malpresentation", "cephalopelvic disproportion", "forceps" and "vacuum".
Initial and follow-up imaging and clinical data on these neonates was reviewed and compiled by two Board-certified pediatric radiologists. The relevant literature was reviewed and findings compared.

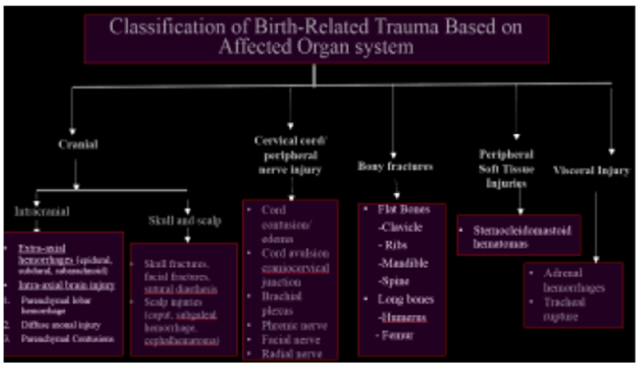

Organ-system based classification scheme for birth-realted trauma.

Results:
In our study, mechanical trauma of birth was seen to manifest within different organ systems, which have been listed below in the order of occurrence within our sample. Injuries to the skull (sutural overlap, dents and fractures), scalp hemorrhages (subgaleal hematoma, cephalhematoma, caput). Intracranial intra- and extra-axial hemorrhages (subdural, subarachnoid, epidural, intraparenchymal). Clavicle fractures Neonatal brachial plexus injury. Sternocleidomastoid hematomas. Adrenal hemorrhages. Cervical spinal cord contusions.

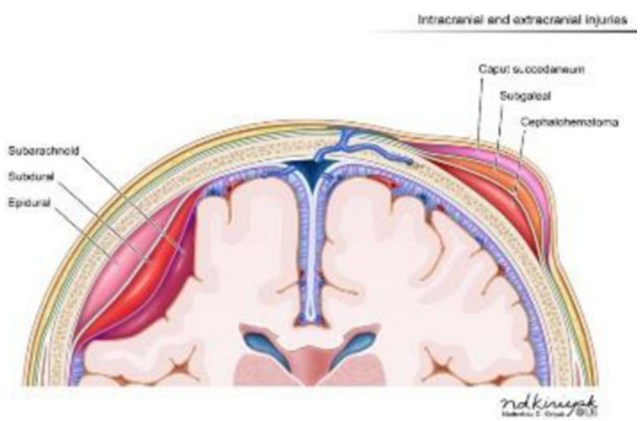

Schematic diagram depicting intra- and extracranial hemorrhages by location.


6-year-old with history of calvarial fracture at birth- fracture did not heal but enlarged secondary to leptomeningeal entrapment at the fracture site- an entity called "growing fracture" or "leptomeningeal cyst".

Conclusion:
Multiple newborn organ systems can be injured from mechanical trauma of birth. Our numbers compare favourably with the existing literature. Mechanical birth-related trauma can occur simultaneously with hypoxic-ischemic birth injury. Although most of these injuries spontaneously and completely resolve, long-term complications can be seen in some cases. Few of these injuries are life-threatening. Imaging plays a crucial role in diagnosis and follow-up, and can assist in decision making as well as in counselling the parents.

SESSION: CASE REPORT PRESENTATION SESSION

Ewing sarcoma of tibia in an infant girl
A. Seehofnerova, J. Skotáková, I. Červinková; Brno/CZ

Objective:
Ewing sarcoma (ES) is the second most common primary bone malignancy in children. It histologically originates from neuroectodermal tissue and consists of small round blue cells. Ewing tumour family is very close to primitive neuroectoderm tumour (PNET) family with diverse stage of differentiation, Ewing sarcoma being less differentiated. Approximately 50 % of the cases occur between ten and twenty years of age with slightly higher prevalence in male gender.

Case presentation:
Nine-month-old Caucasian girl presented to local surgery department after she had wedged her lower leg in a bed. The right lower leg was swollen and painful. She was initially diagnosed with a ligament injury and underwent standard treatment. Oedema gradually disappeared, but swelling and pain increased after three weeks. She also suffered from a fever of 38.1°C (100.58°F). At that point X-ray of her right lower leg was performed with report describing pathologically changed structure of tibia and she was referred to our university centre.

We made a second reading of the plain film, reporting sclerotic heterogeneous bone structure of the right tibial diaphysis and distal metaphysis, onion-like periosteal reaction with sunburst spiculation and cortical bone destruction. Her laboratory results were: CRP 7.2 mg/l, LD 6.2 μkat/l, NSE 44.3 μg/l, ferritin 18 μg/l. CRP has been raising for a week to 25 mg/l, then decreased to normal level.

Differential diagnosis was established as a primary bone malignancy (especially ES) or, less likely, an osteomyelitis.

MRI revealed pathological signal of bone marrow of diaphysis of the whole tibia with cortical scalloping and periosteal spiculated apposition. Epiphyses were spared. Dorsal cortical bone was interrupted with extraosseal spread of the process. Intraosseal part enhanced heterogeneously, whereas extraosseal component enhanced almost homogeneously after contrast medium administration. Total size of the tumour was assessed as 97x23.5x20 mm (22.8 ml). Adjacent muscles were oedematous with post-contrast enhancement. There were also few enlarged lymph nodes in popliteal region.

Results from the biopsy confirmed EWS with positive EWS/FLI1 gene. Tumour was assessed as a localized disease, Enneking IIB. Patient underwent chemotherapy according to AEWS1031DOC protocol and a knee-exarticulation with no traces of tumour in resection lines.

Nowadays she is in the first complete remission.

X-ray: AP view

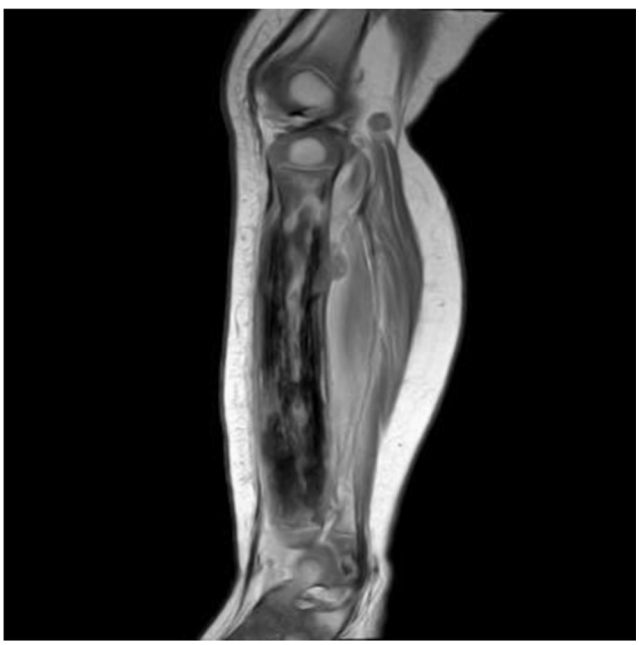

MRI: eTW1_TSE postcontrast, sagittal view, pre-treatment

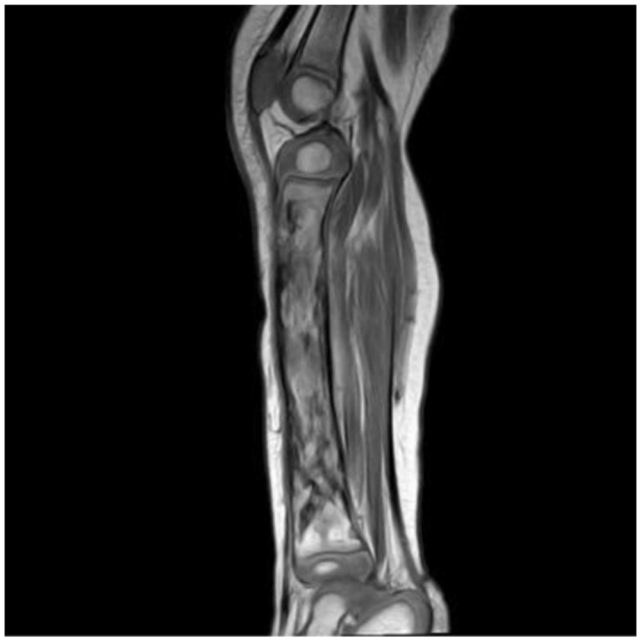

MRI: eTW1_TSE postcontrast, sagittal view, after initial treatment

Unique teaching points:

Ewing sarcoma belongs to common primary bone tumours in children but is a very rare unit in infants. Despite the age predilection it is necessary to consider this diagnosis even in children younger than one year of age.

Scimitar syndrome together with pulmonary sequestration and horseshoe lung: Congenital pulmonary venolobar syndrome

B.E. Derinkuyu, H.N. Özcan, Y. Tasci-Yildiz, H G. Cınar, U.A. Orun; Ankara/TR

Objective:

Congenital pulmonary venolobar syndrome (CPVLS) comprises of a spectrum of pulmonary developmental anomalies. The main components of CPVLS are hypogenetic lung partial anomalous pulmonary venous return, absence of pulmonary artery, pulmonary sequestration, systemic arterialization of lung, absence of inferior vena cava. Minor components of CPVLS include tracheal trifurcation, eventration and partial absence of the diaphragm, phrenic cyst, horseshoe lung, esophageal and gastric lung, anomalous superior vena cava, and absence of the pericardium. In this case presentation, we present a baby with Scimitar syndrome, pulmonary sequestration, horseshoe lung and right aberran subclavian artery.

Case presentation:

A 3 month-old girl was admitted to our hospital with the suspicion of Scimitar syndrome from a different hospital. She did not have any symptoms. The physical examination was unremarkable. On plain radiograph, the baby had dextrocardia. There was a doubtful tubular structure with the shape of scimitar and a nodular radioopacity behind the heart (Figure 1). Transthoracic echocardiography demonstrated the dextrocardia, atrial septal defect and the right pulmonary artery hypoplasia. Afterwards, the CT Angiography was done for confirmation of Scimitar syndrome and other accompanying abnormalities. On the CT angiography, there was a partial anomalous pulmonary venous return to the suprahepatic inferior vena cava known as Scimitar syndrome. Besides this, there was a right pulmonary extralobar sequestration in the lung base. The arterial supply was arising from the celiac trunk, while the venous drainage was going directly to the inferior vena cava. Therefore, the right lung was hypoplastic of which the tongue of the right pulmonary parenchyma passing between the aorta and heart, appearing confluent with the left lung in a horseshoe configuration. There was dextrocardia and right aberran

subclavian artery. The patient was subjected to catheterization and angiography for treatment.

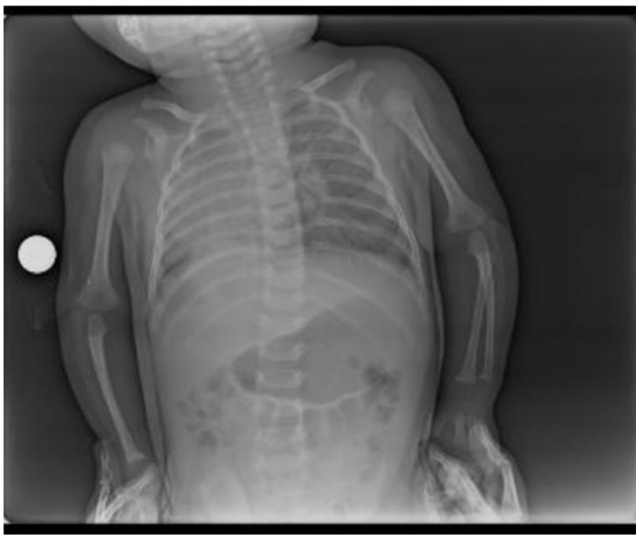

On plain radiograph, the baby had dextrocardia. There was a doubtful tubular structure with the shape of scimitar and a nodular radioopacity behind the heart

Unique teaching points:
The term CPVLS is an umbrella to a group of pulmonary parenchymal and vascular anomalies that may present in combination. MDCT is a helpful diagnostic tool in the preoperative evaluation for delineation of the components of this syndrome.

Congenital pulmonary venolobar syndrome in combination with multiple abnormalities in a child
B.E. Derinkuyu, H.N. Özcan, Y. Tasci-Yildiz, U.A. Orun; Ankara/TR

Objective:
Congenital pulmonary venolobar syndrome refers to a wide spectrum of pulmonary developmental anomalies that may appear single or in combination. The main components of congenital pulmonary venolobar syndrome are hypogenetic lung (including lobar agenesis, aplasia, or hypoplasia), partial anomalous pulmonary venous return, absence of pulmonary artery, pulmonary sequestration, systemic arterialization of lung, absence of inferior vena cava, and accessory diaphragm. In this case presentation, we describe a child with Scimitar syndrome, bilateral sequestration, hypogenetic lung (single lobed left lung) and right aberran subclavian artery.

Case presentation:
An 8 year-old Syrian girl was admitted to our hospital with the history of heart defect. She did not have syncope or ciyanosis whereas she has easy fatigue and palpitation. On plain radiograph the anomalous draining vein was seen as a tubular structure paralleling the right heart border in the shape of a Turkish sword ("scimitar") (Figure 1). Transthoracic echocardiography demonstrated the scimitar vein as well as large patent ductus arteriosus (PDA), atrial septal defect and left pulmonary hypoplasia. Afterwards, the CT Angiography was done for confirmation of Scimitar syndrome and other accompanying abnormalities. On the CT angiography, there was a partial anomalous pulmonary venous return to the suprahepatic inferior vena cava known as Scimitar syndrome. Besides this, there was a bilateral intralobar pulmonary sequestration in the lung bases. The arterial supply of the right side was arising from the celiac trunk, while the left side feeding artery was originating directly from the descending aorta. Therefore, the left lung had a single lobe with single pulmonary vein draining to left atrium. There was a large PDA and right aberran subclavian artery. The patient was subjected to catheterization and angiography for treatment. The right sided anomalous draining pulmonary vein and the feeding artery of the right sequestration were closed in the first session. The procedure was completed without any complication. Afterwards, the closure of the feeding artery of the left pulmonary sequestration and the PDA were planned in the next sessions.

On plain radiograph the anomalous draining vein was seen as a tubular structure paralleling the right heart border in the shape of a Turkish sword ("scimitar")

Unique teaching points: Congenital pulmonary venolobar syndrome comprises a heterogeneous group of uncommon abnormalities that may occur in combination. Diagnosis of congenital pulmonary venolobar syndrome can be confirmed by CT angiography that allows detailed evaluation of vascular, tracheobronchial, and pulmonary parenchymal abnormalities with a single short, noninvasive procedure.

Neck infection disclosing diagnosis of congenital fourth branchial arc anomaly in a girl
H.N. Özcan, Z. Aycan, B. Ardıcl, M. Haliloglu; Ankara/TR

Objective:
Congenital branchial arc anomalies are rare entities. Herein, we describe the imaging findings of acute suppurative infection of the neck caused by fourth branchial fistula in a child.

Case presentation:
An 11-year-old girl presented to our pediatric emergency department with fever, left sided neck swelling and redness. Her complaints were started five days ago. On her physical examination, there was a 4x4 cm, stiff, painful mass lesion with redness on the left side of the neck. Blood count and thyroid function tests were in normal range; however, C-reactive protein level and erythrocyte sedimentation rate were elevated. Neck ultrasonography revealed diffuse soft tissue swelling, a hypoechoic mass consistent with abscess in the left thyroid lobe and perithyroid tissue. The left lobe of the thyroid gland had poorly defined margin and a focus of air. Contrast-enhanced neck MR imaging demonstrated an abscess in the left thyroid and perithyroid tissue (Figure 1) and enhancement of the soft tissue plane around the left pyriform fossa (Figure 2). Barium swallow revealed the sinus tract originating from the left pyriform sinus apex. The patient was operated after antibiotic treatment and sinus tract was surgically excised.

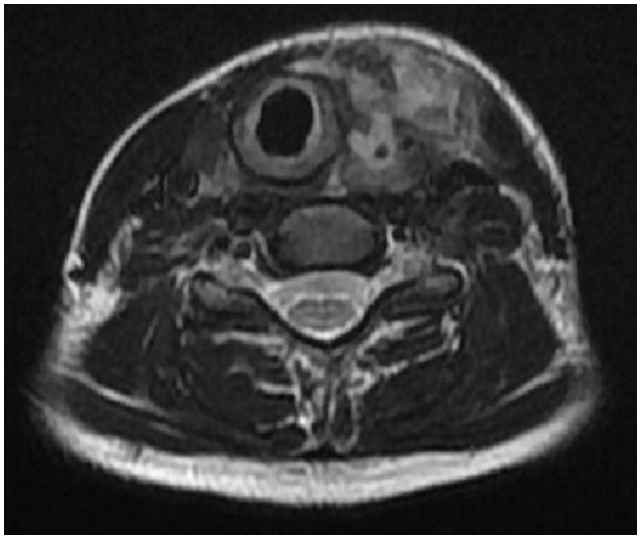

Figure 1

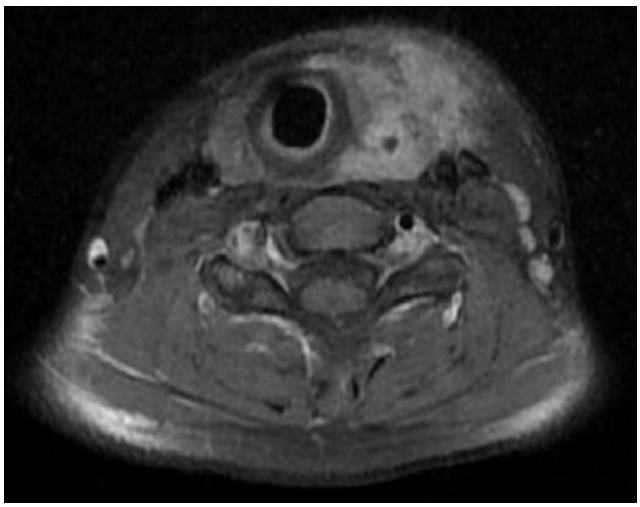

Figure 2

Unique teaching points:
Congenital fourth branchial arc anomaly is an uncommon entity; however, has a characteristic location. It should be kept in mind when an inflammatory infiltration or abscess is present between the pyriform fossa and thyroid gland on the left side of the neck.

Heart and hepatic faillure: Uncommun onset of Wilms' tumor
S.M.S.D. Rocha, A.G. Antón, M.S. Takahashi, M.W. Matsuoka, G.C. Almeida, Y.L. Fugikawa, L. Suzuki; Sao Paulo/BR

Objective:
The aim of this report is to describe three cases of right kidney Wilms' tumor with cavoatrial tumor extension, referred to our Institution between January and September 2016.

Case presentation:
Three children, two girls (3 and 7 years old) and one boy (2 years old) were admitted at the emergency service with cardiac failure symptoms; the latter had also liver failure. Echocardiography showed right atrial thrombus in all three patients, as an extension of massive obstructive thrombosis of the inferior vena cava (IVC). Abdominal ultrasonography revealed in all patients a right renal mass, associated to right renal vein thrombosis that extended to the IVC and to the right hepatic vein. Contrast enhenced computed tomography confirmed findings. Patients were treated primarily with chemotherapy before surgery, with partial regression of the thrombus in two patients and no response in one.

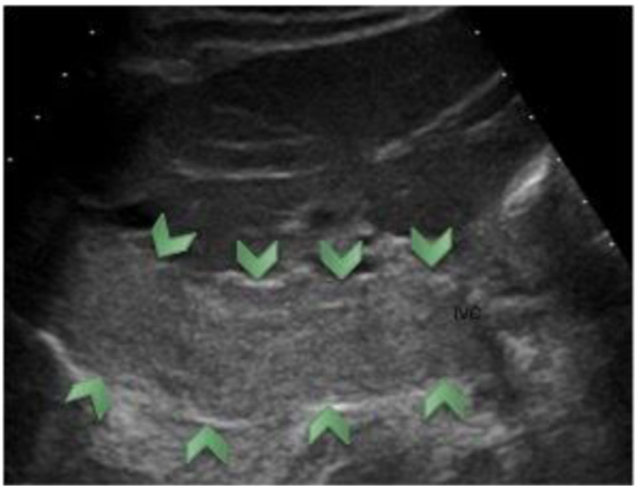

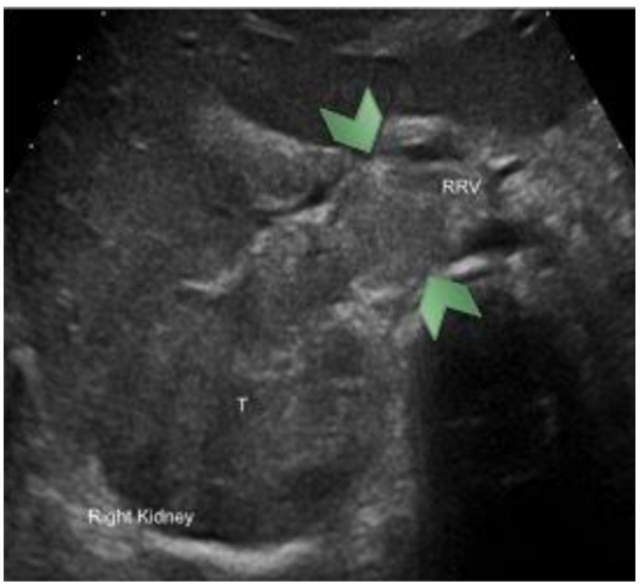

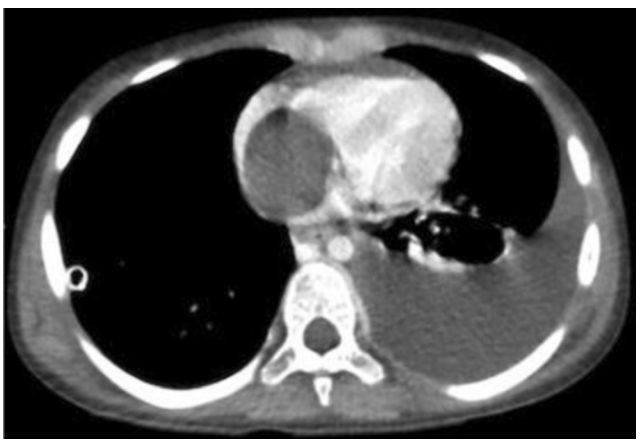

Unique teaching points:
Wilms' tumor is the most common renal malignancy in children and its intravascular extension is a well-recognized event. Incidence of tumor extension to inferior vena cava (IVC) is reported to be of 2-5% and intra-atrial extension of 0,2-1,2%. It occurs most commonly in tumors located in the right kidney (probably due to the shorter path of the right renal vein compared to the left one). This complication does not directly influence the prognosis of malignancy, but the degree of intravascular extension determines technical surgical strategy and increases difficulty of the surgical procedure, especially when there is intracardiac involvement, which increases morbidity.
Several classifications have been proposed in the adult age group, but due to the similarity of the degree of intraoperative difficulty, the same classifications are used in children. Pritchett et al. (1986) described the relation between thrombus and hepatic vessels: Level I - intrahepatic intravascular extension; Level II - intrahepatic extension; and Level III - suprahepatic or atrial extension. Staehler et al. (1987) proposed a different classification that was posteriorly modified and detailed by Daum (1994): Stage I - small extension (thrombus size within IVC <5 cm); Stage II - large thrombus (> 5 cm within the IVC), but still below the hepatic vessels; Stage III - thrombus extending to the level and above the hepatic vessels; Stage IV - intra-atrial thrombus. Abdullah et al. (2013) added a Stage V to the latter classification for intraventricular extension of the tumor thrombus (important in the preoperative management and in the anesthetic approach).

A Case of Angiomatous Fibrous Histiocytoma of the Forearm
S. Ali[1], M. Thyagarajan[1], V. Bhalla[2], Z. Sheikh[1]; [1]Birmingham/UK, [2]Stoke-on-Trent/UK

Objective:
To outline the radiological features of this rare lesion of intermediate malignant potential as demonstrated on ultrasound and magnetic resonance imaging (MR) in our encountered case.

Case presentation:
A 4 year old boy presented with a soft tissue mass in his forearm which appeared to have grown quickly in size over a period of three to four months. Physical examination demonstrated a well-defined mass in the dorsal aspect of the forearm with no pulsatile bruit. Intial differentials included a vascular anomaly or a sarcomatous lesion.
The patient proceeded to have an ultrasound examination which revealed a very well-defined heterogenous subcutaneous mass, mostly solid in substance. The lesion measured 3.5 cm x 1.6 cm x 3.5 cm (transverse x length x depth). There was no evidence of muscle invasion. Prominent internal arterial vascularisation was demonstrated and the mass was classed as inderminate in nature.
Subsequent MR findings demonstrated a mass with T1 signal isointense to muscle, hyperintense T2 signal and marked homogenous enhancement. Small foci of intralesional T1 hyperintensity and larger areas of T2* gradient hypointensity were noted, in keeping with small areas of intralesional blood. Vessels were seen to extend from the subcutaneous fat into the lesion. The mass slightly distorted the underlying extensor muscles and tendons of the forearm but there was no deep extension across the fascia. Findings deemed the lesion to be more malignant in nature.
The patient underwent incisional biopsy and histological findings confirmed a diagnosis of angiomatous fibrous histiocytoma. These tumours are rare soft tissue tumours which most commonly occur in children, adolescents and young adults. While it is rare, there is a potential for local recurrence and metastasis. Therefore, it is essential to identify these tumours where possible or at least consider them as a differential for a soft tissue mass in a child.
The surgeon commented that the imaging findings and report were essential in making the initial decision about whether to perform an incisional or excisional biopsy as the best treatment for the tumour is wide surgical excision with clearance of margins.

Unique teaching points:
Angiomatous fibrous histiocytomas are rare lesions with potential for recurrence and metastasis and therefore should be identified and managed appropriately as a malignant tumour. They are often confused as soft tissue haemangiomas or complex haematomas. It is very important to be aware of the presentation and imaging findings, remembering this form of tumour as a key differential for a soft tissue mass.

Nasopharyngeal anlage tumor in a neonate with the initial presentation of respiratory difficulty: Correlation between imaging and clinicopathologic findings
P.-S. Tsai, D.-C. Lin, S.-L. Shih; Taipei/TW

Objective:
The etiologies of nasal or nasopharygeal obstruction are variable in neonates. The respiratory symptoms are varied in these cases. Mass lesions in nasal cavity or nasopharynx are extremely rare during the neonatal period. However, we must keep it in mind when respiratory problems occur in the neonatal period. Here, we report a case presenting with sleep apnea resulting from nasal obstruction by a rare benign salivary anlage tumor in nasopharynx and discuss the imaging findings as well as clinicopathologic characteristics.

Case presentation:
The 28-day-old female infant had loud breathing sound, slow feeding and sleep apnea since birth. Nasal endoscope and laryngoscope disclosed a polypoid tumor in nasopharyngeal cavity with a stalk connecting with posterior nasal septum.
Further magnetic resonance imaging (MRI) revealed a lobulated mass about 1.6 cm in greatest diameter occupying posterior nasal cavity to the nasopharynx that was intermediate signal intensity on T1-weighted/T2-weighted images and heterogeneous gadolinium enhancement.
The patient then received endoscopic resection. The tumor was shown locating in nasopharyngeal cavity and having a stalk from posterior nasal septum, partially occluding the choanae as well.
Resected tissue fragments displayed tan and whitish in color grossly. Microscopic examination demonstrated duct-like structures and mesenchymal elements in a nodular pattern which are typical features of salivary gland anlage tumor. Until now, there is no tumor recurrence for four years.

Unique teaching points:
"Salivary gland anlage tumor (SGAT)" was firstly introduced in a report by Dehner et al in 1994. The tumor that has histologic resemblance to the developing salivary gland, is believed to be a hamartoma originating from minor salivary gland rather than a true neoplasm.
Congenital SGAT displays male predilection and is a rare cause of neonatal airway obstruction. The mass is usual in the midline and attached to the posterior nasal septum or posterior nasopharygeal wall by a delicate pedicle. Favorable results with simple excision are obtained. Once mass-related airway obstruction is established, further examination with computed tomography (CT) or MRI is helpful in anatomic evaluation, size measurement, characteristics definition and intracranial involvement.
If mass induced airway obstruction is suspected in a neonate and SGAT is considered based on imaging studies, invasive procedure should be careful due to the potential of tumor dislodgement from its fine pedicle resulting in complete airway obstruction.

Sonographic Detection Of Intussception With Malrotation: Waughs Syndrome

A. Sulaiman, E. Arul Raj, N. Praveen Kumar, E.A. Parthasarathy, G. Moorthy; Chennai/IN

Objective:

The association of intussusception with malrotation is referred to as Waugh syndrome.[1] Malrotation occurs in approximately 1 in 500 live births.[2] The incidence of malrotation amongchildren with intussusception is 40%. We hereby present a case report of Waugh's syndrome associated with midgut volvulus.

Case presentation:

A 5 month old male child reported to the emergency department with the clinical history of vomiting, abdominal distension, bloody mucoid stools and incessant cry. Routine blood examination revealed Hb: 12.9 gm%, TLC: 14500/cu mm, PLT-2. 9lac/cu. mm. Ultrasound (US) examination was performed and it revealed dilated fluid-filled small bowel loops with moderate amount of free fluid, Right iliac fossa showed bowel within bowel appearance suggestive of target/pseudo kidney sign of bowel intussusception. No pathologic lead point was identified. Transverse ultrasound image through the upper abdomen showed superior mesenteric vein noted to the left of the superior mesenteric artery hence malrotation should be considered. In view of surgical emergency non contrast enhanced CT was done and axial image showed target/sausage shaped soft tissue density mass it had alternating areas of low and high attenuation due to bowel wall and mesentry. On emergency laparotomy patient was found to have intestinal malrotation with duodenojejunal junction on the right of the midline and 180 mid gut volvulus in clockwise direction. Intussusception with terminal ileum (gangrenous), caecum, appendix, whole of ascending colon, transverse colon were telescoping into descending and sigmoid colon. The volvulus was derotated and the in tussusceptum was reduced. The gangrenous terminal ileum and appendix was resected and Ladd's procedure was done, a diverting ileostomy was created. The patient recovered uneventfully after which an ileo-colonic anastomosis was created

Transverse Ultrasound shows a mass with a swirled appearance of alternating hypoechoic and hyperechoic "bowel-within-bowel" appearance (Target sign)

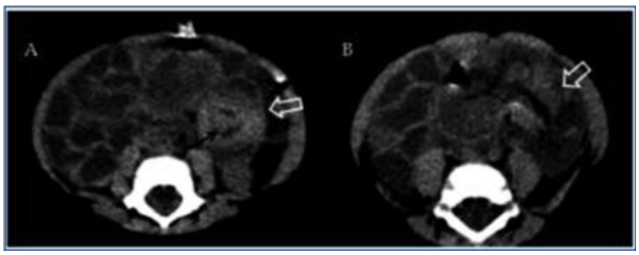

Non contrast enhanced CT scan axial images shows Target shaped (White open arrow in A) /Sausage shaped (White open arrow in B) soft tissue mass with alternating areas of low and high attenuation

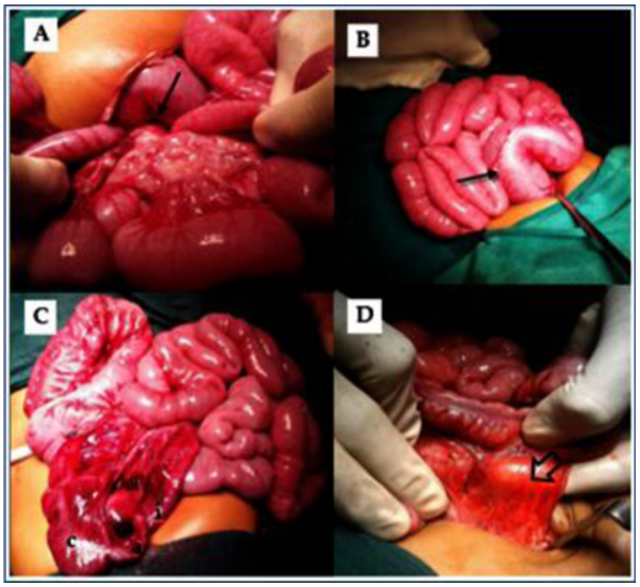

Laparotomy revealed 180° clockwise midgut volvulus with ladd's band. (B) An ileocolic intussusception. (C) Appendix (a) and caecum (c) visualized after manual reduction of intussusception with gangreneous distal ileum (D) Ladd's band with narrow mese

Unique teaching points:

On ultrasonography multiple, concentric, target like appearance of wall layers of invaginated segments (Target sign) on axial scan, as well as pseudokidney sign (sandwich sign) on longitudinal scans were accepted as diagnostic criteria for intussusception.[8] It can assess the relative positions of the SMV and SMA which are mostly abnormal in malrotation. Upper gastrointestinal contrast study is the imaging reference standard for diagnosis of malrotation with or without volvulus. Abnormal position of the duodeno-jejunal junction. Spiral, "corkscrew" or Z-shaped course of the distal duodenum and proximal jejunum, and Location of the proximal jejunum in the right abdomen. [2] A high degree of clinical suspicion and radiologist's awareness of this entity is helpful in guiding the surgeons towards diagnosis and prevention of morbidity and mortality.

A rare case of epidermal naevus syndrome

P. Joshi; Pune/IN

Objective:

To acquaint the radiologists with the entity of Epidermal nevus syndromes (ENSs) which are a group of rare complex disorders characterized by the presence of skin lesions known as epidermal nevi associated with additional extra-cutaneous abnormalities, most often affecting the brain, eye and skeletal systems

Case presentation:

This one and a half year old child was referred to us for neuroimaging. He had multiple hairy naevi over his face, limbs including the palms, since birth, associated with blackish discolouration of his entire trunk.

Brain imaging revealed left temporal lobe cortical dysplasia, an intensely enhancing left choroid plexus lesion in the temporal horn suggestive of a choroid plexus papilloma and a left ocular coloboma. Extraaxial nonenhancing T1 hyper intense lesions were seen in the cerebello medullary cisterns bilaterally showing fat suppression suggestive of lipomas. An extramedullary intra spinal lipoma was also seen in the thoracic region.

Except for a small extraaxial lipoma on the right all the other lesions including the spinal lipoma were on the left

Clinical photo

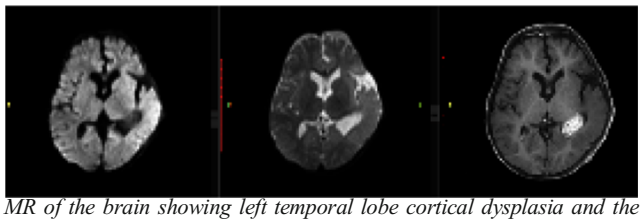

MR of the brain showing left temporal lobe cortical dysplasia and the choroid plexus papilloma

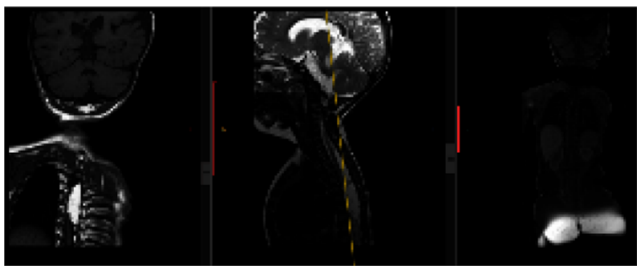

Images through the spine showing the extramedullary thoracic spinal lipoma

Unique teaching points:

Epidermal nevi are overgrowths of structures and tissue of the epidermis, the outermost layer of the skin. The different types of epidermal nevi can vary in size, number, location, distribution and appearance. Neurological abnormalities that can be associated with ENSs can include seizures, cognitive impairment, developmental delays and paralysis of one side of the body (hemiparesis). Skeletal abnormalities can include abnormal curvature of the spine, The term "epidermal nevus syndrome" has generated significant controversy and confusion in the medical literature. Originally, the term was used to denote a disorder that was actually several different disorders erroneously grouped together. In the recent past, the term was used to denote a specific disorder now known as Schimmelpenning syndrome. However, the term epidermal nevus syndrome could be correctly applied to several different disorders. Therefore, the umbrella term "epidermal nevus syndromes" now represents a group of distinct disorders that have in common the presence of one of the various types of epidermal nevi. However, there is so far no general agreement how to classify the types of this diverse group of disorders, adding to the confusion within the medical literature. These disorders are quite different from one another and are not "variants" of each other as is sometimes mistakenly stated in the medical literature. In the future, as the genetic molecular basis of these disorders is better understood, the classification may change or expand.

Bilateral axillary lump in a newborn diagnosed as hematoma

H.N. Özcan, U. Aydingoz, M. Haliloglu; Ankara/TR

Objective:

Most birth traumas are self-limiting and have a favorable outcome. Injuries to the infant that result from mechanical forces during the birth process are not uncommon. They occur most commonly on head and neck after vaginal breech delivery. However, soft tissue hematomas can be rarely seen after caesarian section (C/S). Herein, we describe imaging findings of a newborn with bilateral axillary lump diagnosed as hematoma.

Case presentation:

A 31-year-old woman was admitted to an outside hospital at 38 weeks' gestation for C/S due to prior caesarean operation. It was her fourth pregnancy (G4 P2). The pregnancy was unremarkable and she had normal ultrasounds at gestation. There was no history of trauma or fall during antenatal period. According to the C/S reports, the process of operation was uneventful any undue prolongation and without having used any other instrumentation. The weight of the female baby was 3.1kg at birth. On the 3rd postnatal day, her mother noticed a left axillary swelling, then admitted to a tertiary children's hospital. Her physical examination revealed, bilateral axillary asymmetry with a fluctuant, nontender swellings. There was no redness or discoloration of the skin. There was no clinical feature suggestive of trauma or bleeding diathesis. A superficial ultrasonography showed solid heterogeneous, hyperechogenic masses 38x35 mm in the left axillary region and 15x13 mm in the right side. Doppler study did not reveal any flow in the masses. Contrast enhanced MR imaging demonstrated, bilateral axillary mass lesions with fluid levels and smooth contours (Figure 1 and 2). T1W images demonstrated hyperintense component suggesting hemorrhage. After the administration of the gadolinium-based contrast material, lesions showed peripheral enhancement (Figure 3). A diagnosis of hematoma was entertained. The child was managed non-operatively. She was monitored clinically and radiologically. Follow-up ultrasounds scan revealed significant regression of the swellings.

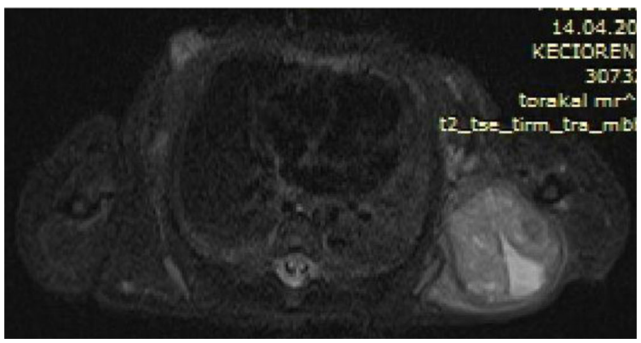

Figure 1

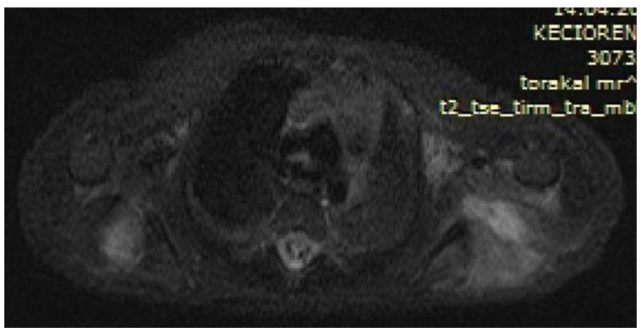

Figure 2

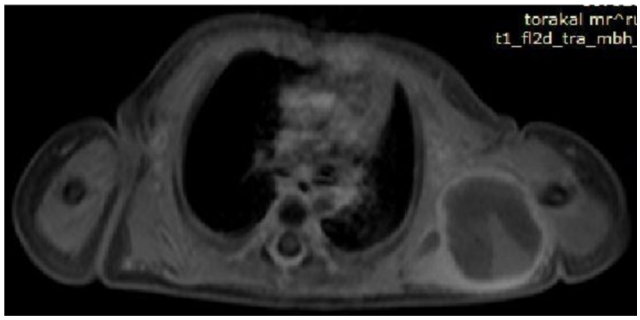

Figure 3

Unique teaching points:
Soft tissue hematomas can be rarely seen in newborns. The formation of axillary hematoma on the background of C/S is a rare complication, which, to the best of our knowledge, has not been previously reported. Ultrasonography and MR imaging readily depicts hematoma and aids in the differential diagnosis.

Pediatric colorectal carcinoma presenting as misleading abdominal pain: A case report

S.K.J. Flores Quispe, A. Cavaliere, M. Cananzi, M. Zuliani, T. Toffolutti; Padua/IT

Objective:
Colorectal carcinoma (CRC) is extremely rare in pediatric age, with an estimated annual incidence of approximately 1 case per million individuals. The majority of reported cases occur in adolescence, while the incidence is further lower for children under 10 years. The distribution between males and females is not equal, with higher prevalence in males (ratio of 2:1). The etiology in children is unclear as these tumors are often sporadic and not linked to a preexisting adenomatous polyp, unlike adults. Predisposing factors such as familial polyposis of the colon, other polyposis syndromes, ulcerative colitis and familial multiple cancer syndromes were reported in 10 % of cases. Advanced stage at diagnosis, aggressive histologic subtypes (poorly differentiated, signet ring and mucinous adenocarcinoma) and poor survival are the hallmarks of pediatric CRC.

Sonographic assessment of bowel wall thickening

Case presentation:
A 15-year-old male presented with a history of dyspeptic symptoms (recurrent epigastric-right flank colic pain and heartburn) for the last eight months, without evidence of irregular bowel function. After a prior diagnosis of esophagitis secondary to a gastro-esophageal reflux disease, physical and laboratory examinations revealed anorexia, progressive body weight loss, microcytic iron deficiency anemia and positive fecal occult blood test. During an emergency access, abdominal ultrasound identified rounded target liver lesions and circumferential heterogeneous mural thickening of the ascending colon. Contrast-enhanced computed tomography scan (CECT) demonstrated a marked circumferential wall thickening of the ascending colon and cecum with a longitudinal extension of 85 mm and thickness of 22 mm; the mass contained low-density areas and calcifications. Furthermore 5 hypovascular hepatic lesions along with lymph node metastases containing calcifications were identified. No lung metastases were found. Histopathological analysis confirmed the diagnosis of metastatic colon adenocarcinoma. After chemo- and radio-therapy, only the hepatic lesions showed reduction in size and number. The patient subsequently underwent right hemicolectomy. One month after surgery he is in a rigorous follow-up through ultrasonographic evaluation of pleural effusion and ascites and CECT.

Hypovascular liver metastasis

Unique teaching points:
CRC, although rare, should be suspected in children presenting with unexplained persistent abdominal pain, progressive body weight loss and positive fecal occult blood test. Ultrasound imaging can be appropriate in the preliminary detection of abnormal bowel wall thickening, lymph node and liver metastases; CECT is mandatory to confirm the radiological diagnosis and complete the staging.

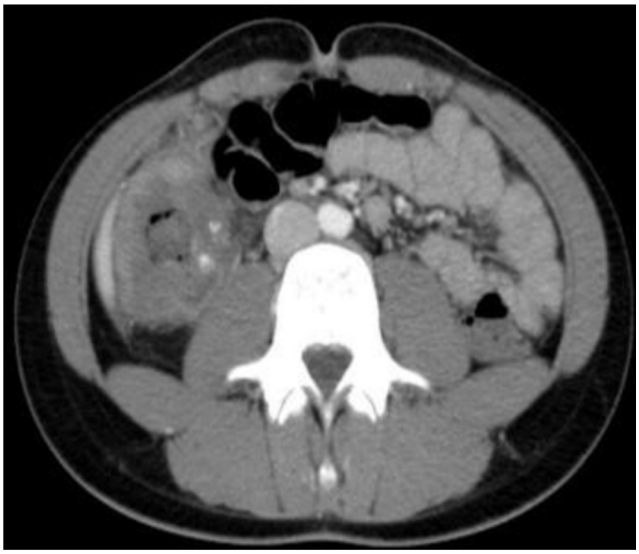

Circumferential wall thickening of the ascending colon with low-density areas and calcifications

Lemierre syndrome: A diagnostic dilemma in paediatric patients

V. Bhalla, S. Ali, S. Al-Ali, M. Thyagarajan; Birmingham/UK

Objective:

To increase awareness of this rare syndrome and its varied presentation in order to facilitate its early diagnosis and treatment to prevent poor prognostic outcomes.

Case presentation:

Lemierre syndrome is a rare disease characterized by an initial infection of the head and neck leading to the development of a septic thrombophlebitis which has a propensity to spread and involve the jugular and facial veins. This progressive infection then leads to the development of metastatic septic emboli to the respiratory tract.

We present the case of a 7 year old boy who attended with a 1 week history of fever and a cough. Initial imaging on admission demonstrated a large left sided hydropneumothorax with multiple cavitating lesions throughout the lung parenchyma in addition to thrombosis of some of the segmental pulmonary veins. The hydropneumothorax was surgically drained and the patient was transferred to the paediatric intensive care unit after further deterioration with the development of a broncho-pleural fistula. Following a short course of antibiotics there was no clinical or radiological improvement and sputum cultures grew coliform organisms which raised suspicion for a more distant source. When pus was noted to be discharging from the left ear, a contrast enhanced CT of the head and neck revealed a left mastoiditis with multiple cerebral abscesses and occlusive thrombi in the left jugular vein, transverse venous sinus, sagittal and straight sinuses. Following this diagnosis antibiotic therapy was modified and targeted at anaerobes, which was vital in assisting the patients recovery and successful discharge home.

Unique teaching points:

Clasically the majority of Lemierres syndrome begins in the oropharynx-involving the palantine tonsils and peritonsillar tissue often presenting with fever, sore throat and neck pain. Our case demonstrates an atypical presentation with sepsis and respiratory symptoms as a result of the septic emboli which delayed diagnosis. We have learnt from this case the importance of considering Lemierres syndrome in patients presenting with signs of a respiratory infection – in particular cavitating pulmonary lesions- that have not improved with conventional therapy and to have a low threshold to investigate the head and neck as a potential source of infection.

When the Working Hypothesis of Meningitis Could Not Help

E. Kovacs[1], N. Pinter[2], G. Balázs[1], A. Machovitsch[1], A. Arany[1], Z. Liptai[1], L. Fonyad[1], P. Benke[1]; [1]Budapest/HU, [2]Amherst/US

Objective:

Neuroinfection still represents a diagnostic challenge in the everyday practice, where clinical evaluation, imaging, laboratory and pathological workup and treatment goes hand in hand under the pressure of time.

We summarized a case in which, despite the extensive multilateral collaboration the battle was lost, to bring attention to the possible causes.

Case presentation:

A two year old, previously healthy female was taken to the emergency department for altered state of consciousness and fever. She also suffered from gingivitis.

The unconscious child underwent an emergency CT scan: hydrocephalus with signs of raised intraventricular pressure was detected. Subsequently MRI of the head and spine was performed, and showed signs of diffuse leptomeningeal enhancement with basal predominance. Multiple DWI restricted parenchymal lesions with basal predominance were also found.

Repeated CSF and blood tests did not reveal any causative organism, although the gradually increasing CRP suggested infection. Two weeks after the onset of symptoms a follow up MRI study showed extensive cerebral and spinal swelling with no focal lesion. The child passed away three days later due to cardiac failure. Autopsy and neuropathological evaluation could not reveal the cause of the disease, which was identified only weeks after the child died, by culturing sputum and CSF.

Unique teaching points:

An overview of the clinical and radiological presentation of meningitis basilaris is carried out. Attention is given to the circumstances, when tuberculotic infection should be suspected, and antituberculotic treatment should be started, even before the confirmation of the presence of mycobacteria can be obtained.

Radial pattern of femoral head edema in chronic non-bacterial osteomyelitis (CNO)

M. Raissaki, K. Spanakis, Z. Korka, M. Bitsori, E. Galanakis, A.H. Karantanas; Heraklion/GR

Objective:

To describe the clinical, laboratory and MRI findings of chronic non-bacterial osteomyelitis(CNO) in a patient with a negative radiograph and emphasize useful imaging findings, including an unusual radial pattern of edema in both femoral heads.

Case presentation:

A 14-year-old adolescent, was referred with progressive debilitating hip pain and inability to walk since 5 days, that was unsuccessfully treated with non-steroidal anti-inflammatory drugs. During hospitalization he developed fever up to 38^{o} with normal full blood count and smear, elevated ESR (95mm/h) and CRP (12.8 mg/dL), positive serologic markers for streptococcus (ASTO) and EBV and received antibiotics with relative good response. Blood cultures did not grow any pathogens, the rest of serology was negative for acute infection, tuberculin skin test was negative and immunological investigation was unremarkable. Pelvic radiographs were negative. MRI showed a symmetric pattern of bone marrow involvement around both triradiate cartillages, at both femoral heads and

major trochanters. Complementary evaluation of tibial areas with a limited protocol disclosed asymptomatic involvement of tibial epiphyses and apophyses. A radial pattern of edema was seen at the femoral heads with alternating stripes of involved and uninvolved areas. Clinical course and imaging appearances were highly suggestive of CNO.
Rapid clinical improvement occurred during hospitalization while a repeat MRI 6 months later showed complete resolution of hip findings and the patient was free of any symptoms or signs.

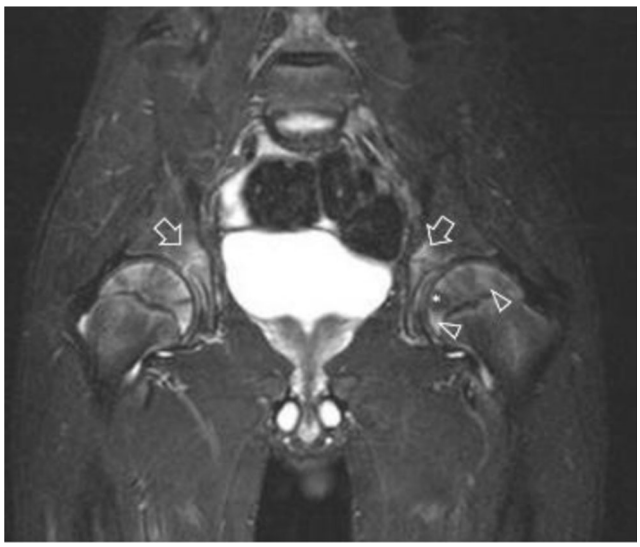

Coronal STIR sequence at presentation showing the radial pattern of bone marrow edema (arrowheads) alternating with stripes of normal marrow (*) at both femoral epiphyses. Note hyperinense edema (arrows) around triradial cartillages.

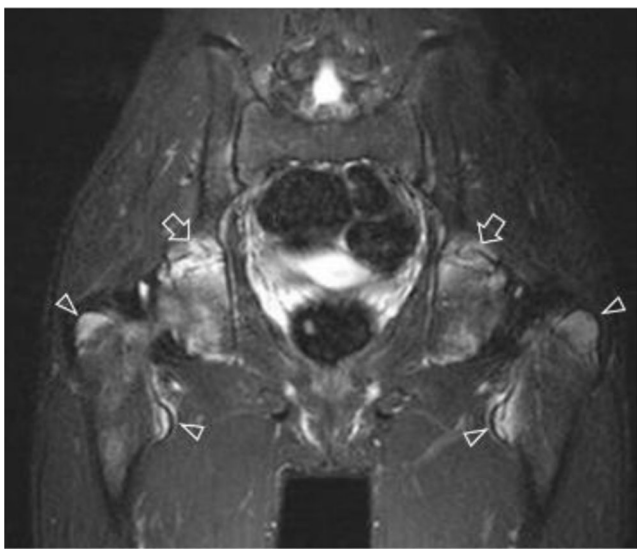

Coronal STIR sequence showing the predilection of bone marrow edema symmetrically around triradial cartillages (arrows) and at major and minor trochanters (arrowheads).

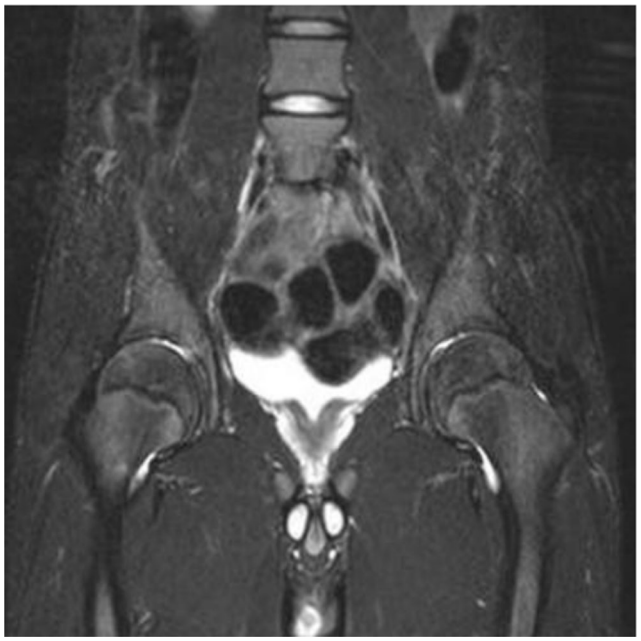

Coronal STIR sequence at 6-months follow-up shows resolution of edema.

Unique teaching points:
CNO is a not well known chronic autoinflammatory bone disorder affecting primarily children and adolescents.
Positive serology for streptococcus or other infectious agents has been previously reported as in our case and may be a triggering factor.
Striking MRI findings with a negative radiograph may occur at initial stages. Symmetrical distribution of non-specific bone marrow edema around epiphyses and apophyses is highly suggestive of the diagnosis in the appropriate clinical setting and following exclusion of suppurative bone infections as well as bone or hematologic malignancies.
The radial pattern of edema in our patient is unusual and considered to comply with the direction of main trabecular systems in femoral heads.

SESSION: SCIENTIFIC SESSION: ONCOLOGY AND WHOLE BODY IMAGING

Detection and prevalence of pulmonary nodules in young children with and without cancer

M. Verhagen[1], J. van Schuppen[1], E. Deurloo[1], C. Schaefer-Prokop[2], A. Smets[1]; [1]Amsterdam/NL, [2]Amersfoort/NL

Objective:
To determine the optimal reconstruction technique of CT data for the detection and characterization of pulmonary nodules in children under 13 years. To study the prevalence and characteristics of pulmonary nodules in children with and without a malignancy.
Materials:
We compared 5 mm maximum intensity projections (MIPs) used in conjunction with 1 mm slices (A) to 1 mm (B) and 3 mm scans alone (C) of chest CTs of 36 children (median age 6.9 years, range 2.1-12.7), half of whom (18/36) had known extra-thoracic malignancies. After consensus, five chest CTs were excluded. Subgroups were defined based on a 4.5-year clinical and radiological follow-up. Typical perifissural nodules were registered.
Results:

In 26/31 chest CTs, 103 nodules (median size 2.0 mm) were detected. Display mode A with 5 mm MIP yielded the best interreader variability (κ=0.294) and the highest sensitivity (73.9%) compared to mode B and C (κ=0.218, sensitivity 61.2% and κ=0.238, sensitivity 59.3%, respectively). Perifissural nodules were detected in all subgroups.

Conclusion:

MIP improves the detection of pulmonary nodules in chest CTs of young children, but overall interreader agreement is only fair. Nodules, including perifissural nodules, occur in children with and without malignancy.

The acquisition of a diagnostic CT improves the diagnostic value of combined integrated FDG PET/CT in pediatric oncology

C. Loberg, C. Kuhl, F. Mottaghy, A. Heinzel, U. Kontny, T. Braunschweig, A. Bartella, F. Verburg; Aachen/DE

Objective:

Combined integrated [^{18}F] 2-fluoro-2-deoxyglucose (FDG) positron emission tomography and X-ray computed tomography (PET/CT) is proven to be useful in pediatric oncology. However, it is unclear whether a contrast-enhanced diagnostic (ceCT) has an additional value as part of the integrated scan protocol.

Aim: To study the additional diagnostic value of ceCT as part of FDG PET/CT in pediatric oncology.

Materials:

We reviewed the first available FDG PET/CT of 37 pediatric oncology patients referred for PET/CT between January 2007 and October 2015. Images were subsequently read and interpreted by board-certified radiologists and nuclear medicine physicians in communal reading. In case of identifying suspicious lesions in ceCT additional imaging (MRI) or biopsy was performed.

Results:

Compared to PET/CT employing only low dose CT (ldCT), the use of ceCT resulted in the identification of 19 additional suspicious lesions in 13 patients. Furthermore the use of ceCT allowed us to qualify 3 lesions as benign/physiologic which in PET/ldCT were identified as suspicious and 16 lesions suspect for metastases or tumor. In those 37 patients who received combined integrated FDG PET/CT including both ldCT and ceCT the CTDI ranged in between 1,3-15.5 mGy (n= 10.2 mGy) and the dose length product (DLP) ranged in between 82.4-2464 mGy *cm (n= 812.6 mGy *cm)

Specificity was significantly higher combining PET and CT compared to stand-alone CT and PET.

Conclusion:

Our study showed that the acquisition of ceCT in combined integrated PET/CT leads to an increased specificity and thus represents an essential component of a good FDG PET/CT in pediatric oncology. In assessment of lymph nodes, inflammatory foci and liver lesions diagnostic contrast enhanced CT is essential.

Comparison of the Detectability of UBOs in Neurofibromatosis Type I patients with Proton density-weighted and FLAIR sequences in 3T MRI

L. Porto, S. Lescher, N. Hillenbrand; Frankfurt/DE

Objective:

Neurofibromatosis Type 1 (NF1) is an autosomal-dominant congenital disease. In NF1 patients, significant numbers of so-called unidentified bright objects (UBOs) can be found in brain imaging, with predilection sites at the basal ganglia and the dentate nucleus. UBOs seem to develop at a very early age, contrary to other criteria leading to diagnosis. The detection of UBOs might therefore prove helpful in the early diagnosis of NF1, complementing the clinical diagnosis based on criteria of the "National Institutes of Health Consensus Development Conference". The aim of the study was to investigate whether the detectability of UBOs increases at 3T by comparing Proton density-weighted images (PDw) with fluid-attenuated inversion recovery (FLAIR) sequences.

Materials:

A total of 14 NF1 patients (7 male, 7 female, between 8 and 26 years old, mean age 15.4 years) were examined by a 3T magnetic resonance scanner. The presence of UBOs was evaluated on PD-w and FLAIR images by 4 evaluators (2 experienced neuroradiologists, 1 junior radiologist and 1 student in his final year). Detectability was rated by a three-point scoring system for dedicated regions: lesions which were "well defined/detectable", "suspicious" or "detected after a second look". The Wilcoxon signed-rank test was used for comparisons between the raters. The level of significance was $P<0.05$.

Results:

Significantly more lesions were marked as "well defined/detectable" in the PD-w Sequence compared to FLAIR ($P<0,001$ for all four evaluators together, as well as for each evaluator separately). In particular, PD-w proved to be superior for detecting UBOs located in the medulla oblongata (P=0,001) dentate nucleus (P=0,002) and hippocampal region (P=0,007), regardless of the level of the raters' experience.

Conclusion:

This is the first study that compares FLAIR and PD-w at T3 for the diagnosis of UBOs in NF1. Significantly more UBOs are detected in the PD-w compared to FLAIR sequences, especially for the infratentorial regions. As UBOs occur at very early stages of the disease in patients with suspected NF1, PD-w might aid an early diagnosis in these patients.

Assessment of radiation doses from diagnostic imaging in the follow-up of paediatric oncology patients

P. Logan[1], R. Harbron[2], K. McHugh[1]; [1]London/UK, [2]Newcastle-upon-Tyne/UK

Objective:

Previous literature (1,2) has suggested paediatric oncology patients accumulate a large radiation burden as a consequence of routine diagnostic imaging examinations during therapy. We retrospectively looked at the effective doses from routine CT and nuclear medicine in three cohorts of children, namely patients with hepatoblastoma, Wilms' tumours and rhabdomyosarcoma (RMS). Of note, in our centre we rely on repeated MRIs of the primary site for many tumours.

Materials:

Effective doses (E), in millisieverts (mSv), were estimated using the NCICT dose estimation tool (Lee et al 2015), based on details specific to each procedure: patient age, scan region, scanner type and CT dose index (CTDI - an indicator of radiation exposure recorded at the time of each scan). Doses for general radiography were estimated using PCXMC V2.0 Monte Carlo simulations, assuming standard exposure factors and field size.

Results:

There were 59 patients in total (18 hepatoblastoma, 21 Wilms', 20 RMS). There were 33 boys. The mean age was 3 years 2 months (ranging from 14 days – 11 years 10 months). The mean and median cumulative effective doses from CT for the whole cohort were 7.88 mSv and 4.24 mSv respectively. Four patients in the Wilms' cohort had a DMSA nuclear scintigram (0.7 – 1.0 mSv), no hepatoblastoma patient had any nuclear medicine imaging, and 16 patients with RMS received a bone scan (3 – 3.5 mSv) or a PET scan (approximately 8mSv).

Conclusion:

Cumulative radiation doses from routine radiological investigations in paediatric oncology can be kept in a much lower range than reported in the literature (1,2). In our institution, the follow-up of solid intra-abdominal tumours with MRI, with additional CT or nuclear medicine only when clinically justified, has resulted in a significantly low radiation exposure in these patient cohorts. MRI of the primary tumour site should be implemented as a replacement for CT imaging when there is no significant detriment to the diagnostic information obtained.

MRI-based evaluation of multiorgan iron overload is a predictor of adverse outcomes in pediatric patients undergoing allogeneic hematopoietic stem cell transplantation

F. Zennaro[1], D. Zanon[2], R. Simeone[2], G. Boz[2], F. Degrassi[2], M. Gregori[2], G. Schillani[2], C. Boyer[1], N. Maximova[2]; [1]Nice/FR, [2]Trieste/IT

Objective:
Iron overload is associated with poor clinical outcomes in patients undergoing allogeneic hematopoietic stem cell transplantation (HSCT). Although the effects of hepatic and cardiac siderosis on patient outcomes have been extensively studied, less is known about the effects of siderosis in other organs.
Materials:
The medical records of 44 consecutive pediatric patients who underwent allogeneic HSCT in our Institute from 2011 to 2015 were retrospectively reviewed. MRI was used to measure iron concentrations in the liver, spleen, pancreas and bone. These patients were divided into two groups, 18 with non-elevated (<100 μmol/g; Group 1) and 26 with elevated (>100 μmol/g; Group 2) liver iron concentration (LIC) at baseline.
Results:
In Group 1, only two patients had normal iron concentrations in all organs. None of the patients of Group 2 presented with pathological iron concentrations in only two organs. Comparisons of baseline data with results of the first follow-up MRI performed 1-6 months after HSCT, showed a general worsening of iron accumulation. In Group 1, none of the patients showed complete absence of iron overload in a single organ. In Group 2, none of the patients showed a total absence of siderosis involving fewer than three organs.
Conclusion:
This study confirms the correlations between iron overload and the risks of transplant-related complications, such as transplant related mortality, sinusoidal obstruction syndrome, infections, pancreatic insufficiency, and metabolic syndrome, in transplant recipients with systemic siderosis.
Another important finding of this study was the close correlations between pre-transplant BIC and times to neutrophil and platelet engraftment (p<0.001 each).

Quantitative Diffusion weighted MR Imaging in children with Neuroblastoma

B. Ammann, A.-L. Peschmann, H. Cario, D. Steinbach, C. Beltinger, K. Kneer, A.J. Beer, S. Dürr, M. Beer; Ulm/DE

Objective:
Neuroblastoma (NB) is the most common extracranial solid tumor in children. Previous studies indicated that diffusion-weighted (DW) magnetic resonance imaging (MRI) allows deep insights into tumor biology prior and during therapy or observation.
Materials:
Eighteen children, NBs (15), Ganglioneuromas (GN, 2) and Ganglioneuroblastoma (GNB, 1), examined by 3T MRI were retrospectively grouped according to tumor entity, risk factors (bone marrow metastasis, *MYCN* amplification or 1p36 deletion) and therapeutic regime (observation versus chemotherapy). DW (b values 0, 400 and 800) and conventional MRI images (T2, T1 pre and post contrast) were analyzed for tumor size, relative SI- and absolute ADC-values at baseline (base; no therapy), and after 3 (FU1) and 12 (FU2) months.
Results:
ADC values in NB were lower than in GNB and GN ($0.75*10^{-3}mm^2/s$ versus $1.28*10^{-3}mm^2/s$; p<0.05). There was a tendency towards lower ADC values in tumors with risk factors (n=6) versus no risk factors (n=7) at baseline, which did not reach statistical significance (p=0.08). During follow-up shrinkage of tumor volume was noted (baseline 1206 ml, FU1 159 ml, FU2 51 ml; p<0.05 baseline vs. FU1; p=0.08 baseline vs. FU2). In the observation group, tumor ADC values rose without relapse ($0.89*10^{-3}$ to $1.07*10^{-3}mm^2/s$). Only in eventually relapsing tumors ADC values tended to decrease further ($0.95*10^{-3}$ to $0.71*10^{-3}mm^2/s$, p=0.17), despite initial reduction in tumor size.
Conclusion:
ADC values differ between NB and GNB/GN. Tumor volume decreased during follow-up. While increasing ADC values might predict relapse free survival, ADC decreasing during therapy might herald relapse.

Pulmonary Nodule Detection and Characterisation in Children with Wilms Tumours: Do Radiologists Agree?

S.C. Shelmerdine[1], S. Irtan[2], J. Brok[1], A. Nair[1], V. Hedayati[1], J. Jacob[1], S. Swinson[3], A. Smets[4], K. Pritchard-Jones[1], O. Olsen[1]; [1]London/UK, [2]Paris/FR, [3]Leeds/UK, [4]Amsterdam/NL

Objective:
To establish inter and intra-observer variability in the radiological detection and assessment of pulmonary nodules at diagnosis in children with Wilms tumours.
Materials:
A test set of CT thoraxes at diagnosis from 15 patients enrolled in the multicentre 'Improving Population Outcomes of Renal Tumours of childhood' (IMPORT) study in the UK were assessed.
Five radiologists (3 chest, 2 paediatric) from 5 different centres (4 UK, 1 Netherlands) completed a scoring sheet for nodule assessment on the same studies on two occasions, 6 months apart. The readers were blinded to patient respiratory symptoms, the original radiology reports and also that they were scoring identical cases.
Descriptive statistics, modified Bland Altman graph and Fleiss kappa scores were used for statistical assessment.
Results:
In total, 93 different pulmonary nodules across the 15 CT Thoraces at both rounds were scored by at least one reader. 81 (87%) were seen by at least one reader in round 1 and 81 (87%) in round 2, 69 (85.2%) nodules were seen by at least one reader in both rounds.
Only 20 (21%) nodules were scored by all 5 readers in round 1, 16 (17%) by all 5 readers in round 2, and 14 (7%) nodules by all 5 readers in both rounds. Of the 20 nodules seen in the first round, 11 were measured to be >5mm in at least one dimension and of these, 7 were classified as malignant by all 5 readers. The limits of agreement for mean difference in nodule size in anterior-posterior, transverse and longitudinal measurements were ±1.85mm, ±1.76mm and ±1.88mm respectively. The Fleiss kappa scores ranked from poor to fair agreement for nodule border smoothness (0.03), nodule shape (0.2), solidity (0.2) and impression of malignancy (0.4).
Within the same readers for both rounds, nodule detection rates of agreement were between 60.7-82.9%. The average intra-reader percentage of observed agreements for nodule border smoothness, shape, solidity and impression of malignancy were 84.2%,63.9%, 90.6% and 84.8% respectively.
Conclusion:
Detection and characterisation of pulmonary nodules on CT thorax shows both intra- and inter-observer variability. This has important implications for the interpretation of metastatic disease at presentation.

Whole-Body MRI (WB-MRI) in the diagnosis of children with fever without a focus

J. Delgado, N.A. Chauvin, M.A. Bedoya, S.J. Patel, K. Darge, S.A. Anupindi; Philadelphia/US

Objective:
Fever without a focus is defined as febrile illness without an initial obvious cause or localizing signs. Our aim is to assess the diagnostic value of Whole-Body MRI (WB-MRI) in the diagnostic work-up of children with fever without a focus.
Materials:
We retrospectively searched for subjects who underwent WB-MRI for fever without a focus. A total of 29 children (M=17, F=12), mean age 6.1 years (range: 0.08 – 17.61) were included. 8/29 (27.6%) subjects were immunosuppressed and 6/29 (20.7%) subjects were hospitalized at onset of fever. The reference standard was based on positive cultures, biopsy or surgery. When this was not possible, a probable diagnosis was made based on clinical follow-up or serology.

Initially, the WB-MRI images were reviewed independently by 2 pediatric radiologists blinded to all clinical information. At the end of each case the final diagnosis and the diagnostic category (5 categories: a. Normal, b. Infection, c. Oncologic, d. Rheumatologic, e. Miscellaneous) was recorded. This was followed by a consensus read for comparison with the reference standard. For statistical analyses all subjects were treated as fever without a focus.

Results:

Reference standard: The diagnostic category of the reference standard was as follows: Infectious 12/29 (44.8%), oncologic 1/29 (3.4%), rheumatologic 8/29 (27.6%), miscellaneous. 1/29 (3.4%). Even after extensive work-up in 7/29 (20.7%) no clear cause for the fever was found **Table 1**.

WB-MRI: WB-MRI diagnosed the cause of fever without a focus in 7/29 subjects (24.1%) **(Table 1)**. In 2 subjects (6.8%) WB-MRI results were falsely positive (1 JIA and 1 myositis), and in the remaining 20 subjects no imaging findings compatible a cause of febrile disease were found. Interobserver agreement was fair (Kappa 0.53).

Reference standard diagnosis	Number of cases	Number of cases diagnosed with WB-MRI
Infectious		
• Bacteremia without a focus	3	0
• Osteomyelitis	2	2
• B. cepaciae Pneumonia	1	0
• Viral Fever	1	0
• Lyme	1	0
• Pyelonephritis	2	2
• Cystitis	1	0
• Sinusitis	1	0
Oncologic		
• Hodgkin Lymphoma	1	1
Rheumatologic		
• Kawasaki Disease	2	0
• CRMO	2	1
• Acute Rheumatic Fever	1	0
• JIA and Macrophage activation Syndrome	1	1
• Lupus	1	0
• Pauci-immune glomerulonephritis	1	0
Miscellaneous		
• Familial Mediterranean Fever	1	0
Unexplained fever after work-up	7	0
TOTAL	**29**	**7**

Table 1. Final diagnoses and number of cases diagnosed with WB-MRI for each disease.

Conclusion:

In children with fever without a focus WB-MRI provided the diagnosis in in almost a quarter of the cases. Given the multiplicity of causes of fever without a focus, some of them not possible to visualize on MR imaging, WB-MRI may be considered in routine imaging practice when evaluating pediatric patients with fever without a focus.

Subjective Differences in Solid Tumor Measurements by Pediatric Radiologists Results in Inconsistent Reporting of Tumor Burden Which Could Adversely Affect Treatment Decisions

D.M.E. Bardo, R. Southard, S. Jorgensen, H. Hu, S. Bailey, D.R. Biyyam, M. Patel, C. Barnes, I.L.S. Cassell, R. Augustyn, S. Willard, L. Dance, C. Pfeifer, M. Thorkelson, P. Chatfield, R.B. Towbin; Phoenix/US

Objective:

To investigate inter-reader variability in measurement of solid tumors amongst Pediatric Radiologists.

To compare linear measurement/volume to direct volumetric measurements using 3 dimensional(3D) post-processing software.

Materials:

For this IRB approved study initial diagnostic CT or MR exams in 100 patients(11mo-20yr) with solid tumors were reviewed by 11 Radiologists and 3 Technologists. Radiologists recorded measurements in 3 axes in their routine method, described tumor shape (sphere, ellipse, cone) and surface texture (smooth, almost smooth, or mildly, moderately, markedly irregular). Three Technologists individually, and 3 Radiologists by consensus, used 3D processing software (Intellispace Portal, Philips, Cleveland, OH) to directly measure tumor volume.

Tumor volume (V) was calculated from linear measuments using the following equations: sphere $V=4/3\pi r^3$, ellipsoid $V=8\pi r^2$ or $16\pi r^2$, conical$V=2\pi r^2$ or $4\pi r^2$, and cuboid V=(xyz).

Inter-reader variability in tumor measurement in all tumors and for tumors divided by surface characteristics was assessed amongst radiologists and technologists, and Radiologist consensus using coefficient of variation (CoV).

Results:

Tumor shape analysis was reported as 14 sphere, 84 ellipse, 2 cone, and surface texture 8 smooth, 10 almost smooth, 32 mildly irregular, 31 moderately irregular, 19 markedly irregular.

Inter-reader variability of as much as 1,119cc above to 383cc below the mean tumor volume was found when using Radiologist determined linear measurements, with standard deviation (SD), range 0.65-413. Inter-reader variability amongst technologist derived volumes was considerably less, range 102cc above to 90cc below the mean, with SD, range 0.03-97.

CoV analysis shows a greater degree of variation in tumor volume calculated from linear measurements [smooth(7%), almost smooth(12%), mildly(20%), moderately(18%), markedly(27%) irregular] than direct volume determination [smooth(5%), almost smooth(6%), mildly(3%), moderately(3%), markedly(5%) irregular]. Variation was significant only for tumor with irregular surface texture [smooth (p=0.26), almost smooth (p=0.23), mildly (p=0.003), moderately (p=0.001), or markedly (p=0.002) irregular].

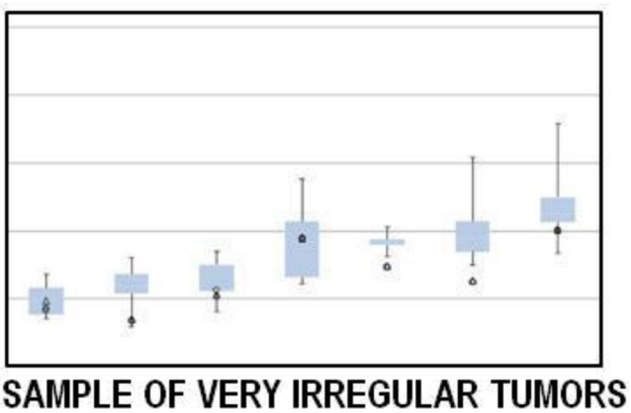

Variation in linear/volume measurements in very irregular tumors. Light blue=middle 50% tumor volume measurements by Pediatric Radiologists. Whiskers mark limits of range. ▲♦● markers =measurements by technologists. Note broad degree of variation.

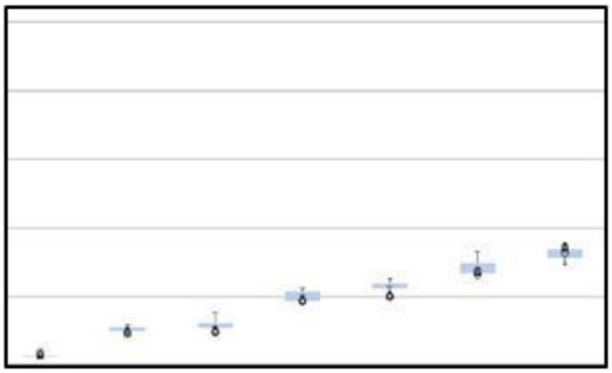

Variation in linear/volume measurements in almost smooth tumors. Light blue=middle 50% tumor volume measurements by Pediatric Radiologists. Whiskers mark limits of range. ▲♦● markers =measurements by technologists. Note narrow degree of variation.

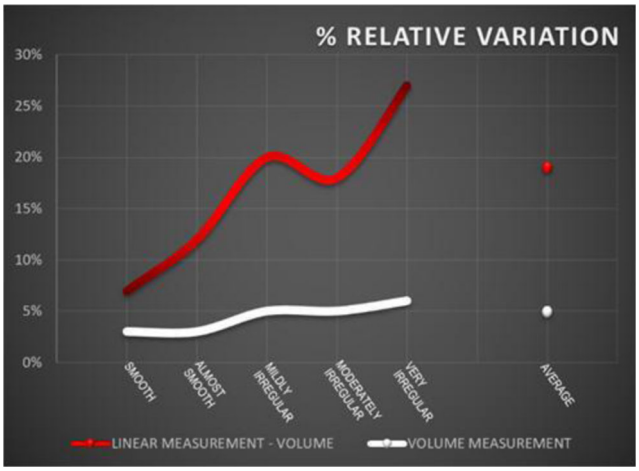

Both graphs show the same information – the % relative variation in tumor volume measurements determined by 3 dimensional linear measurements (11 Pediatric Radiologists) v. volumetric processing (Technologists & consensus group).

Conclusion:
Radiologist generated measurements are subjective and unreliable.
Variation in measurement technique leads to differences in calculated tumor volume which significantly over or under estimate volume in tumors with irregular texture and is not significant in smooth tumors.

Quail-quantitative MRI-based evaluation of pancreatic iron overload in pediatric patients undergoing allogeneic hematopoietic stem cell transplantation

F. Zennaro[1], M. Gregori[1], F. Degrassi[1], E. Cattaruzzi[2], Y. Diascorn[3], C. Boyer[3], N. Maximova[1]; [1]Trieste/IT, [2]Muggia/IT, [3]Nice/FR

Objective:
Iron overload (IO) is a relatively common but often neglected transplant-related complication and has been associated with poor prognosis in patients undergoing allogeneic HSCT for hemato-oncological disease. Pancreatic IO is frequent among patients with transfusion-dependent anemias, but is uncommon among patients with hematologic malignancies. The causes of pancreatic IO and the potential effects of pancreas iron deposits on transplant outcomes or on the risk of developing significant late effects in long-term HSCT survivors have not been yet determined.
Materials:
Our Institute routinely uses magnetic resonance imaging (MRI) with various gradient-recalled-echo (GRE) sequences to quantitatively measure the iron concentration in abdominal parenchymal organs in all pediatric patients before and after allogeneic HSCT. This study retrospectively analyzes the correlations of pancreas IO with the type of conditioning regimen and pre-transplant liver iron concentration (LIC) in 50 pediatric patients who underwent allogeneic HSCT in our Transplant Unit over the last 5 years.
Results:
We enrolled 50 patients, age 1–17 years. Pre-transplant mean LIC was 147,55 μmol/g (normal values 36 μmol/g). 3 (6%) patients had mild liver IO and 25 (50%) had moderate or severe IO. Pre-transplant mean pancreatic iron concentration (PIC) was 29,59 μmol/g, whose only 4 (8%) had mild pancreatic IO and none had severe IO. Post-transplant mean LIC was 162,6 μmol/g, only one patient had mild liver IO but 36 patients (72%) had moderate or severe IO. Post-transplant mean PIC was 66,22 μmol/g, 12 (22%) patients had moderate or severe IO. Mean pre-transplant pancreatic volume was 33,41 cm^3, while mean post-transplant pancreatic volume (evaluated 30 days after transplantation) was 25,41 cm^3. 11 (91,7%, p<0,001) patients with post-transplant moderate or severe pancreatic IO underwent TBI-based conditioning. Mean reduction of pancreas volume in TBI group was 12,02 cm^3 (p< 0,001). No pancreatic volume reduction was observed in chemotherapy-based group. All patients with pancreatic IO have had exocrine pancreatic insufficiency and 9 (83,3%) patients have had metabolic syndrome. Volume reduction well correlate (mean 49,8%, p<0,0001) with pancreatic IO.
Conclusion:
This study confirms that pancreatic iron overload is not so rare in patients with hematologic malignancy underwent allogeneic HSCT, with increased risk of metabolic syndrome and total deficit of exocrine pancreatic activity, but not of endocrine activity.
Iron overload monitoring allows for chelation therapy optimization. MR is fast, reproducible and more reliable compared to serum ferritin and transfusional history and allows a multi organ evaluation.

SATURDAY, JUNE 03, 2017

SESSION: SCIENTIFIC SESSION: CARDIAC AND THORACIC

Comparison of Chest X-ray findings in ambulatory and hospitalised children with suspected pulmonary TB

G.D. Baker[1], S. Andronikou[2], S. Lucas[1], H. Zar[3]; [1]Johannesburg/ZA, [2]Bristol/UK, [3]Cape Town/ZA

Introduction:
Pulmonary TB is common in South Africa, with many children affected. Diagnosis can be challenging and chest x-ray remains fundamental for diagnosis. Interpretation is difficult and shown to have wide inter-reader variability. No study however has compared CXR findings and inter-reader agreement between ambulatory and hospitalised patients.
Aim:
This study compares the frequency of CXR changes, as well as inter-reader agreement in ambulatory compared to hospitalised children with suspected TB.
Method:
A pre-existing database containing CXR data of children worked up for PTB from 2008-2013 was used. Retrospective analysis of 69 ambulatory and 112 hospitalised patients, aged 0-12 years

from Nolungile clinic and Red Cross Children's Hospital respectively was done. Each sample contained 50% proven TB and 50% negative controls. Two paediatric radiologists and one paediatrician served as blinded, independent readers for the database using standardised ticksheets.

Results:

Finding frequency; Weighted Kappa (ambulatory and hospitalised respectively):

Overall TB: 27.5% and 35.7%; -0.07 and 0.12

Parenchymal change: 34.8% and 67.9%; 0.24 and 0.49

Lymphadenopathy: 24.6% and 33.9%; 0.01 and 0.13

Pleural effusion: 7.3% and 18.8%; 0.27 and 0.61

Conclusion:

Our study demonstrated no significant difference in lymphadenopathy, but an increase in parenchymal change in the hospitalised group. We otherwise showed similar results to literature regarding finding frequency, but poor inter-observer agreement. If the least expert reader were removed, results were comparable with available literature. This highlights the need for development and study of explicit CXR criteria for lymphadenopathy to improve the value of CXR for paediatric TB in all settings.

Lung ultrasound in pediatric pneumonia - why is it necessary to use the additional trans-abdominal approach?

J. Lovrenski; Novi Sad/RS

Objective:

To emphasize the need of lung ultrasound (LUS) technique modification, which enables detection of pneumonia in children not visualized by using solely the standard trans-thoracic approach.

Materials:

A prospective study was carried out in the regional children's hospital, and comprised a 2-year period. The inclusion criterion was US finding of pneumonia detected by trans-abdominal, and not with trans-thoracic approach. LUS examinations were performed using a combined, trans-abdominal and trans-thoracic approach. Longitudinal, transversal (intercostal), and oblique sections were used. Trans-abdominal examination included trans-hepatic and trans-splenic approach. The ultrasound probe was angulated from the most anterior to the most posterior sections while examining the lung bases by trans-abdominal approach. A pneumonia-positive LUS finding included subpleural consolidation with air-bronchogram, or with an adjacent area of interstitial/alveolar-interstitial edema. LUS was always performed before the other diagnostic modalities (chest X-ray (CXR) and computed tomography (CT)), if they were indicated by pediatrician or radiologist.

Results:

Within a 2-year period in 14 children (mean age 3.9y, SD 2.3y) the pneumonic focus was discovered using the trans-abdominal approach, while the trans-thoracic approach showed a normal LUS pattern. All the children had the clinical symptoms of pneumonia (fever and cough, with or without dyspnea/tachypnea). The auscultatory finding was positive in 4 children. CXR was performed in three children, showed a right-sided pneumonia in two, and was negative in one patient. One child had a contrast-enhanced chest CT, which confirmed a left-sided pulmonary base abscess detected during LUS examination by trans-splenic approach only (Figures 1, 2). Apart from pulmonary symptoms, there has not been any other associated diseases found, apart from otitis media in two children. Each child responded to the antibiotics treatment with resolution of infection and US signs of pneumonia. In this oral presentation we will explain and give anatomical and technical reasons for pneumonia-positive US findings within lung bases, that remained undetected by the trans-thoracic approach.

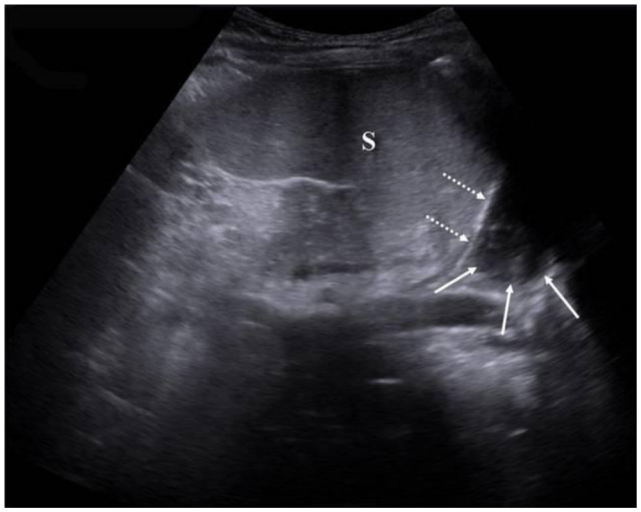

Figure 1. Trans-splenic approach to the left lung base enabled detection of the hypoechogenic area (arrows), representing abscess. Dotted arrows - left hemidiaphragm, S-spleen.

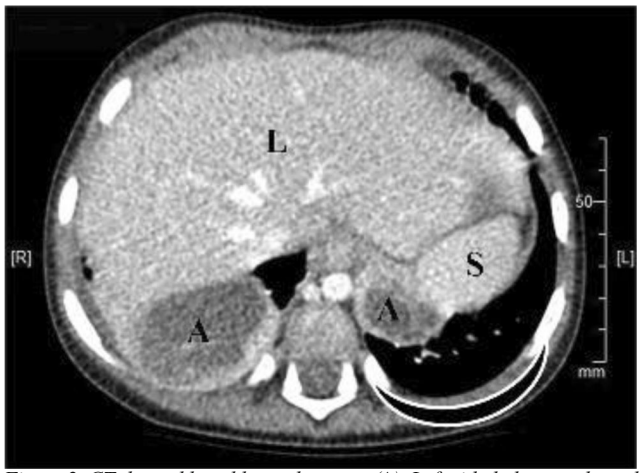

Figure 2. CT showed basal lung abscesses (A). Left-sided abscess abutted on the spleen (S), and was detected by trans-splenic US approach. It did not contact the pleural surface approachable by trans-thoracic ultrasound (black semi-lunar mark). L-liver.

Conclusion: Trans-abdominal (trans-hepatic and trans-splenic) approach should become an inseparable part of each LUS examination, along with a standard trans-thoracic approach. This modification of technique is expected to result in a further increase of LUS sensitivity in diagnosing pneumonia.

Is thoracic ultrasound really competitive to computed tomography in children – A two-year retrospective study

J. Lovrenski, K. Antolović; Novi Sad/RS

Objective:

To compare diagnostic accuracy of thoracic ultrasound (US) and computed tomography (CT) in children.

Materials:

A retrospective study was conducted in the regional children's hospital, and comprised a 2-year period. The inclusion criteria were: chest CT performed within 24h after the US examination of thorax, and US and CT examinations in the same patient performed by different pediatric radiologists. All US examinations were performed using a combined transabdominal-transthoracic approach. CT examinations were done

according to the body mass based pediatric CT protocols. Each hemithorax was analyzed separately in terms of comparison between US and CT findings. Statistical analysis included the calculation of sensitivity, specificity, positive predictive value (PPV) and negative predictive value (NPV) of ultrasound in diagnosis of pulmonary pathological entities.

Results:

Out of 176 children with chest CT, 21 of them (mean age 8,2y, SD 5,6y) fulfilled the criteria to enter the study group. Lung US showed sensitivity, specificity, PPV and NPV in diagnosis of pleural effusion: 100%, 96,4%, 91%, 100%; lung consolidation: 100%, 100%, 100%, 100%; lung abscess: 75%, 100%, 100%, 97%; and interstitial lung disease: 57%, 100%, 100%, 91%, respectively. Within 3 hemithoraces multiseptation of pleural effusion was observed by US only. Air bronchogram within lung consolidation was observed in 5 hemithoraces both by US and CT examinations. Necrotic areas within pulmonary consolidations were detected by US in 4 hemithoraces, which was later confirmed by CT examination. Lung abscesses were diagnosed in 3 hemithoraces by both US and CT. Two small lung abscesses filled with air (1 hemithorax) and bronchiectasis (2 hemithoraces) were detected only by CT examinations. Other pathological findings detected both by US and CT examinations were: congenital pulmonary airway malformation (CPAM) (1 hemithorax), pulmonary sequestration (1 hemithorax), partial pneumothorax (2 hemithoraces), hidropneumotorax (1 hemithorax), inflamed pneumatocele (1 hemithorax), hydatid cyst (1 hemithorax), pericardial effusion (2 patients), soft tissue masses of thoracic wall with initial bone destruction (2 patients), and lymphomas (2 patients) (Figures 1-3). In one patient US and CT revealed cysts and an extremely dilated bronchus within lung consolidation (pathohistological finding: CPAM type 2 combined with subsegmental bronchial atresia, and extensive bronchopneumonia). US examination, unlike CT, could not differentiate between eventration of the left hemidiaphragm and diaphragmatic hernia in one patient.

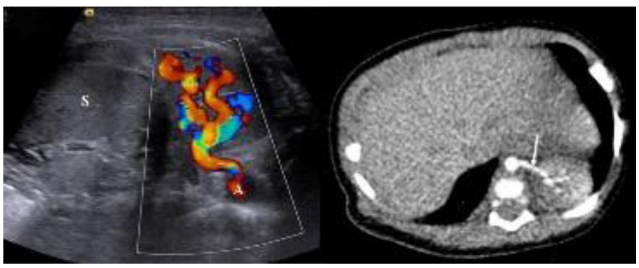

Fig. 1. Color Doppler ultrasound (left image) and axial contrast-enhanced CT in the arterial phase (right image) showed a systemic arterial supply (arrow) from the descending aorta (A) of the left lung base sequestration. S - spleen.

Fig. 2. US revealed the presence of air (arrows) and multiseptated pleural effusion (dotted arrows) within the pleural space (left image). CT showed a classic pattern of hydropneumothorax, without detection of septa within pleural space (right image).

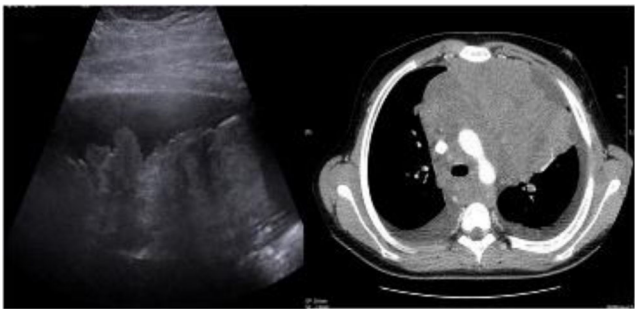

Fig. 3. US revealed a soft tissue mass within mediastinum and left hemithorax with irregular, undulating border and pleural effusion next to it (left image). Contrast-enhanced CT confirmed the finding (right image). Final diagnosis - Hodgkin's lymphoma.

Conclusion:

US and CT of thorax are diagnostic modalities of similar diagnostic accuracy, with each of them being superior in detection of certain fields of thoracic pathology.

The value of lateral chest X-rays for the diagnosis of lymphadenopathy in children with pulmonary tuberculosis

T. Poyiadji[1], N. Mahomed[1], S. Andronikou[2], H. Zar[3]; [1]Johannesburg/ZA, [2]Bristol/UK, [3]Cape Town/ZA

Objective:

To determine and compare the accuracy of frontal CXRs alone and 'combination frontal-lateral' set of CXRs for diagnosing lymphadenopathy in children with TB using patients with confirmed TB and controls without TB, and to compare findings in HIV-infected and HIV-uninfected children.

Materials:

A total of 172 children (ie: 88 children with gene Xpert confirmed TB and 84 control patients admitted with lower respiratory tract infections), which were part of a larger South African study, who had both frontal and lateral CXRs, were included. Three qualified radiologists read the CXRs in 2 separate sittings one month apart (one for the frontal X-ray alone and one for the 'combination frontal-lateral' CXRs) for the presence of lymphadenopathy. Odds ratios and 95% confidence intervals were calculated to determine the presence of lymphadenopathy using a consensus reading on the frontal CXR and frontal-lateral CXR combination according to the final diagnosis of TB. Inter reader agreement was determined using the kappa statistic.

Results:

Lymphadenopathy was reported in 86 (50%) patients on the frontal CXR alone and in 143 (83%) patients on the frontal-lateral CXR combination. 52 (60%) of the 86 patients with lymphadenopathy on the frontal CXR alone were gene Xpert positive versus 72 (50%) of the 143 patients with lymphadenopathy on the frontal-lateral CXR combination.

In all patients, the consensus reading using a frontal-lateral CXR combination resulted in a 5-fold increase (OR 4,9; 95% CI 2,9-8,4) in calling lymphadenopathy compared to using a frontal CXR only

In the gene Xpert positive group, the consensus reading using a frontal and lateral CXR combination resulted in a 3 fold increase (OR 3,1; 95% CI 1,5-6,6) in calling lymphadenopathy compared to a frontal CXR only.

Overall inter reader agreement for all 3 readers when evaluating for lymphadenopathy was 'fair' on both the frontal CXR (K= 0,2088) and the frontal-lateral CXR combination (K=0,273).

Conclusion:

The addition of a lateral view to the standard frontal CXR increased the rate of calling lymphadenopathy. However, the accuracy of diagnosing lymphadenopathy on chest X-ray as a marker for TB was poor. This poor accuracy was further hampered by only 'fair' inter reader agreement for the presence of lymphadenopathy on chest X-ray.

Pitfalls encountered when setting up a 4D CT service for dynamic airway imaging in children

S. Andronikou, M. Chopra, J. Green, E. Norbury, E. Simpson; Bristol/UK

Objective:

Dynamic 4D CT imaging in children has significant advantages over routine CT scanning, bronchography and bronchoscopy for diagnosing trachebronchomalacia because it can be performed during free breathing without anaesthesia or invasive airway access. It can also demonstrate vascular causes of tracheo-bronchomalacia in the same sitting. The technique is currently performed in 1 paediatric center in the UK. We aimed to report pitfalls encountered while setting up a dynamic 4D CT imaging service for children and report the findings of studies performed.

Materials:

Dynamic 4D CT scanning was introduced after installation of a large array (320 slice) CT scanner, applications specialist training and review of the literature. Imaging parameters in use by Greenberg and colleagues (Arkansas children's hospital, USA) were applied. Referral indications, pitfalls encountered, quality of scanning and imaging findings/diagnoses were reviewed and enumerated.

Results:

Nineteen paediatric dynamic 4D CT scans (9 females, 10 males; 11 days – 3 years 9 months; mean 12 months) were performed over 15 months.

The first 4 studies were performed without IVI contrast due to lack of experience and 13 subsequent studies were performed with contrast (Figure 1 and 2) [2 no vascular access].

Three patients were intubated. The first study was performed with the ET tube in situ which compromised the diagnosis - the subsequent 2 studies had the ET tubes withdrawn under guidance of the scanogram.

Motion artefact compromised quality in 7 cases (37%) which compromised diagnosic confidence. Studies improved over time by use of a vaccuum restrainer and presence of the radiologist within the scanner for the duration of the scan.

In 6 patients vascular anomalies were identified as the cause of tracheobronchomalacia. There was tracheomalacia in 5 (26%), bronchomalacia of the right main bronchus in 3 (16%) and of the left main bronchus in 14 (74%).

Figure 1: 3D volume rendered representation of the airway during expiration from a cine loop during free breathing without any abnormality shown.

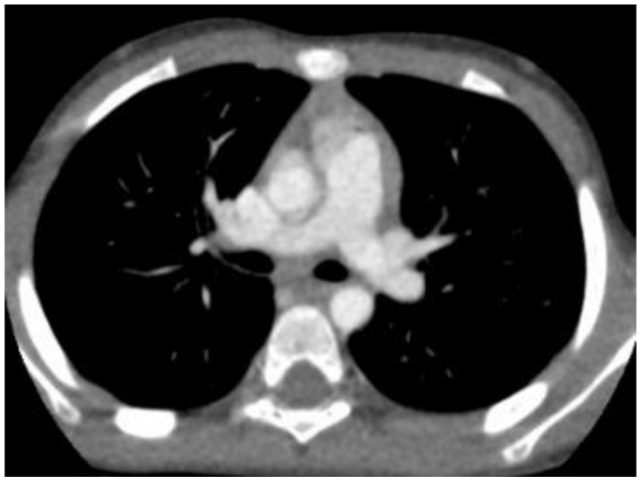

Figure 2: Source image of one of the CT volumes used to create the dynamic airway assessment for figure 1 to demonstrate the vascular anatomy in the conventional way.

Conclusion:

Major pitfalls included initial failure to perform contrasted studies for simultaneous evaluation of vessels, initial failure to withdraw the endotracheal tube, patient motion under care of nurses and clinicians, failure to appreciate the value of imaging the full lung volume while trying to keep Dose Length Product to a minimum and failure to appreciate that collapse of the airway is often in the AP plane and not appreciated on coronal slab projections - rotating 3D volume rendered images is a requirement (figure 3). Additional obstacles were initial clinician and radiologist lack of support after early failures and colleague concerns regarding the radiation dose.

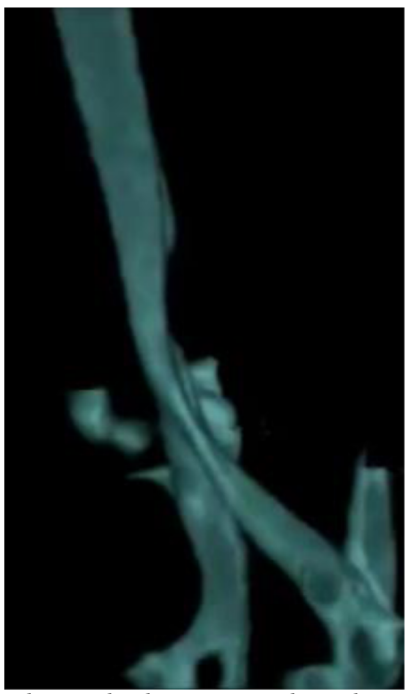

Figure 3: 3D volume rendered representation during the expiratory phase of a cine loop demonstrating the compressed and collapsed airway due to an abnormal vessel (not shown) which is only evident in the lateral view.

Assessment of airway compression on chest radiographs in children with pulmonary tuberculosis

L. Richter-Joubert[1], S. Andronikou[2], L. Workman[1], H. Zar[1]; [1]Cape Town/ZA, [2]Bristol/UK

Objective:

Diagnosis of pulmonary tuberculosis (PTB) in children relies on chest radiography, however there is wide inter-observer agreement in detecting lymphadenopathy, the hallmark of PTB. Paediatric airways are pliable, thus detection of airway compression may be a more objective criterion for the presence of lymphadenopathy.

Thus the objctive was to assess the usefulness of airway compression on chest radiographs for diagnosis of PTB in children.

Materials:

Chest radiographs of children admitted to Red Cross Children's Hospital with suspected PTB were read by two readers according to a standardised format and a 3rd when there was disagreement. Radiographs of children with definite PTB were compared to those with lower respiratory tract infection (LRTI) from another cause. The prevalence and location of airway compression was evaluated. Findings were correlated with HIV status and age. Inter-observer agreement was assessed using kappa statistic.

Results:

Radiographs of 505 children [median age 25.9 months (IQ 14.3-62.2)] were reviewed; 19% were HIV-infected. Airway compression occurred in 28.7% of 188 definite PTB cases versus 7.6 % of the 317 other LRTI cases (OR 4.9; 95%CI 2.9–8.3). The left main bronchus was the most commonly affected airway at 10.3%. A higher prevalence of airway compression (21.9%) occurred in infants compared to 13.9% in older children (OR 1.7; 95%CI 1.00–3.00). No association with airway compression and HIV infection was found. Inter-observer agreement ranged from 0.0-0.4.

Eighteen-month-old male patient diagnosed with PTB; HIV negative. Majority agreement of airway compression at LMB indicative of lymphadenopathy. Left upper lobe opacity is in keeping with a Ghon focus.

Conclusion:

There is a strong association between airway compression on chest radiographs and confirmed PTB, particularly in infants, irrespective of HIV status. However, clinical use is limited by poor inter-observer agreement.

Paediatric Ultrasound-guided Biopsies in a Tertiary Oncology Centre: Five Years Experience

N. Parvizi, M. Smedley, S. Chakraborty; Oxford/UK

Objective:

Histological diagnosis is almost always essential to guide appropriate therapy for children diagnosed with cancer. Tissue can either be obtained by surgical/open or image-guided percutaneous biopsy. The aim of this study is to assess the safety and diagnostic accuracy of ultrasound-guided biopsies in a tertiary oncology referral centre.

Materials:

A retrospective analysis of clinical data, imaging findings and histological diagnosis of patients aged 0 to 18 years between January 2010 and December 2015 was carried out. A total of 113 ultrasound-guided biopsies were performed in our institution on 110 patients. Most of the biopsies were performed in theatre with the patient under general anesthetic and with an 18-gauge spring-loaded core biopsy needle with a minimum of two cores per patient.

Results:

In 99% of lesions the needle biopsy was diagnostic. The single non-diagnostic case did not have sufficient material to make a full diagnosis and a surgical biopsy was required. Eighty-two of the biopsied lesions were malignant and 31 were benign. In no cases was a repeat biopsy required. The vast majority of the biopsies were performed within one week of request with over half performed within 3 days. All biopsies were performed without complication and in the majority of cases the patients were discharged the same day or following an overnight stay.

Conclusion:

Ultrasound-guided percutaneous biopsy is an accurate and safe technique in order to acquire tissue from suspected malignant lesions in children. These can be performed instead of or in addition to open biopsy and will often result in a shorter hospital admission and recovery time.

The role of imaging in the diagnosis of thymoma in paediatric patients with myasthenia gravis

J. Adu, T. A. Watson; London/UK

Objective:

Thymomas are exceedingly rare tumours in the paediatric age group, with only very few cases having been reported in the literature. Thymomas are commonly associated with myasthenia gravis (MG), with thymectomy being potentially curative. CT is the mainstay imaging modality for thymoma diagnosis in the adult population. While, chemical shift MR imaging can be helpful to distinguish thymoma from other anterior mediastinal abnormalities. Currently, there is no consensus on the imaging pathway for children with MG with suspected thymoma. Our aim is to review the imaging of patients who were referred to our institution for management of MG, and suggest an imaging pathway in cases where thymoma is suspected.

Materials:

We performed a retrospective search of the local PACS system of cases between 2000 and 2016 using the search terms "thymoma" and "myasthenia gravis" in the clinical indication for the study and the body of the final report.

Results:

Forty-three cases were identified using the search criteria. Eight cases were excluded owing to an absence of cardiothoracic imaging.

20/35 of all cases (57%) had chest x-rays (CXR's), of these 17/20 (85%) were normal. The three remaining patients who had abnormal CXR's went on to have CT scans, which confirmed an anterior mediastinal mass (AMM) in all three cases.

26/35 of all cases (74%) had cross-sectional imaging (MRI 15/26 cases, CT 11/26 cases). Of those, 21/26 of cases (81%) had normal studies. Specifically, all 15 MRI studies (100% of cases) were normal, while only 5/15 CT scans (66%) demonstrated an anterior mediastinal abnormality.

12/35 of all cases (34%) had both CXR and cross sectional studies. 9/12 of these cases (75%) had a normal CT or MRI. In the remaining three cases, the AMM was clearly demonstrated on both CXR and the cross-sectional imaging.

Conclusion:

In our series, radiography, CT and MRI studies were normal in the vast majority of cases. However, given that thymectomy is potentially

curative, it is appreciated that clinicians may still be keen to radiologically investigate paediatric patients with myasthenia gravis. CXR is not an efficacious imaging modality in this context, as patients with a normal CXR may be falsely negative, and patients with an abnormal CXR may undergo cross-sectional imaging regardless. We propose that MRI should be used as first line investigation for patients in this population. This approach will negate the need for ionizing radiation, maximize diagnostic yield, and facilitate surgical planning if deemed clinically appropriate.

Increased Risk of Venous Thrombosis of the Arm with Multiple Peripherally Inserted Central Catheters Insertion in Paediatric patients

R. Gnannt[1], N. Waespe[2], J. Donnellan[2], K. Liu[2], L. Brandao[2], B. Connolly[2]; [1]Zurich/CH, [2]Toronto/CA

Objective:
Peripherally inserted central catheters (PICCs) are associated with superficial and deep venous thrombosis of the arm. The impact on the incidence of developing a thrombosis of the arm when inserting a subsequent PICC remains unclear. The purpose of this study was to analyze the incidence of deep, upper limb thrombosis of repeated upper limb PICCs in children.
Materials:
The study population included all patients who underwent their first successful arm PICC insertion between January 2010 and December 2015. Subsequent ipsilateral arm PICCs were included in the analysis. Patients were followed until March 2016 or until any alternative central venous line insertion (jugular, femoral, saphenous or umbilical vein lines - because of their thrombogenic effect). For each PICC insertion the following data were collected: date of insertion and removal, weight of the patient, type of PICC (1.9Fr, 2.6Fr, 3Fr, 4Fr, 5Fr), left or right arm, and vein cannulated (basilic, brachial, cephalic). All symptomatic deep and superficial thrombosis of the arm were correlated with the PICC database.
Results:
Four thousand one hundred thirty-eight PICCs were inserted. Applying inclusion and exclusion criteria, 1955 PICCs remained for analysis. First, 2nd, 3rd, and 4th PICC insertions in the same arm were identified in 1773, 146, 30 and 6 patients, respectively. In total there were 57 upper body deep symptomatic thrombotic events diagnosed with ultrasound. A 1st, 2nd, 3rd, and 4th PICC insertion was associated with 46/1773 (incidence 2.6%), 6/146 (4.1%), 4/30 (13.3%), and 1/6 (16.7%) thrombotic events, respectively. An increasing hazard ratio was seen with higher numbers of PICC insertions, which was significant when comparing the 1st with the 3rd PICC insertion in the same arm (HR 3.9, CI95%1.3-11.4, P=0.01). After excluding any confounder, double lumen PICCs were associated with a significantly higher risk of thrombosis than single lumen (OR 5.3, CI 1.2 – 23.4, P=0.026).
Conclusion:
Repetitive PICC insertions in the same arm are associated with an increased risk of thrombosis. Double lumen PICCs are associated with a higher risk of thrombosis compared to single lumen lines.

Diagnostic performance of lung ultrasound for the detection of community acquired pneumonia in children

J.A.M. Stadler[1], S. Androunikou[2], H. Zar[3]; [1]Paarl/ZA, [2]Bristol/UK, [3]Cape Town/ZA

Objective:
Chest radiographs (CXR) are considered the first line imaging modality when investigating cases of suspected community acquired pneumonia (CAP) in children. However, CXR interpretation is limited by moderate sensitivity and specificity and poor inter- and intra-rater reliability and expose children to potentially harmful ionizing radiation. Point-of-care lung ultrasound (LUS) has been proposed as alternative to CXR for diagnosis of pneumonia in children and some published data suggest accuracy and reliability as good as or better than CXR. Most of these studies however, were performed in in-hospital settings creating a bias for selceting more severe disease and consequently more overt radiological findings. The mean age of children in most of these studies were also well above one year, while the highest incidence and risk of complicated pneumonia occurs during the first year of life. The purpose of our study was to assess the diagnostic performance of LUS for the diagnosis of pneumonia in both hospitalised and non-hospitalised children in an age group representative of the most at risk segment of the population.
Materials:
We performed a LUS on 147 children who presented with clinical signs consistent with the WHO case definition for childhood pneumonia. One hundred of these patients also had chest radiographs performed as part of routine clinical care. Inter-rater reliability (IRR) between a general practitioner and an expert paediatric radiologist were assessed for the interpretation of LUS findings consistent with pneumonia. Where radiographs were available concordance between LUS and CXR findings of pneumonia were also assessed.
Results:
Seventy-four hospitalised and 73 non-hospitalised clinically defined pneumonia cases were included with a median age of 10.3 years. Our general practitioner reported LUS findings consistent with pneumonia in 77/147 (52%) compared with 66/147 (45%) by the paediatric radiologist. Substantial overall agreement between the reporters was found with an overall agreement proportion of 0.79 and kappa=0.62. Agreement for the presence of lung consolidation or for a normal scan was also substantial with kappa of 0.67 and 0.68 respectively. Agreement on the finding of interstitial syndrome was moderate with kappa=0.45. Agreement was higher in hospitalised than in non-hospitalised cases with kappa of 0.62 and 0.56 for the respective categories. Results showing concordance between LUS and CXR findings are pending.
Conclusion:
LUS shows substantial IRR for the diagnosis of pneumonia in children. IRR are higher for the detection of consolidation or for no pathology than for interstitial syndrome. IRR also appears to be lower in clinically less severe disease.

SESSION: CASE REPORT PRESENTATION SESSION

'White-out' on plain chest radiograph- a late presentation of congenital diaphragmatic hernia

A. Fagan[1], C. Stewart[2], K. Halliday[3], S. Rao[2], D.T. Chang Kwok[2]; [1]Peterborough/UK, [2]Lincoln/UK, [3]Nottingham/UK

Objective:
Awareness of the limitations of plain radiograph and computed tomography in diagnosis of late presentation of congenital diaphragmatic hernia.
Case presentation:
A 2 year old boy presented with a 6 day history of pyrexia, vomiting and respiratory distress. He was haemodynamically stable, and had no audible air entry over his upper left thorax with occasional wheeze over the left base. He had bronchiolitis previously but did not require ventilatory support. He was otherwise well with unremarkable antenatal scans.
Initial chest X-ray showed a large air collection with fluid or soft tissue density within the left hemi-thorax and mediastinal shift to the right. Repeat X-ray (**Figure 1**) demonstrated the nasogastric tube below the diaphragm. Complicated pneumonia was suspected but as the findings were atypical a non-contrast CT was performed. This was interpreted as showing a large hydropneumothorax. (**Figure 2**). A chest drain was inserted which drained only a small volume of fluid, and a repeat chest film showed no change. CT chest and abdomen with oral and intravenous contrast revealed a Bochdalek diaphragmatic hernia (**Figure 3**). Fortunately the chest drain had not entered the herniated stomach. The hernia was surgically corrected and the child recovered well.

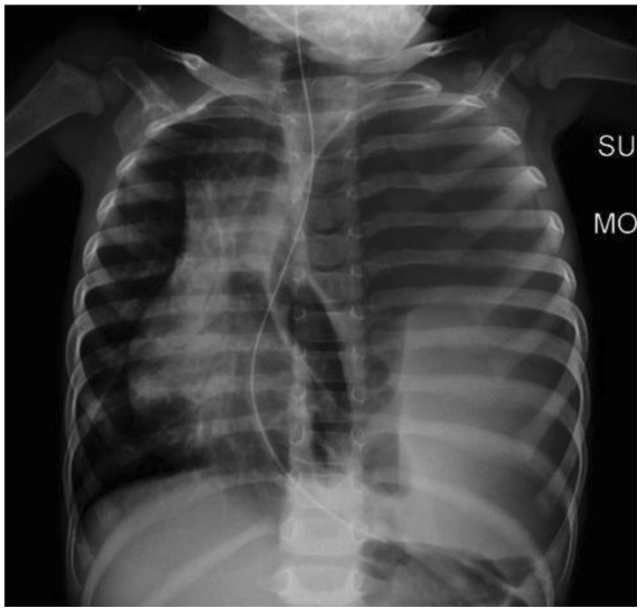

Figure 1: Chest X-ray showing fluid and air within the left hemi-thorax with mediastinal shift. The nasogastric tube passes below the diaphragm.

Figure 2: Initial CT scan showing fluid and air within the pleural space.

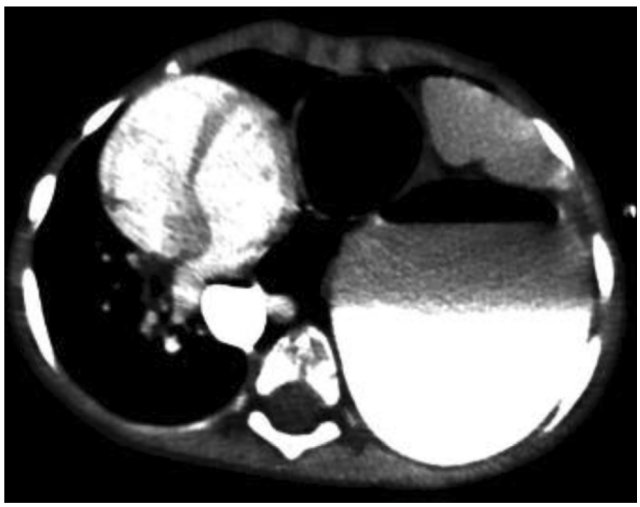

Figure 3: CT with oral and intravenous contrast shows the stomach and spleen in the left hemi-thorax.

Unique teaching points:

Bochdalek is the most common congenital diaphragmatic hernia (CDH). It is often diagnosed on prenatal ultrasound, with MRI used for confirmation.

CDH which is not diagnosed in the perinatal period may be asymptomatic and imaging findings can be confusing. Postnatal X-ray typically shows an opacified hemi-thorax with or without gas bubbles. There can be mass effect with mediastinal shift. The position of an NG tube can be helpful in localising the stomach, but in this case the infradiaphragmatic position of the tube gave false reassurance. In neonates, the position of an umbilical venous catheter may demonstrate abnormal location of the liver.

Computed tomography generally demonstrates a posterolateral defect (foramen of Bochdalek), which is located on the left in 80% of cases. CT is useful for excluding lung masses or bronchopulmonary foregut malformations, which may appear similar to CDH on X-ray. CT can also identify anatomical abnormalities associated with CDH. Late presenting CDH is often misdiagnosed as pleural effusion or pneumothorax. There are other case reports published where chest drains were inserted before CDH was diagnosed.

It is important to keep CDH in mind as a potential cause of unilateral hemithorax opacification, even in previously asymptomatic older children. CT with oral contrast can be useful in diagnosis.

Ovarian tuberculosis with peritoneal dissemination mimicking ovarian tumor with peritoneal seeding

D. Grassi, V. Tostes, A. Duarte, S. Abib, H.M. Lederman; Sao Paulo/BR

Objective:

Consider tuberculosis (TB) as a differential diagnosis whenever the case enrolls in an endemic region.

Case presentation:

Female, 13 years old adolescent, who presents with abdominal pain and weight loss. Abdominal sonography was performed in a public family practice location and bilateral ovarian masses were detected. She was referred to an oncology pediatric facility for further investigation. Abdominal MRI and chest CT were performed where dissemination through the peritoneal and mesenteric lymph nodes could be detected; chest CT was normal. The patient underwent surgical intervention for diagnosis and on pathology the findings in the bilateral ovarian masses were secondary to TB involvement.

Sonography showing bilateral pelvic masses.

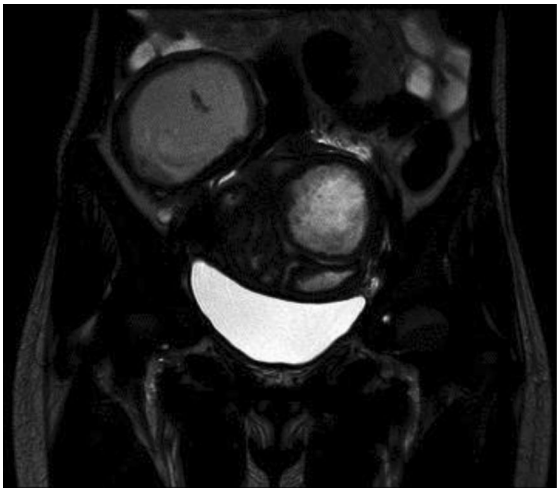

Bilateral ovarian masses.

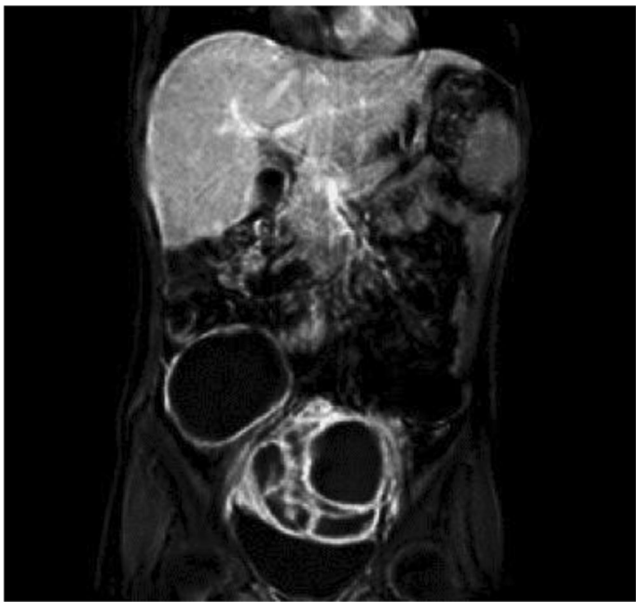

T2- weighted coronal overview bilateral ovarian masses.

Unique teaching points:
Whenever a case enrolls in an endemic region of tuberculosis, it is important to consider it as a possible differential diagnosis. In this case, the initial presentation mimicked ovarian tumor with mesenteric seeding. However, only after surgical approach was possible to diagnose ovarian tuberculosis with mesenteric lymph nodes and peritoneal involvement. Retrospectively, patient's uncle was discovered as having pulmonary TB.

Langerhans'-cell histiocytosis with thoracic involvement in infant and young child: CT findings
S.-L. Shih[1], K. Tsai[1], W. Huang[2], F.-S. Yang[1]; [1]Taipei/TW, [2]Taitung/TW

Objective:
The purpose of the study was to evaluate the CT changes of thorax in the patients with Langerhans'-cell histiocytosis.

Case presentation:
Case 1
The 3-month-old female infant presented with generalized hemorrhagic macular rash over the skin for 2 months. The laboratory findings showed hemoglobin 7.8gm/dL (normal 11.0~16.0gm/dL). The chest radiograph showed bilateral reticulonodular infiltration. High-resolution computed tomography (HRCT) of chest showed multiple cystic-like lesions (1-6mm) in the right middle and bilateral lower lobes. The pathological report was Langerhans'-cell histiocytosis after skin biopsy from upper chest. Then she was on scheduled chemotherapy. She was in remission after one-year treatment.
Case 2
The 1y10m-old girl presented with fever for 3 months. The physical examination revealed hemorrhagic-macular rash over the skin in the anterior chest wall and hepatosplenomegaly. The laboratory findings revealed albumin 2.5g/dL (normal 3.8-4.7g/dL) and hemoglobin 7.0g/dL (normal 11.0-16.0g/dL). HRCT of chest showed multiple cystic-like lesions (1-6mm) in the bilateral lower lobes with left pleural effusion as well as multiple osteolytic lesions in the vertebral bodies of T7, T8, T11 and T12. The pathological report was Langerhans'-cell histiocytosis after skin biopy from anterior chest wall. Then she was on scheduled chemotherapy. She was doing well 10 years after treatment.
Case 3
The 1y6m-old girl presented with yellowish discoloration of skin for one month. The laboratory findings revealed direct/total bilirubin 4.4/7.9mg/dL (normal 0.1-0.5/0.3-1.2mg/dL), GOT 223IU/L (24-46IU/L) and GPT 220IU/L (12-27IU/L). The chest radiograph revealed enlargement of upper mediastinum. The CT scan of chest and upper abdomen showed punctuate calcification with heterogeneous enhancement in the upper mediastinum and several minute cysts in the lower lobes of lung (HRCT) as well as dilatation of bilateral intrahepatic bile ducts in the liver. The pathological report was Langerhans'-cell histiocytosis after biopsy from thymus and liver. Then she was on scheduled chemotherapy and got initial response.
Unique teaching points:
Langerhans'-cell histiocytosis affecting the lungs and thymus may be in isolation or as part of a multiorgan disease. The pulmonary changes on CT scan may not have corresponding respiratory symptoms. CT scan of thorax may have multiple minute cysts (1-6mm) in the lungs, pleural effusion, calcification in the thymus and osteolytic lesions in the thoracic spine.

Case of fungal infection of the soft tissue in a child with acute myeloid leukemia (ultrasound aspects of diagnosis)
I. Begun, S. Kondaurova; Minsk Region/BY

Objective:
Early diagnosis of fungal infections of the tissues is essential for a successful and complete recovery. We describe a clinical case of fungal infection of the soft tissue in a child with acute myeloid leukemia (AML). Ultrasound were made for the characteristics of the structural changes in the area of interest to perform biopsies followed by bacteriological culture studies.
Case presentation:
Patient K., 13 years old, diagnosed with AML, from which after a course of induction chemotherapy with neutropenia about 3 weeks on the skin of the foreskin appeared removable hard white coating. Cultures of plaque it possible to establish the presence of fungi of the genus Trichosporon spp. After 4 days, there were hyperemia, compaction and ulceration of the glans penis, which led to extensive tissue defects. With help ultrasound were determined the structural deformation of the glans penis with the pronounced around changed tissues vascularization. After 7 days in the rear surface projection of the left thigh and the lateral surface of the left calf were defined erythematous papules which progressed to ulceration with central black scab. By standard

ultrasound were visualized: subcutaneous nodal education oval 1,0x0,4 sm on hip and echogenic skin thickened portion having an average degree of severity of dorsal acoustic shadow on the lower leg (weakening of the signal behind scab). In cultures of biopsies of subcutaneous foci were revealed fungi of the genus Trichosporon spp too. The patient received the combination treatment (intravenous liposomal amphotericin B and surgical rehabilitation of lesions of glans and corpus cavernosum of penis). After the stabilization of patient state the treatment of the underlying disease was continued.

Unique teaching points:

For some patients, lesions of superficial tissues may be the only sign of systemic fungal infections, and rapid recognition of these lesions may contribute to early diagnosis and treatment. Ultrasound examination in such a situation naturally becomes an main imaging tool and by choice method. The scanning High-resolution of foci of the thigh of the patient K. in grayscale made possibility to determine the configuration consisting of the central echogenic focus surrounded by a hypoechoic rim (Fig. 1) with peripheral changes in the type of "infiltrative" according by the active fungal infection at the exit of cytopenia. Duplex and triplex ultrasound scanning were indicating to the perifocal vascularization with low level vascular resistance around of the affected area (see Fig.2-3).

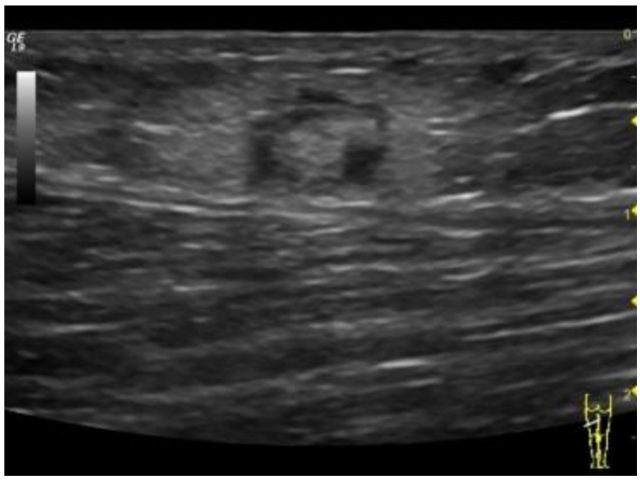

Fig. 1. Grayscale mode. The configuration of the lesion.

Fig. 2. Duplex scanning. Perifocal vascularization.

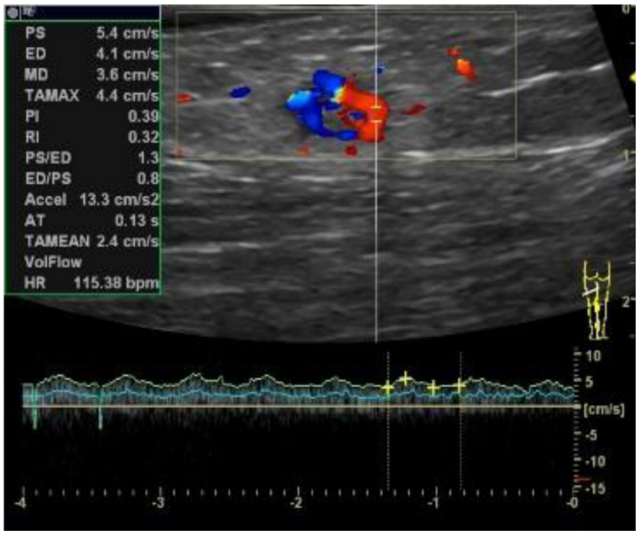

Fig. 3. Triplex scanning. Quantitative assessment of perifocal blood flow.

Unfortunate outcome of the first infantile hepatic hemangioendothelioma to be diagnosed in the district of Bethlehem due to lack of medical experience with such rare cases

R. Albad; Bethlehem/PS

Objective:

To increase knowledge and awareness of rare cases and diseases in order to be able to better manage and treat patients in the future.

Case presentation:

An 3-month-old female was presented to our hospital with abdominal distention that increased in the past 3 months associated with low-grade fever, loss of weight and mild respiratory distress.

Abdominal ultrasonography revealed an enlarged liver with multifocal hypoechoic lesions scattered all over the liver (fig 1).

A CT scan with IV contrast (MRI was not available at that time in our district) revealed severe hepatomegaly with the presence of multiple, variable in size, hepatic hypodense lesions which had peripheral (ring) enhancement after contrast injection in the arterial phase (Fig 2).

Progressive centripetal filling in portal phase is seen and in the delayed images many of the lesions were completely filled (Fig 3).

Reduction in the aortic caliber (mid-aortic syndrome) below the level of celiac branch was noted.

A diagnosis of hemangioendothelioma was made although liver biopsy was not done due to fear of hemorrhage.

Alternative diagnosis to infantile hemangioendothelioma in this age group is hepatoblastoma, mesenchymal hamartoma and metastatic neuroblastoma.

The patient was transferred to another city to a hospital with pediatric oncology department for follow up and treatment. Unfortunately the lack of experience and knowledge of such rare cases led to mismanagement and delayed treatment and after less than 2 months the patient was brought back to our hospital to the pediatric ICU due to deterioration of her status due to congestive heart failure. Unfortunately the patient died shortly afterwards.

Hemangioendothelioma is twice as common in girls and can have complications due to high output CHF secondary to arteriovenous shunting

Hemangioendotheliomas tend to involute spontaneously without therapy over a course of months to years. They are followed with sequential ultrasounds. Medical therapy is reserved for severely symptomatic lesions (e.g. anemia, consumptive coagulopathy, high-output CHF) and includes high-dose steroids or alpha-interferon. In cases of failed medical management, surgical resection should be performed. If partial hepatectomy is not technically achievable, transarterial embolization should be used either as definitive therapy or as a temporizing measure until liver transplantation is possible.

Fig 1

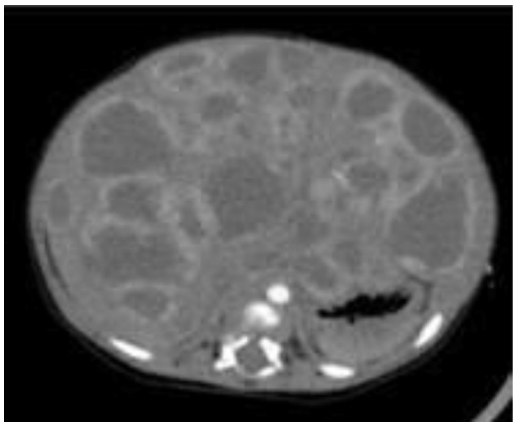

Fig 2

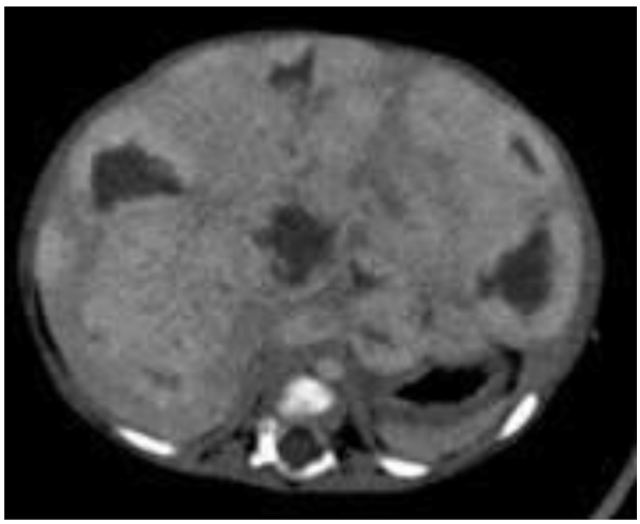

Fig 3

Unique teaching points:
The sad outcome of this case was mainly due to mismanagment due to lack of medical experience and knowledge of such rare cases so we suggest that such rare cases should be catalogued in a national data bank for future consultation and teaching purposes.

Fatal Outcome of Acute Gastric Dilatation Causing Acute Abdomen Compartment Syndrome in a Child: A Case Review
C.S. Yoon; Seoul/KR

Objective:
To describe and review presumed acute abdominal compartment syndrome in a child.
Case presentation:
A 3 years and 5months old boy was admitted to emergency room due to abdominal distention. He suffered abdominal pain and vomited since yesterday after lunch. On physical examination, his abdomen was rigid and distended. Body temperature is 37.2 °C. The white cell count was increased (24,140/μL). ESR is 25 mm/hr and C-reactive protein was 123.4 mg/L. Creatinine was increased (1.24mg/dL). Amylase and lipase were increased (164 U/L and 104 U/L respectively). Prothrombin time was prolonged (15.5 sec). Plain abdomen radiograph shows markedly distended stomach with air-fluid level (Fig.1). First trial of nasogastric tube insertion was failed due to kinking of tube at gastro-esophageal junction. Contrast-enhanced abdomen CT scan shows marked distension of stomach with large amount of food materials and intraluminal air with prominent external compression in the duodenal 3rd-4th junction. Esophageal air distention is also markedly noted with L-tube insertion. No opacification of large vessel with contrast media, without contrast enhancement of spleen, pancreas and left kidney is noted (Fig.2). Prob. markedly compressed and poorly defined lower abdominal aorta with faintly visible both common iliac arteries and femoral arteries. After CT scan, nasogastric tube exchange was performed due to poor drainage of gastric fluid. About 700cc of gastric fluid was drained. However, sudden cardiac arrest of the patient was developed. Although vigorous cardiopulmonary resuscitation was performed, the patient was died.

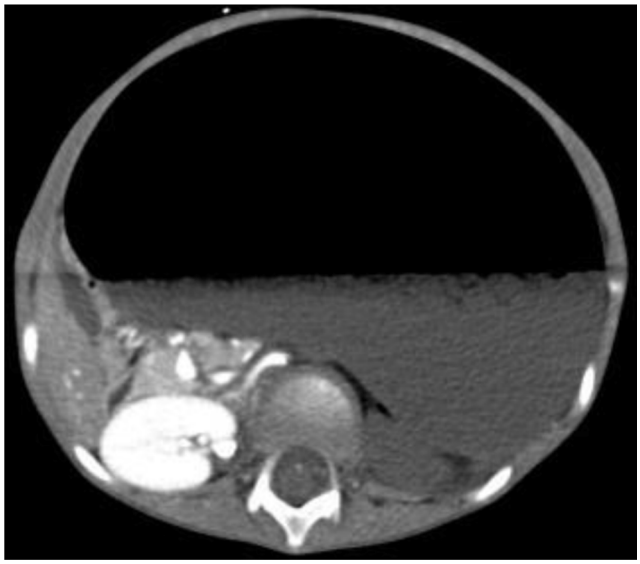

Unique teaching points:

Acute abdomen compartment syndrome is a very serious and life-threatening disease. As soon as possible, rapid diagnosis and adequate treatment are necessary for good prognosis. Delayed diagnosis and treatment may result in fatal outcome.

Pleuroperitoneal fistula in a pediatric patient with primary hyperoxaluria type 1

W.P. Chu; Hang Hau/HK

Objective:

To illustrate the imaging features of pleuroperitoneal fistula in a pediatric patient suffering from primary hyperoxaluria type 1

Case presentation:

An 11-year-old girl with the history of primary hyperoxaluria type 1 was repeatedly admitted to the hospital for recurrent right pleural effusion despite chest drain insertion. The right pleural fluid was transudative in nature and the microbiological cultures for bacteria and mycobacterial species were negative. The radiographic examination **[Figure 1]** showed moderate right pleural effusion and features of oxalosis including bilateral cortical nephrocalcinosis and generalized increased in bone sclerosis. Delayed planar images of the peritoneal scinitigraphy **[Figure 2]** obtained 3 and 5 hours after injection of Technetium-99 m suphlur colloid found diffuse tracer activity at the right hemithorax, suggestive of pleuro-peritoneal fistula. The patient subsequently required thoracoscopy and surgical decortication at the right hemithorax and renal transplantation.

Primary hyperoxaluria is due to defective glyoxylate metabolism and results in increased synthesis of oxalic acid. Cortical nephrocalcinosis and diffusely increased bone sclerosis are characteristic radiographic features. Pleuroperitoneal fistula is unusual in patients without peritoneal dialysis. Possible cause in this patient is increased intra-abdominal pressure related to portal hypertension and cirrhosis.

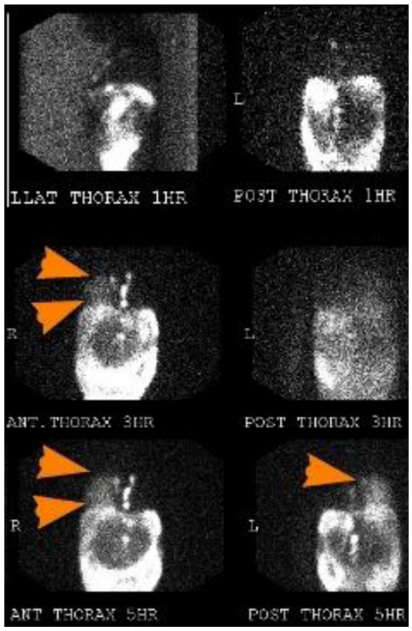

Figure 2. Delayed planar images of the peritoneal scinitigraphy found diffuse tracer activity at the right hemithorax (orange arrowheads)

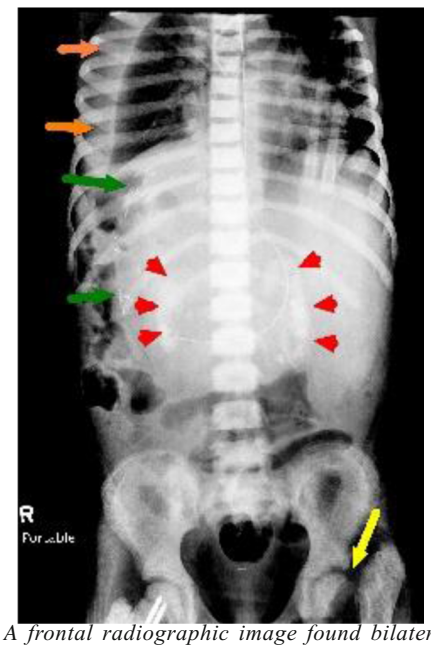

Figure 1. A frontal radiographic image found bilateral cortical nephrocalcinosis (red arrowheads), pathological fracture of the left proximal femur (yellow arrow) and surgical clips related to liver transplantation (green arrows)

Unique teaching points:

High index for suspicion of pleuroperitoneal fistula is necessary for patients with primary hyperoxaluria and recurrent unilateral pleural effusion. Imaging work-up of pleuroperitoneal fistula includes peritoneal

scintigraphy and CT peritoneography. Peritoneal scintigraphy allows dynamic and delayed imaging and can confirmation of the diagnosis.

Osteosarcoma with Pulmonary Intra-arterial Tumor Embolism Metastasis

A. Alzaher, F. Alzaher; Dammam/SA

Objective:

Osteosarcoma rarely invade the veins and small number of cases has been reported with venous invasion at the presentation. However, to our knowledge, no case has been reported with venous invasion and isolated distal metastasis as intra-arterial pulmonary embolisms. We are presenting a case of pediatric pelvic osteosarcoma with venous invasion and pulmonary arterial tumor embolisms as isolated distant metastasis at the presentation.

The purpose of this case report is to describe the rare presentation of distant metastasis as isolated pulmonary arterial embolism that might be overlooked radiological. Additionally, such tumor embolism might cause respiratory symptoms and differentiating tumor emblism from pulmonary thromboembolism is crucial to avoid the unnecessary anticoagulation.

Case presentation:

Fourteen year old boy who presented with 3 months history of right hip and lower limb pain after trauma. This was associated with lower limb swelling. The plain radiography showed right pelvic iliac bone aggressive mass, along with lobulated, soft-tissue components, extensive areas of osseous matrix, and malignant periosteal reaction. The patient could not tolerate the MRI and CT scan was performed and it showed that the mass was invading the right external and internal iliac vein with imaging appearance was most consistent with osteosarcoma.

Patient staging was then carried on with MRI under anesthesia and chest, abdomen and pelvic CT scan. The unenhanced and IV contrast enhanced chest CT scan showed multiple beaded expansion of sub segmental pulmonary arteries with soft tissue destinies and calcification suggestive of intra-arterial pulmonary tumor embolisms. There was no isolated pulmonary nodule or any other site of distant metastasis.

Unique teaching points:

We present this case to increase the awareness of isolated intra-arterial pulmonary tumor embolisms as osteosarcoma metastasis especially with the present of venous invasion. Additionally, such condition might be with respiratory symptoms and differentiating the tumor embolism from pulmonary thromboembolism is crucial to avoid the unnecessary anticoagulation.

Endovascular embolization of left gastric artery pseudoaneurysm for acute upper gastrointestinal hemorrhage in a child with pancreatitis

J. Donnellan, P. Muthusami, M. Temple; Toronto/CA

Objective:

To describe transcatheter embolization with N-Butyl cyanoacrylate (NBCA) of left gastric artery (LGA) pseudoaneurysm in a 14-year old child with acute upper gastrointestinal (GI) bleed.

Case presentation:

A 14-year old boy with acute myelodysplastic syndrome presented with recurrent, acute severe anemia (hemoglobin 68 g/dL) and melena. His past history was significant for bone marrow transplant twice followed by graft-versus-host-disease of intestines, bilateral lung transplants for bronchiolitis obliterans, renal failure, scleroderma and acute pancreatitis. CT angiography performed previously did not identify active extravasation. Several days before, upper GI endoscopy had demonstrated ulceration of the greater curvature of the gastric wall that was initially treated with epinephrine injection and surgical clip placement. At the time of referral, endoscopic interventions were unsuccessful leading to progressive clinical deterioration. A decision was taken to proceed to angiography to isolate the arterial source of hemorrhage, with an intention to embolize, if feasible.

Catheter angiography via transfemoral 4Fr access revealed a left gastric artery pseudoaneurysm with active extravasation into the gastric lumen through the ulcer. After selecting the feeding pedicle of the left gastric artery with a microcatheter, the pseudoaneurysm was embolized using 40% NBCA in lipiodol, resulting in complete angiographic obliteration of the bleeding source.

On repeat CBC 6 hours post-procedure, the hemoglobin had increased from 80 to 115 g/dL. The patient remained hemodynamically stable in the intensive care unit. There is no evidence of bleeding recurrence 25 days later.

Unique teaching points:

Catheter angiography can define the bleeding source with greater accuracy than CTA in children. There should be a low threshold to perform catheter angiography, with an intention to proceed to treatment. NBCA embolization is a feasible and effective option for treatment of acute GI bleeding in children.

A case of neonatal hemochromatosis

G. Perucca, P.L. Calvo, R. Cotti, G. Di Rosa, G. Gandini; Torino/IT

Objective:

Showing the main clinical and radiological features of neonatal hemochromatosis.

Case presentation:

An infant born by cesarean section at 38 weeks of gestation, after nonreassuring cardiotocoghraphy, with meconium aspiration at birth, severe hepatocellular failure with hyperbilirubinemia, signs of hemorrhage, edema, ascites, hypoglycemia, increased ferritin values, and lactic acidosis was referred for ultrasound and magnetic resonance.

Both examinations showed signs of liver cirrhosis with portal hypertension; in addition, on T2-weighted images and gradient-echo images, the signal intensity of the liver and the pancreas was lower than that of the spleen and skeletal muscle, a finding consistent with abnormal iron deposition in those organs.

A biopsy of the lower lip confirmed the diagnosis of neonatal hemochromatosis.

Unique teaching points:

Although the diagnosis may be suspected clinically, it must be confirmed by demonstrating the generalized iron overload affecting, among other organs, the salivary glands, liver and pancreas, with sparing of the reticuloendothelial system.

The underlying cause may be associated with an an alloimmune mechanism; thus, intravenous immunoglobulin during gestation is administered in selected cases to prevent the severity of neonatal hemochromatosis. Diagnosis is then crucial not only for management of the affected infant, but also for prevention in the future offspring.

Fishing for the answer – A rare case of paediatric exogenous lipoid pneumonia secondary to fish oil aspiration

H. Moodley, D. White, G.D. Baker; Johannesburg/ZA

Objective:

Lipoid pneumonia is a rare condition caused by the intrapulmonary accumulation of endogenous or exogenous fat containing substances. In the acute exogenous form secondary to aspiration of oil, it is important to make the diagnosis and remove the causative agent to prevent or arrest the progression of pulmonary fibrosis. Radiopathological findings usually prompt the diagnosis, as aspiration of mineral oils is usually unnoticed due to the lack of reactive airway symptoms and patients present with vague chronic respiratory symptoms.

Case presentation:

We present the clinical, radiological and pathological correlation of exogenous lipoid pneumonia in a 4-month-old male patient with recurrent respiratory tract infections. A CT chest demonstrated an extensive crazy paving pattern of the dependent lung segments bilaterally. The lung biopsy findings of occasional intra - alveolar macrophages with larger

foamy cytoplasmic vacuoles, raised the possibility of an exogenous lipoid pneumonia secondary to aspiration. On further history, the patient was found to have been fed fish oil by his mother, confirming the diagnosis.

Unique teaching points:

The rare diagnosis of exogenous lipoid pneumonia can be confirmed on CT chest by measuring the Hounsfield Units in the most hyperdense components of consolidation (typically -150 to -30 HU). Histopathological confirmation can be obtained provided that the specimens are not embedded in paraffin.

The possible role of visual evaluation of DWIBS in childhood renal masses based on our five cases

E. Varga, G. Rudas; Budapest/HU

Objective:

Nowadays, the diffusion-weighted MRI has a great importance not only in the differential diagnosis and follow-ups of childhood renal tumors, but in the early detection of recurrence of the disease as well. The DWIBS with appropriate b-values and the ADC calculation can be helpful in distinguishing between benign and malignant processes. However, the ADC calculation is a time consuming method and in addition, there are cases when we cannot use this technique, but we can still apply the visual evaluation of diffusion.

Case presentation:

Between 2013-2016, we had 5 cases in which the visual assessment of DWIBS was the best method which helped to make the appropriate therapeutic decisions. Left kidney of an infant with nephroblastomatosis was removed because of an arising Wilms tumor. 2,5 years later, in the contralateral kidney, a small area of diffusion restriction appeared on the DWIBS in one of the cystic residual lesions, but the anatomic sequences haven't showed any changes comparing with the previous examinations. In another patient with Beckwidt-Wiedemann syndrome, the follow-up ultrasound examination showed a little bulging of the surface of the left kidney. Accordingly, the MRI showed a barely distinguishable nodule, but the DWIBS referred to a Wilms tumor. In a 17-month-old child, more nodules were visible in both kidney on the DWIBS than on other sequences. With the help of visual evaluation of DWIBS, we were able to detect the malignant lesion easily and quickly, among a lot of cystic and solid nodules of the kidneys in a seven years old patient with sclerosis tuberosa. An 8-month-old infant was followed with a benign cystic renal disease and a new small solid nodule was found on the last ultrasound examination. Instead, the visual assessment of DWIBS indicated a multilocular cystic Wilms' tumor.

Unique teaching points:

The diffusion-weighted MRI is suitable for differentiate benign and malignant renal lesions in children. The DWIBS (with appropriate b-values) and the ADC calculation are very sensitive methods in pediatric oncoradiology. The ADC calculation is a long process and – as our cases demonstrated - we cannot apply in every cases. The visual evaluation of DWIBS is a time saving method which is spared from limitations of ADC histogram-based assessment, so it may become very useful in the everyday practice. We can use it in the differential diagnosis and follow-ups of childhood renal tumors and we can detect the recurrence of the malgnancy very early and easily.

MR Urography in a 9-years-old female with unusual urinary dribbling

M.C. Terranova, C. Tudisca, D. Narese, G. Li Voti, S. Salerno; Palermo/IT

Objective:

Congenital anomalies of kidney and urinary tract (CAKUT) occurs in up to 3.2% of infants, and clinically they can range from asymptomatic patients, in which anomaly is detected incidentally even in adulthood, to ante-natal or post-natal mortality due to bilateral kidney agenesis or acute renal failure.

DMSA Renal scintigraphy is considered gold standard, for evaluation of those cases electable for surgery, in order to assess renal function, depict and locate ectopic kidney and guide surgical management, but has the important limit of radiation exposure and may undetect poorly functional renal moieties.

The advent of modern Magnetic Resonance technics proven to be able to assess anatomical malformations and renal function, overcoming the limits of DMSA Scintigraphy, may be used as a valid alternative, especially in vulnerable pediatric population.

We herein describe a case of a young girl with small left renal bud and ectopic ureter, draining in vagina, discovered by MR and undetected by previous DSMA Scintigraphy.

Case presentation:

A 9 years old girl was referred for continuous urinary dribbling, after starting toilet training, with normal bladder voiding pattern, unrelated to any physical and psychological events, and no history of urinary tract infections.

Physical examination revealed vaginal septa and micturition training was practiced, with no symptoms improvement.

Abdominal US study was performed, reporting empty left renal fossa and hypertrophic right kidney; no ectopic kidney nor sign of urine stasis or other urogenital anomalies were detected, and DMSA Renal scintigraphy was planned.

It depicted only normal right kidney radionuclide uptake but no evidence of left renal or ectopic renal tissues activity.

Patient then underwent MR evaluation for suspected genito urinary malformation, that revealed a small cystic formation, with a slight cortex, at the level of the IV lumbar vertebra - that represented the left immature renal bud - supplied by a short fluid-filled tubular structure, located postero-medially to the bladder - that configured the left ectopic ureter, draining in left vaginal wall. Bladder was normal, and regularly connected with the right orthotopic ureter (FIG 1).

Pre-surgical cystoscopy and vaginoscopy, followed by left ascending urethrogram were performed, confirmed previous MR findings, and patient underwent successfull laparoscopic left nephron-ureterectomy.

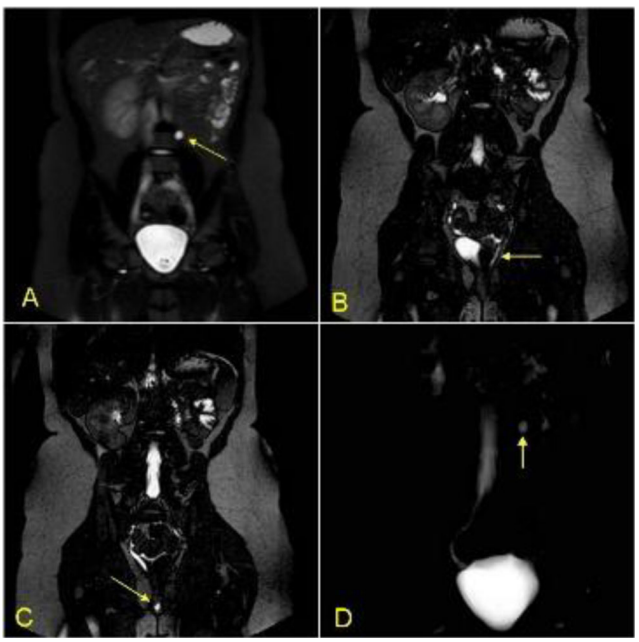

FIG 1A. T2 SPAIR CORONAL: Right orthotopic kidney, and left renal bud (arrow); 1B-C. Ectopic left ureter, that drains caudally to the bladder; 1D. Radial T2 MIP post-processed. Right orthotopic ureter, and left renal bud (arrow).

Unique teaching points:
MR Urography has proven to be a rapid, safe, radiation free, systematic diagnostic tool especially in the evaluation of poorly functioning renal systems, and of collecting system, bladder and ureteral abnormalities, overcoming the limits of conventional imaging technics

Agenesis of the dorsal pancreas: Case report

C. Lanza, G. Pieroni, L. Amici, A. Giovagnoni; Ancona/IT

Objective:
Agenesis of the dorsal pancreas (ADP) is a rare malformation. Since 1911 and until 2008, 53 cases have been reported. Majority of the patients with this anomaly are asymptomatic or associated with abdominal pain, hyperglycemia, diabetes mellitus, and acute or chronic pancreatitis.
Case presentation:
We present a case report of a 11-year-old girl with ADP, diagnosed incidentally during radiological evaluation for abdominal pain. She was hospitalized in the pediatric department for recurrent abdominal pain for the past 10 months. There was no history of nausea, vomiting or trauma.
Biochemical investigations showed a normal random serum glucose, serum amylase levels slightly increased (149 U/L; reference value 28-100 U/L) and slightly elevated serum pancreatic lipase levels (138 U/L; reference value 22-51 U/L). The day after serum amylase levels decresed up to 80 U/L and lipase levels to 78 U/L.
US revealed increased - size pancreatic head with normal contour and echotexture with no parenchymal calcification or duct dilatation. The body and the tail of the pancreas were poorly visualized. MR imaging examinations revealed only a partial visualization of the pancreas: the pancreatic head and the uncinate process were visualized with defined margins with peripancreatic fat stranding, but the distal neck, body, and tail of the pancreas were absent.
On MRCP, the dorsal pancreatic duct of Santorini and the minor duodenal papilla could not be visualized. The ventral pancreatic duct of Wirsung and the common bile duct were normal and clearly visualized. These findings were compatible with complete ADP, eliminating the need for ERCP.
Unique teaching points:
The clinical presentation of DPA varies greatly ranging from incidental detection on X-ray, surgery or autopsy through to the development of a ductal adenocarcinoma of the pancreas. Abdominal pain and diabetes are the most frequent clinical manifestations reflecting exocrine and endocrine insufficiency as most of the islands of Langerhans are located in the tail of the pancreas. There have also been reports of an increase in the size of the remnant pancreas and recurrent acute pancreatitis as a form of presentation. Diagnosis requires confirmation of the absence of the neck, body and tail of the pancreas and duct of Wirsung using endoscopic retrograde cholangiopancreatography (ERCP) or MRCP.

SESSION: SCIENTIFIC SESSION: FETAL AND POSTMORTEM

Malformations of cortical development associated with corpus callosum dysgenesis (CCD): Diagnostic value of foetal MRI in prenatal counseling

A. Antonelli, S. Bernardo, E. Marchionni, V. Vinci, M. Saldari, A. Pizzuti, C. Catalano, L. Manganaro; Rome/IT

Objective:
To define the diagnostic role of foetal MRI in the assessment of cortical dysplasias and other malformations of the developing cerebral cortex, in foetuses with different forms of Agenesis of the Corpus Callosum (ACC).
Materials:
One hundred four MR images of foetal CNS with a US suspicion of ACC were retrospectively reviewed. Foetal MRI was performed at 1.5 T Magnetom Avanto (Siemens, Erlangen, Germany) without mother-foetal sedation. Polymicrogyria, lissencephaly, schizencephaly, subependymal heterotopias and migration disorders were evaluated. Cortical findings were compared to three types of ACC (complete agenesis, partial agenesis and hypoplasia). Genetic tests were collected. Postnatal MRI or foetopsy for diagnostic confirmation were collected.
Results:
On 104 foetuses, fetal MRI was able to detect cortical malformations in 32 cases even in early gestational ages (<24GW). The mean Gestational Weeks (GW) at MR diagnosis was 26 (range: 22-36GW). MR imaging found 13/32 polymicrogyria, 7/32 lissencephaly, 5/32 schizencephaly, 4/32 subependymal heterotopias and 3/32 neuronal migration disorders. 22/32 had complete ACC, 4/32 had partial ACC and 6/32 had CC hypoplasia. Statistically significant correlations (p<0.005) between complete ACC, focal polymicrogyria and cortical dysmorphism affecting frontal lobes were found.
Conclusion:
Fetal CNS MRI can detect cortical development malformations in complex ACC, providing further information for the clinician to assess the severity of perinatal outcome. MRI is a useful tool in improving obstetrical genetic prenatal counselling to predict pregnancy and foetal prognosis.

Recognition of Neonatal Lymphatic Flow Disorder: Fetal MR Findings and Postnatal Dynamic MR Lymphangiogram Correlation

D.M. Biko, J.A. Johnstone, Y. Dori, M. Itkin, E.R. Oliver, T. Victoria; Philadelphia/US

Objective:
Clinical signs of the Neonatal Lymphatic Flow Disorder (NLFD) are a combination of the congenital chylothorax, chylous ascites and body edema. It can present as neonatal chylothorax (NC), neonatal chylous ascites, or congenital lymphatic dysplasia (CLD). The prenatal appearance of lymphangiectasia has been described as nutmeg lung. The purpose of this study is to describe prenatal and postnatal imaging features and outcomes of neonates with NLFD.
Materials:
This is a retrospective case series of neonates in our institution that had pre- and postnatal lymphatic imaging and NLFD. All patients had prenatal imaging (fetal MRI and US) and underwent postnatal dynamic contrast MR lymphangiography (DCMRL) with a three-dimensional (3D) T2 SPACE. Conventional lymphangiography (CL) when performed was also reviewed.
Results:
Six patients with NLFD were identified (3 with NC and 3 with CLD). One patient had congenital heart disease. Nutmeg lung was seen in all patients on fetal MRI and 4 patients on fetal US. 5/6 patients had pleural effusions, 2/6 had ascites and 1/6 had body wall edema prenatally. Postnatal MRI with 3D T2 SPACE revealed soft tissue edema in the upper chest and neck (5/6 patients), mediastinal edema (5/6 patients), interstitial lung edema (6/6 patients), retroperitoneal edema (5/6 patients), and ascites (6/6 patients). DCMRL demonstrated lymphatic flow to the pleural space (5/6 patients) and to the abdominal cavity (1/6 patients) and dermal backflow (2/6 patients). CL was performed in 4 patients, all of which had collateral lymphatic flow to the lung. Lymphatic intervention was performed in 3 patients, lipiodol injection for 2 patients with NC and thoracic duct embolization (TDE) for 1 patient with CLD. Mean hospital duration in the first 4 months of life was 51 days (range 5-113) for NC and 105 days (range 75-120) for CLD. All 3 patients with CLD died after 4 months of age due to respiratory distress including the patient that had TDE and both with findings of dermal backflow. The pleural effusions in the 2 patients with NC resolved post lipiodol injection and in the other patient with NC it resolved with conservative therapy.
Conclusion:
NLFD is a disorder that can be recognized on prenatal and postnatal imaging. In this small series, nutmeg lung was present in all patients with NLFD and may be easier to recognize with fetal MR than US. Dermal backflow on DCMRL suggests a poor prognosis. Both prenatal and postnatal imaging may guide treatment and interventions in NLFD.

Congenital bronchopulmonary malformation: Prenatal MR and postnatal CT and histopathological correlation

M. Kočí, M. Kyncl, D. Maslava, B. Prosova, O. Fabian, L. Hornhofova, M. Pychova, J. Snajdauf, M. Rocek; Prague/CZ

Objective:
Study evaluated the accuracy of fetal magnetic resonance imaging (MRI) in the identification of congenital bronchopulmonary malformation (BPM) in comparison with postnatal computed tomography (CT) and histopathological correlation.
Materials:
Fetal MRI and postnatal CT scans of prenatally diagnosed BPMs from 10 patients with available histology were analyzed retrospectively. The fetal MRI and CT images were reviewed by two radiologists blinded to histological findings. Specific diagnosis was assigned based on predetermined criteria. The accuracy of fetal MRI was evaluated.
Results:
The agreement rate in fetal MRI diagnosis between two radiologists was 100 %. An overlap of 80% in fetal MRI and histopathological diagnosis was reached. When comparing fetal MRI and postnatal CT examinations, the agreement of the results was also 80%. The least matching histological diagnosis was bronchopulmonary sequestration (BPS).

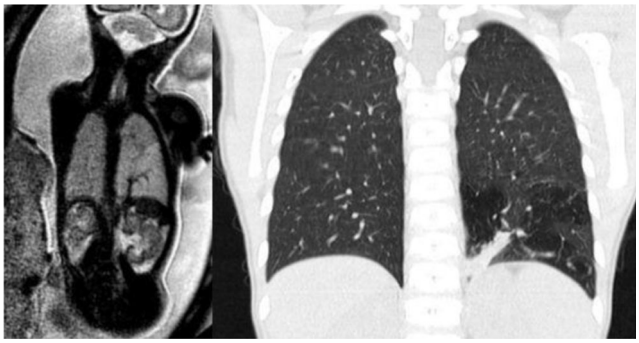

BPS with feeding vessel

Conclusion:
Fetal MRI is very accurate in characterizing the BPM spectrum and provides important information on lesion type and structure when compared with histology. With relatively small number of patients high correlation between prenatal MRI and postnatal CT was reached. Therefore, further investigation with more patients is needed. We hypotethise that fetal MRI in late pregnancy could in the future replace early (neonatal) CT examinations if fetal MRI provides sufficient inforfmation for clinical management.

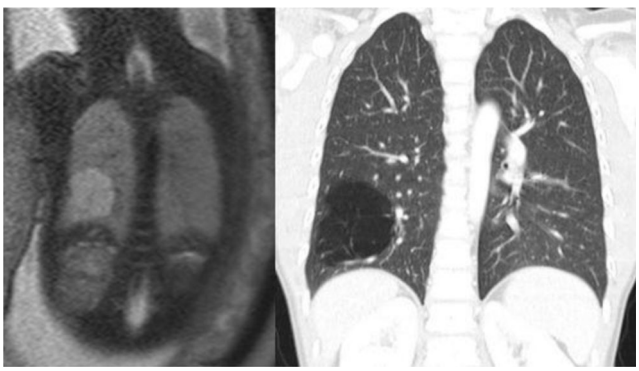

CLO on prenatal MRI and postnatal CT

Real Time Virtual Sonography: A new integrated approach for the evaluation of fetal cerebral pathologies?

S. Bernardo, A. Antonelli, V. Vinci, M. Saldari, C. Catalano, L. Manganaro; Rome/IT

Objective:
Real-time virtual sonography (RVS) is a new technique that uses magnetic navigation and computer software for the synchronized display of real-time US and multiplanar reconstruction MRI images. The purpose of this study was to evaluate the feasibility and ability of RVS to assess the main cerebral pathologies in fetuses with suspected US anomalies.
Materials:
This is a prospective study. Fusion imaging (Hitachi HI Vision Ascendus) was offered to 35 patients undergone Fetal MRI for a US suspicion of cerebral pathology. The MRI image dataset acquired was loaded into the fusion system using a CD support and displayed together with the US image. Both sets of images were then manually synchronized and images were registered. The possibility to record the images in a video format allowed, however, the possibility to re-evaluated the examination.
Results:
RVS was technically possible in all cases. Data registration, matching and fusion imaging were performed in 25 minutes at the beginning and in less than 15-20 minutes after practice. The ability of RVS imaging to assess the main anatomical sites and fetal anomalies was evaluated and compared with standard US and MRI images. The principal application of RVS was the study of midline, cerebral gyration and vascular malformations because it also allowed adding a real time Doppler signal on MRI images. Fusion imaging helped the diagnosis in 25%. In the 25/35 cases of encephalic pathology, fusion imaging improved the diagnosis; in the other cases MRI was superior to US even using the RVS.
Conclusion:
This is a preliminary study on the feasibility and practical use of a Fetal MRI-US real-time fusion imaging. Both techniques are complementary but still independent and the retrospective synthesis of these exams allows optimal analysis of fetal cerebral anomalies. This technique has many advantages especially on the pedagogic plan. However, RVS is currently limited to the research area.

Role of foetal MRI in the evaluation of ischaemic-haemorrhagic lesions of the foetal brain

S. Bernardo, A. Antonelli, V. Vinci, M. Saldari, C. Catalano, L. Manganaro; Rome/IT

Objective:
The aim of this study was to define the role of fetal magnetic resonance imaging in the evaluation of cerebral ischaemic-haemorrhagic lesions and the extension of parenchymal injuries.
Materials:
From September 2010 to December 2016 we performed 271 fetal MRI of cerebral region in foetuses with suspected abnormalities on ultrasound or CMV infection and Toxoplasma serum conversion. Fetal MRI was performed with a 1.5-T Magnet System without materno-fetal sedation.
Results:
Fetal MRI detected ischaemic-haemorrhagic lesions in 14/271 fetuses, revealing a 5% pathology incidence. MRI confirmed the diagnosis in 3/14 cases with US suspect of ischaemic-haemorrhagic lesions associated with ventriculomegaly. In 1/14 cases with US findings of cerebellar haemorrhage, MRI confirmed and provided additional information regarding the parenchymal ischaemic injury. In 8/14 cases with US suspect of ventriculomegaly (n=3), corpus callosum agenesis (2), cerebellar vermis hypoplasia (1), holoprosencephaly (1), spina bifida (1) MRI detected ischaemic and haemorrhagic lesions unidentified at US examination. In 2/14 fetuses with US suspicion of intracerebral tissue space-occupying lesion, MRI modified the diagnosis to extra-axial haematoma associated with dural sinus malformation. Results were compared to fetopsy or after-birth follow up.

Conclusion:
Fetal MRI is an additional imaging modality in the diagnosis of cerebral ischaemic-haemorrhagic lesions and it is useful in providing further information on the extension of parenchyma injury and associated abnormalities and in improving delivery management.

The contribution of mid-trimester virtual autopsy with MR imaging
A. D'hondt, N. D'haene, J. Rommens, M. Cassart, F.E. Avni; Brussels/BE

Objective:
The aim of the study was to assess the potential contribution of fetal virtopsy (Post-mortem MR imaging (PM-MRI)) in the second trimester of pregnancy.
Materials:
During a one-year period, post-mortem MR imaging (PM-MRI) was performed in all fetuses who died in utero or whose pregnancy was interrupted due to major malformations. The study was performed in agreement with the local ethical committee. Fetuses of <26 weeks that underwent obstetrical ultrasound and PM-MR were included.
MR imaging examination was performed on a 1.5 tesla magnet with a standardized protocol.
The findings on PM-MRI were compared to obstetrical sonographic findings (and to pathology when available). We have analyzed separately the findings in the central nervous system and those in the rest of the fetus (Chest, abdomen and skeleton). The results were classified in three categories according to the diagnostic accuracy: ultrasound>PM-MRI, ultrasound=PM-MRI and PM-MRI>ultrasound.
Results:
The US and PM-MRI data of ten fetuses were analyzed. Their gestational age ranged from 17.6-26 weeks and their bodyweight ranged from 160-930g.
For the CNS malformation: PM-MRI offered a better diagnostic accuracy than US in 7 cases (70%) (e.g. agenesis of the corpus callosum and holoprosencephaly). In 3 cases (30%) US offered the same information than PM- MRI. There was no case where US was more accurate than PM-MRI.
For the rest of the body malformations: PM-MRI offered a better diagnostic accuracy in 5 cases (50%) (e.g. heterotaxy anomalies or vertebral segmentation anomalies). In 3 cases (30%), US offered the same information as PM- MRI. There were 2 cases (20%) where US showed major malformations that were not diagnosed on the PM-MRI (Two cases of cardiac malformation).
Conclusion:
Post mortem MR imaging is more accurate than obstetrical ultrasound in detecting major malformations in the CNS as well as in the rest of the body. The present exceptions are cardiac malformations. The examination offers an easy evaluation of the deceased fetus. It provides, in most cases, important additional information.

Diffusion coefficient and perfusion fraction parameters correlate with gestational age in normal human in vivo placenta: A preliminary study
A. Antonelli, M. Guerreri, S. Bernardo, S. Capuani, C. Catalano, L. Manganaro; Rome/IT

Objective:
To investigate the potential of diffusion parameters derived from a bi-exponential analysis as marker to evaluate the perfusion quality of normal in vivo placenta.
Materials:
Eighteen normal pregnancies, fulfilling the study inclusion criteria, have been analysed at 1.5 T Magnetom Avanto (Siemens, Erlangen, Germany) without mother-foetal sedation. DW imaging was collected using seven b values: 0, 50, 100, 150, 400, 700, 1000 (s/mm^2). Three regions of interest (ROIs) have been considered - central (C), peripheral (P) and umbilical (U) regions. A bi-exponential model was used to obtain perfusion fraction (f), pseudo-perfusion (D*) and apparent diffusion (D) coefficients. Pearson test was performed to investigate correlation between diffusion parameters and gestation weeks (GW), body mass index (BMI) and basal glycaemia (bG).
Results:
The average values on all ROIs were D=1.41±0.16·10^{-3} (mm^2/s), D*=1.81 ±1.28·10^{-2} (mm^2/s), f=3.28±0.18·10^{-1}, in good agreement with the literature. In the C ROI, a positive correlation (p<0.04) was observed between f and GW. After 30 GW in the P ROI a positive correlation between f and GW (p<0.05) and a negative correlation between D and GW (p<0.0001) were found. No correlation was found between D, D*, f, BMI and bG.
Conclusion:
The f increase reflects normal placenta perfusion physiology. On the other hand, the decrease of D highlights placental parenchyma maturation becoming more fibrotic during late gestational age. Bi-exponential model provides more and useful information about placental morphological changes compared to mono-exponential diffusion model.

Central Nervous System involvement in congenital heart diseases: Is fetal MRI mandatory?
A. Antonelli, S. Bernardo, V. Vinci, M. Saldari, F. Ventriglia, C. Catalano, L. Manganaro; Rome/IT

Objective:
To demonstrate the diagnostic value of fetal MRI in the detection of fetal Central Nervous system (CNS) impairment in prenatally echocardiographic diagnosed congenital heart diseases.
Materials:
We retrospectively examined 24 fetuses between 19 gestational weeks and 33 gestational weeks who performed a fetal MRI in our institution after a second-line ultrasonography, between April 2010 and October 2015. Fetal heart and CNS studies were performed with a 1.5 Tesla magnet (Siemens Magnetm Avanto) without maternal sedation. Prenatal findings were compared to fetopsy results, fetal MRI after 30 GW or postnatal MRI.
Results:
In our sample of 24 cases, 7/24 had interatrial septal defect (IASD),intervertricular septal defect (IVSD), and atrioventricular canal defect (CAVC), 6/24 had cardiac rhabdomyomas, 3/24 had hypoplastic left heart syndrome and hypoplastic aorta, 2/24 had Transposition of the great vessels, 2/24 had Fallot Tetralogy, 2/24 had aorta coartation and 2/24 had intracardiac masses of uncertain significance. Magnetic resonance imaging was able to detect CNS impairment: we recognize 11/24 Corpus Callosum (CC) Dysgenesis (4/13 CC hypoplasia, 4/13 complete CC agenesis, 3/13 partial CC agenesis), 7/24 Ventriculomegalies or hydrocephalus, 3/24 subtentorial anomalies (Dandy-Walker, vermian hypoplasia and vermian malrotation) and 3/24 gyration anomalies.
Conclusion:
Due to the high risk of CNS involvement in prenatal congenital heart diseases, it is essential to suggest an MRI study of the evolving fetal brain especially in complexes forms that suggest a syndromic background. Fetal MRI of the CNS is mandatory in the study of congenital heart disease due to the high rate of encephalic anomalies associated, particularly in IASD, IVSD and CAVC.

First experiences and diagnostic utility of micro-CT for fetal autopsy
J.C. Hutchinson[1], X. Kang[2], S.C. Shelmerdine[3], M. Cannie[2], V. Segers[2], N. Sebire[3], J. Jani[2], O.J. Arthurs[3]; [1]Newcastle upon Tyne/UK, [2]Brussels/BE, [3]London/UK

Objective:
Perinatal autopsy remains poorly accepted by parents, despite yielding information that affects the management of future pregnancies in around 30% of cases. Microcomputed tomography (micro-CT) has shown promising results in the examination of ex-vivo fetal organs, and may provide diagnostic imaging in cases where traditional autopsy is challenging, and

existing post mortem imaging techniques (CT and MRI) provide insufficient diagnostic resolution. Our objective was to examine whole fetuses non-invasively using micro-CT, and compare the findings with standard autopsy as the gold standard.

Materials:

In this ethically approved double blinded study, terminated fetuses or miscarriages underwent iodinated micro-CT examination followed by conventional autopsy. Images were acquired using a Nikon XTH225ST microfocus-CT scanner with individual specimen image optimisation. Forty indices normally assessed at perinatal autopsy were evaluated for each imaging dataset by two independent reporters and a consensus report produced. Autopsies were performed blinded to the imaging findings by one of two perinatal pathologists.

Results:

We examined 8 fetuses, with a gestational age range of 11–16 gestational weeks. 36/320 indices were non-diagnostic (11%), but there was agreement for 271/284 diagnostic indices (overall concordance of 95.4% (95% CI 92.3, 97.3%). In seven out of eight fetuses (87.5%), the same final diagnosis was made following micro-CT examination and autopsy examination; in one case, micro-CT was non-diagnostic. Ten false negatives indices included a VSD, laryngeal anomaly, ambiguous genitalia and incomplete bowel rotation, none of which changed the overall diagnosis. Three apparent false positives on micro CT were a cloacal anomaly, incidental cystic neck lesion and thymic atrophy, which were not detected at autopsy.

Conclusion:

Micro-CT of early gestation whole fetuses can provide highly accurate datasets with three-dimensional renderings of complex disease processes. This approach confirms the potential of this technology for non-invasive examination of small fetuses.

Investigation of perinatal body organ diffusion-weighted post mortem MRI

S.C. Shelmerdine[1], M. Cheryl[2], J.C. Hutchinson[1], N. Sebire[1], O.J. Arthurs[1]; [1]London/UK, [2]Southampton/UK

Objective:

Diffusion weighted magnetic resonance imaging (DWI) uses water molecule diffusion to generate MR contrast images, and can reveal microstructural or functional changes in tissues, quantified by measuring the apparent diffusion coefficient (ADC). The application of DWI to the post mortem setting is appealing as it does not require the administration of an exogenous contrast agent. A recent pilot study of 15 paediatric cases suggested that lung ADC values at PM MRI may be a useful marker of post mortem interval (time since death; PMI) which has forensic relevance, but other body organs have not been comprehensively evaluated. The aim of this study was therefore to evaluate the relationship between PMI and body organ ADC values in a larger cohort of subjects across a wider gestational range in the setting of perinatal death.

Materials:

Whole body perinatal postmortem MRI with DWI sequences were performed at 1.5T, with b values of 0, 500, 1000 mm^2/s. Mean ADC values were calculated from regions of interest (ROIs) placed in the lungs, myocardium, spleen, renal cortex, liver and psoas muscle. The values were measured by two independent readers, correlated against gestational age and post mortem interval (PMI) using the Pearson product-moment correlation coefficient. Bland-Altman plots were created, and the limits of agreement used to assess the inter-observer agreement of mean ADC values.

Results:

Eighty fetal deaths and stillbirths were imaged with mean gestational age 31.5 weeks (range: 20 – 41 weeks). The mean PMI was 8.9 days (range 2-20 days). There was a weakly positive correlation between PMI and mean lung ADC (R^2=0.03) and spleen ADC (R^2=0.08). No correlation was found with between ADC and PMI for the other body organs. There was reasonable inter-observer agreement between the two readers, with mean ADC difference 11.8 mm^2/s (+/- 135.1 mm^2/s).

Conclusion:

Perinatal lung and splenic ADC values show a mild increase with increasing PMI. Together with other imaging parameters, this may be useful to evaluate organ-specific changes which occur in the post mortem period, particularly in a forensic setting. Further research is needed to understand the organ-specific changes which occur in the post-mortem period.

SESSION: SCIENTIFIC SESSION: ABDOMINAL (GI & GU) IMAGING

Usefulness of combined grey-scale and color Doppler ultrasonography(US) findings in the evaluation of acute pyelonephritis in children

K. Lee, J.H. Lee; Anyang/KR

Objective:

US diagnosis of APN in children can give a valuable information to the clinicians for the early treatment. But the problem of US in the diagnosis of APN is wide range of sensitivity, which is 11-69%. The purpose of this presentation is to evaluate the usefulness of grey-scale US and color Doppler US in the diagnosis of acute pyelonephritis in children.

Materials:

From March 2007 to February 2014, 154 children(308 kidneys), 108 boys and 46 girls, aged 2 weeks to 9 years (mean age, 7.7 months) underwent kidney US as an initial diagnostic tool for acute pyelonephritis and follow up DMSA scintigraphy within a week. Criteria for acute pyelonephritis on grey-scale image were focal/diffusely increased/decreased echogenicity or loss of corticomedullary differentiation. On color Doppler sonography, the criterion was decreased color flow. We classified the US diagnosis of APN into 4 categories. Definite, suggestive, possible and normal. When above two grey-scale US criteria and color Doppler US criterion are seen, we classified it as 'definite'. When one of grey-scale US and color Doppler US finding are seen, it was classified as 'suggestive' of APN. 'Possible' APN was abnormal finding either on grey-scale or color Doppler US. 'Normal' was no abnormal findings on grey-scale and color Doppler US. We compared above findings with DMSA scan, which is considered as gold standard for diagnosing APN. Statistical analysis was performed on all 308 kidneys.

Results:

The overall sensitivity of our study was 68%(88/129) and specificity was 72%(123/177). The positive predictive value for each Definite, Suggestive, Possible groups were 86%, 60%, and 38% respectively. The negative predictive value for normal group was 75%, which means the false PPV was 25%. The p-value of the Definite and Suggestive was statistically significant, but the Possible was statistically insignificant.

Conclusion:

In the diagnosis of APN in children, abnormal US finding either on grey-scale or color Doppler US is not optimal. Abnormal US findings both grey-scale US and color Doppler US showed good association with DMSA scan and statistically significant. Combined grey-scale and color Doppler US findings can give a more reliable information in the diagnosis of APN in children.

Colonic Strictures in Children and Young Adults with Crohn's Disease: Recognition on MRE

D.M. Biko, P. Mamula, N.A. Chauvin, S.A. Anupindi; Philadelphia/US

Objective:

MR enterography (MRE) plays an important role in childhood inflammatory bowel disease (IBD) imaging. Even without colon preparation, colonic pathology can be evaluated. The objective of this study is to identify the MRE features associated with colonic strictures in Crohn's disease

Materials:
Gastroenterology and radiology records were searched to identify IBD patients with colonic strictures. All patients underwent an MRE within 3 months of colonoscopy. The following colonic parameters were evaluated: bowel wall thickening with luminal narrowing, pre-stenotic bowel dilatation, bowel wall enhancement, and diffusion restriction (if performed). Colonoscopy and operative notes were correlated.
Results:
Fourteen patients met the inclusion criteria, one with 2 colonic strictures. Bowel wall thickening with luminal narrowing at the site of the reported stricture was present in all cases. Pre-stenotic bowel dilatation (>3.0 cm) proximal to the reported stricture was present in 11/15 cases. Using luminal narrowing and prestenotic dilatation as criteria for diagnosis of a colonic stricture, 11/15 cases were therefore positive on MRE. When comparing to colonoscopy, MRE diagnosed colonic strictures in 8/12 cases (67%). In the six patients who had surgery, MRE accurately diagnosed colonic strictures in 5/6 cases (83%).

MRE, colonoscopy, and surgical findings of patients in patient population with reported colonic strictures (M: male, F: female, yrs: years, BWT: bowel wall thickening, PSD: Prestenotic Dilatation, DR: Diffusion Restriction, BWHE: Bowel Wall Hyperenhancement)

Sex (M,F)/Age (yrs)	Location	MRE Findings				Stricture on Colonoscopy (Y,N)	Surgery Findings (if applicable)
		BWT (mm)	PSD (cm)	DR (Y, N, N/A)	BWHE (Y,N)		
F/16	distal transverse	7	6.7	Y	Y	N	Ileostomy, no stricture
M/16	proximal transverse	7	5.3	N/A	Y	N	
F/16	ascending	7	6.8	Y	Y	N	
M/17	cecum	8	2.2	Y	N	Y	Large inflammatory mass, no stricture
M/16	ascending	7	N/A	Y	Y	Y	
F/17	rectosigmoid	4	4.6	Y	Y	Y	
M/14	ascending	11	2.6	Y	Y	Y	
F/19	rectum	6	3.4	N	Y	Y	Rectal stricture, rectal dilatation
F/18	Sigmoid	8	3.5	Y	N	Y	Partial colectomy, severe sigmoid disease with central stricture
M/17	Cecum/ ascending	11	2.4	Y	Y	Y	
M/11	rectum	9	4.5	Y	Y	Y	Rectal stricture, rectal dilatation
M/17	cecum	11	5.2	Y	N	Y	Ileocecotomy, stricture
M/10	sigmoid	6	3.6	N/A	Y	Y	
M/19	sigmoid	5	3.0	N/A	N	Y	
	transverse	4	3.8	N/A	N	Y	

MRE, colonoscopy, and surgical findings of patients in patient population with reported colonic strictures

Conclusion:
MRE is not the primary modality for colonic evaluation, yet diagnosing colonic pathology on MRE, particularly strictures, may be beneficial for the referring gastroenterologist in the assessment of these patients. Potential strictures on colonoscopy did not agree with MRE in all cases, but when correlating with surgery 83% of colonic strictures were accurately diagnosed in a small subset. Although MRE is not optimized for the evaluation of the colon, colonic strictures can be recongnized in children with Crohn's disease.

Disorders of sexual differentiations in neonates: Standardized sonographic evaluation and proposal of a reading grid
H. Lerisson, E. Amzallag - Bellenger, F.E. Avni, M. Cartigny; Lille/FR

Objective:
To propose a systematic and structured sonographic approach in neonates with disorders of sexual differentiation (DSD)
Materials:
Review of the US pelvic, external genital and adrenal findings in 20 consecutive patients with clinical suspicion of DSD evaluated in the neonatal period. The US survey included: The uterus (absent or visible - with or without hormonal impregnation), the vagina (absent or present (complete or partial)), the gonads (ovaries, testis or unsetermined – dysgenetic) as well as the adrenals (normal, too small or enlarged). The US conclusions were correlated with the endocrinological and genetical work-up of each patient
Results:
Twenty cases of DSD have been included
US had correctly identified the presence of a uterus in 11 patients. There was one false positive case; 6 among the 11 patients did not show the physiological hormonal impregnation. The 5 vaginal anomalies were correctly evaluated. The gonads were defined correctly as normal testis in 6 patients, normal ovaries in 4 and dysgenetic gonads in 4. They could not be visualized in 6 patients.
Adrenals were considered normal in 17 patients (one false negative), hypertrophied in 2 and small in one patient.
Conclusion:
A structured and standardized US evaluation provides significative information in neonates with DDS. Visualization of intraabdominal dysgenetic gonads is the most difficult part of the study.
A lecture grid will be proposed

Hepatic Shear Wave Elastography in Children under Free-Breathing and Breath-Hold Conditions
J. Herrmann[1], C. Jung[1], M. Groth[1], K.-U. Petersen[2], A. Hammel[1], G. Adam[1]; [1]Hamburg/DE, [2]Tubingen/DE

Objective:
To compare hepatic 2D shear wave elastography (2D SWE) in children between free-breathing and breath-hold conditions, in terms of measurement agreement and time expenditure.
Materials:
A cohort of 57 children (12.7±4.3 years) who underwent standardized 2D SWE between May and October 2015 were retrospectively evaluated. Liver elastograms were obtained under free-breathing and breath-hold conditions and time expenditure was measured. Median stiffness, interquartile range (IQR), and IQR/median ratio were calculated based on 12, six, and three elastograms. Results were compared using Pearson correlation coefficient, intraclass correlation coefficient (ICC), Bland-Altman analysis, and Student's *t*.
Results:
Median liver stiffness under free-breathing and breath-hold conditions correlated strongly (7.22±4.5kPa vs. 7.21±4.11kPa; r=0.97, P<0.001). Time to acquire 12 elastograms with free-breathing was lower than that with breath-holding (79.3±32.5sec vs. 143.7±51.8sec, P<0.001). Results for median liver stiffness based of 12, six, and three elastograms demonstrated very high agreement for free-breathing (ICC 0.993) and for breath-hold conditions (ICC 0.994).
Conclusion:
Hepatic 2D SWE performed with free-breathing yields results similar to the breath-hold condition. With a substantially lower time requirement, which can be further reduced by lowering the number of elastograms, the free-breathing technique may be suitable for infants and less cooperative children not capable of breath-holding.

Hydronephrosis and crossing vessels in children: Sensitivity of Colour-Doppler Ultrasound and Magnetic Resonance Urography
M.B. Damasio, M.C.Y. Wong, G. Piaggio, G. Mattioli, M. Bodria, G. Ghiggeri, G. Magnano; Genoa/IT

Objective:
Abstract: Pelvi-ureteric junction obstruction (PUJO), classified into intrinsic and estrinsic is one of the most frequent urological diseases affecting the pediatric population. Extrinsic causes include the presence of crossing vessels, kinks or adhesions. In cases with extrinsic obstruction of PUJ, Colour Doppler Ultrasound (CD-US) can detect the presence of crossing vessels. In presence of crossing vessels pyeloplasty or vascular hitch can be performed. The aim of the study is to analyze the sensitivity of CD-US and Magnetic Resonance Urography (MRU) in visualizing crossing vessels in extrinsic pediatric hydronephrosis in order to decide the correct diagnostic pathway and evaluate in the pre-operative phase which surgical technique and approach (open, laparoscopic or robotic) is the ideal to be performed.
Materials:
A retrospective review of medical records for patients who underwent surgical treatment for hydronephrosis from August 2006 to February 2016 was performed. A descriptive statistical analysis was performed. The presence of crossing vessels at surgery was considered the gold standard. The sensitivity was calculated for both the imaging techniques as a measure of accuracy, evaluating the ratio between the positive cases divided by the those with aberrant vessels identified at surgery.
Results:
Results 220 clinical charts were reviewed. Crossing vessels identified at surgery were 73 (33,2% of PUJO). The median age was higher in the group with crossing vessels compared to the group without crossing vessels ($p<$ 0,0001). The sensitivity of CD-US was higher compared to MRU (93,3% vs 71,7%). Before the surgical time knowing which technique and approach have to be managed in hydronephrotic patients with crossing vessels could be very important. According to our preliminary datacollection CD-US has got a higher sensitivity and could be the gold standard technique. Study limitations include the absence of specificity, positive and negative predictive values. In the future it could be useful to perform a double blind trial in which children with moderate-severe hydronephrosis will be subjected to both imaging techniques to evaluate not only the sensitivity, but also the specificity, the positive predictive value and the negative predictive value
Conclusion:
Conclusions In the pre-operative phase, CD-US could be sufficient for the surgeon to discern between PUJO with the presence or the absence of crossing vessels, as it has a higher sensitivity and lower costs compared to MRU.

Urosonography - Nonradiant alternative for voiding cystourethrography

O.M. Fufezan, C.A. Asavoaie, S. Tatar; Cluj-Napoca/RO

Objective:
Voiding cystourethrography (VCUG) was considered the gold standard in the diagnosis and monitoring of vesicoureteric reflux (VUR). This method is invasive due to the radiation exposure. In the present the diagnosis of VUR can also be established by contrast ultrasound examination, also known as voiding urosnography (VUS). The authors will present the role of VUS in the diagnosis and grading of the VUR and the role of patient position in the detection of VUR.
Materials:
The infants and children with congenital anomalies of the urinary tract and/or urinary tract infection have been evaluated with VUS. Iatrogenic VUR, neurogenic bladder and urogenital sinus anomalies were excluded. The presence and the degree of the VUR were evaluated. VUS has been performed using a protocol similar to the one used for VCUG. In conditions of sterile urine, 0.5 ml Sonovue and saline solution have been introduced into the bladder until voiding started. The patients were examined both in a supine and an upright position and the following structures have been scanned: urinary bladder, distal part of the ureters and both pelvicaliceal systems during bladder filling, during and after voiding. The visualisation of the ultrasound contrast agent in the upper urinary tract represented a positive VUR diagnosis. The grading of the VUR has been established based on the same criteria as in VCUG.
Results:
Sixty five patients (130 renal units), ages between 2 weeks and 17 years were evaluated (median age ± SD: 3 years ± 4 years and 2 months) through VUS. VCUG was performed in 6 patients in a maximum of 48 hours after VUS. VUR has been identified in 35 patients (40.7% renal units). A high VUR grade (IV-V) was identified in 19.2% of renal units. For the patients investigated with both methods, the results were concordant in 4 patients. In two patients VUR has not been identified by VCUG, but was detected during VUS. The upright position (in addition to decubitus) revealed VUR in 3 renal units in which the reflux was not detected in decubitus.
Conclusion:
VUS is extremely useful and reliable in diagnosing and grading VUR in pediatrics. The changing of the patient position during examination can improve VUR detection.

New sonographic features useful in differentiating congenital duodenal anomalies from malrotation: Gastric and duodenal wall thickening and hyperechogenicity

P. Caro Dominguez[1], S. Hameed[2], A. Zani[3], R. Moineddin[3], O.M. Navarro Kunstmann[3], A. Daneman[3]; [1]Cordoba/ES, [2]London/UK, [3]Toronto/CA

Objective:
The clinical and plain radiographic differentiation of congenital duodenal anomalies (atresia, web, stenosis) and intestinal malrotation is not always clear. Although sonography has been documented as an important diagnostic tool to differentiate these two entities, its role is still not widely appreciated. The purpose of this study was to assess the sonographic features of the gastric and duodenal wall in a large series of neonates with congenital duodenal obstruction as these have not been reported previously.
Materials:
Neonates who had surgically proven congenital duodenal anomalies or malrotation were identified from the surgical database in a tertiary pediatric hospital in a period of 15 years (2000-2015). Those with an ultrasound performed within 48 hours of surgery were included in the study. Imaging was retrospectively and independently reviewed by two readers in chronological order blinded to final diagnosis. A wall thickness of ≥ 2 mm of a distended loop was considered abnormal. Hyperechogenicity was recorded when the wall of the stomach or duodenum was brighter than liver or splenic parenchyma. Imaging findings in the group with congenital duodenal anomalies was compared to the group with malrotation using Fisher's exact test.
Results:
One hundred eight neonates were included in the study, 40 with a congenital duodenal anomaly, 49 with malrotation (36 with volvulus) and 19 with both. UGI was performed in 61 neonates who had US. The correct diagnosis was provided only by US in 24 of these 61 newborns (39%), only by UGI in 5 (8%), by both in 26 (43%) and by neither in 6 (10%). UGI was performed in 21 children with malrotation and volvulus, eight were diagnosed only by US, four only by UGI and nine by both.
The gastric and/or duodenal wall was significantly thicker and more hyperechoic in neonates with congenital duodenal anomalies than those with malrotation (p<0.0001) [Fig 1, Table 1]. Conversely an abnormal relationship between the superior mesenteric artery and vein, abnormal position of the third part of the duodenum and the whirlpool sign were found more commonly in neonates with malrotation than those with congenital anomalies (p<0.0001).

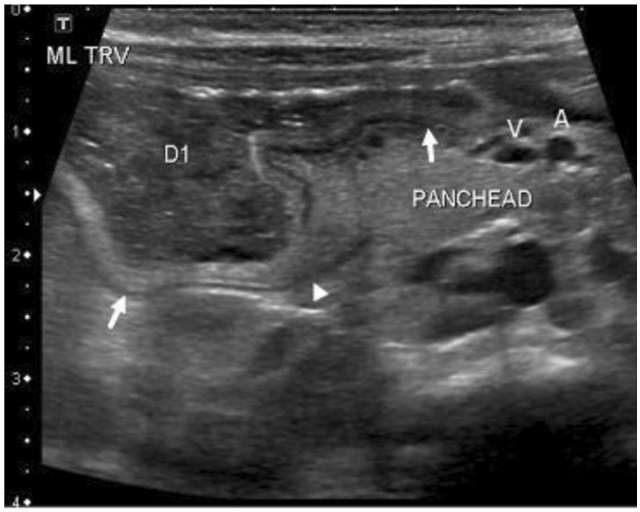

Fig 1 1-day-old baby girl with atresia of the first portion of the duodenum (D1). Transverse ultrasound image of the upper abdomen demonstrate thickening and hyperechogenicity of the stomach and duodenum (arrow) and an abrupt stop of D1 (arrowhead). Note the normal relationship of the superior mesenteric artery (A) and vein (V)

			Malrotation with or without volvulus n = 49	Duodenal atresia/web/ stenosis n = 41	Malrotation + duodenal anomaly n = 18
Ultrasound findings n = 108	Abnormal SMA/SMV relationship		44 - 90%	3 - 7%	11 - 67%
	Whirlpool sign		34 - 69%	0	1 - 6%
	Abnormal position of D3		40 - 82%		3 - 17%
	Gastric wall	Thickening	6 - 12%	33 - 79%	10 - 59%
		Hyperechogenicity	7 - 14%	36 - 86%	14 - 82%
	Duodenal wall	Thickening	9 - 18%	35 - 83%	9 - 53%
		Hyperechogenicity	9 - 18%	38 - 90%	12 - 71%

Conclusion:
The greater degree of gastric and/or duodenal wall thickening and increased echogenicity are helpful sonographic features in differentiating congenital duodenal anomalies from malrotation. Our findings confirm the superiority of US vs UGI for evaluation of duodenal obstruction in neonates and evaluation of gastric and duodenal wall must be added to the constellation of other features to be assessed on US examinations.

A Measure of Renal Morphology as an Indicator for Potential Renal Failure

A.C. Eichenberger, P. Grehten, C. Kellenberger; Zurich/CH

Objective:
This study introduces a measure of renal morphology, herein labelled Split Renal Volume (SRV), that should be applied as an indicator for potential renal failure and eventual surgical treatment of obstructive uropathy in children. Current practice applies dynamic contrast enhanced Functional Renal Imaging (FRI) with complex post-processing methods. FRI generates a measure of Split Renal Function (SRF). Reduced values of SRF under 45% are currently considered to be an indicator for surgical treatment. This retrospective study compares the accuracy of SRV with the accuracy of SRF as methods for assessing potential renal failure.
Materials:
SRV is a quotient of volumetric measurements. Total renal volume is described by the sum of parenchymal volume and intra-renal collecting system volume. SRV is designated in this study as the quotient of two ratios: first, the ratio of total renal volume to parenchymal volume of the left kidney; and second, the ratio of total renal volume to parenchymal volume of the right kidney.
Twenty-two children were studied: 16 (age 3.1±4.5y) with unilateral asymptomatic intrinsic uretero-pelvic-junction obstruction (UPJO), and 6 normal controls (age 6.6±4.0y). All subjects underwent MR Urography at 1.5T, which provided estimates of SRF and SRV for each of the 44 examined kidneys. The sensitivity and specificity of both SRF and SRV for predicting surgical management were determined by comparing the indicators with an expert review panel's decision to operate. The panel was blinded to values of SRV.
Results:
When a cut-off value of 45% for SRF was used, the resultant sensitivity and specificity of SRF for the detection of kidneys at risk were found to be 44% and 86%. The values of SRV ranged between 0.3 and 3.5. It was found that a value greater than 1.1 indicated kidneys at risk. When the cut-off value of 1.1 for SRV was used, the resultant sensitivity and specificity of SRV for the detection of kidneys at risk were both 100%.
Conclusion:
In this small population, SRV proved to be 100% accurate and is superior to SRF for detecting kidneys at risk of failure due to obstruction. Routine application of SRV promises to simplify MR Urography by obviating dynamic contrast enhanced imaging studies. Further prospective studies are necessary in order to select an optimal cut-off value of SRV.

Factors that can distort the DJ flexure mimicking malrotation

V. Bhalla[1], S. Mohan[2], K.A. Bradshaw[2], M. Thyagarajan[2]; [1]Stoke-on-Trent/UK, [2]Birmingham/UK

Objective:
To highlight the varied radiological appearances and position of the Duodenal-jejunal flexure in children and to discuss its importance in assessing for malrotation
Materials:
Retrospective analysis of the multiple fluoroscopic examinations performed in the assessment for malrotation over the past 5 years in a busy tertiary centre
Results:
The classic position of the DJ flexure is to the left of left pedicle of L1 and at the level of the duodenal bulb on frontal views and posterior (retroperitoneal) on lateral views. However variations of the normal location can appear, particularly on frontal views, in the upper GI series that can mimic malrotation which has shown to be more common in neonates. We present cases with examples to illustrate the variability in position due to various causes and its implications in the diagnosis of Malrotation and volvulus. Our case mix includes patients with excessively distended stomachs, large bowel obstruction, renal pelvic dilatation, repeated naso-jejunal and gastro-jejunal tube insertion and in patients post liver transplantation.
Conclusion:
Malrotation and its assessment have serious management and prognostic implications. This presentation demonstrates that the imaging features can be varied, and knowledge about factors distorting the position of the DJ flexure is vital in the accurate management of neonates presenting with bilious vomits.

16 year experience of Native Paediatric Renal Biopsies

K.S. Minhas, A. Parthipun, S. Stuart, P. Patel, N. Sabire, D. Roebuck; London/UK

Objective:
Report the results of a single centre prospective study investigating native paediatric renal biopsies. The success rate, outcome and complication rates were evaluated.
Materials:

Retrospective study of prospectively collected data performed at a single tertiary paediatric institution over a 16.5 year period. A total of 1000 consecutive patients, aged <18 years, were reviewed who underwent native renal biopsy. All biopsies were performed within the Interventional Radiology Department. All patients had renal disease requiring a renal biopsy for diagnosis. Outcome measures include technical success, early and late complications and the adequacy of histological samples. In addition, age, body weight, glomeruli number, histological data, number of cores, size of the biopsy needle, use of co-axial needle and the rate of tract embolisation/plugging were recorded.

Results:

From September 1999 to April 2016, 1000 patients (mean age: 10.07 years +/- 4.65; range 0.14 – 18.0 years) underwent native renal biopsy. One hundred ninety-one patients were <5 years of age. Nine hundred forty-six patients (94.6%) had a biopsy of the right kidney, 53 patients (5.3%) had a biopsy of the left kidney and 1 patient (0.1%) had a biopsy of a horseshoe kidney.

Five hundred fifteen patients were female (51.5%). Seven hundred sixty-nine patients (76.9%) had the procedure performed under general anaesthetic and 227 of patients (22.7%) had the procedure performed under local anaesthetic (+/- sedation/Entonox). Mean number of passes of the core biopsy needle through the renal capsule was 2.7. A 16 gauge core biopsy needle was used in 100% of the patients. 81.9% of the patients had three or less passes of the biopsy needle though the renal capsule. The overall complication rate was 2.6% (n= 26). 1.2% (n= 12) of patients had a non- diagnostic biopsy.

Fifty-five patients underwent a post biopsy ultrasound due to clinical concerns. Twenty patients developed perinephric haematoma (19 were treated conservatively; one underwent embolisation and subsequent nephrectomy). Four patients developed arteriovenous fistulas. Two patients developed post procedure infections (one at the skin site and one a perinephric collection).

Histology results were reviewed in all patients. The mean number of glomeruli obtained was 26.97 (range 2-87). Glomerulonephritis was the most common histological diagnosis (n=464; 46.4%)

Conclusion:

Renal biopsy is an extremely useful diagnostic tool for renal disease. There is no published data of this size assessing the outcome of native renal biopsies in the paediatric population.